ANALYTICAL ELECTROCHEMISTRY

Second Edition

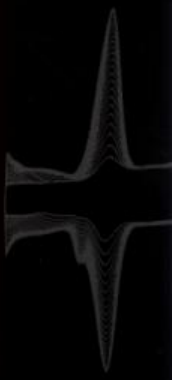

Joseph Wang

WILEY-VCH

Analytical Electrochemistry, Second Edition. Joseph Wang

ISBNs: 0-471-28272-3 (Hardback); 0-471-22823-0 (Electronic)

ANALYTICAL ELECTROCHEMISTRY

SECOND EDITION

ANALYTICAL ELECTROCHEMISTRY

Second Edition

JOSEPH WANG

A JOHN WILEY & SONS, INC., PUBLICATION

New York / Chichester / Weinheim / Brisbane / Singapore / Toronto

ISBN 0-471-22823-0.

This title is also available in print as ISBN 0-471-28272-3.

For more information about Wiley products, visit our web site at www.Wiley.com.

Dedicated to the memory of my parents, Elka and Moshe Wang

CONTENTS

PREFACE

The goal of this textbook is to cover the full scope of modern electroanalytical techniques and devices. The main emphasis is on electroanalysis, rather than physical electrochemistry. The objective is to provide a sound understanding of the fundamentals of electrode reactions and of the principles of electrochemical methods, and to demonstrate their potential for solving real-life analytical problems. Given the impressive progress in electroanalytical chemistry, and its growing impact on analytical chemistry, this work offers also an up-to-date, easy-to-read presentation of recent advances including new methodologies, sensors, detectors, and microsystems. The book is suitable for a graduate-level course in electroanalytical chemistry or as a supplement to a high-level undergraduate course in instrumental analysis. It should also be very useful to those considering the use of electroanalysis in their laboratories.

The material is presented in six roughly equal chapters. The first chapter is devoted to fundamental aspects of electrode reactions and the structure of the interfacial region. Chapter 2 discusses the study of electrode reactions and high-resolution surface characterization. Chapter 3 gives an overview of finite-current controlled-potential techniques. Chapter 4 describes the electrochemical instrumentation and electrode materials (including new modified and microelectrodes). Chapter 5 deals with the principles of potentiometric measurements and various classes of ion-selective electrodes, while Chapter 6 is devoted to the growing field of chemical sensors (including modern biosensors, gas sensors, solid-state devices, and sensor arrays). I have tried to provide numerous references to review literature at the end of each chapter. By discussing the very latest advances, it is hoped to bridge the common gap between recent research literature and standard textbooks.

This second edition of *Analytical Electrochemistry* is extensively revised and updated, and reflects the rapid growth of electroanalytical chemistry during the 1990s. It contains a number of new topics, including self-assembled monolayers, DNA biosensors, sol-gel surface modification, detection for capillary electrophoresis, single molecule detection, and micromachined analyzers ("Lab-on-a-Chip"). Other topics such as the fundamentals of faradaic processes, principles of potentiometric measurements, spectroelectrochemistry, modified and microelectrodes, scanning electron microscopy, electrical communication between redox enzymes and electrodes, and enzyme and immunoelectrodes, have been greatly expanded. The entire text has been updated to cover the very latest (as of 1999) developments in electroanalytical chemistry. Numerous new worked examples and end-of-chapter questions have been added to this edition. The organization of the book has been changed somewhat, by moving the study of electrode reactions forward to Chapter 2. In the five years since the first edition I received numerous suggestions, many of which have been incorporated in the second edition.

Finally, I wish to thank my wife, Ruth, and my daughter, Sharon, for their love and patience; the editorial and production staff of Wiley Inc. for their help and support; and the numerous electrochemists across the globe who led to the advances reported in this textbook. Thank you all!

Joseph Wang
Las Cruces, New Mexico, U.S.A.

ABBREVIATIONS AND SYMBOLS

a	Activity
A	Absorbance
A	Area of electrode
Ab	Antibody
AdSV	Adsorptive stripping voltammetry
AES	Auger electron spectroscopy
AFM	Atomic force microscopy
Ag	Antigen
ASV	Anodic stripping voltammetry
B	Adsorption coefficient
C	Concentration
C_{dl}	Differential capacitance
C_{Hg}	Concentration in amalgam
CSV	Cathodic stripping voltammetry
CWE	Coated-wire electrode
CME	Chemically modified electrode
CV	Cyclic voltammetry
CZE	Capillary zone electrophoresis
D	Diffusion coefficient
DC	Direct current
DNA	Deoxyribonucleic acid

DME	Dropping mercury electrode
DPV	Differential pulse voltammetry
E	Potential (V)
ΔE	Pulse amplitude; step height
E_B	Binding energy (in XPS)
E_{eq}	Equilibrium potential
E°	Standard electrode potential
$E_{1/2}$	Half wave potential
E_p	Peak potential
E_{pzc}	Potential of zero charge
EC	Electrode process involving an electrochemical reaction followed by a chemical step
ECL	Electrochemiluminescence
EQCM	Electrochemical quartz crystal microbalance
ESCA	Electron spectroscopy for chemical analysis
EXAFS	X-ray adsorption fine structure
F	Faraday constant
FET	Field-effect transistor
FIA	Flow injection analysis
f	Activity coefficient; frequency
Δf	Frequency change (in EQCM)
ΔG	Free energy
$\Delta G^\ddagger$	Free energy of activation
HMDE	Hanging mercury drop electrode
i	Electric current
i_c	Charging current
i_l	Limiting current
i_t	Tunneling current
Δi	Current difference
IHP	Inner Helmholtz plane
IRS	Internal reflectance spectroscopy
ISE	Ion-selective electrode
ISFET	Ion-selective field-effect transistor
J	Flux
k_{ij}^{pot}	Potentiometric selectivity coefficient
k°	Standard rate constant
K_m	Michaelis–Menten constant; mass transport coefficient

l	Film thickness
LCEC	Liquid chromatography/electrochemistry
LEED	Low-energy electron diffraction
m	Mercury flow rate (in polarography); electron mass (in STM)
Δm	Mass charge (in EQCM)
M	Mediator
MFE	Mercury film electrode
N	Collection efficiency
NADH	Dihydronicotinamide adenine dinucleotide
n	Number of electrons transferred
NP	Normal pulse
O	The oxidized species
OHP	Outer Helmholtz plane
OTE	Optically transparent electrode
PAD	Pulsed amperometric detection
PSA	Potentiometric stripping analysis
q	Charge
QCM	Quartz crystal microbalance
r	distance; radius
R	Resistance; gas constant
RDE	Rotating disk electrode
Re	Reynolds number
RRDE	Rotating ring disk electrode
RVC	Reticulated vitreous carbon
S	Barrier width (in STM)
SAM	Self-assembled monolayers
Sc	Schmidt number
SECM	Scanning electrochemical microscopy
SERS	Surface enhanced Raman scattering
STM	Scanning tunneling microscopy
SWV	Square-wave voltammetry
T	Temperature
t	Time
t_d	Deposition time
t_{m}	Transition time (in PSA)
U	Flow rate, stirring rate

v	Potential scan rate
V_{Hg}	Volume of mercury electrode
V_{max}	Maximum rate
$W_{1/2}$	Peak width (at half height)
WE	Working electrode
WJD	Wall jet detector
XPS	X-ray photoelectron spectroscopy
α	Transfer coefficient
Γ	Surface coverage
ε	Dielectric constant; molar absorptivity
γ	Surface tension
δ	Thickness of the diffusion layer
δ_H	Thickness of the hydrodynamic boundary layer
η	Overvoltage
μ	Ionic strength
ν	Kinematic viscosity
ω	Angular velocity

Analytical Electrochemistry, Second Edition. Joseph Wang

ISBNs: 0-471-28272-3 (Hardback); 0-471-22823-0 (Electronic)

CHAPTER 1

FUNDAMENTAL CONCEPTS

1-1 WHY ELECTROANALYSIS?

Electroanalytical techniques are concerned with the interplay between electricity and chemistry, namely the measurements of electrical quantities, such as current, potential, or charge, and their relationship to chemical parameters. Such use of electrical measurements for analytical purposes has found a vast range of applications, including environmental monitoring, industrial quality control, and biomedical analysis. Advances in the 1980s and 1990s—including the development of ultramicroelectrodes, the design of tailored interfaces and molecular monolayers, the coupling of biological components and electrochemical transducers, the synthesis of ionophores and receptors containing cavities of molecular size, the development of ultratrace voltammetric techniques or of high-resolution scanning probe microscopies, and the microfabrication of molecular devices or efficient flow detectors—have led to a substantial increase in the popularity of electroanalysis, and to its expansion into new phases and environments. Indeed, electrochemical probes are receiving a major share of the attention in the development of chemical sensors.

In contrast to many chemical measurements that involve homogeneous bulk solutions, electrochemical processes take place at the electrode–solution interface. The distinction between various electroanalytical techniques reflects the type of electrical signal used for the quantitation. The two principal types of electroanalytical measurements are potentiometric and potentiostatic. Both types require at least two electrodes (conductors) and a contacting sample (electrolyte) solution, which constitute the electrochemical cell. The electrode surface is thus a junction between an ionic conductor and an electronic conductor. One of the two electrodes responds

to the target analyte(s) and is thus termed the indicator (or working) electrode. The second one, termed the reference electrode, is of constant potential (that is, independent of the properties of the solution). Electrochemical cells can be classified as electrolytic (when they consume electricity from an external source) or galvanic (if they are used to produce electrical energy).

Potentiometry (discussed in Chapter 5), which is of great practical importance, is a static (zero current) technique in which the information about the sample composition is obtained from measurement of the potential established across a membrane. Different types of membrane materials, possessing different ion-recognition processes, have been developed to impart high selectivity. The resulting potentiometric probes have thus been widely used for several decades for direct monitoring of ionic species such as protons or calcium, fluoride, and potassium ions in complex samples.

Controlled-potential (potentiostatic) techniques deal with the study of charge-transfer processes at the electrode–solution interface, and are based on dynamic (no zero current) situations. Here, the electrode potential is being used to derive an electron-transfer reaction and the resultant current is measured. The role of the potential is analogous to that of the wavelength in optical measurements. Such a controllable parameter can be viewed as "electron pressure," which forces the chemical species to gain or lose an electron (reduction or oxidation, respectively).

TABLE 1-1 Properties of Controlled-Potential Techniques

Technique[a]	Working Electrode[b]	Detection Limit (M)	Speed (time per cycle) (min)	Response Shape
DC polarography	DME	10^{-5}	3	Wave
NP polarography	DME	5×10^{-7}	3	Wave
DP polarography	DME	10^{-8}	3	Peak
DP voltammetry	Solid	5×10^{-7}	3	Peak
SW polarography	DME	10^{-8}	0.1	Peak
AC polarography	DME	5×10^{-7}	1	Peak
Chronoamperometry	Stationary	10^{-5}	0.1	Transient
Cyclic voltammetry	Stationary	10^{-5}	0.1–2	Peak
Stripping voltammetry	HMDE, MFE	10^{-10}	3–6	Peak
Adsorptive stripping voltammetry	HMDE	10^{-10}	2–5	Peak
Adsorptive stripping voltammetry	Solid	10^{-9}	4–5	Peak
Adsorptive-catalytic stripping voltammetry	HMDE	10^{-12}	2–5	Peak

[a]DC = direct current; NP = normal pulse; DP = differential pulse; SW = square wave; AC = alternating current.

[b]DME = dropping mercury electrode; HMDE = hanging mercury drop electrode; MFE = mercury film electrode.

Accordingly, the resulting current reflects the rate at which electrons move across the electrode–solution interface. Potentiostatic techniques can thus measure any chemical species that is electroactive, in other words, that can be made to reduce or oxidize. Knowledge of the reactivity of functional group in a given compound can be used to predict its electroactivity. Nonelectroactive compounds may also be detected in connection with indirect or derivatization procedures.

The advantages of controlled-potential techniques include high sensitivity, selectivity towards electroactive species, a wide linear range, portable and low-cost instrumentation, speciation capability, and a wide range of electrodes that allow assays of unusual environments. Several properties of these techniques are summarized in Table 1-1. Extremely low (nanomolar) detection limits can be achieved with very small sample volumes (5–20 μl), thus allowing the determination of analyte amounts of 10^{-13} to 10^{-15} mol on a routine basis. Improved selectivity may be achieved via the coupling of controlled-potential schemes with chromatographic or optical procedures.

This chapter attempts to give an overview of electrode processes, together with discussion of electron transfer kinetics, mass transport, and the electrode–solution interface.

1-2 FARADAIC PROCESSES

The objective of controlled-potential electroanalytical experiments is to obtain a current response that is related to the concentration of the target analyte. This objective is accomplished by monitoring the transfer of electron(s) during the redox process of the analyte:

$$\mathrm{O} + ne^- \rightleftharpoons \mathrm{R} \tag{1-1}$$

where O and R are the oxidized and reduced forms, respectively, of the redox couple. Such a reaction will occur in a potential region that makes the electron transfer thermodynamically or kinetically favorable. For systems controlled by the laws of thermodynamics, the potential of the electrode can be used to establish the concentration of the electroactive species at the surface [$C_{\mathrm{O}}(0, t)$ and $C_{\mathrm{R}}(0, \mathrm{t})$] according to the Nernst equation:

$$E = E^\circ + \frac{2.3RT}{nF} \log \frac{C_{\mathrm{O}}(0, t)}{C_{\mathrm{R}}(0, t)} \tag{1-2}$$

where E° is the standard potential for the redox reaction, R is the universal gas constant (8.314 J K^{-1} mol^{-1}), T is the Kelvin temperature, n is the number of electrons transferred in the reaction, and F is the Faraday constant (96,487 coulombs). On the negative side of E°, the oxidized form thus tends to be reduced, and the forward reaction (i.e., reduction) is more favorable. The current resulting from a change in oxidation state of the electroactive species is termed the *faradaic*

current because it obeys Faraday's law (i.e. the reaction of 1 mole of substance involves a change of $n \times 96{,}487$ coulombs). The faradaic current is a direct measure of the rate of the redox reaction. The resulting current–potential plot, known as the *voltammogram*, is a display of current signal (vertical axis) versus the excitation potential (horizontal axis). The exact shape and magnitude of the voltammetric response is governed by the processes involved in the electrode reaction. The total current is the summation of the faradaic currents for the sample and blank solutions, as well as the nonfaradaic charging background current (discussed in Section 1-3).

The pathway of the electrode reaction can be quite complicated, and takes place in a sequence that involves several steps. The rate of such reactions is determined by the slowest step in the sequence. Simple reactions involve only mass transport of the electroactive species to the electrode surface, the electron transfer across the interface, and the transport of the product back to the bulk solution. More complex reactions include additional chemical and surface processes that precede or follow the actual electron transfer. The net rate of the reaction, and hence the measured current, may be limited either by mass transport of the reactant or by the rate of electron transfer. The more sluggish process will be the rate-determining step. Whether a given reaction is controlled by the mass transport or electron transfer is usually determined by the type of compound being measured and by various experimental conditions (electrode material, media, operating potential, mode of mass transport, time scale, etc.). For a given system, the rate-determining step may thus depend on the potential range under investigation. When the overall reaction is controlled solely by the rate at which the electroactive species reach the surface (i.e., a facile electron transfer), the current is said to be mass transport-limited. Such reactions are called nernstian or reversible, because they obey thermodynamic relationships. Several important techniques (discussed in Chapter 4) rely on such mass transport-limited conditions.

1-2.1 Mass Transport-Controlled Reactions

Mass transport occurs by three different modes:

- *Diffusion*—the spontaneous movement under the influence of concentration gradient (i.e., from regions of high concentration to regions of lower concentration), aimed at minimizing concentration differences.
- *Convection*—transport to the electrode by a gross physical movement; such fluid flow occurs with stirring or flow of the solution and with rotation or vibration of the electrode (i.e., forced convection) or due to density gradients (i.e., natural convection);
- *Migration*—movement of charged particles along an electrical field (i.e., the charge is carried through the solution by ions according to their transference number).

These modes of mass transport are illustrated in Figure 1-1.

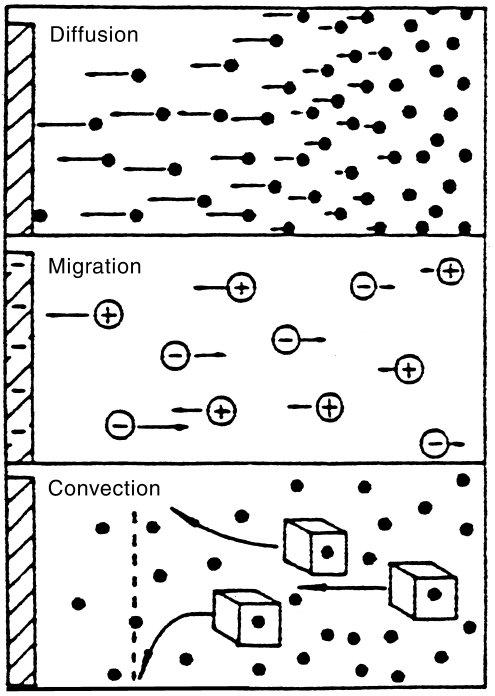

FIGURE 1-1 The three modes of mass transport. (Reproduced with permission from reference 1.)

The flux (J) is a common measure of the rate of mass transport at a fixed point. It is defined as the number of molecules penetrating a unit area of an imaginary plane in a unit of time, and has the units of mol cm^{-2} s^{-1}. The flux to the electrode is described mathematically by a differential equation, known as the Nernst–Planck equation, given here for one dimension:

$$J(x, t) = -D\frac{\partial C(x, t)}{\partial x} - \frac{zFDC}{RT}\frac{\partial \phi(x, t)}{\partial x} + C(x, t)V(x, t) \tag{1-3}$$

where D is the diffusion coefficient (cm^{-2} s^{-1}), $\partial C(x, t)/\partial x$ is the concentration gradient (at distance x and time t), $\partial \phi(x, t)/\partial x$ is the potential gradient, z and C are the charge and concentration, respectively, of the electroactive species, and $V(x, t)$ is the hydrodynamic velocity (in the x direction). In aqueous media, D usually ranges between 10^{-5} and 10^{-6} cm^{-2} s^{-1}. The current (i) is directly proportional to the flux:

$$i = -nFAJ \tag{1-4}$$

As indicated by equation (1-3), the situation is quite complex when the three modes of mass transport occur simultaneously. This complication makes it difficult to relate the current to the analyte concentration. The situation can be greatly simplified by suppressing the electromigration or convection, through the addition of excess inert salt or use of a quiescent solution, respectively. Under these conditions, the movement of the electroactive species is limited by diffusion. The reaction occurring at the surface of the electrode generates a concentration gradient adjacent to the surface, which in turn gives rise to a diffusional flux. Equations governing diffusion processes are thus relevant to many electroanalytical procedures.

According to Fick's first law, the rate of diffusion (i.e., the flux) is directly proportional to the slope of the concentration gradient:

$$J(x, t) = -D \frac{\partial C(x, t)}{\partial x} \tag{1-5}$$

Combination of equations (1-4) and (1-5) yields a general expression for the current response:

$$i = nFAD \frac{\partial C(x, t)}{\partial x} \tag{1-6}$$

Hence, the current (at any time) is proportional to the concentration gradient of the electroactive species. As indicated by the above equations, the diffusional flux is time dependent. Such dependence is described by Fick's second law (for linear diffusion):

$$\frac{\partial C(x, t)}{\partial t} = D \frac{\partial^2 C(x, t)}{\partial x^2} \tag{1-7}$$

This equation reflects the rate of change with time of the concentration between parallel planes at points x and $(x + dx)$ (which is equal to the difference in flux at the two planes). Fick's second law is valid for the conditions assumed, namely planes parallel to one another and perpendicular to the direction of diffusion, i.e., conditions of linear diffusion. In contrast, for the case of diffusion toward a spherical electrode (where the lines of flux are not parallel but are perpendicular to segments of the sphere), Fick's second law has the form

$$\frac{\partial C}{\partial t} = D\left(\frac{\partial^2 C}{\partial r^2} + \frac{2}{r} \frac{\partial C}{\partial r}\right) \tag{1-8}$$

where r is the distance from the center of the electrode. Overall, Fick's laws describe the flux and the concentration of the electroactive species as functions of position and time. The solution of these partial differential equations usually requires the application of a (Laplace transformation) mathematical method. The Laplace transformation is of great value for such applications, as it enables the conversion

of the problem into a domain where a simpler mathematical manipulation is possible. Details of use of the Laplace transformation are beyond the scope of this text, and can be found in reference 2. The establishment of proper initial and boundary conditions (which depend upon the specific experiment) is also essential for this treatment. The current–concentration–time relationships that result from such treatment will be described below for several relevant experiments.

1-2.1.1 Potential-Step Experiment Let us see, for example, what happens in a potential-step experiment involving the reduction of O to R, a potential value corresponding to complete reduction of O, a quiescent solution, and a planar electrode imbedded in a planar insulator. (Only O is initially present in solution.) The current–time relationship during such an experiment can be understood from the resulting concentration–time profiles. Since the surface concentration of O is zero at the new potential, a concentration gradient is established near the surface. The region within which the solution is depleted of O is known as the *diffusion layer*, and its thickness is given by δ. The concentration gradient is steep at first, and the diffusion layer is thin (see Figure 1-2, for t_1). As time goes by, the diffusion layer expands (to δ_2 and δ_3 at t_2 and t_3), and hence the concentration gradient decreases.

Initial and boundary conditions in such experiment include $C_O(x, 0) = C_O(b)$ (i.e., at $t = 0$, the concentration is uniform throughout the system and equal to the bulk concentration; $C_O(b)$), $C_O(0, t) = 0$ for $t > 0$ (i.e., at later times the surface concentration is zero); and $C_O(x, 0) \rightarrow C_O(b)$ as $x \rightarrow \infty$ (i.e., the concentration increases as the distance from the electrode increases). Solution of Fick's laws (for

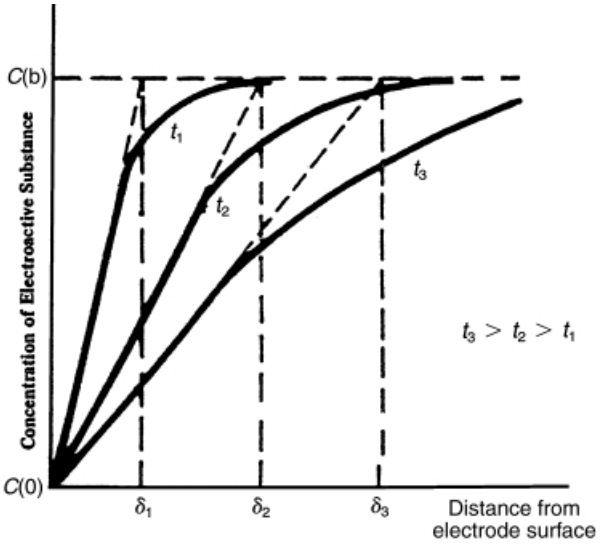

FIGURE 1-2 Concentration profiles for different times t after the start of a potential-step experiment.

linear diffusion, i.e., a planar electrode) for these conditions results in a time-dependent concentration profile,

$$C_O(x, t) = C_O(b)\{1 - \text{erf}[X/(4D_O t)^{1/2}]\} \tag{1-9}$$

whose derivative with respect to x gives the concentration gradient at the surface,

$$\frac{\partial C}{\partial x} = \frac{C_O(b)}{(\pi D_O t)^{1/2}} \tag{1-10}$$

when substituted into equation (1-6) leads to the well-known *Cottrell equation*:

$$i(t) = \frac{nFAD_O C_O(b)}{(\pi D_O t)^{1/2}} \tag{1-11}$$

That is, the current decreases in proportion to the square root of time, with $(\pi D_O t)^{1/2}$ corresponding to the diffusion layer thickness.

Solving equation (1-8) (using Laplace transform techniques) yields the time evolution of the current of a spherical electrode:

$$i(t) = \frac{nFAD_O C_O(b)}{(\pi D_O t)^{1/2}} + \frac{nFAD_O C_O}{r} \tag{1-12}$$

The current response of a spherical electrode following a potential step thus contains time-dependent and time-independent terms, reflecting the planar and spherical diffusional fields, respectively (Figure 1-3), becoming time independent at long time scales. As expected from equation (1-12), the change from one regime to another is strongly dependent upon the radius of the electrode. The unique mass transport properties of ultramicroelectrodes (discussed in Section 4-5.4) are attributed to the shrinkage of the electrode radius.

1-2.1.2 Potential-Sweep Experiments Let us move to a voltammetric experiment involving a linear potential scan, the reduction of O to R and a quiescent solution. The slope of the concentration gradient is given by $(C_O(b, t) - C_O(0, t))/\delta$ where $C_O(b, t)$ and $C_O(0, t)$ are the bulk and surface concentrations of O. The change in the slope, and hence the resulting current, is due to changes of both $C_O(0, t)$ and δ. First, as the potential is scanned negatively, and approaches the standard potential (E°) of the couple, the surface concentration rapidly decreases in accordance to the Nernst equation (equation 1-2). For example, at a potential equal to E° the concentration ratio is unity $(C_O(0, t)/C_R(0, t) = 1)$. For a potential 59 mV more negative than E°, $C_R(0, t)$ is present at 10-fold excess $(C_O(0, t)/C_R(0, t) = 1/10, n = 1)$. The decrease in $C_O(0, t)$ is coupled with an increase in the diffusion layer thickness, which dominates the change in the slope after $C_O(0, t)$ approaches zero. The net result is a peak-shaped voltammogram. Such

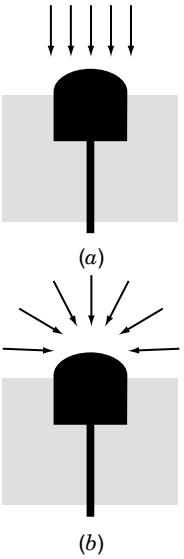

FIGURE 1-3 Planar (*a*) and spherical (*b*) diffusional fields at spherical electrodes.

current–potential curves and the corresponding concentration–distance profiles (for selected potentials along the scan) are shown in Figure 1-4. As will be discussed in Section 4-5.4, shrinking the electrode dimension to the micrometer domain results in a sigmoidal-shaped voltammetric response under quiescent conditions, characteristic of the different (radial) diffusional field and higher flux of electroactive species of ultramicroelectrodes.

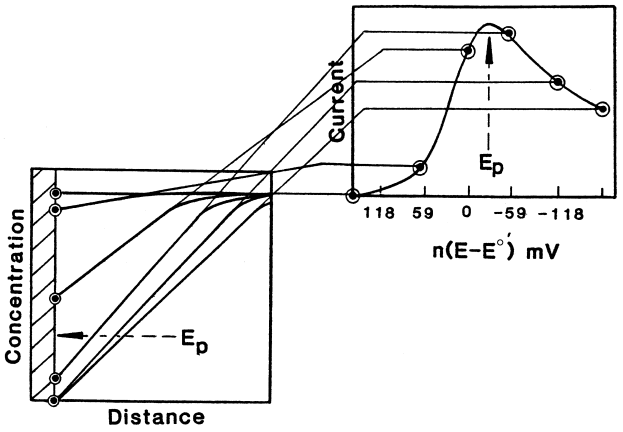

FIGURE 1-4 Concentration profiles (left) for different potentials during a linear sweep voltammetric experiment in unstirred solution. The resulting voltammogram is shown on the right, along with the points corresponding to each concentration gradient. (Reproduced with permission from reference 1.)

Let us see now what happens in a similar linear scan voltammetric experiment, but utilizing a stirred solution. Under these conditions, the bulk concentration ($C_O(b, t)$) is maintained at a distance δ by the stirring. It is not influenced by the surface electron transfer reaction (as long as the ratio of electrode area to solution volume is small). The slope of the concentration–distance profile $[(C_O(b, t) - C_O(0, t))/\delta]$ is thus determined solely by the change in the surface concentration ($C_O(0, t)$). Hence, the decrease in $C_O(0, t)$ during the potential scan (around E°) results in a sharp rise in the current. When a potential more negative than E° by 118 mV is reached, $C_O(0, t)$ approaches zero, and a limiting current (i_l) is achieved:

$$i_l = \frac{nFAD_O C_O(b, t)}{\delta} \tag{1-13}$$

The resulting voltammogram thus has a sigmoidal (wave) shape. If the stirring rate (U) is increased, the diffusion layer thickness becomes thinner, according to

$$\delta = \frac{B}{U^\alpha} \tag{1-14}$$

where B and α are constants for a given system. As a result, the concentration gradient becomes steeper (see Figure 1-5, curve b), thereby increasing the limiting current. Similar considerations apply to other forced convection systems, e.g., those relying on solution flow or electrode rotation (see Sections 3-6 and 4-5, respectively). For all of these hydrodynamic systems, the sensitivity of the measurement can be enhanced by increasing the convection rate.

Initially it was assumed that no solution movement occurs within the diffusion layer. Actually, a velocity gradient exists in a layer, termed the *hydrodynamic boundary layer* (or the *Prandtl layer*), where the fluid velocity increases from zero at the interface to the constant bulk value (U). The thickness of the hydrodynamic layer, δ_H, is related to that of the diffusion layer:

$$\delta \cong \left(\frac{D}{v}\right)^{1/3} \delta_H \tag{1-15}$$

where v is the kinematic viscosity. In aqueous media (with $v \simeq 10^{-2}$ cm^2 s^{-1} and $D \simeq 10^{-5}$ cm^2 s^{-1}), δ_H is $\sim$10-fold larger than δ, indicating negligible convection within the diffusion layer (Figure 1-6). The above discussion applies to other forced convection systems, such as flow detectors or rotating electrodes (see Sections 3-6 and 4-5, respectively). δ values of 10–50 μm and 100–150 μm are common for electrode rotation and solution stirring, respectively. Additional means for enhancing the mass transport and thinning the diffusion layer, including the use of power ultrasound, heated electrodes, or laser activation, are currently being studied (3,4a). These methods may simultaneously minimize surface fouling effects, as desired for retaining surface reactivity.

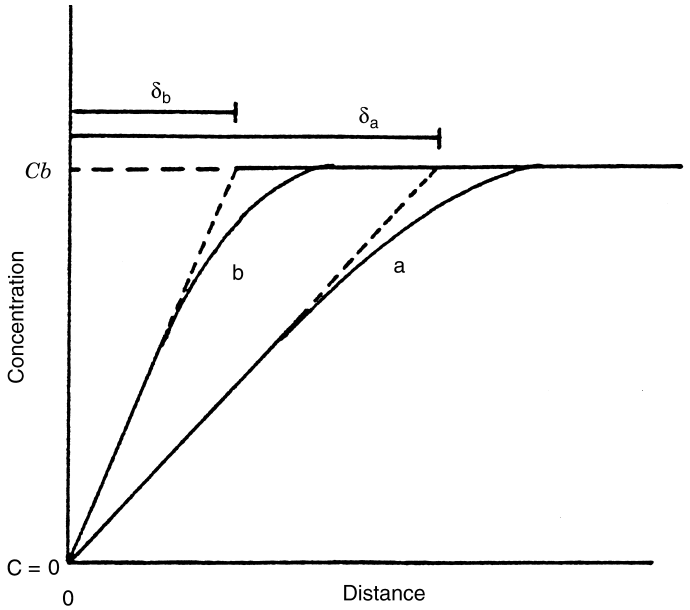

FIGURE 1-5 Concentration profiles for two rates of convection transport: low (curve a) and high (curve b).

1-2.2 Reactions Controlled by the Rate of Electron Transfer

In this section we consider experiments in which the current is controlled by the rate of electron transfer (i.e., reactions with sufficiently fast mass transport). The current–potential relationship for such reactions is different from those discussed (above) for mass transport-controlled reactions.

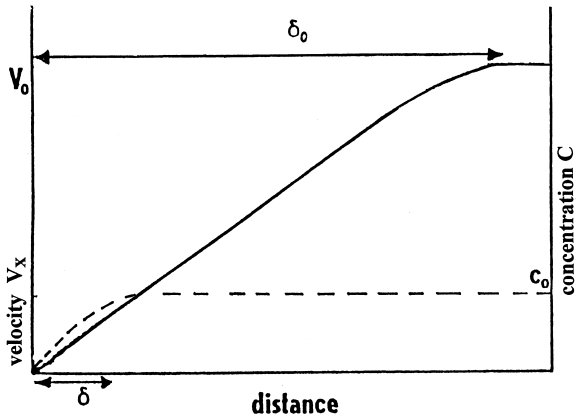

FIGURE 1-6 The hydrodynamic boundary (Prandtl) layer. Also shown (as dotted line), is the diffusion layer.

Consider again the electron-transfer reaction: $O + ne^- \rightleftharpoons R$; the actual electron transfer step involves transfer of the electron between the conduction band of the electrode and a molecular orbital of O or R (e.g., for a reduction, from the conduction band into an unoccupied orbital in O). The rate of the forward (reduction) reaction, V_f, is first order in O:

$$V_f = k_f C_O(0, t) \tag{1-16}$$

while that of the reversed (oxidation) reaction V_b, is first order in R:

$$V_b = k_b C_R(0, t) \tag{1-17}$$

where k_f and k_b are the forward and backward heterogeneous rate constants, respectively. These constants depend upon the operating potential according to the following exponential relationships:

$$k_f = k^\circ \exp[-\alpha nF(E - E^\circ)/RT] \tag{1-18}$$

$$k_b = k^\circ \exp[(1 - \alpha)nF(E - E^\circ)/RT] \tag{1-19}$$

where k° is the standard heterogeneous rate constant, and α is the transfer coefficient. The value of k° (in cm s^{-1}) reflects the reaction between the particular reactant and the electrode material used. The value of α (between zero and unity) reflects the symmetry of the free energy curve (with respect to the reactants and products). For symmetric curves, α will be close to 0.5; α is a measure of the fraction of energy that is put into the system that is actually used to lower the activation energy (see discussion in Section 1-2.2.1). Overall, equations (1-18) and (1-19) indicate that by changing the applied potential we influence k_f and k_b in an exponential fashion. Positive and negative potentials thus speed up the oxidation and reduction reactions, respectively. For an oxidation, the energy of the electrons in the donor orbital of R must be equal or higher than the energy of electrons in the electrode. For reduction, the energy of the electrons in the electrode must be higher than their energy in the receptor orbital of R.

Since the net reaction rate is

$$V_{net} = V_f - V_b = k_f C_O(0, t) - k_b C_R(0, t) \tag{1-20}$$

and as the forward and backward currents are proportional to V_f and V_b, respectively,

$$i_f = nFAV_f \tag{1-21}$$

$$i_b = nFAV_b \tag{1-22}$$

the overall current is given by the difference between the currents due to the forward and backward reactions:

$$i_{\text{net}} = i_f - i_b = nFA[k_f C_{\text{O}}(0, t) - k_b C_{\text{R}}(0, t)] \tag{1-23}$$

By substituting the expressions for k_f and k_b (equations 1-17 and 1-18), one obtains

$$\begin{aligned} i = nFAk^{\circ}\{&\text{C}_{\text{O}}(0, t) \exp[-\alpha nF(E - E^{\circ})/RT] \\ &- C_{\text{R}}(0, t) \exp[(1 - \alpha)nF(E - E^{\circ})/RT]\} \end{aligned} \tag{1-24}$$

which describes the current–potential relationship for reactions controlled by the rate of electron transfer. Note that the net current depends on both the operating potential and the surface concentration of each form of the redox couple. For example, Figure 1-7 displays the current–potential dependence for the case where $C_{\text{O}}(0, t) = C_{\text{R}}(0, t)$ and $\alpha = 0.50$. Large negative potentials accelerate the movement of charge in the cathodic direction, and also decelerate the charge movement in the opposite direction. As a result the anodic current component becomes negligible and the net current merges with the cathodic component. The acceleration and deceleration of the cathodic and anodic currents are not necessarily as symmetric as depicted in Figure 1-7, and would differ for α values different than 0.5. Similarly, no cathodic current contribution is observed at sufficiently large positive potentials.

When $E = E_{\text{eq}}$, no net current is flowing. This situation, however, is dynamic, with continuous movement of charge carriers in both directions, and equal opposing anodic and cathodic current components. The absolute magnitude of these compo-

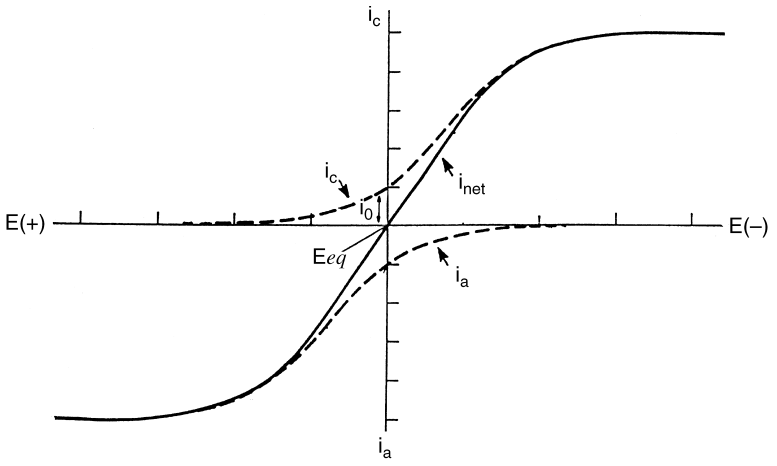

FIGURE 1-7 Current–potential curve for the system $\text{O} + ne^- \rightleftharpoons \text{R}$, assuming that electron-transfer is rate limiting, $C_{\text{O}} = C_{\text{R}}$, and $\alpha = 0.5$. The dotted lines show the cathodic (i_c) and anodic (i_a) components.

nents at E_{eq} is the *exchange current* (i_o) which is directly proportional to the standard rate constant:

$$i_o = i_c = i_a = nFAk^{\circ}C \tag{1-25}$$

where i_c and i_a are the cathodic and anodic components, respectively.

The exchange current density for common redox couples (at room temperature) can range from $10^{-6}\,\mu A\,cm^{-2}$ to $A\,cm^{-2}$. Equation (1-24) can be written in terms of the exchange current to give the *Butler–Volmer equation*:

$$i = i_0\{\exp(-\alpha nF\eta/RT) - \exp[(1-\alpha)nF\eta/RT]\} \tag{1-26}$$

where $\eta = E - E_{eq}$ is called the *overvoltage* (i.e., the extra potential beyond the equilibration potential leading to a net current i). The overvoltage is always defined with respect to a specific reaction, for which the equilibrium potential is known.

Equation (1-26) can be used for extracting information on i_0 and α, which are important kinetic parameters. For sufficiently large overvoltages ($\eta > 118\,mV/n$), one of the exponential terms in equation (1-26) will be negligible compared with the other. For example, at large negative overpotentials, $i_c \gg i_a$ and equation (1-26) becomes

$$i = i_0 \exp(-\alpha nF\eta/RT) \tag{1-27}$$

and hence we get

$$\ln i = \ln i_0 - \alpha nF\eta/RT \tag{1-28}$$

This logarithmic current–potential dependence was derived by Tafel, and is known as the *Tafel equation*. By plotting log i vs. η one obtains the Tafel plots for the cathodic and anodic branches of the current–overvoltage curve (Figure 1-8). Such plots are linear only at high values of overpotentials; severe deviations from linearity are observed as η approaches zero. Extrapolation of the linear portions of these plots to the zero overvoltage gives an intercept that corresponds to log i_0; the slope can be used to obtain the value of the transfer coefficient α. Another form of the Tafel equation is obtained by rearrangement of equation (1-28):

$$\eta = a - b \log i \tag{1-29}$$

with b, the Tafel slope, having the value of $2.303\,RT/\alpha nF$. For $\alpha = 0.5$ and $n = 1$, this corresponds to 118 mV (at 25 °C). Equation (1-29) indicates that the application of small potentials (beyond the equilibrium potential) can increase the current by many orders of magnitude. In practice, however, the current could not rise to an infinite value due to restrictions from the rate at which the reactant reaches the surface. (Recall that the rate-determining step depends upon the potential region.)

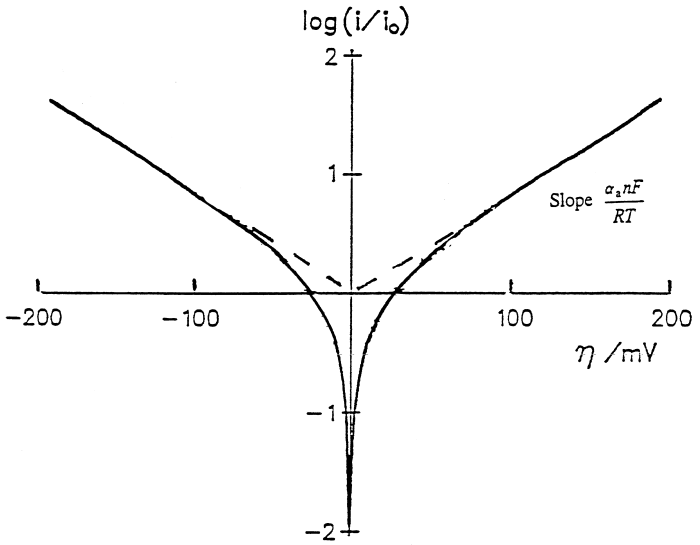

FIGURE 1-8 Tafel plots for the cathodic and anodic branches of the current–potential curve.

For small departures from E°, the exponential term in equation (1-27) may be linearized and the current is approximately proportional to η:

$$i = i_0\, nF\eta/RT \tag{1-30}$$

Hence, the net current is directly proportional to the overvoltage in a narrow potential range near E°.

Note also that when $i_{net} = 0$ (i.e., when $E = E_{eq}$) one can obtain the following from equation (1-24):

$$C_O(0, t)\exp[-\alpha nF(E_{eq} - E^\circ)/RT] = C_R(0, t)\exp[(1-\alpha)nF(E_{eq} - E^\circ)/RT] \tag{1-31}$$

Rearrangement of equation (1-31) yields the exponential form of the Nernst equation:

$$\frac{C_O(0, t)}{C_R(0, t)} = \exp[nF(E_{eq} - E^\circ)/RT] \tag{1-32}$$

expected for equilibrium conditions.

The equilibrium potential for a given reaction is related to the formal potential:

$$E_{eq} = E^\circ + (2.3RT/nF)\log Q \tag{1-33}$$

where Q is the equilibrium ratio function (i.e., ratio of the equilibrium concentrations).

1-2.2.1 Activated Complex Theory The effect of the operating potential upon the rate constants (equations 1-18 and 1-19) can be understood in terms of the free energy barrier. Figure 1-9 shows a typical Morse potential energy curve for the reaction: $O + ne^- \rightleftharpoons R$, at an inert metallic electrode (with O and R being soluble). Because of the somewhat different structures of O and R, there is a barrier to electron transfer (associated with changes in bond lengths and bond angles). In order for the transition from the oxidized form to occur, it is thus necessary to overcome the free energy of activation, $\Delta G^{\ddagger}$. The frequency with which the electron crosses the energy barrier as it moves from the electrode to O (i.e., the rate constant) is given by

$$k = Ae^{-\Delta G^{\ddagger}/RT} \tag{1-34}$$

Any alteration in $\Delta G^{\ddagger}$ will thus affect the rate of the reaction. If $\Delta G^{\ddagger}$ is increased, the reaction rate will decrease. At equilibrium, the cathodic and anodic activation energies are equal ($\Delta G^{\ddagger}_{c,0} = \Delta G^{\ddagger}_{a,0}$) and the probability of electron transfer is the

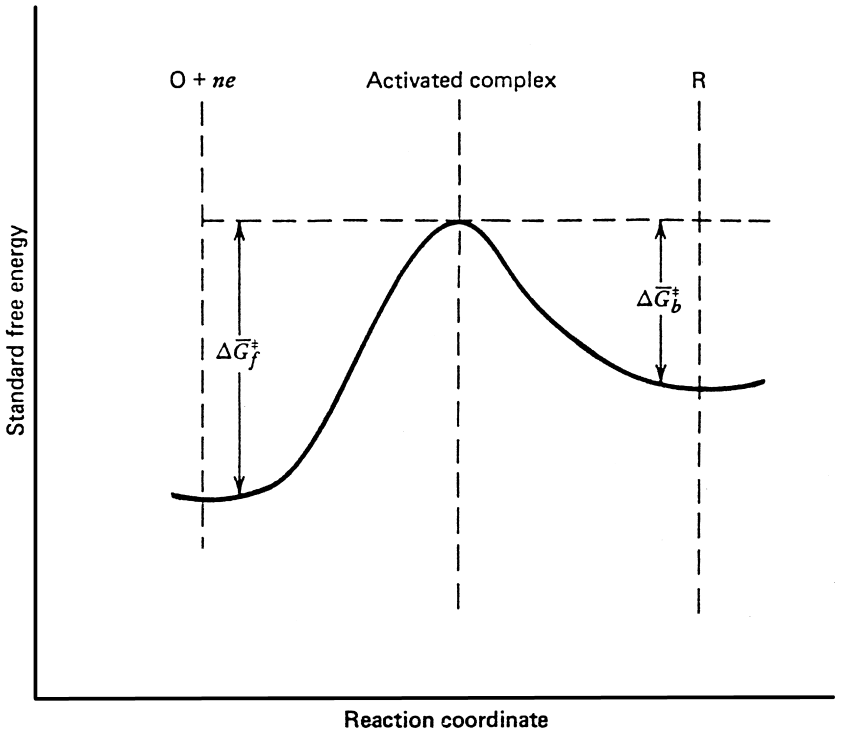

FIGURE 1-9 Free energy curve for a redox process at a potential more positive than the equilibrium value.

same in both directions. A, known as the *frequency factor*, is given as a simple function of the Boltzmann constant k' and the Planck constant, h:

$$A = \frac{k'T}{h} \tag{1-35}$$

Now let us discuss nonequilibirum situations. By varying the potential of the working electrode, we can influence the free energy of its resident electrons, thus making one reaction more favorable. For example, a potential shift E from the equilibrium value moves the $O + ne^-$ curve up or down by $\phi = -nFE$. The dotted line in Figure 1-10 displays such a change for the case of a positive E. Under this condition the barrier for reduction, $\Delta G_c^{\ddagger}$, is larger than $\Delta G_{c,0}^{\ddagger}$. A careful study of the new curve reveals that only a fraction (α) of the energy shift ϕ is actually used to increase the activation energy barrier, and hence to accelerate the rate of the reaction. Based on the symmetry of the two potential curves, this fraction (the transfer coefficient) can range from zero to unity. Measured values of α in aqueous solutions have ranged from 0.2 to 0.8. The term α is thus a measure of the symmetry of the activation energy barrier. An α value of 0.5 indicates that the activated complex is exactly halfway between the reagents and products on the reaction coordinate (i.e.,

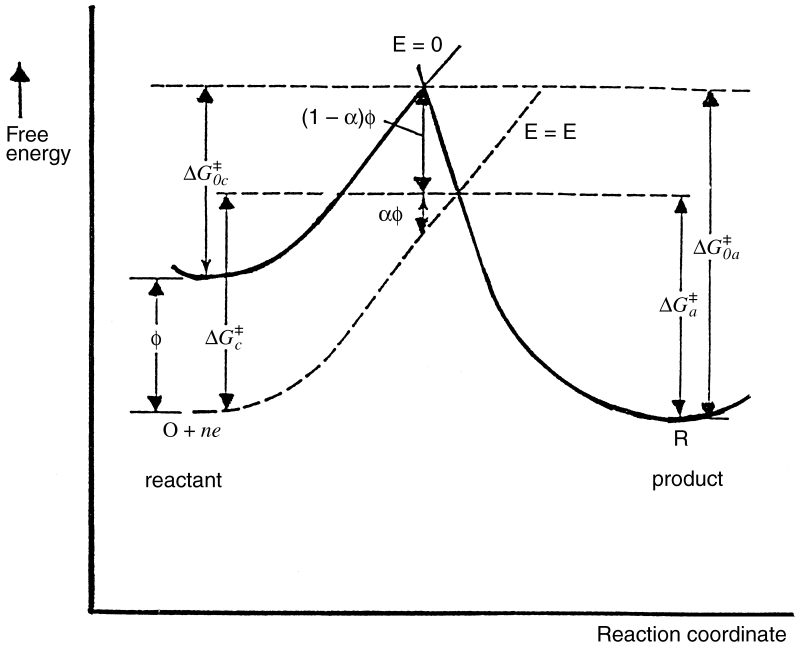

FIGURE 1-10 Effect of a change in the applied potential on the free energies of activation for reduction and oxidation.

an idealized curve). Values of α close to 0.5 are common for metallic electrodes with a simple electron transfer process. The barrier for reduction at E is thus given by

$$\Delta G_c^{\ddagger} = \Delta G_{c,0}^{\ddagger} + \alpha nFE \tag{1-36}$$

Similarly, examination of the figure reveals also that the new barrier for oxidation, $\Delta G_a^{\ddagger}$ is lower than $\Delta G_{a,0}^{\ddagger}$:

$$\Delta G_a^{\ddagger} = \Delta G_{a,0}^{\ddagger} - (1-\alpha)nFE \tag{1-37}$$

By substituting the expressions for $\Delta G^{\ddagger}$ (equations 1-36 and 1-37) in equation (1-34), we obtain for reduction

$$k_f = A \exp[-\Delta G_{c,0}^{\ddagger}/RT] \exp[-\alpha nFE/RT] \tag{1-38}$$

and for oxidation

$$k_b = A \exp[-\Delta G_{a,0}^{\ddagger}/RT] \exp[(1-\alpha)nFE/RT] \tag{1-39}$$

The first two factors in equations (1-38) and (1-39) are independent of the potential, and thus these equations can be rewritten as

$$k_f = k_f^{\circ} \exp[-\alpha nFE/RT] \tag{1-40}$$

$$k_b = k_b^{\circ} \exp[(1-\alpha)nFE/RT] \tag{1-41}$$

When the electrode is at equilibrium with the solution, and when the surface concentrations of O and R are the same, $E = E^{\circ}$, and k_f and k_b are equal:

$$k_f^{\circ} \exp[-\alpha nFE/RT] = k_b^{\circ} \exp[(1-\alpha)nFE/RT] = k^{\circ} \tag{1-42}$$

and correspond to the standard rate constant k°. By substituting for k_f° and k_b° (using equation 1-42) in equations (1-40) and (1-41), one obtains equations (1-18) and (1-19) (which describe the effect of the operating potential upon the rate constants).

1-3 THE ELECTRICAL DOUBLE LAYER

The *electrical double layer* is the array of charged particles and/or oriented dipoles that exists at every material interface. In electrochemistry, such a layer reflects the ionic zones formed in the solution to compensate for the excess of charge on the electrode (q_e). A positively charged electrode thus attracts a layer of negative ions (and vice versa). Since the interface must be neutral, $q_e + q_s = 0$ (where q_s is the charge of the ions in the nearby solution). Accordingly, such a counterlayer is made

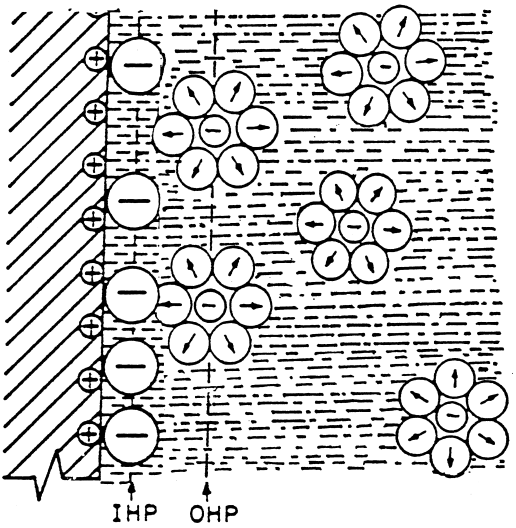

FIGURE 1-11 Schematic representation of the electrical double layer. IHP = inner Helmholtz plane; OHP = outer Helmoltz plane.

of ions of opposite sign to that of the electrode. As illustrated in Figure 1-11 the electrical double layer has a complex structure of several distinct parts.

The inner layer (closest to the electrode), known as the inner Helmholtz plane (IHP), contains solvent molecules and specifically adsorbed ions (which are not fully solvated). It is defined by the locus of points for the specifically adsorbed ions. The next layer, the outer Helmholtz plane (OHP), reflects the imaginary plane passing through the center of solvated ions at their closest approach to the surface. The solvated ions are nonspecifically adsorbed and are attracted to the surface by long-range coulombic forces. Both Helmholtz layers represent the *compact layer.* Such a compact layer of charges is strongly held by the electrode and can survive even when the electrode is pulled out of the solution. The Helmholtz model does not take into account the thermal motion of ions, which loosens them from the compact layer.

The outer layer (beyond the compact layer), referred to as the *diffuse layer* (or *Gouy layer*), is a three-dimensional region of scattered ions, which extends from the OHP into the bulk solution. Such an ionic distribution reflects the counterbalance between ordering forces of the electrical field and the disorder caused by a random thermal motion. Based on the equilibrium between these two opposing effects, the concentration of ionic species at a given distance from the surface, $C(x)$, decays exponentially with the ratio between the electrostatic energy ($zF\Phi$) and the thermal energy (RT), in accordance with the Boltzmann equation:

$$C(x) = C(0)\exp(-zF\Phi)/RT) \tag{1-43}$$

The total charge of the compact and diffuse layers equals (and is opposite in sign to) the net charge on the electrode side. The potential–distance profile across the double-

layer region involves two segments, with a linear increase up to the OHP and an exponential increase within the diffuse layer. These potential drops are displayed in Figure 1-12. Depending upon the ionic strength, the thickness of the double layer may extend to more than 10 nm.

The electrical double layer resembles an ordinary (parallel-plate) capacitor. For an ideal capacitor, the charge (q) is directly proportional to the potential difference:

$$q = CE \tag{1-44}$$

where C is the capacitance (in farads, F), the ratio of the charge stored to the applied potential. The potential–charge relationship for the electrical double layer is

$$q = C_{\text{dl}}A(E - E_{\text{pzc}}) \tag{1-45}$$

where C_{dl} is the capacitance per unit area and E_{pzc} is the potential of zero charge (i.e., where the sign of the electrode charge reverses and no net charge exists in the double layer). C_{dl} values are usually in the range 10–40 μF cm^{-2}.

The capacitance of the double layer consists of combination of the capacitance of the compact layer in series with that of the diffuse layer. For two capacitors in series, the total capacitance is given by

$$\frac{1}{C} = \frac{1}{C_H} + \frac{1}{C_G} \tag{1-46}$$

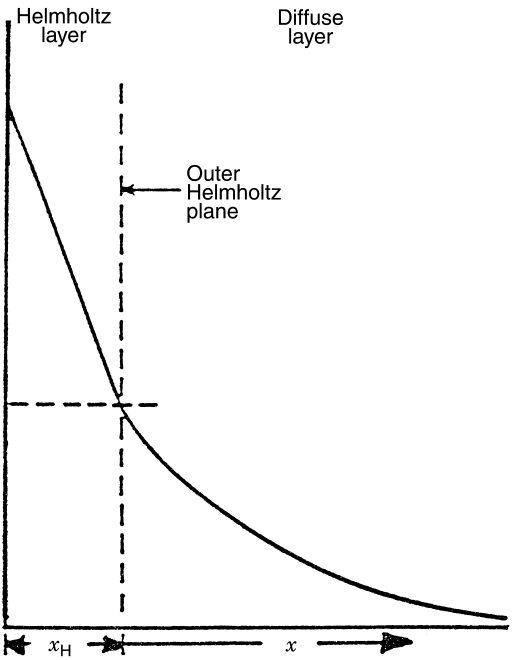

FIGURE 1-12 Variation of the potential across the electrical double layer.

where C_H and C_G represent that capacitance of the compact and diffuse layers, respectively. The smaller of these capacitances determines the observed behavior. By analogy with a parallel-plate (ideal) capacitor, C_H is given by

$$C_H = \frac{-\varepsilon}{4\pi d} \tag{1-47}$$

where d is the distance between the plates and ε the dielectric constant ($\varepsilon = 78$ for water at room temperature.) Accordingly, C_H increases with decreasing separation between the electrode surface and the counterionic layer, as well as with increasing dielectric constant of the intervening medium. The value of C_G is strongly affected by the electrolyte concentration; the compact layer is largely independent of the concentration. For example, at sufficiently high electrolyte concentration, most of the charge is confined near the Helmholz plane, and little is scattered diffusely into the solution (i.e., the diffuse double layer becomes small). Under these conditions, $1/C_H \gg 1/C_G$, $1/C \simeq 1/C_H$ or $C \simeq C_H$. In contrast, for dilute solutions, C_G is very small (compared to C_H) and $C \simeq C_G$.

Figure 1-13 displays the experimental dependence of the double-layer capacitance upon the applied potential and electrolyte concentration. As expected for the parallel-plate model, the capacitance is nearly independent of the potential or concentration over several hundreds of millivolts. Nevertheless, a sharp dip in the capacitance is observed (around -0.5 V; i.e., the E_{pzc}) with dilute solutions, reflecting the contribution of the diffuse layer. Comparison of the double layer with the parallel-plate capacitor is thus most appropriate at high electrolyte concentrations (i.e., when $C \simeq C_H$).

The charging of the double layer is responsible for the background (residual) current known as the charging current, which limits the detectability of controlled-potential techniques. Such a charging process is *nonfaradaic* because electrons are not transferred across the electrode–solution interface. It occurs when a potential is applied across the double layer, or when the electrode area or capacitances are changing. Note that the current is the time derivative of the charge. Hence, when such processes occur, a residual current flows based on the differential equation

$$i = \frac{dq}{dt} = C_{\text{dl}} A \frac{dE}{dt} + C_{\text{dl}}(E - E_{\text{pzc}}) \frac{dA}{dt} + A(E - E_{\text{pzc}}) \frac{dC_{\text{dl}}}{dt} \tag{1-48}$$

where dE/dt and dA/dt are the potential scan rate and rate of area change, respectively. The second term is applicable to the dropping mercury electrode (discussed in Section 4-2). The term dC_{dl}/dt is important when adsorption processes change the double-layer capacitance.

Alternately, for potential-step experiments (e.g., chronoamperometry, see Section 3-1), the charging current is the same as that obtained when a potential step is applied to a series RC circuit:

$$i_c = \frac{E}{R_S} e^{-t/RC_{\text{dl}}} \tag{1-49}$$

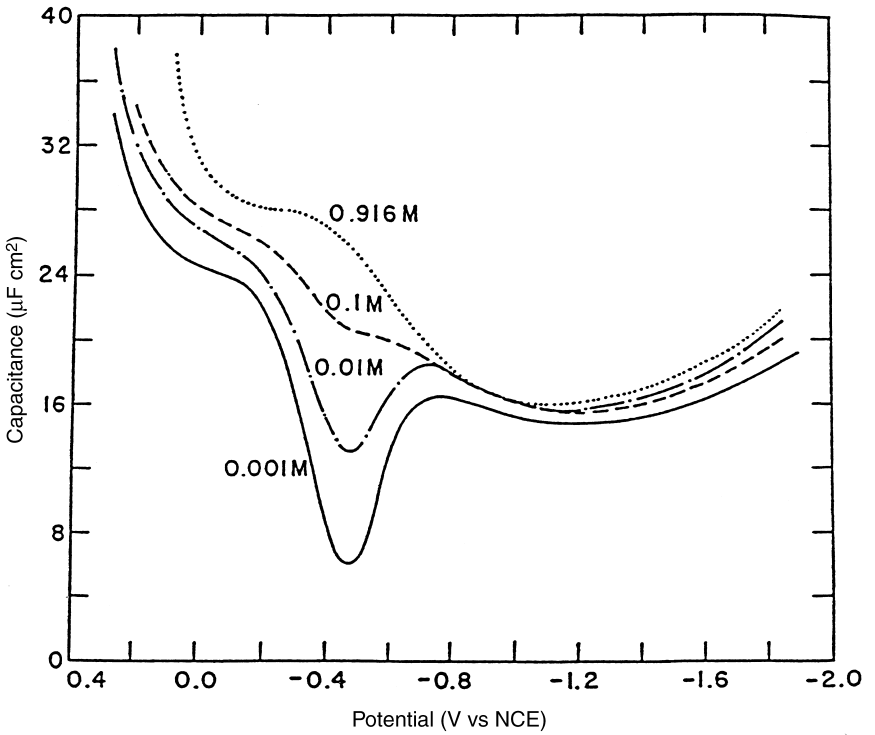

FIGURE 1-13 Double-layer capacitance of a mercury drop electrode in NaF solutions of different concentrations. (Reproduced with permission from reference 5.)

that is, the current decreases exponentially with time. E is the magnitude of the potential step, while R_S is the (uncompensated) solution resistance.

Equation (1-48) can be used for calculating the double-layer capacitance of solid electrodes. By recording linear scan voltammograms at different scan rates (using the supporting electrolyte solution), and plotting the charging current (at a given potential) versus the scan rate, one obtains a straight line with slope corresponding to $C_{\text{dl}}A$.

Measurements of the double-layer capacitance provide valuable insights into adsorption and desorption processes, as well as into the structure of film-modified electrodes (6).

Further discussion of the electrical double layer can be found in several reviews (5,7–11).

1-4 ELECTROCAPILLARY EFFECT

Electrocapillarity is the study of the interfacial tension as a function of the electrode potential. Such a study can provide useful insight into the structure and properties of

the electrical double layer. The influence of the electrode–solution potential difference upon the surface tension (γ) is particularly pronounced at nonrigid electrodes (such as the dropping mercury electrode discussed in Section 4-5). A plot of the surface tension versus the potential (like those shown in Figure 1-14), is called an *electrocapillary curve*.

The excess charge on the electrode can be obtained from the slope of the electrocapillary curve (at any potential), by the *Lippman equation*:

$$\left(\frac{\partial \gamma}{\partial E}\right)_{\text{const. pressure}} = q \tag{1-50}$$

The more highly charged the interface becomes, the more the charges repel each other, thereby decreasing the cohesive forces, lowering the surface tension, and flattening the mercury drop. The second differential of the electrocapillary plot gives directly the differential capacitance of the double layer:

$$\left(\frac{\partial^2 \gamma}{\partial E^2}\right) = -C_{\text{dl}} \tag{1-51}$$

Hence, the differential capacitance represents the slope of the plot of q vs. E.

An important point of the electrocapillary curve is its maximum. Such maximum value of γ, obtained when $q = 0$, corresponds to the potential of zero charge (E_{pzc}). The surface tension is a maximum because on the uncharged surface there is no repulsion between like charges. The charge on the electrode changes its sign after the

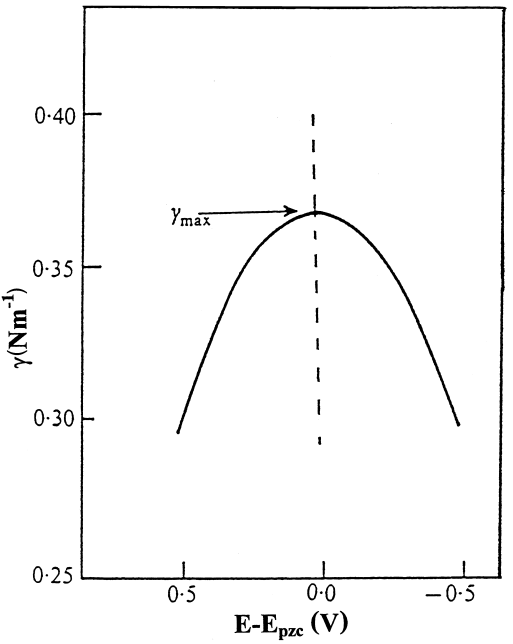

FIGURE 1-14 Electrocapillary curve (surface tension γ vs. potential).

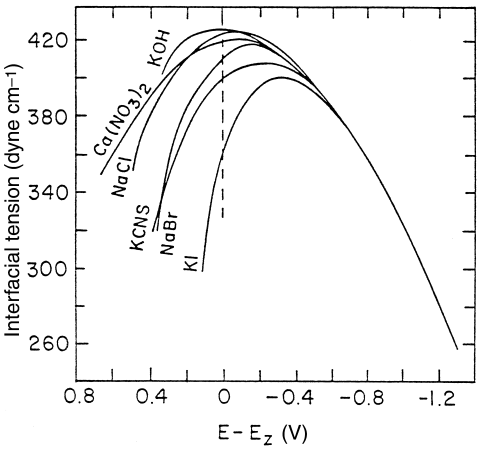

FIGURE 1-15 Electrocapillary curves for different electrolytes showing the relative strength of specific adsorption. (Reproduced with permission from reference 5.)

potential passes through the E_{pzc}. Experimental electrocapillary curves have a nearly parabolic shape around E_{pzc}. Such a parabolic shape corresponds to a linear change of the charge with the potential. The deviation from a parabolic shape depends on the solution composition, particularly on the nature of the anions present in the electrolyte. In particular, specific interaction of various anions (e.g., halides) with the

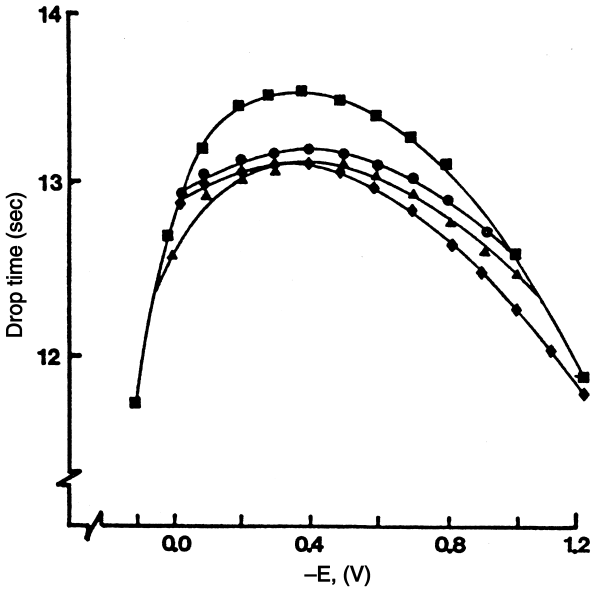

FIGURE 1-16 Electrocapillary curves of background (■), ethynylestradiol (●), β-estradiol (▲) and morgestrel (◆). (Reproduced with permission from reference 12.)

mercury surface, occurring at positive potentials, causes deviations from parabolic behavior (with shifts of E_{pzc} to more cathodic potentials). As shown in Figure 1-15, the change in the surface tension, and the negative shift in the E_{pzc}, increase in the order: $I^- > Br^- > CNS^- > NO_3^- > OH^-$. (These changes are expected from the strength of the specific adsorption.) Such ions can be specifically adsorbed because they are not solvated. Inorganic cations, in contrast, are less specifically adsorbed (because they are usually hydrated). Similarly, blockage of the surface by a neutral adsorbate often causes depressions in the surface tension in the vicinity of E_{pzc} (Figure 1-16). Note the reduced dependence of γ on the potential around this potential. At more positive or negative potentials, such adsorbates are displaced from the surface by oriented water molecules. The electrocapillary approach is not suitable for measuring the E_{pzc} of solid (i.e., rigid) electrodes.

SUPPLEMENTARY READING

Several international journals bring together papers and reviews covering innovations and trends in the field of electroanalytical chemistry:

Bioelectrochemistry and Bioenergetics
Biosensors and Bioelectronics
Electroanalysis
Electrochimica Acta
Journal of Applied Electrochemistry
Journal of Electroanalytical and Interfacial Electrochemistry
Journal of the Electrochemical Society
Langmuir
Sensors and Actuators

Useful information can be found in many prominent journals that cater to all branches of analytical chemistry including *The Analyst*, *Analytica Chimica Acta*, *Analytical Chemistry*, *Talanta*, *Analytical Letters*, and *Fresenius Zeitschrift für Analytical Chemie*. Biennial reviews published in the June issue of *Analytical Chemistry* offer comprehensive summaries of fundamental and practical research work.

Many textbooks and reference works dealing with various aspects of electroanalytical chemistry have been published in recent decades. Some of these are given below as suggestions for additional reading, in alphabetic order:

W.J. Albery, *Electrode Kinetics*, Clarendon Press, Oxford, 1975.

A.J. Bard and L. Faulkner, *Electrochemical Methods*, Wiley, New York, 1980.

J.M. Bockris and A. Reddy, *Modern Electrochemistry*, Vol. 1,2, Plenum Press, New York, 1970.

A.M. Bond, *Modern Polarographic Methods in Analytical Chemistry*, Dekker, New York, 1980.

C. Brett and A.M. Oliveira Brett, *Electrochemistry: Principles, Methods and Applications*, Oxford University Press, Oxford, 1993.

D. Diamond, *Chemical and Biological Sensors*, Wiley, New York, 1998.

E. Gileadi, *Electrode Kinetics*, VCH Publishers, New York, 1993.

P. Kissinger and W. Heineman, *Laboratory Techniques in Electroanalytical Chemistry*, (2nd ed.), Dekker, New York, 1996.

J. Janata, *Principles of Chemical Sensors*, Plenum Press, New York, 1989.

J. Koryta and J. Dvorak, *Principles of Electrochemistry*, Wiley, Chichester, 1987.

P. Rieger, *Electrochemistry*, Prentice-Hall, Englewood Cliffs, NJ, 1987.

D. Sawyer and J. Roberts, *Experimental Electrochemistry for Chemists*, Wiley, New York, 1974.

M. Smyth and J. Vos, *Analytical Voltammetry*, Elsevier, Amsterdam, 1992.

A.P. Turner, I. Karube and G. Wilson, *Biosensors*, Oxford University Press, Oxford, 1987.

J. Wang, *Electroanalytical Techniques in Clinical Chemistry and Laboratory Medicine*, VCH Publishers, New York, 1988.

REFERENCES

1. J.R. Maloy, *J. Chem. Educ.*, 60, 285 (1983).
2. M.G. Smith, *Laplace Transform Theory*, Van Nostrand, London, 1966.
3. R.G. Compton, J. Eklund, and F. Marken, *Electroanalysis*, 9, 509 (1997).
4. P. Grundler, and A. Kirbs, *Electroanalysis*, 11, 223 (1999).

4a. J. Alden, and R.G. Compton, *Anal. Chem*., 72, 198A (2000).

5. D. Grahame, *Chem. Rev.* 41, 441 (1947).
6. A. Swietlow, M. Skoog, and G. Johansson, *Electroanalysis*, 4, 921 (1992).
7. D.C. Grahame, *Annu. Rev. Phys. Chem.*, 6, 337 (1955).
8. D. Mohilner, *Electroanal. Chem.*, 1, 241 (1966).
9. O'M. Bockris, M.A. Devanathan, and K. Muller, *Proc. R. Soc.*, 55, A274 (1963).
10. R. Parsons, *J. Electrochem. Soc.*, 127, 176C (1980).
11. H.B. Mark, *Analyst* 115, 667 (1990).
12. A.M. Bond, I. Heritage, and M. Briggs, *Langmuir*, 1, 110 (1985).

Questions

1. Show or draw the concentration profile/gradient near the electrode surface during a linear scan voltammetric experiment in *stirred* a solution. (Use 5–6 potentials on both sides of E°.) Show also the resulting voltammogram, along with points for each concentration gradient (in a manner analogous to Figure 1-4).

2. Describe and draw clearly the structure of the electrical double layer (with its

several distinct parts).

3. Use the activated complex theory for explaining clearly how the applied potential affects the rate constant of an electron-transfer reaction. Draw free energy curves and use proper equations for your explanation.

4. Use equations to demonstrate how an increase of the stirring rate will effect the mass transport-controlled limiting current.

5. Derive the Nernst equation from the Butler–Volmer equation.

6. Explain clearly why polyanionic DNA molecules adsorb onto electrode surfaces at potentials more positive than E_{pzc}, and suggest a protocol for desorbing them back to the solution.

7. Which experimental conditions assure that the movement of the electroactive species is limited by diffusion? How do these conditions suppress the migration and convection effects?

8. Explain clearly the reason for the peaked response of linear sweep voltammetric experiments involving a planar macrodisk electrode and a quiescent solution.

9. The net current flowing at the equilibrium potential is zero, yet this is a dynamic situation with equal opposing cathodic and anodic current components (whose absolute value is i_0). Suggest an experimental route for estimating the value of i_0.

10. Explain clearly why only a fraction of the energy shift (associated with a potential shift) is used for increasing the activation energy barrier.

Analytical Electrochemistry, Second Edition. Joseph Wang

ISBNs: 0-471-28272-3 (Hardback); 0-471-22823-0 (Electronic)

CHAPTER 2

STUDY OF ELECTRODE REACTIONS

2-1 CYCLIC VOLTAMMETRY

Cyclic voltammetry is the most widely used technique for acquiring qualitative information about electrochemical reactions. The power of cyclic voltammetry results from its ability to rapidly provide considerable information on the thermodynamics of redox processes, on the kinetics of heterogeneous electron-transfer reactions, and on coupled chemical reactions or adsorption processes. Cyclic voltammetry is often the first experiment performed in an electroanalytical study. In particular, it offers a rapid location of redox potentials of the electroactive species, and convenient evaluation of the effect of media upon the redox process.

Cyclic voltammetry consists of scanning linearly the potential of a stationary working electrode (in an unstirred solution) using a triangular potential waveform (Figure 2-1). Depending on the information sought, single or multiple cycles can be used. During the potential sweep, the potentiostat measures the current resulting from the applied potential. The resulting plot of current versus potential is termed a *cyclic voltammogram*. The cyclic voltammogram is a complicated, time-dependent function of a large number of physical and chemical parameters.

Figure 2-2 illustrates the expected response of a reversible redox couple during a single potential cycle. It is assumed that only the oxidized form O is present initially. Thus, a negative-going potential scan is chosen for the first half-cycle, starting from a value where no reduction occurs. As the applied potential approaches the characteristic E° for the redox process, a cathodic current begins to increase, until a peak is reached. After traversing the potential region in which the reduction process takes place (at least $90/n$ mV beyond the peak), the direction of the potential

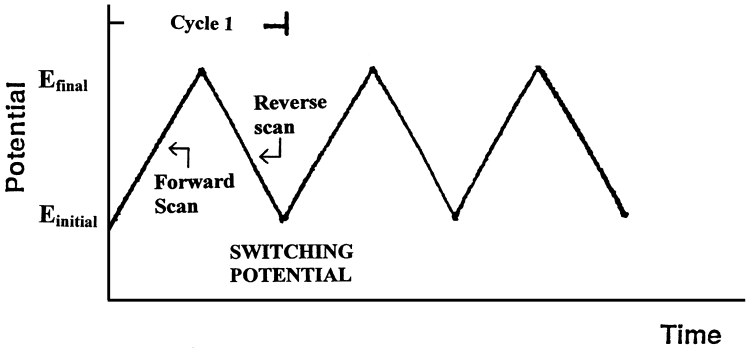

FIGURE 2-1 Potential–time excitation signal in cyclic voltammetric experiment.

sweep is reversed. During the reverse scan, R molecules (generated in the forward half cycle, and accumulated near the surface) are reoxidized back to O and an anodic peak results.

The characteristic peaks in the cyclic voltammogram are caused by the formation of the diffusion layer near the electrode surface. These can best be understood by carefully examining the concentration–distance profiles during the potential sweep (see Section 1-2.1.2). For example, Figure 2-3 illustrates four concentration gradients for the reactant and product at different times corresponding to (*a*) the initial potential value, (*b*) and (*d*) the formal potential of the couple (during the forward and reversed scans, respectively), and (*c*) to the achievement of a zero reactant surface concentration. Note that the continuous change in the surface concentration is coupled with an expansion of the diffusion layer thickness (as

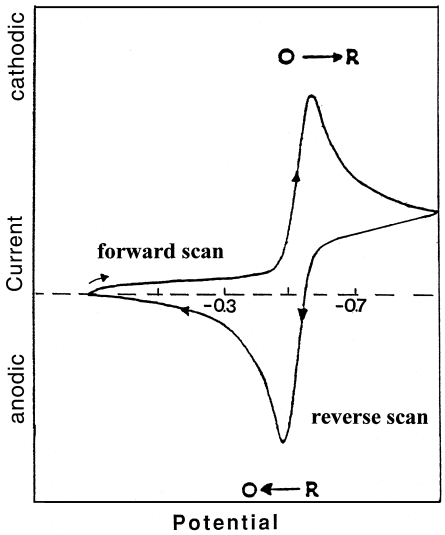

FIGURE 2-2 Typical cyclic voltammogram for a reversible $O + ne^- \rightleftharpoons R$ redox process.

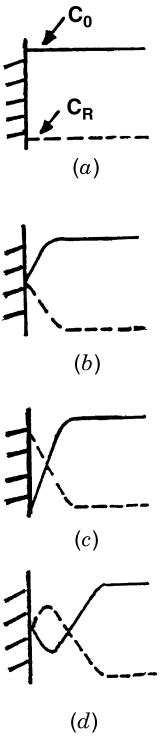

FIGURE 2-3 Concentration distribution of the oxidized and reduced forms of the redox couple at different times during a cyclic voltammetric experiment corresponding to the initial potential (*a*), to the formal potential of the couple during the forward and reversed scans (*b*, *d*), and to the achievement of a zero reactant surface concentration (*c*).

expected in quiescent solutions). The resulting current peaks thus reflect the continuous change of the concentration gradient with the time. Hence, the increase to the peak current corresponds to the achievement of diffusion control, while the current drop (beyond the peak) exhibits a $t^{-1/2}$ dependence (independent of the applied potential). For the above reasons, the reversal current has the same shape as the forward one. As will be discussed in Chapter 4, the use of ultramicroelectrodes—for which the mass transport process is dominated by radial (rather than linear) diffusion—results in a sigmoidal-shaped cyclic voltammogram.

2-1.1 Data Interpretation

The cyclic voltammogram is characterized by several important parameters. Four of these observables, the two peak currents and two peak potentials, provide the basis for the diagnostics developed by Nicholson and Shain (1) for analyzing the cyclic voltammetric response.

2-1.1.1 Reversible Systems The peak current for a reversible couple (at 25°C), is given by the *Randles–Sevcik equation*:

$$i_p = (2.69 \times 10^5)\, n^{3/2} A C D^{1/2}\, v^{1/2} \tag{2-1}$$

where n is the number of electrons, A is the electrode area (in cm^2), C is the concentration (in mol cm^{-3}), D is the diffusion coefficient (in $cm^2\ s^{-1}$), and v is the scan rate (in V s^{-1}). Accordingly, the current is directly proportional to concentration and increases with the square root of the scan rate. The ratio of the reverse-to-forward peak currents, $i_{p,r}/i_{p,f}$, is unity for a simple reversible couple. As will be discussed in the following sections, this peak ratio can be strongly affected by chemical reactions coupled to the redox process. The current peaks are commonly measured by extrapolating the preceding baseline current.

The position of the peaks on the potential axis (E_p) is related to the formal potential of the redox process. The formal potential for a reversible couple is centered between $E_{p,a}$ and $E_{p,c}$:

$$E^\circ = \frac{E_{p,a} + E_{p,c}}{2} \tag{2-2}$$

The separation between the peak potentials (for a reversible couple) is given by

$$\Delta E_p = E_{p,a} - E_{p,c} = \frac{0.059}{n} \quad \text{V} \tag{2-3}$$

Thus, the peak separation can be used to determine the number of electrons transferred, and as a criterion for a Nernstian behavior. Accordingly, a fast one-electron process exhibits a ΔE_p of about 59 mV. Both the cathodic and anodic peak potentials are independent of the scan rate. It is possible to relate the half-peak potential ($E_{p/2}$, where the current is half of the peak current) to the polarographic half-wave potential, $E_{1/2}$:

$$E_{p/2} = E_{1/2} \pm \frac{0.028}{n} \quad \text{V} \tag{2-4}$$

(The sign is positive for a reduction process.)

For multielectron-transfer (reversible) processes, the cyclic voltammogram consists of several distinct peaks if the E° values for the individual steps are successively higher and are well separated. An example of such a mechanism is the six-step reduction of the fullerenes C_{60} and C_{70} to yield the hexaanion products C_{60}^{6-} and C_{70}^{6-}. Such six successive reduction peaks are observed in Figure 2-4.

The situation is very different when the redox reaction is slow or coupled with a chemical reaction. Indeed, it is these "nonideal" processes that are usually of greatest chemical interest and for which the diagnostic power of cyclic voltammetry is most useful. Such information is usually obtained by comparing the experimental

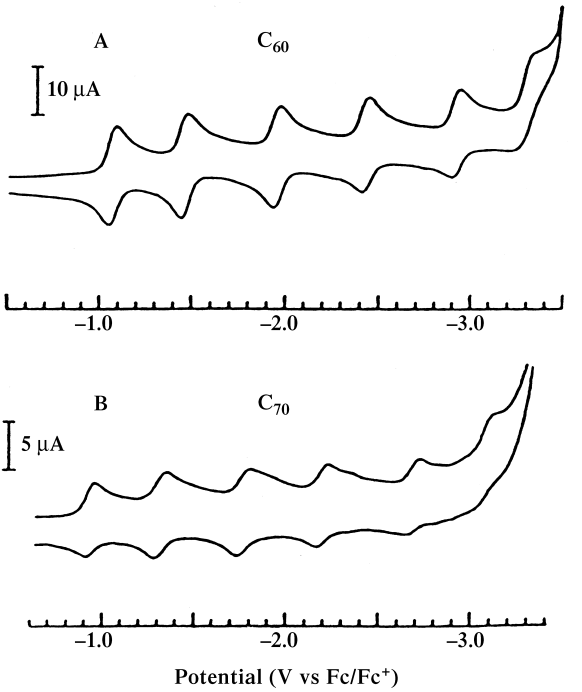

FIGURE 2-4 Cyclic voltammetry of C_{60} and C_{70} in an acetonitrile–toluene solution. (Reproduced with permission from reference 2.)

voltammograms with those derived from theoretical (simulated) ones (1). Proper compensation of the ohmic drop (see Section 4-4) is crucial for such diagnostic applications of cyclic voltammetry.

2-1.1.2 Irreversible and Quasi-Reversible Systems For irreversible processes (those with sluggish electron exchange), the individual peaks are reduced in size and widely separated (Figure 2-5, curve A). Totally irreversible systems are characterized by a shift of the peak potential with the scan rate:

$$E_p = E^\circ - \frac{RT}{\alpha n_a F}\left[0.78 - \ln\frac{k^\circ}{D^{1/2}} + \ln\left(\frac{\alpha n_a F v}{RT}\right)^{1/2}\right] \tag{2-5}$$

where α is the transfer coefficient and n_a is the number of electrons involved in the charge-transfer step. Thus, E_p occurs at potentials higher than E°, with the overpotential related to k° and α. Independent of the value k°, such peak displacement can be compensated by an appropriate change of the scan rate. The peak potential and the half-peak potential (at 25°C) will differ by $48/\alpha n$ mV. Hence, the voltammogram becomes more drawn-out as αn decreases.

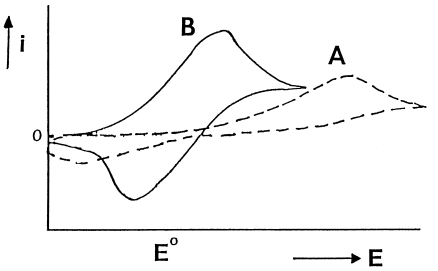

FIGURE 2-5 Cyclic voltammograms for irreversible (curve A) and quasi-reversible (curve B) redox processes.

The peak current, given by

$$i_p = (2.99 \times 10^5)n(\alpha n_a)^{1/2}ACD^{1/2}v^{1/2} \tag{2-6}$$

is still proportional to the bulk concentration, but will be lower in height (depending upon the value of α). Assuming a value of 0.5, the ratio of the reversible-to-irreversible current peaks is 1.27 (i.e., the peak current for the irreversible process is about 80% of the peak for a reversible one).

For quasi-reversible systems (with $10^{-1} > k^\circ > 10^{-5}$ cm s^{-1}) the current is controlled by both the charge transfer and mass transport. The shape of the cyclic voltammogram is a function of $k^\circ/\sqrt{\pi aD}$ (where $a = nFv/RT$). As $k^\circ/\sqrt{\pi aD}$ increases, the process approaches the reversible case. For small values of $k^\circ/\sqrt{\pi aD}$ (i.e., at very fast v) the system exhibits an irreversible behavior. Overall, the voltammograms of a quasi-reversible system are more drawn-out and exhibit a larger separation in peak potentials compared to those of a reversible system (Figure 2-5, curve B).

2-1.2 Study of Reaction Mechanisms

One of the most important applications of cyclic voltammetry is for qualitative diagnosis of chemical reactions that precede or succeed the redox process (1). Such reaction mechanisms are commonly classified by using the letters E and C (for the redox and chemical steps, respectively) in the order of the steps in the reaction scheme. The occurrence of such chemical reactions, which directly affect the available surface concentration of the electroactive species, is common to redox processes of many important organic and inorganic compounds. Changes in the shape of the cyclic voltammogram, resulting from the chemical competition for the electrochemical reactant or product, can be extremely useful for elucidating these reaction pathways and for providing reliable chemical information about reactive intermediates.

For example, when the redox system is perturbed by a following chemical reaction, that is, an EC mechanism,

$$O + ne^- \rightleftharpoons R \rightarrow Z \tag{2-7}$$

the cyclic voltammogram will exhibit a smaller reverse peak (because the product R is chemically removed from the surface). The peak ratio $i_{p,r}/i_{p,f}$ will thus be smaller than unity; the exact value of the peak ratio can be used to estimated the rate constant of the chemical step. In the extreme case, the chemical reaction may be so fast that all of R will be converted to Z, and no reverse peak will be observed. A classic example of such an EC mechanism is the oxidation of the drug chlorpromazine to form a radical cation that reacts with water to give an electroinactive sulfoxide. Ligand exchange reactions (e.g., of iron porphyrin complexes) occurring after electron transfer represent another example of such a mechanism.

Additional information on the rates of these (and other) coupled chemical reactions can be achieved by changing the scan rate (i.e., adjusting the experimental time scale). In particular, the scan rate controls the time spent between the switching potential and the peak potential (during which the chemical reaction occurs). Hence, as illustrated in Figure 2-6, i is the ratio of the rate constant (of the chemical step) to the scan rate, which controls the peak ratio. Most useful information is obtained when the reaction time lies within the experimental time scale. For scan rates between 0.02 and 200 V s^{-1} (common with conventional electrodes), the accessible

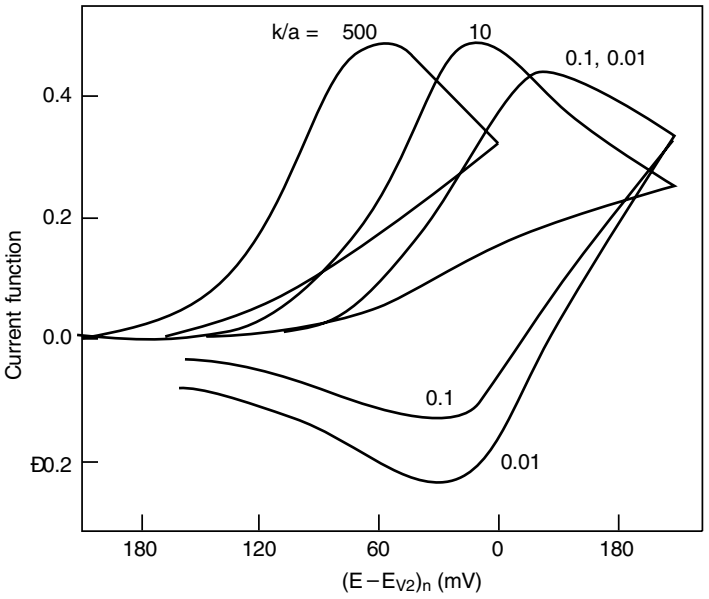

FIGURE 2-6 Cyclic voltammograms for a reversible electron transfer followed by an irreversible step for various ratios of chemical rate constant to scan rate, k/a, where $a = nFv/RT$. (Reproduced with permission from reference 1.)

time scale is around 0.1–1000 ms. Ultramicroelectrodes (discussed in Section 4-5.4) offer the use of much faster scan rates and hence the possibility of shifting the upper limit of follow-up rate constants measurable by cyclic voltammetry (3). For example, highly reactive species generated by the electron transfer, and living for 25 ns can be detected using a scan rate of 10^6 V s^{-1}. A wide variety of fast reactions (including isomerization and dimerization) can thus be probed. The extraction of such information commonly requires background subtraction to correct for the large charging current contribution associated with ultrafast scan rates.

A special case of the EC mechanism is the catalytic regeneration of O during the chemical step:

$$O + ne^- \rightleftharpoons R \tag{2-8}$$

$$R + A \rightleftharpoons O \tag{2-9}$$

An example of such a catalytic EC process is the oxidation of dopamine in the presence of ascorbic acid (4). The dopamine quinone formed in the redox step is reduced back to dopamine by the ascorbate ion. The peak ratio for such a catalytic reaction is always unity.

Other reaction mechanisms can be elucidated in a similar fashion. For example, for a CE mechanism, where a slow chemical reaction precedes the electron transfer, the ratio of $i_{p,r}/i_{p,f}$ is generally larger than unity, and approaches unity as the scan rate decreases. The reverse peak is usually not affected by the coupled reaction, while the forward peak is no longer proportional to the square root of the scan rate.

ECE processes, with a chemical step being interposed between electron transfer steps,

$$O_1 + ne^- \rightleftharpoons R_1 \rightarrow O_2 + ne^- \rightarrow R_2 \tag{2-10}$$

are also easily explored by cyclic voltammetry, because the two redox couples can be observed separately. The rate constant of the chemical step can thus be estimated from the relative sizes of the two cyclic voltammetric peaks.

Many anodic oxidations involve an ECE pathway. For example, the neurotransmitter epinephrine can be oxidized to its quinone, which proceeds via cyclization to leukoadrenochrome. The latter can rapidly undergo electron transfer to form adrenochrome (5). The electrochemical oxidation of aniline is another classical example of an ECE pathway (6). The cation radical thus formed rapidly undergoes a dimerization reaction to yield an easily oxidized *p*-aminodiphenylamine product. Another example (of industrial relevance) is the reductive coupling of activated olefins to yield a radical anion, which reacts with the parent olefin to give a reducible dimer (7). If the chemical step is very fast (in comparison to the electron-transfer process), the system will behave as an EE mechanism (of two successive charge-transfer steps). Table 2-1 summarizes common electrochemical mechanisms involving coupled chemical reactions. Powerful cyclic voltammetric computational simulators, exploring the behavior of virtually any user-specific mechanism, have

TABLE 2-1 Electrochemical Mechanisms Involving Coupled Chemical Reactions

1. Reversible electron transfer, no chemical complications:

$$O + ne^- \rightleftharpoons R$$

2. Reversible electron transfer followed by a reversible chemical reaction, E_rC_r mechanism:

$$O + ne^- \rightleftharpoons R$$
$$R \underset{k_{-1}}{\overset{k_1}{\longleftrightarrow}} Z$$

3. Reversible electron transfer followed by an irreversible chemical reaction, E_rC_i mechanism:

$$O + ne^- \rightleftharpoons R$$
$$R \xrightarrow{k} Z$$

4. Reversible chemical reaction preceding a reversible electron transfer, C_rE_r mechanism:

$$Z \underset{k_{-1}}{\overset{k_1}{\longleftrightarrow}} O$$
$$O + ne^- \rightleftharpoons R$$

5. Reversible chemical reaction preceding an irreversible electron transfer, C_rE_i mechanism:

$$Z \underset{k_{-1}}{\overset{k_1}{\longleftrightarrow}} O$$
$$O + ne^- \rightleftharpoons R$$

6. Reversible electron transfer followed by an irreversible regeneration of starting materials, catalytic mechanism:

$$O + ne^- \rightleftharpoons R$$
$$R + Z \xrightarrow{k} O$$

7. Irreversible electron transfer followed by an irreversible regeneration of starting material:

$$O + ne^- \rightleftharpoons R$$
$$R + Z \xrightarrow{k} O$$

8. Multiple electron transfer with intervening chemical reaction—ECE mechanism

$$O + n_1e^- \rightleftharpoons R \qquad R \rightleftharpoons Y$$
$$Y + n_2e^- \rightleftharpoons Z$$

Adapted with permission from reference 88.

been developed (9). Such simulated voltammograms can be compared with and fitted to the experimental ones. The new software also provides movie-like presentations of the corresponding continuous changes in the concentration profiles.

2-1.3 Study of Adsorption Processes

Cyclic voltammetry can also be used for evaluating the interfacial behavior of electroactive compounds. Both the reactant and the product can be involved in an

adsorption–desorption process. Such interfacial behavior can occur in studies of numerous organic compounds, as well as of metal complexes (if the ligand is specifically adsorbed). For example, Figure 2-7 illustrates repetitive cyclic voltammograms, at the hanging mercury drop electrode, for riboflavin in a sodium hydroxide solution. A gradual increase of the cathodic and anodic peak currents is observed, indicating progressive adsorptive accumulation at the surface. Note also that the separation between the peak potentials is smaller than expected for solution-phase processes. Indeed, ideal Nernstian behavior of surface-confined nonreacting species is manifested by symmetrical cyclic voltammetric peaks ($\Delta E_p = 0$), and a peak half-width of $90.6/n$ mV (Figure 2-8). The peak current is directly proportional to the surface coverage (Γ) and potential scan rate:

$$i_p = \frac{n^2F^2\Gamma Av}{4RT} \tag{2-11}$$

Recall that Nernstian behavior of diffusing species yields a $v^{1/2}$ dependence. In practice, the ideal behavior is approached for relatively slow scan rates, and for an adsorbed layer that shows no intermolecular interactions and fast electron transfers.

The peak area at saturation (i.e., the quantity of charge consumed during the reduction or adsorption of the adsorbed layer) can be used to calculate the surface coverage:

$$Q = nFA\Gamma \tag{2-12}$$

This can be used for calculating the area occupied by the adsorbed molecule and hence to predict its orientation on the surface. The surface coverage is commonly

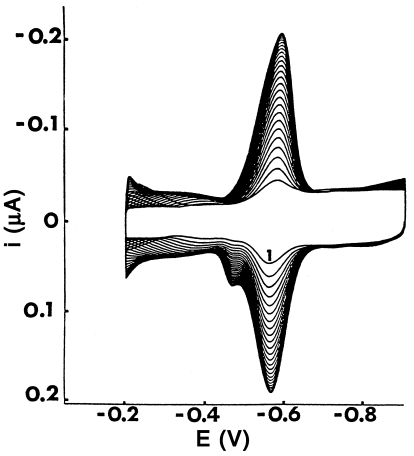

FIGURE 2-7 Repetitive cyclic voltammograms for 1×10^{-6} M riboflavin in a 1 mM sodium hydroxide solution. (Reproduced with permission from reference 10.)

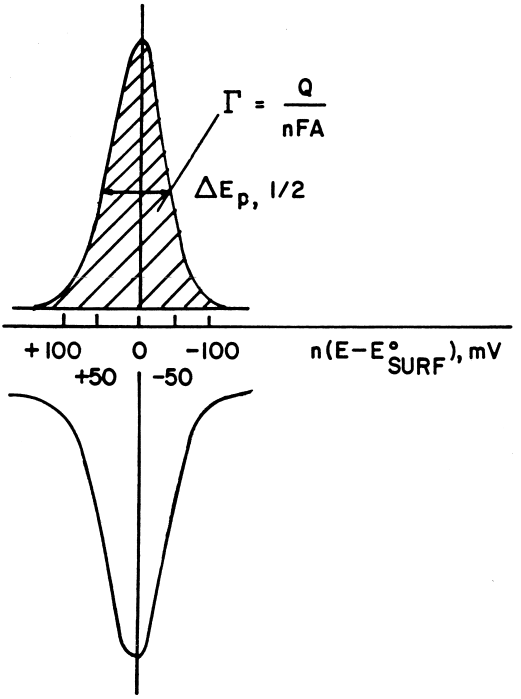

FIGURE 2-8 Ideal cyclic voltammetric behavior for a surface layer on an electrode. The surface coverage, Γ, can be obtained from the area under the peak. (Reproduced with permission from reference 11.)

related to the bulk concentration via the adsorption isotherm. One of the most frequently used at present is the *Langmuir isotherm*:

$$\Gamma = \Gamma_m \left(\frac{BC}{1 + BC} \right) \tag{2-13}$$

where Γ_m is the surface concentration corresponding to a monolayer coverage (mol cm^{-2}), and B is the adsorption coefficient. A linearized isotherm, $\Gamma = \Gamma_m BC$, is obtained for low adsorbate concentrations (i.e., when $1 \gg BC$). The Langmuir isotherm is applicable to a monolayer coverage and assumes that there are no interactions between adsorbed species. Other isotherms (e.g., those of Frumkin or Temkin) take such interactions into account. Indeed, the Langmuir isotherm is a special case of the Frumkin isotherm when there are no interactions.

When either the reactant (O) or product (R) is adsorbed (but not both), one expects to observe a postpeak or prepeak, respectively (at potentials more negative or positive than the diffusion-controlled peak).

Equations have been derived for less ideal situations, involving quasi-reversible and irreversible adsorbing electroactive molecules and different strengths of adsorption

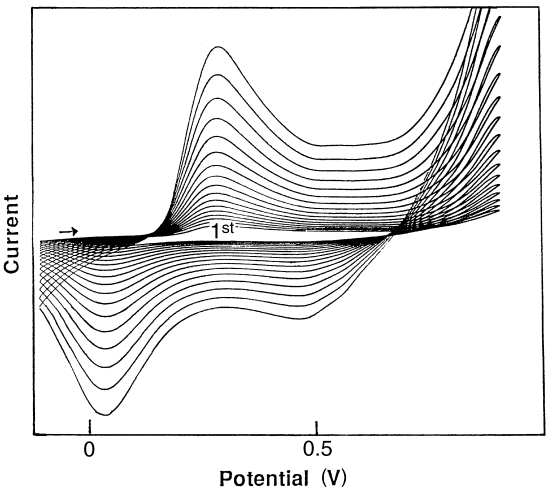

FIGURE 2-9 Repetitive cyclic voltammograms illustrating the continuous growth of polyaniline on a platinum surface.

of the reactant and product (11–14). The rates of fast adsorption processes can be characterized by high-speed cyclic voltammetry at ultramicroelectrodes (15).

Two general models can describe the kinetics of adsorption. The first involves fast adsorption with mass transport control, while the other involves kinetic control of the system. Under the latter (and Langmuirian) conditions, the surface coverage of the adsorbate at time t, Γ_t, is given by.

$$\Gamma_t = \Gamma_e\left[1 - \exp(-k'C_t t)\right] \tag{2-14}$$

where Γ_e is the surface coverage and k' is the adsorption rate constant.

The behavior and performance of chemically modified electrodes based on surface-confined redox modifiers and conducting polymers (Chapter 4) can also be investigated by cyclic voltammetry, in a manner similar to that for adsorbed species. For example, Figure 2-9 illustrates the use of cyclic voltammetry for in-situ probing of the growth of an electropolymerized film. Changes in the cyclic voltammetric response of a redox marker (e.g., ferrocyanide) are commonly employed for probing the blocking/barrier properties of insulating films (such as self-assembled monolayers).

2-1.4 Quantitative Applications

Cyclic voltammetry can also be useful for quantitative purposes, based on measurements of the peak current (equation 2-1). Such quantitative applications require the establishment of the proper baseline. For neighboring peaks (of a mixture), the baseline for the second peak is obtained by extrapolating the current decay of the

first one (in accordance with $t^{-1/2}$). Background reactions, primarily those associated with the double-layer charging and redox-surface processes, limit the detection limit to around the 1×10^{-5} M level. Background-subtracted cyclic voltammetry can be employed for measuring lower concentrations (16). In particular, fast-scan ($1000\ \mathrm{V\ s^{-1}}$) background-subtracted cyclic voltammetry is seeing increased use for the in-vivo monitoring of neurotransmitters (such as dopamine or serotonin) in the brain. Such coupling of digital background subtraction and fast voltammetric measurements provides the subsecond temporal resolution necessary for detecting dynamic concentration changes in the micromolar range occurring in the extracellular environment of the brain. The good temporal and chemical resolution of such in-vivo cyclic voltammetric experiments offers improved understanding of the chemistry of the brain. These repetitive scanning in-vivo experiments generate large quantities of data that are best represented as three-dimensional (potential, current, time) color contour images (17). For example, the temporal release of dopamine following electrical stimulation is evidenced from the rapid increase in color around its peak potential. The ultrafast scanning also eliminates interferences from adsorption processes and chemical reactions that are coupled to the primary oxidation reaction of catecholamine neurotransmitters (18):

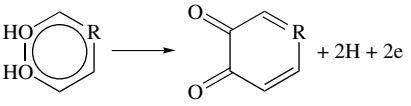

(2-15)

For more detailed information on the theory of cyclic voltammetry, and the interpretation of cyclic voltammograms, see references (1,7,19,20).

2-2 SPECTROELECTROCHEMISTRY

The coupling of optical and electrochemical methods—*spectroelectrochemistry*—has been employed for over two decades to investigate a wide variety of inorganic, organic, and biological redox systems (21,22). Such a combination of electrochemical perturbations with the molecular specificity of optical monitoring successfully addresses the limited structural information available from the current response. It can be extremely useful for the elucidation of reaction mechanisms, and for the delineation of kinetic and thermodynamic parameters. A variety of informative optical methods have thus been coupled with electrochemical techniques. While the following sections will focus primarily on transmission/absorption UV-visible spectroscopic procedures, powerful spectroelectrochemical data can be obtained in reflectance experiments (in which the light beam is reflected from the electrode surface), using vibrational spectroscopic investigations, as well as from luminescence and scattering spectrochemical studies.

2-2.1 Experimental Arrangement

Optically transparent electrodes (OTEs), which enable light to be passed through their surface and the adjacent solution, are the keys for performing transmission

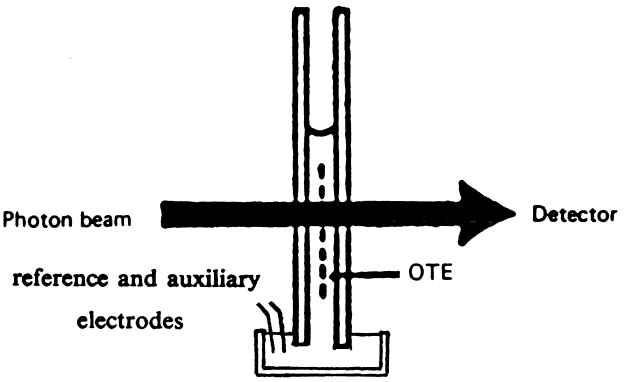

FIGURE 2-10 Thin-layer spectroelectrochemical cell. OTE = optically transparent electrode.

spectroelectrochemical experiments. One type of OTE consists of a metal (gold, silver, nickel) micromesh containing small (10–30 μm) holes, which couples good optical transmission (over 50%) with good electrical conductivity. Such a minigrid is usually sandwiched between two microscopic slides, which form a thin-layer cell (Figure 2-10). The resulting chamber, containing the electroactive species in solution, contacts a larger container that holds the reference and auxiliary electrodes. The OTE is placed in the spectrophotometer so that the optical beam is passed directly through the transparent electrode and the solution. The working volume of the cell is only 30–50 μL, and complete electrolysis of the solute requires only 30–60 s. Alternately, the OTE may consist of a thin (100–5000 Å) film of a metal (e.g., gold or platinum) or a semiconductor (e.g., tin oxide), deposited on a transparent material such as quartz or glass substrate. The film thickness is often selected as a compromise between its electrical conductivity and optical transmission.

Improvements in cell designs have been reported in recent years, including the use of fiber optics for the illumination and collection of light near electrode surfaces (23), the fabrication of long-path-length OTEs via drilling of a small hole through a solid conducting material for sensitive optical monitoring of weakly absorbing species (24,25), and the incorporation of open porous materials (particularly reticulated vitreous carbon) within a thin-layer compartment (26).

2-2.2 Principles and Applications

The primary advantage of spectroelectrochemistry is the cross-correlation of information from the simultaneous electrochemical and optical measurements. In a typical experiment, one measures absorption changes resulting from species produced (or consumed) in the redox process. The change in absorbance is related to concentration and optical path length. Careful evaluation of the temporal absorbance response (A–t curve) during the electrochemical generation (or consumption) of an optically active species can yield extremely useful insights on reaction

mechanisms and kinetics. Such experiments are particularly useful when the reactant and product have sufficiently different spectra.

Consider, for example, the general redox process:

$$O + ne^- \rightleftharpoons R \tag{2-16}$$

When the potential of the OTE is stepped to a value such that reaction (2-16) proceeds at a diffusion-controlled rate, the time-dependent absorbance of R is given by

$$A = \frac{2C_O\varepsilon_R D_O^{1/2} t^{1/2}}{\pi^{1/2}} \tag{2-17}$$

where ε_R is the molar absorptivity of R and D_O and C_O are the diffusion coefficient and concentration of O, respectively. Hence, A increases linearly with the square root of time ($t^{1/2}$), reflecting the continuous generation of R at a rate determined by the diffusion of O to the surface. Equation (2-17) is valid when the generated species is stable. However, when R is a short-lived species (i.e., in an EC mechanism), the absorbance response will be smaller than that expected from equation (2-17). The rate constant for its decomposition reaction can thus be calculated from the decrease in the absorbance. Many other reaction mechanisms can be studied in a similar fashion from the deviation of the A–t curve from the shape predicted by equation (2-17). Such a potential-step experiment is known as chronoabsorptometry.

Thin-layer spectroelectrochemistry can be extremely useful for measuring the formal redox potential (E°) and n values. This is accomplished by spectrally determining the concentration ratio of oxidized to reduced ([O]/[R]) species at each applied potential (from the absorbance ratio at the appropriate wavelengths). Since bulk electrolysis is achieved within a few seconds (under thin-layer conditions), the whole solution rapidly reaches an equilibrium with each applied potential (in accordance to the Nernst equation). For example, Figure 2-11 shows spectra for the complex $[Tc(dmpe)_2Br_2]^+$ in dimethylformamide using a series of potentials [dmpe is 1,2-bis(dimethylphosphine)ethane]. The logarithm of the resulting concentration ratio ([O]/[R]) can be plotted against the applied potential to yield a straight line, with an intercept corresponding to the formal potential. The slope of this Nernstian plot ($0.059/n$ V) can be used to determine the value of n.

Besides potential-step experiments, it is possible to employ linear potential scan perturbations of an OTE (27). This voltabsorptometric approach results in an optical analogue of a voltammetric experiment. A dA/dE vs. E plot (obtained by differentiating the absorbance of the reaction product with respect to the changing potential) is morphologically identical to the voltammetric response for the redox process (Figure 2-12). Depending upon the molar absorptivity of the monitored species, the derivative optical response may afford a more sensitive tool than the voltammetric one. This concept is also not prone to charging-current background contributions and holds considerable promise for mechanism diagnosis and kinetic characterization of coupled chemical reactions.

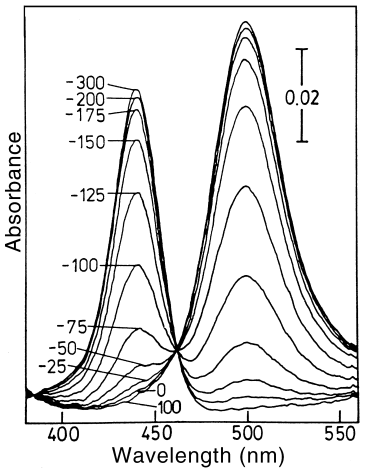

FIGURE 2-11 Spectra for a series of applied potentials (mV vs. Ag/AgC1) during thin-layer spectroelectrochemical experiment on 1.04×10^{-3} M $[Tc(III)(dmpe)_2Br_2]^+$. Medium is dimethylformamide containing 0.5 M TEAP = tetraethylammonium perchlorate. (Reproduced with permission from reference 27.)

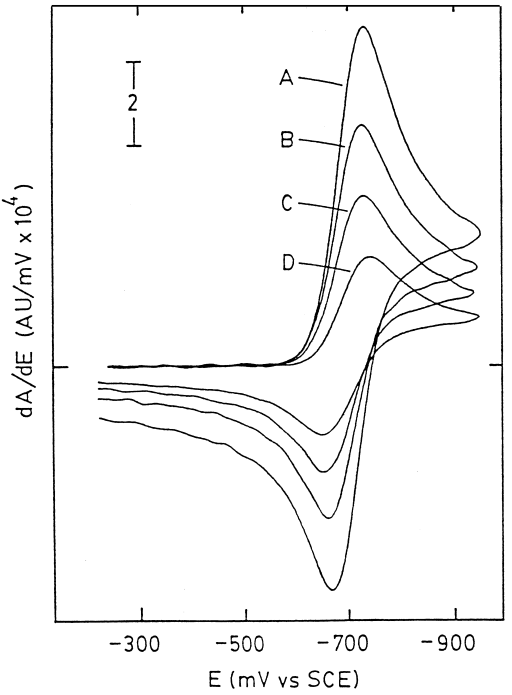

FIGURE 2-12 Plot of dA/dt vs. E for 1.55×10^{-3} M methyl viologen at tin oxide optically transparent electrode, using scan rates of (A) 25, (B) 50, (C) 97.2 and (D) 265 mV s^{-1}. (Reproduced with permission from reference 28.)

Spectroelectrochemical experiments can be used to probe various adsorption/desorption processes. In particular, changes in the absorbance accruing from such processes can be probed utilizing the large ratio of surface area to solution volume of OTEs with long optical path length (29). Additional information on such processes can be obtained from the Raman spectroelectrochemical experiments described later.

In addition to transmission experiments, it is possible to use more sensitive reflectance protocols. In particular, in internal reflectance spectroscopy (IRS) the light beam is introduced to the electrode at an angle, and the spectrum is recorded from the reflected beam at the solid–solution interface. Prisms are used to allow the radiation enter and leave. In addition to its higher sensitivity, IRS is less prone to solution resistance effects.

Infrared spectroelectrochemical methods, particularly those based on Fourier transform infrared (FTIR) spectroscopy can provide structural information that UV-visible absorbance techniques do not. FTIR spectroelectrochemistry has thus been fruitful in the characterization of reactions occurring on electrode surfaces. The technique requires very thin cells to overcome solvent absorption problems.

Besides its widespread use for investigating the mechanism of redox processes, spectroelectrochemistry can be useful for analytical purposes. In particular, the simultaneous profiling of optical and electrochemical properties can enhance the overall selectivity of different sensing (30) and detection (31) applications. Such coupling of two modes of selectivity is facilitated by the judicious choice of the operating potential and wavelength.

2-2.3 Other Spectroelectrochemical and Spectroscopic Techniques

In addition to UV-visible absorption measurements, other spectroscopic techniques can be used for monitoring the dynamics of electrochemical events or the fate of electrogenerated species. Particularly informative are the couplings of electrochemistry with electron spin resonance, nuclear magnetic resonance, and mass spectroscopy. A variety of specially designed cells have been constructed to facilitate such studies, and several reviews have been published (32–36). Electrochemiluminescence (ECL) is another useful technique for studying the fate of electrogenerated radicals that emit light. It involves the formation of light-emitting excited-state species as a result of fast and highly energetic electron-transfer reactions of reactants formed electrochemically (37,38). Various organic and inorganic substances (e.g., polycyclic hydrocarbons, nitro compounds, luminol, $Ru(bpy)_3^{2+}$) can produce ECL upon electron transfer from electrodes, in connection with the formation of radical ions. The electrogenerated radicals behave as very strong redox agents, and their reactions with each other or with other substances are sufficiently energetic to be able to populate excited states. ECL experiments are usually carried out by recording the spectra of the emitted light using a deoxygenated nonaqueous medium (e.g., highly purified acetonitrile or dimethylformamide). Analytical applications of ECL relying on the linear dependence of the ECL intensity and the reactant concentration have also been realized (39).

Additional spectroscopic techniques can be used for probing the molecular structure of electrode–solution interfaces, as desired for understanding the fundamentals of electrode surfaces. The focus of these surface techniques is the correlation of the surface structure with electrochemical reactivity. Such surface-sensitive analytical tools can be classified as in-situ or ex-situ. In particular, the high sensitivity of molecular vibrations to the chemical environment has led to the widespread use of vibrational spectroscopies, such as surface enhanced Raman scattering (SERS), for monitoring the surface composition before, during, and after the electrochemical experiment. In these experiments, a small fraction of the photons exchange energy with the sample and are inelastically scattered, with a change of their wavelength characteristic of the energy change. Such Raman scattering effect can be enhanced by factors of up to 10^8 when the compound is adsorbed on the metallic surface (40). The enhancement process is believed to result from the combination of several electromagnetic and chemical effects between the molecule and the metal surface. Since this scattering efficiency increases dramatically in the adsorbate state, Raman spectroelectrochemistry has been used primarily for investigating species adsorbed on electrodes (41). Another powerful in-situ structural characterization technique, X-ray adsorption fine structure (EXAFS), refers to the modulation in the X-ray adsorption coefficient beyond the adsorption edge. Readers interested in these in-situ techniques are referred to a monograph (42). Scanning electron microscopy (SEM) represents another widely used technique for obtaining ex-situ information on the surface morphology and chemical composition (see, for example, Figure 4-17).

Other powerful ex-situ techniques are based on the detection of charged particles derived from or interacting with the surface. Among these are low-energy electron diffraction (LEED), Auger electron spectroscopy (AES), and X-ray photoelectron spectroscopy (XPS), which are carried out in ultrahigh vacuum (UHV). In LEED, electrons directed at the sample at low energies (20–200 eV) are diffracted to produce a pattern unique to each substrate and adsorbed layer. In AES, electron bombardment creates a vacancy in the electronic level close to the nucleus. This vacancy is filled by an electron coming from another electronic level, with the excess energy being dissipated through ejection of a secondary electron (an Auger electron). The resulting energy spectrum consists of Auger peaks that are unique to each element. XPS (also known as ESCA for electron spectroscopy for chemical analysis) can also provide atomic information about the surface region. In this technique, electrons are emitted from the sample upon its irradiation with monochromatic X rays. The photon energy is related to the ionization (binding) energy E_B, i.e., the energy required to remove the electron from the initial state. Most elements (with the exception of hydrogen and helium) produce XPS signals with distinct E_B. In view of the limited penetration of X rays into solids, the technique gives useful information about surface structures or layers. The appearance of new XPS peaks can thus be extremely useful for studies of modified electrodes. The reliability of information gained by such ex-situ analysis depends on knowledge of what happens during vacuum exposure. Uncertainties associated with potential loss of material during such exposure have led to renewed emphasis on direct (in-situ) probes.

2-3 SCANNING PROBE MICROSCOPY

The recently developed scanning probe microscopies (SPM) promise to revolutionize the understanding of electrode processes. The purpose of this family of microscopes is to acquire high-resolution data of surface properties. The various scanning probe microscopies have similar subcomponents but different sensing probes. These high-resolution microscopies rely on sensing the interactions between a probe tip and the target surface while scanning the tip across the surface. Different types of interactions can be sensed by the tip to yield different imaging signals. Such signals are displayed as gray-scale portraits, reflecting the extent of the tip–surface interaction. With microcomputers, the image processing becomes possible in very short times. Among the various scanning probe microscopies, scanning tunneling microscopy, atomic force microscopy, and scanning electrochemical microscopy have been useful for imaging electrode surfaces directly (under potential control), and have thus dramatically improved the understanding of electrode reactions.

2-3.1 Scanning Tunneling Microscopy

Scanning tunneling microscopy (STM) has revolutionized the field of surface science by allowing the direct imaging of surfaces on the atomic scale. The scanning tunneling microscope consists of a very sharp metallic tip that is moved over the surface of interest with a ceramic piezoelectric translator. The basis for its operation is the electron tunneling between the metal tip and the sample surface. The tunneling current (i_t) that flows when a voltage is applied between the sample and the tip is extremely sensitive to the sample–tip separation. In the simplest one-dimensional treatment i_t is given by

$$i_t \alpha \exp[(-4S\pi/h)(2m\phi)^{1/2}] \tag{2-18}$$

where S is the barrier width (equivalent to the shortest distance between the sample surface and the end of the tip), h is the Planck constant, m is the electron mass, and ϕ is the barrier height (equivalent to the local work function). In practice, i_t can change by a factor of 2 or more with a change of the tip-sample separation of only 1 Å. Accordingly, i_t tends to vary with the sample topography.

Although much of the early STM work has focused on investigating surfaces in vacuum, recent work has demonstrated that surface images can also be obtained in liquid and air. In particular, the STM probing of electrode–electrolyte interfaces has attracted considerable attention (43–45). The ability of STM to offer structural information at the atomic level makes it highly suitable for in-situ studies of time-dependent electrochemical processes, such as corrosion, electrodeposition, adsorption, as well as surface modification, passivation, and activation. For example, Figure 2-13 shows a representative three-dimensional STM view of an electrochemically pretreated glassy carbon electrode, while Figure 2-14 illustrates a STM image of a spontaneously adsorbed alkanethiol monolayer on a gold surface. Useful insights into the structural–preparation relationships of conducting polymers can also be

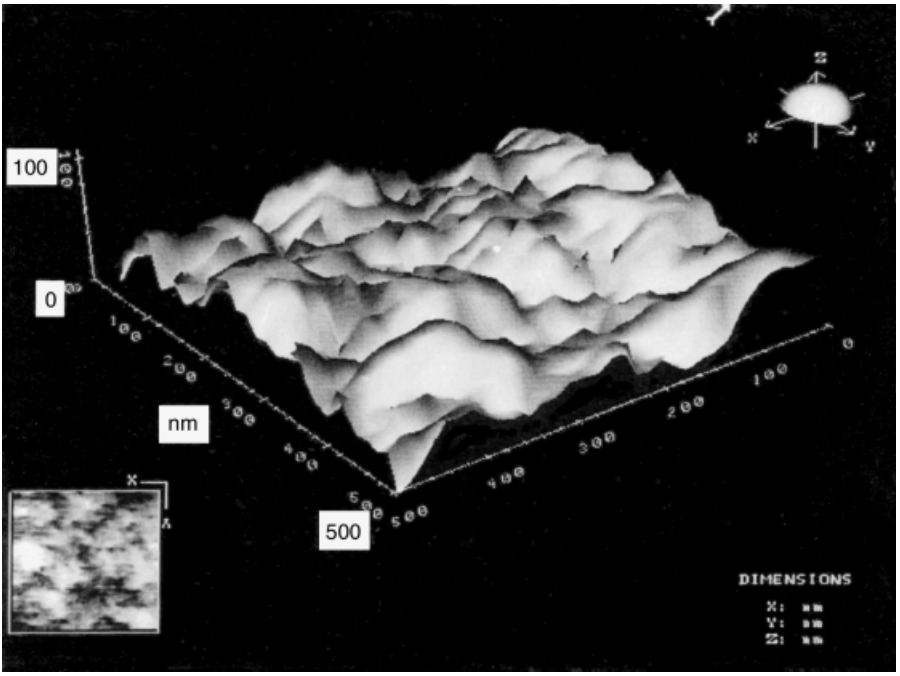

FIGURE 2-13 STM image of an electrochemically activated glassy-carbon surface. (Reproduced with permission from reference 46.)

achieved by monitoring the growth of such films under different conditions (48). In addition to topographic information, the high sensitivity of the tunneling current to changes in the local work function (i.e., surface conductivity) offers a distinct visualization of composite electrode surfaces (49).

The recent introduction of commercial STM machines incorporating a potentiostat and an electrochemical cell has greatly facilitated in-situ investigations of electrochemical processes. A block diagram of such a STM/electrochemical system is shown in Figure 2-15. Coupled with powerful software, such instruments allow the simultaneous acquisition and display of the electrochemical and topographic data. Extremely useful insights can thus be obtained by correlating the surface microstructures and the electrochemical reactivity. The interpretation of STM images requires extreme caution, and the tip should be shielded properly (from the electrolyte) to minimize the stray capacitance. Nevertheless the powerful coupling of STM and electrochemical systems offers many exciting future opportunities.

2-3.2 Atomic Force Microscopy

Atomic force microscopy (AFM) has become a standard technique for high-resolution imaging of the topography of surfaces. It enables one to see nanoscopic

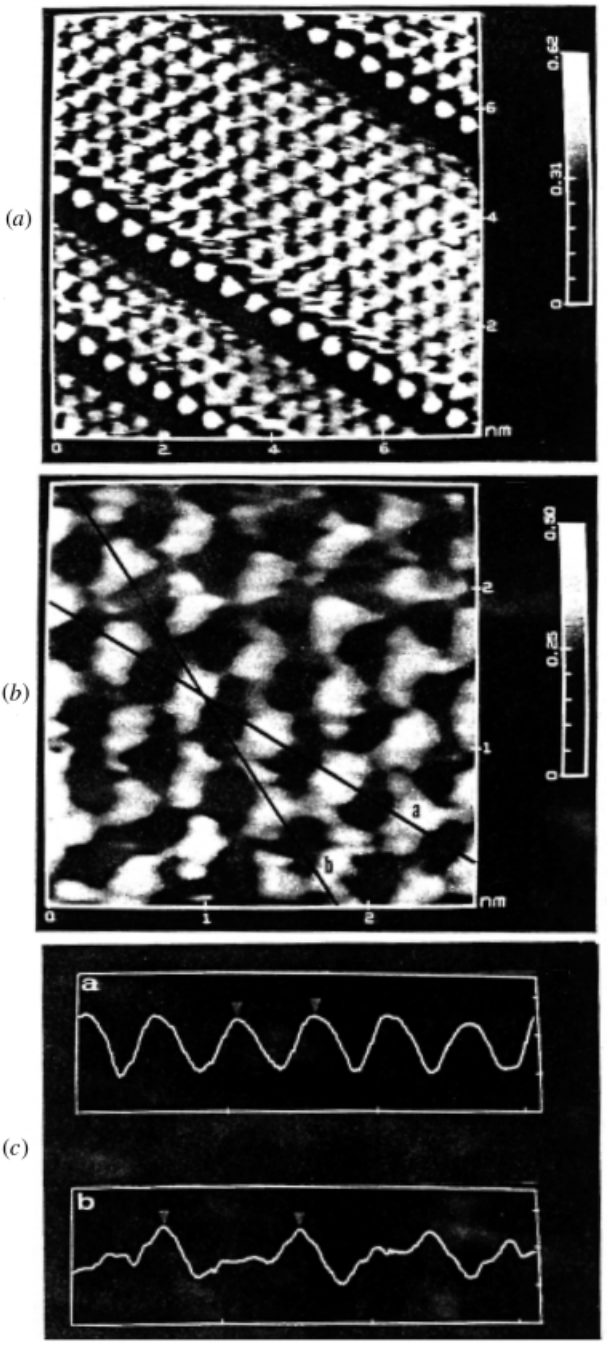

FIGURE 2-14 STM images of (a) 7.7 nm × 7.7 nm and (*b*) 2.65 nm × 2.65 nm sections of an ethanethiolate monolayer on a gold film. (*c*) Contours of the image along the lines a and b in (*b*). (Reproduced with permission from reference 47.)

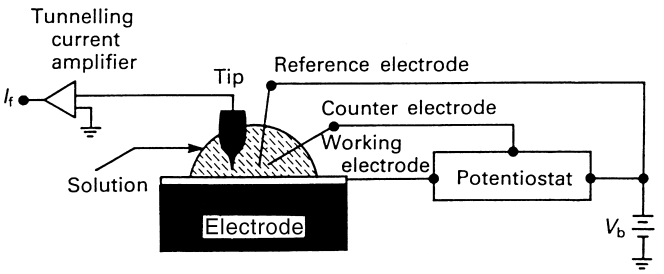

FIGURE 2-15 Design of a system for in-situ electrochemical scanning tunneling microscopy.

surface features while the electrode is under potential control. This powerful probe microscopy operates by measuring the force between the probe and the sample (50). This force is attributed to repulsion generated by the overlap of the electron cloud at the probe tip with the electron cloud of surface atoms. It depends in part on the nature of the electrode, the distance between the electrode and the tip, any surface contamination, and the tip geometry. The interaction of the force fields is sensed by a cantilever beam, to which the tip is attached. An image (revealing individual atoms) is created as the probe is translated across the surface. Such images can be formed by constant-force or constant-height modes (with known or measured deflections of the cantilever, respectively). Since AFM does not involve passage of current between the tip and the surface, it is useful for exploring both insulating and conducting regions.

2-3.3 Scanning Electrochemical Microscopy

The scanning tunneling microscope (STM) has led to several other variants (51). Particularly attractive for electrochemical studies is scanning electrochemical microscopy (SECM) (52–55). In SECM, faradaic currents at an ultramicroelectrode tip are measured while the tip is moved (by a piezoelectric controller) in close proximity to a substrate surface that is immersed in a solution containing an electroactive species (Figure 2-16). These tip currents are a function of the conductivity and chemical nature of the substrate, as well as of the tip–substrate distance. The images thus obtained offer valuable insights into the microdistribution of the electrochemical and chemical activity, as well as the substrate topography. A wide range of important applications involving different electrochemical systems has been developed.

The most common version of SECM, the feedback mode, involves recycling of an electroactive material between the tip and substrate surfaces (Figure 2-17). When the microelectrode is distant from the surface by several electrode diameters, a steady-state current $i_{T,\infty}$ is observed at the tip (*a*). When the tip is brought near a conductive substrate (held at sufficiently positive potential), the tip-generated product R can be oxidized back to O, and the tip current will be greater than $i_{T,\infty}$ (*b*). In contrast, when the tip passes over an insulating region (on the substrate), diffusion to the tip is hindered, and the feedback current diminishes (*c*). For example, Figure 2-18 displays a two-dimensional scan of a gold minigrid surface. The

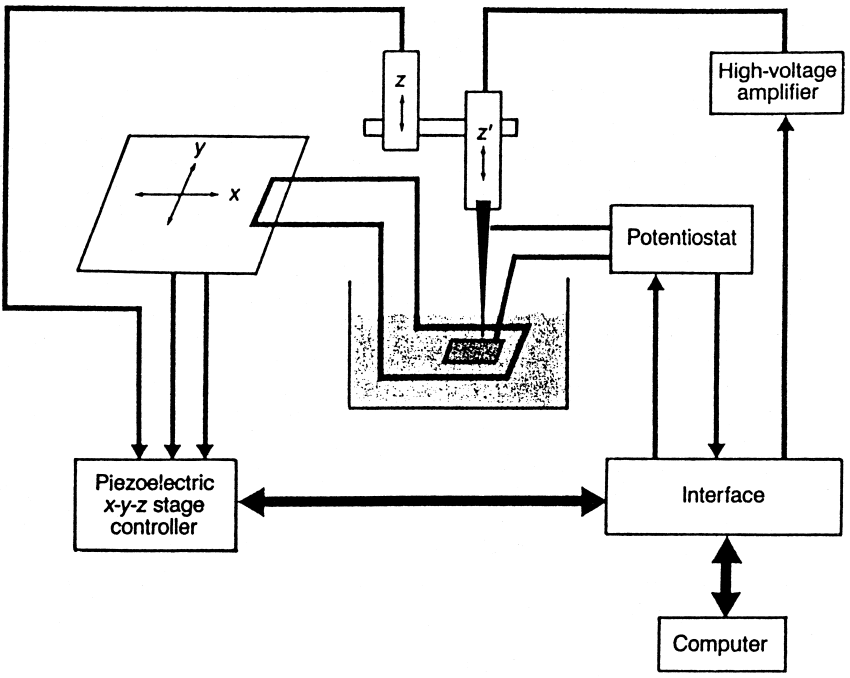

FIGURE 2-16 Design of a scanning electrochemical microscope. (Reproduced with permission from reference 56.)

conducting gold lines are clearly observed from the enhanced recycling current. Alternately, in the collection mode, the tip is used only as a detector of species generated at the substrate. The distribution of the electrochemical activity of the surface can thus be mapped. The submicrometer resolution of SECM images is controlled by the size and shape of the tip, and it can be further improved by using digital image processing techniques. However, unlike in STM or AFM, atomic resolution cannot be achieved in SECM. Scanning electrochemical microscopy can also be used to investigate heterogeneous reaction kinetics. This is accomplished by forming a twin-electrode thin layer between the tip and a conducting substrate. Such a configuration induces high rates of mass transfer and leads to tip currents limited by the intrinsic electron-transfer rates. The volume reduction has also been exploited for electrochemical studies at the level of single molecules that allow the elucidation of new effects that are not apparent in experiments involving a large number of molecules (58). For this purpose, the tip is insulated (e.g., with a wax) to trap the single molecule in a tiny pocket (e.g., Figure 2-19).

Scanning electrochemical microscopy can also be applied to study localized biological activity, as desired, for example, for in-situ characterization of biosensors (59,60). In this mode, the tip is used to probe the biological generation or consumption of electroactive species, for example, the product of an enzymatic surface reaction. The utility of potentiometric (pH-selective) tips has also been

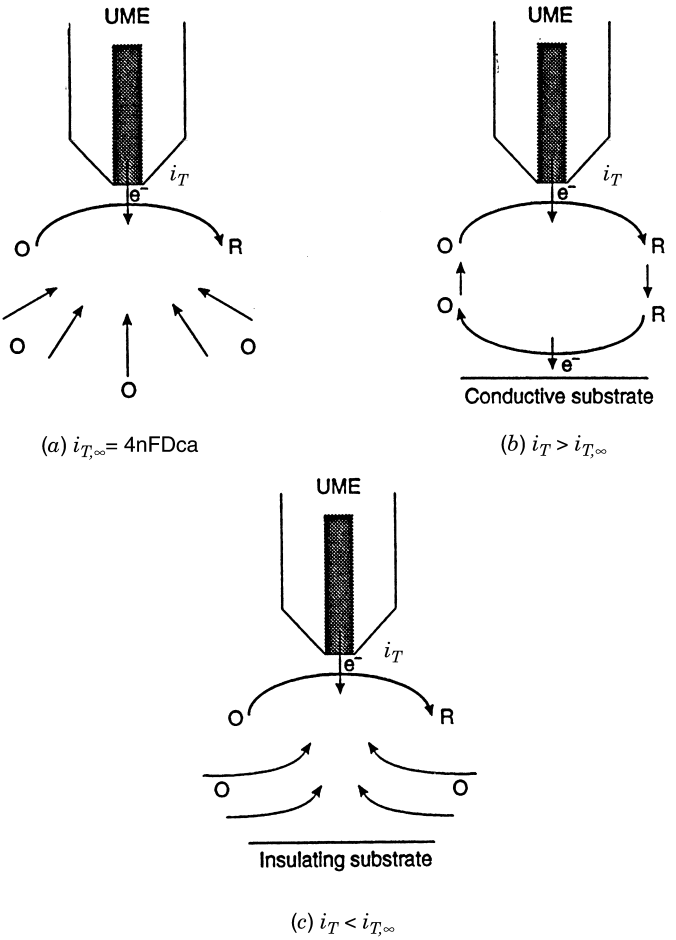

FIGURE 2-17 Principles of SECM. (*a*) Tip far from the substrate surface; diffusion of O leads to steady-state current. (*b*) Tip near a conductive substrate; positive feedback of O. (*c*) Tip near the insulating substrate; hindered diffusion of O. c = concentration; a = radius of tip. (Reproduced with permission from reference 55.)

documented recently for imaging pH profiles such as those generated by enzymatic (urease) reactions (61). These and other (62) potentiometric tips are expected to probe different reactions that are not accessible with voltammetric tips, e.g., determining local concentrations of electroinactive species. Double-barreled tips, integrating the working and reference microelectrodes, are preferred for such potentiometric imaging. Unlike their voltammetric counterparts, potentiometric tips serve as purely passive sensors. In addition to its extensive use for surface characterization, SECM has been used as a microfabrication tool (63), with its tip acting as an electrochemical "pen" or "eraser." Various electrochemical processes (e.g., electroplating, etching) can thus be carried out at high resolution while moving

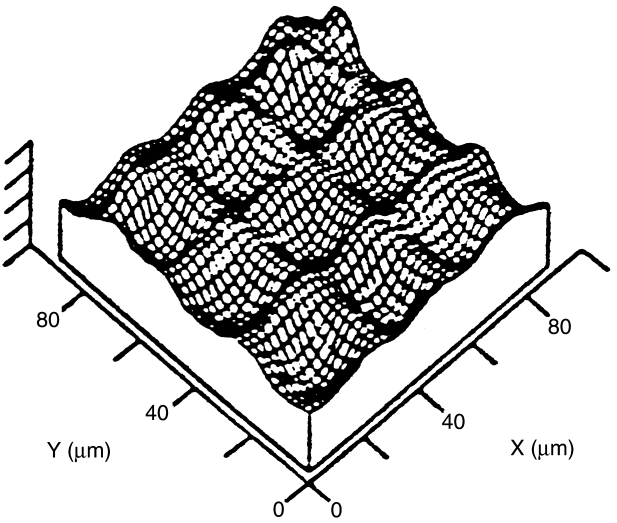

FIGURE 2-18 SECM image of a gold minigrid surface. (Reproduced with permission from reference 57.)

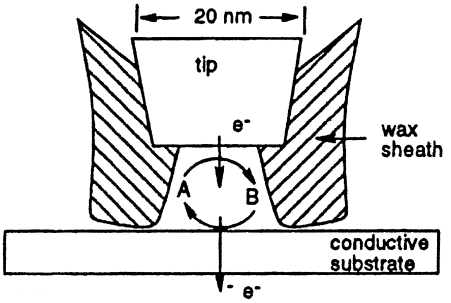

FIGURE 2-19 Single-molecule detection with SECM. Molecule A is trapped between the tip and the surface. (Reproduced with permission from reference 58.)

the tip over the substrate surface. Recently introduced commercial SECM instruments (64) will undoubtedly increase the scope and power of SECM.

2-4 ELECTROCHEMICAL QUARTZ CRYSTAL MICROBALANCE

The electrochemical quartz crystal microbalance (EQCM) is a powerful tool for elucidating interfacial reactions based on the simultaneous measurement of electrochemical parameters and mass changes at electrode surfaces. The microbalance is based on a quartz crystal wafer, which is sandwiched between two electrodes, used to induce an electric field (Figure 2-20). The field produces a mechanical oscillation

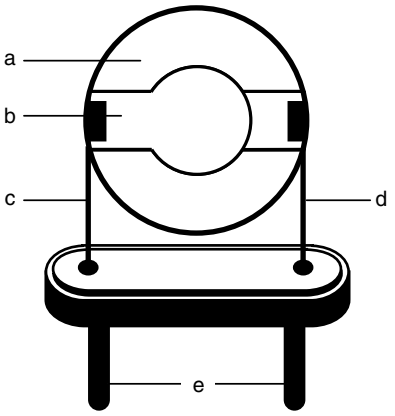

FIGURE 2-20 The quartz crystal microbalance: a, the quartz crystal; b, the gold electrode; c and d, connecting metal wires; e, the base.

in the bulk of the wafer. Surface reactions involving minor mass changes can cause perturbation of the resonant frequency of the crystal oscillator. The frequency change (Δf) is related to the mass change (Δm) according to the Sauerbrey equation:

$$\Delta f = -2\ \Delta m n f_0^2 / A\sqrt{\mu\rho} \tag{2-19}$$

where n is the overtone number, f_0 is the base resonant frequency of the crystal (prior to the mass change), A is the area (cm^2), μ is the shear modulus of quartz (2.95×10^{11} g cm^{-1} s^{-1}), and ρ is the density of quartz (2.65 g cm^{-3}). As expected from the negative sign, decreases in mass correspond to increases in frequency and vice versa. The Sauerbrey equation forms the basis for the excellent mass sensitivity of the EQCM. In-situ mass changes of 1 ng cm^{-2} can thus be detected. Such high sensitivity and in-situ capability represent the major advantages of EQCM experiments.

The EQCM is very useful for probing processes that occur uniformly across the surface. Numerous surface reactions have been investigated, including deposition or dissolution of surface layers and various uptake processes (such as doping/undoping of conducting polymers or ion-exchange reactions at polymer films). Such changes can be probed using various controlled-potential or controlled-current experiments. In these experiments, one of the electrodes (on the wafer) contacts the solution and serves as the working electrode in the electrochemical cell, to allow simultaneous frequency and current measurements. For example, Figure 2-21 displays the frequency (mass) versus potential profiles, and the corresponding cyclic voltammograms, during the uptake of a multiply charged complex ion at an ion exchanger-coated electrode. Other useful examples of probing the uptake of mobile species by polymer-coated electrodes have been given by Hillman et al. (66). Application of the Sauerbrey equation to the study of polymeric films in solutions requires adherence to the rigid film approximation (i.e., behavior of an elastic, solvent-free thin layer).

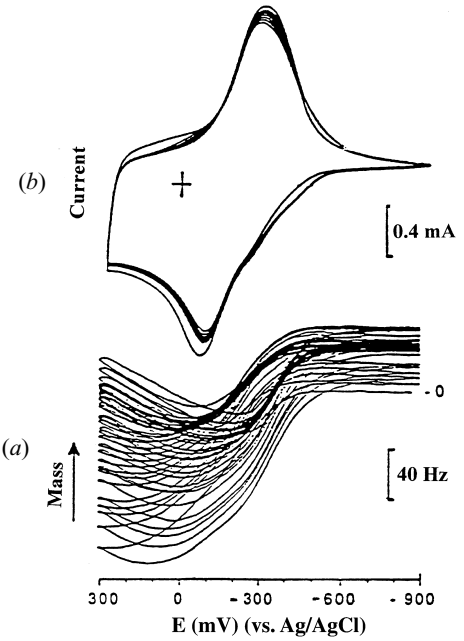

FIGURE 2-21 EQCM (*a*) and cyclic voltammetry (*b*) profiles at an ion exchanger-coated electrode in the presence of 6×10^{-3} M $Ru(NH_3)_6Cl_6$. (Reproduced with permission from reference 65.)

Such approximation is valid when the thickness of the polymeric layer is small compared to the thickness of the crystal, and the measured frequency change is small with respect to the resonant frequency of the unloaded crystal. Mass changes up to 0.05% of the crystal mass commonly meet this approximation. In the absence of molecular specificity, EQCM cannot be used for molecular-level characterization of surfaces. Electrochemical quartz crystal microbalance devices also hold promise for the task of affinity-based chemical sensing, as they allow simultaneous measurements of both the mass and the current. The principles and capabilities of EQCM have been reviewed (67,68). The combination of EQCM with scanning electrochemical microscopy has also been reported recently for studying the dissolution and etching of various thin films (69). The recent development of a multichannel quartz crystal microbalance (70), based on arrays of resonators, should further enhance the scope and power of EQCM.

REFERENCES

1. R.S. Nicholson and I. Shain, *Anal. Chem.*, 36, 706 (1964).
2. L. Echegoyen, and L.E. Echegoyen, *Acc. Chem. Res.*, 31, 593 (1998).
3. C.P. Andrieux, P. Hapiot, and J.M. Savéant, *Electroanalysis*, 2, 183 (1990).

4. M.B. Gelbert, and D.J. Curran, *Anal. Chem.*, 58, 1028 (1986).
5. M.D. Hawley, S.V. Tatawawdi, S Piekarski, and R.N. Adams, *J. Am. Chem. Soc.*, 89, 447 (1967).
6. D.M. Mohilner, R.N. Adams and W.R. Argersinger, *J. Am. Chem. Soc.*, 84, 3816 (1962).
7. D. Evans, *Acc. Chem. Res.*, 10, 313 (1977).
8. G. Mabbott, *J. Chem. Educ.*, 60, 697 (1983).
9. M. Rudolph, D. Reddy and S.W. Feldberg, *Anal. Chem.*, 66, 589A (1994).
10. J. Wang, D.B. Luo, P.A.M. Farias and J.S. Mahmoud, *Anal. Chem.*, 57, 158 (1985).
11. P.J. Pearce and A.J. Bard, *J. Electroanal. Chem.*, 114, 89 (1980).
12. R.H. Wopschall and I. Shain, *Anal. Chem.*, 39, 1514 (1967).
13. M. Sluyters-Rehbach and J.R. Sluyter, *J. Electroanal. Chem.*, 65, 831 (1975).
14. A.P. Brown and F.C. Anson, *Anal. Chem.*, 49, 1589 (1977).
15. J. Stamford, P. Hurst, W. Kuhr and R.M. Wightman, *J. Electroanal. Chem.*, 265, 291 (1989).
16. J. Baur, E. Kristensen, L. May, D. Wiedemann and R.M. Wightman, *Anal. Chem.*, 60, 1268 (1988).
17. D. Michael, E. Travis and R.M. Wightman, *Anal. Chem.*, 70, 586A (1998).
18. B. Jackson, S. Dietz and R.M. Wightman, *Anal. Chem.*, 67, 1115 (1995).
19. J. Heinze, *Angew. Chem. (Int. Ed. Engl.)*, 23, 831 (1984).
20. R.P. Baldwin, K. Ravichandran and R.K. Johnson, *J. Chem. Educ.*, 61, 820 (1984).
21. T. Kuwana and W. Heineman, *Acc. Chem. Res.*, 9, 241 (1976).
22. W. Heineman, F. Hawkridge and H. Blount, "Spectroelectrochemistry at Optically Transparent Electrodes" in A.J. Bard, Ed., *Electroanalytical Chemistry*, Vol. 13, Marcel Dekker, New York, 1986.
23. D.A. Van Dyke and H.Y. Cheng, *Anal. Chem.*, 60, 1256 (1988).
24. M. Porter and T. Kuwana, *Anal. Chem.*, 56, 529 (1984).
25. J. Brewster and J.L. Anderson, *Anal. Chem.*, 54, 2560 (1982).
26. V. Norvell and G. Mamantov, *Anal. Chem.*, 49, 1470 (1977).
27. W.R. Heineman, *J. Chem. Educ.*, 60, 305 (1983).
28. E. Bancroft, J. Sidwell and H. Blount, *Anal. Chem.*, 53, 1390 (1981).
29. Y.P. Gui, M. Porter and T. Kuwana, *Anal. Chem.*, 57, 1474 (1985).
30. Y. Shi, A. Slaterbeck, C. Seliskar and W.R. Heineman, *Anal. Chem.*, 69, 3676 (1997).
31. H.D. Dewald and J. Wang, *Anal. Chim. Acta*, 166, 163 (1984).
32. R.N. Bagchi, A.M. Bond and F. Scholz, *Electroanalysis*, 1, 1 (1989).
33. J.A. Richards and D.H. Evans, *Anal. Chem.*, 47, 964 (1965).
34. H. Chang, D.C. Johnson and R.S. Houk, *Trends Anal. Chem.*, 8, 328 (1989).
35. M.C. Regino and A. Brajter-Toth, *Anal. Chem.*, 69, 5067 (1997).
36. Y. Tong, E. Oldfield and A. Wieckowski, *Anal. Chem.*, 70, 518A (1998).
37. L Faulkner and A.J. Bard, "Electrochemiluminescence" in A.J. Bard, Ed., *Electroanalytical Chemistry*, Vol. 10, Marcel Dekker, New York, 1977.
38. J.G. Velasco, *Electroanalysis*, 3, 261 (1991).
39. A.W. Knight and G. Greenway, *Analyst*, 119, 879 (1994).
40. D. Jeanmarie and R. Van Duyne, *J. Electroanal. Chem.*, 84, 1 (1977).

41. R.L. McCreery and R.T. Packard, *Anal. Chem.*, 61, 775A (1989).
42. H.D. Abruna, *Electrochemical Interfaces*, VCH Publishers, New York, 1991.
43. A.J. Arvia, *Surface Science*, 181, 78 (1987).
44. T.R. Cataldi, I. Blackham, A. Briggs, J. Pethica and H.A. Hill, *J. Electroanal. Chem.*, 290, 1 (1990).
45. J. Wang, *Analyst*, 117, 1231 (1992).
46. J. Wang, T. Martinez, D. Yaniv and L.D. McCormick, *J. Electroanal. Chem.*, 278, 379 (1990).
47. C. Widrig, C. Alves and M. Porter, *J. Am. Chem. Soc.*, 113, 2805 (1991).
48. T. Kim, H. Yang and A. Bard, *J. Electrochem. Soc.*, 138, L71 (1991).
49. J. Wang, T. Martinez, D. Yaniv and L.D. McCormick, *J. Electroanal. Chem.*, 286, 265 (1990).
50. H. Hansma, A. Weisenhorm, A. Edmundson, H. Gaub and P. Hansma, *Clin. Chem.*, 37, 1497 (1991).
51. H. Wickramaasinghe, *Scientific American*, 98 (Oct. 1989).
52. R. Engstrom and C. Pharr, *Anal. Chem.*, 61, 1099A (1989).
53. A.J. Bard, G. Denuault, C. Lee, D. Mandler and D. Wipf, *Acc. Chem. Res.*, 23 (1990) 357.
54. M.V. Mirkin, *Anal. Chem.*, 68, 177A (1996).
55. M. Arca, A.J. Bard, B. Horrocks, T. Richards and D. Treichel, *Analyst*, 119, 719 (1994)
56. H. Liu, F. Fan, C. Lin and A.J. Bard, *J. Am. Chem. Soc.*, 108, 3838 (1986).
57. J. Kwak and A.J. Bard, *Anal. Chem.*, 61, 1794 (1989).
58. F. Fan, J. Kwak and A.J. Bard, *J. Am. Chem. Soc.*, 118, 9669 (1996).
59. J. Wang, L. Wu and R. Li, *J. Electroanal. Chem.*, 272, 285 (1989).
60. D. Pierce, P. Unwin and A.J. Bard, *Anal. Chem.*, 64, 1795 (1992).
61. B. Horrocks, M. Mirkin, D. Pierce, A.J. Bard, G. Nagy and K. Toth, *Anal. Chem.*, 65, 1304 (1993).
62. C. Wei, A.J. Bard, G. Nagy and K. Toth, *Anal. Chem.*, 67, 1346 (1995).
63. W. Nowall, D. Wipf and W.G. Kuhr, *Anal. Chem.*, 70, 2601 (1998).
64. "Scanning Electrochemical Microscope", CH Instruments, 1998.
65. S. Basak, C. Bose and K. Rajeshwar, *Anal. Chem.*, 64, 1813 (1992).
66. A.R. Hillman, D. Loveday, M. Swann, S. Bruckenstein and C.P. Wildle, *Analyst*, 117, 1251 (1992).
67. M. Deakin and D. Buttry, *Anal. Chem.*, 61, 1147A (1989).
68. M.D. Ward and D.A. Buttry, *Science*, 249, 1000 (1990).
69. D. Cliffel and A.J. Bard, *Anal. Chem.*, 70, 1993 (1998).
70. T. Tatsuma, Y. Watanabe, N. Oyama, K. Kiakizaki and M. Haba, *Anal. Chem.*, 71, 3632 (1999).

EXAMPLES

Example 2-1 The reversible oxidation of dopamine (DA) is a two-electron process. A cyclic voltammetric anodic peak current of 2.2 μA is observed for a

0.4 mM solution of dopamine in phosphate buffer at a glassy carbon disk electrode of 2.6 mm^2 area with a scan rate of 25 mV s^{-1}. What will i_p be for $v = 100$ mV s^{-1} and 1.2 mM DA?

Solution From equation (2-1):

$$i_p = kCv^{1/2} \qquad 2.2 = k\ 0.4(25)^{1/2} \qquad k = 1.1$$

Under the new experimental conditions, i_p is given by

$$i_p = 1.1 \times 1.2 \times (100)^{1/2} = 13.2\ \mu A$$

Example 2-2 The following cyclic voltammogram was recorded for a reversible couple: Calculate the number of electrons transferred and the formal potential for the couple.

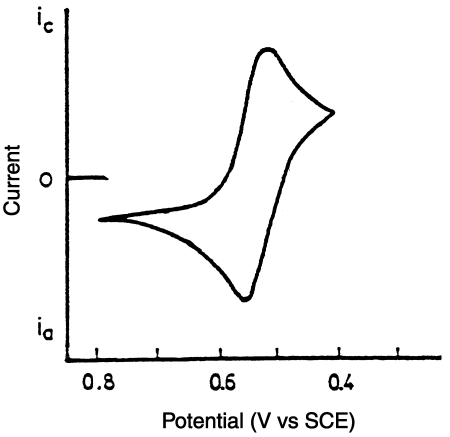

Solution From equation (2-3),

$$n = 0.059/\Delta E_p = 0.059/(0.555 - 0.495) = 0.983 \cong 1.0$$

The formal potential can be calculated from equation (2-2):

$$E^0 = (0.555 + 0.495)/2 = 0.525\ V$$

Example 2-3 The electropolymeric growth of 2 ng polyphenol onto a gold QCM crystal ($A = 1\ cm^2$; $f_0 = 5$ MHz) resulted in a frequency change of 12 Hz. Calculate the frequency change associated with the deposition of 4 ng polyphenol onto a 0.5 cm^2 crystal ($f_0 = 8$ MHz).

Solution From equation (2-19)

$$\Delta f = -K\,\Delta m f_0^2/A$$

$$5 = -K2 \times 5^2/1 \qquad K = -0.1$$

Under the new experimental conditions, Δf is given by

$$\Delta f = -(-0.1) \times 4 \times 8^2/0.5 = 51.2 \text{ Hz}$$

Example 2-4 A potential-step spectroelectrochemistry experiment using a reactant concentration of 2 mM generated a product with an absorbance (sampled after 25 s) of 0.8. Calculate the reactant concentration that yielded an absorbance of 0.4 upon sampling at 16 s.

Solution From equation (2-17),

$$A = KC_0 t^{1/2} \qquad 0.8 = K2(25)^{1/2} \qquad K = 0.08$$

Accordingly,

$$0.4 = 0.08C_0(16)^{1/2} \qquad C_0 = 5\text{mM}$$

QUESTIONS

1. Explain and demonstrate clearly how spectroelectrochemistry can provide useful information about a reaction mechanism involving a redox process followed by a chemical reaction (EC mechanism), involving decomposition of the reaction product. Draw an absorbance–time plot for different rate constants of the decomposition reaction.
2. Which voltammetric technique can be used for estimating the surface coverage of an adsorbed molecule? How?
3. Draw an EQCM (mass–potential) profile for a metal deposition-stripping process during a cycling voltammetric scanning.
4. A cyclic-voltammetric peak current of 12.5 μA was observed for the reversible reduction of a 1.5 mM lead solution using a 1.2 mm-diameter disk electrode and a 50 mV s^{-1} scan rate. Calculate the lead concentration that yields a peak current of 20.2 μA at 250 mV s^{-1}.
5. Explain clearly how SECM images the microdistribution of the electrochemical activity of composite electrode materials.

6. Describe clearly how thin-layer spectroelectrochemistry is used for measuring the values of E° and n.

7. Summarize the different features of the cyclic voltammogramic response for reversible and quasi-reversible systems.

8. Explain the use of cyclic voltammetry for estimating the values of E° and n for a reversible system.

9. What is the reason for the gradual increase of the cathodic and anodic cyclic-voltammetric peak currents observed upon repetitive scanning?

10. How would you use EQCM for elucidating the electrostatic desorption of anionic DNA molecules from gold electrodes?

11. Propose a SECM experiment for mapping the distribution of an oxidase enzyme within a carbon composite surface. (Note that the enzyme generates hydrogen peroxide in the presence of its substrate and oxygen.)

12. How does the increase of the scan rate affect the ratio of peak currents (backward/forward) in a cyclic voltammetric experiment involving a redox process followed by a chemical reaction?

Analytical Electrochemistry, Second Edition. Joseph Wang

ISBNs: 0-471-28272-3 (Hardback); 0-471-22823-0 (Electronic)

CHAPTER 3

CONTROLLED-POTENTIAL TECHNIQUES

The basis of all controlled-potential techniques is the measurement of the current response to an applied potential. There exist a multitude of potential excitations, including a ramp, potential steps, pulse trains, a sine wave, and various combinations thereof. The present chapter reviews those techniques that are widely used.

3-1 CHRONOAMPEROMETRY

Chronoamperometry involves stepping the potential of the working electrode from a value at which no faradaic reaction occurs to a potential at which the surface concentration of the electroactive species is effectively zero (Figure 3-1*a*). A stationary working electrode and unstirred solution are used. The resulting current–time dependence is monitored. As mass transport under these conditions is solely by diffusion, the current–time curve reflects the change in the concentration gradient in the vicinity of the surface (recall Section 1.2). This involves a gradual expansion of the diffusion layer associated with the depletion of the reactant, and hence decreased slope of the concentration profile as time progresses (see Figure 3-1*b*). Accordingly, the current (at a planar electrode) decays with time (Figure 3-1*c*), as given by the *Cottrell equation:*

$$i(t) = \frac{nFACD^{1/2}}{\pi^{1/2}\, t^{1/2}} = kt^{-1/2} \tag{3-1}$$

Such an $it^{1/2}$ constancy is often termed "Cottrell behavior." Deviations from such behavior occur at long times (usually over 100 s) as a result of natural convection

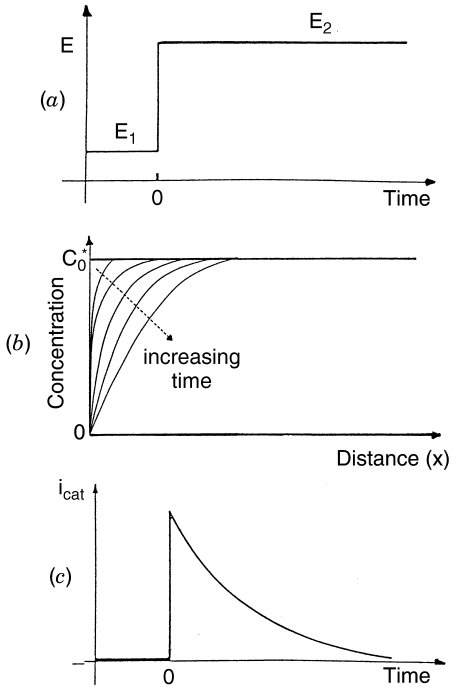

FIGURE 3-1 Chronoamperometric experiment: (*a*) potential–time waveform; (*b*) change of concentration profiles with time; (*c*) the resulting current–time response.

effects, or when using microelectrodes with high perimeter-to-area ratios (see Section 4-5.4). In the latter case, a time-independent current (proportional to the concentration) is obtained for $t > 0.1$ s due to a large radial diffusion contribution. Similar considerations apply to spherical electrodes whose current response following a potential step contains a time-dependent and time-independent terms (equation 1-12). Recall also that for small values of t ($t < 50$ ms) the chronoamperometric signal contains a background contribution of the charging current (equation 1-49). Additional transient background contributions (associated with surface redox reactions) are common to solid-electrode chronamperometric experiments.

Chronoamperometry is often used for measuring the diffusion coefficient of electroactive species or the surface area of the working electrode. Analytical applications of chronoamperometry (e.g., in-vivo bioanalysis) rely on pulsing of the potential of the working electrode repetitively at fixed time intervals. Chronoamperometry can also be applied to the study of mechanisms of electrode processes. Particularly attractive for this task are reversal double-step chronoamperometric experiments (where the second step is used to probe the fate of a species generated in the first step).

The potential-step experiment can also be used to record the charge versus time dependence. This is accomplished by integrating the current resulting from the

potential step. Such a charge measurement procedure, known as chronocoulometry, is particularly useful for measuring the quantity of adsorbed reactants (because of the ability to separate the charges produced by the adsorbed and solution species). A plot of the charge (Q) vs. $t^{1/2}$ yields an intercept at $t = 0$ that corresponds to the sum of the charge due to the reaction of the adsorbed species and the double-layer charging. The former can be estimated by subtracting the intercept obtained in an identical experiment carried out in the blank solution.

3-2 POLAROGRAPHY

Polarography is a subclass of voltammetry in which the working electrode is the *dropping mercury electrode* (DME). Because of the special properties of this electrode, particularly its renewable surface and wide cathodic potential range (see Section 4-5 for details), polarography has been widely used for the determination of many important reducible species. This classical technique was invented by J. Heyrovsky in Czechoslovakia in 1922, and had an enormous impact on the progress of electroanalysis (through many subsequent developments). Accordingly, Heyrovsky was awarded the 1959 Nobel Prize in Chemistry.

The excitation signal used in conventional (DC) polarography is a linearly increasing potential ramp. For a reduction, the initial potential is selected so that the reaction of interest does not take place. The potential is then scanned cathodically while the current is measured. The current is proportional to the slope of the concentration–distance profile (see Section 1-2.1.2). At a sufficiently negative potential, reduction of the analyte commences, the concentration gradient increases, and the current rises rapidly to its limiting (diffusion-controlled) value. At this plateau, any analyte particle that arrives at the electrode surface instantaneously undergoes an electron-transfer reaction, and the maximum rate of diffusion is achieved. The resulting polarographic wave is shown in Figure 3-2. The current oscillations reflect the growth and fall of the individual drops.

To derive the expression for the current response, one must account for the variation of the drop area with time:

$$A = 4\pi\left(\frac{3mt}{4\pi d}\right)^{2/3} = 0.85(mt)^{2/3} \tag{3-2}$$

where t is the time and m and d are the mass flow rate and density of mercury, respectively. By substituting the surface area (from equation 3-2) into the Cottrell equation (equation 3-1), and replacing D by $7/3D$ (to account for the compression of the diffusion layer by the expanding drop), we obtain the *Ilkovic equation* for the limiting diffusion current (1):

$$i_d = 708nD^{1/2}m^{2/3}t^{1/6}C \tag{3-3}$$

Here, i_d will have units of amperes (A) when D is in $cm^2\ s^{-1}$, m is in $g\ s^{-1}$, t is in seconds and C is in mol cm^{-3}. This expression represents the current at the end of

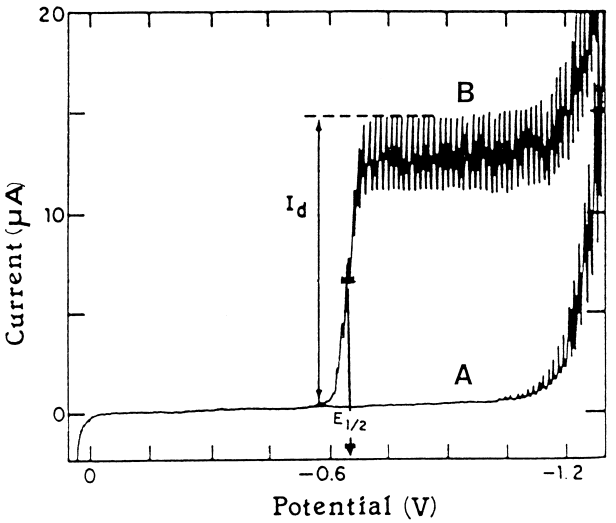

FIGURE 3-2 Polarograms for 1 M hydrochloric acid (Curve A) and 4×10^{-4} M Cd^{+2} in 1 M hydrochloric acid B. i_d represents the limiting current; $E_{1/2}$ is the half-wave potential.

the drop life. The average current over the drop life is obtained by integrating the current over this time period:

$$i_{\text{aver}} = 607nD^{1/2}m^{2/3}t^{1/6}C \tag{3-4}$$

To determine the diffusion current, it is necessary to subtract the residual current. This can be achieved by extrapolating the residual current prior to the wave or by recording the response of the deaerated supporting electrolyte (blank) solution. Addition of a standard or a calibration curve are often used for quantitation. Polarograms to be compared for this purpose must be recorded in the same way.

The potential at which the current is one-half of its limiting value is called the half-wave potential, $E_{1/2}$. The half-wave potential (for electrochemically reversible couples) is related to the formal potential, E°, of the electroactive species according to

$$E_{1/2} = E^\circ + \frac{RT}{nF} \log(D_{\text{R}}/D_{\text{O}})^{1/2} \tag{3-5}$$

where D_{R} and D_{O}, are the diffusion coefficients of the reduced and oxidized forms of the electroactive species, respectively. Because of the similarity in the diffusion coefficients, the half-wave potential is usually similar to the formal potential. Thus, the half-wave potential, which is a characteristic of a particular species in a given supporting electrolyte solution, is independent of the concentration of that species. Therefore, by measuring the half-wave potential, one can identify the species responsible for an unknown polarographic wave. Typical half-wave potentials for

TABLE 3-1 Functional Groups Reducible at the Dropping Mercury Electrode

Class of Compound	Functional Group	$E_{1/2}$(V)[a]
Azo	−N=N−	−0.4
Carbon–carbon double bond[b]	−C=C−	−2.3
Carbon–carbon triple bond[b]	−C≡C−	−2.3
Carbonyl	>C=O	−2.2
Disulfide	S−S	−0.3
Nitro	NO_2	−0.9
Organic halides	C−X (X = Br, Cl, I)	−1.5
Quinone	C=O	−0.1

[a] Against the saturated calomel electrode at pH 7.
[b] Conjugated with a similar bond or with an aromatic ring.

several reducible organic functionalities common in organic compounds are given in Table 3-1. Compounds containing these functionalities are ideal candidates for polarographic measurements. (Additional oxidizable compounds can be measured using solid-electrode voltammetric protocols.) Since neutral compounds are involved, such organic polarographic reductions commonly involve hydrogen ions. Such reactions can be represented as

$$\mathrm{R} + n\mathrm{H}^+ + ne^- \rightleftharpoons \mathrm{RH}_n \tag{3-6}$$

where R and RH_n are oxidized and reduced forms of the organic molecule. For such processes, the half-wave potential will be a function of pH (with a negative shift of about $59\,\mathrm{mV}/n$ for each unit increase in pH, due to decreasing availability of protons). Thus, in organic polarography, good buffering is vital for generating reproducible results. Reactions of organic compounds are also often slower and more complex than those of inorganic cations.

For the reduction of metal complexes, the half-wave potential is shifted to more negative potentials (vs. the true metal ion), reflecting the additional energy required for the decomposition of the complex. Consider the reversible reduction of a hypothetical metal complex, ML_p:

$$\mathrm{ML}_p + ne^- + \mathrm{Hg} \rightleftharpoons \mathrm{M(Hg)} + p\mathrm{L} \tag{3-7}$$

where L is the free ligand and p is the stoichiometric number. (The charges are omitted for simplicity.) The difference between the half-wave potential for the complexed and uncomplexed metal ion is given by (2):

$$(E_{1/2})_c - (E_{1/2})_{\text{free}} = \frac{RT}{nF}\ \ln K_d - \frac{RT}{nF}\ p\ \ln[\mathrm{L}] + \frac{RT}{nF}\ \ln\left(\frac{D_{\text{free}}}{D_c}\right)^{1/2} \tag{3-8}$$

where K_d is the formation constant. The stoichiometric number can thus be computed from the slope of a plot of $(E_{1/2})_c$ vs. In [L]. It is possible to exploit equation (3-8) to improve the resolution between two neighboring polarographic waves, based on a careful choice of the ligand and its concentration.

For reversible systems (with fast electron-transfer kinetics), the shape of the polarographic wave can be described by the *Heyrovsky–Ilkovic equation*:

$$E = E_{1/2} + \frac{RT}{nF} \ln\left(\frac{i_d - i}{i}\right) \tag{3-9}$$

It follows from equation (3-9) that a plot of E vs. $\log[(i_d - i)/i]$ should yield a straight line with a slope of $0.059/n$ at 25°C. Such a plot offers a convenient method for the determination of n. In addition, the intercept of this line will be the half-wave potential. Another way to estimate n is to measure $(E_{3/4} - E_{1/4})$, which corresponds to $56.4/n$ mV for a reversible system. ($E_{3/4}$ and $E_{1/4}$ are the potentials for which $i = 0.75i_d$ and $i = 0.25i_d$, respectively.) It should be emphasized that many polarographic processes, especially those of organic compounds, are not reversible. For those that depart from reversibility, the wave is "drawn out," with the current not rising steeply, as is shown in Figure 3-2. The shape of the polarographic response for an irreversible reduction process is given by

$$E = E^\circ + \frac{RT}{\alpha nF} \ln\left[1.35k_f \left(\frac{i_d - i}{i}\right)\left(\frac{t}{D}\right)^{1/2}\right] \tag{3-10}$$

where α is the transfer coefficient and k_f is the rate constant of the forward reaction.

In a few instances, the polarographic wave is accompanied by a large peak (where the current rises to a maximum before returning to the expected diffusion current plateau). Such an undesired peak, known as the polarographic maximum, is attributed to a hydrodynamic flow of the solution around the expanding mercury drop, and can be suppressed by adding a small amount of a surface-active material (such as Triton X-100).

When the sample solution contains more than one reducible species, diffusion currents resulting from each of them are observed. The heights of the successive waves can be used to measure the individual analytes, provided there is a reasonable difference (>0.2 V) between the half-wave potentials. The baseline for measuring the limiting current of the second species is obtained by extrapolation of the limiting current of the first process. With a potential window of about 2 V, five to seven individual polarographic waves might be observed. Solution parameters, such as the pH or concentration of complexing agents, can be manipulated to deliberately shift the peak potential and hence improve the resolution of two successive waves. Successive waves are observed also for samples containing a single analyte that undergoes reduction in two or more steps (e.g., 1,4-benzodiazepine or tetracycline).

The background (residual) current that flows in the absence of the electroactive species of interest is composed of contributions due to double-layer charging process and redox reactions of impurities, as well as of the solvent, electrolyte, or electrode.

The latter processes (e.g., hydrogen evolution and mercury oxidation) are those that limit the working potential range. In acidic solutions, the negative background limit shifts by approximately 59 mV per pH unit to more positive potentials with decreasing pH. Within the working potential window, the charging current is the major component of the background (which limits the detection limit). It is the current required to charge the electrode–solution interface (which acts as a capacitor) upon changing the potential or the electrode area (see Section 1-3). Thus, the charging current is present in all conventional polarographic experiments, regardless of the purity of reagents. Because of the negligible potential change during the drop life, the charging associated with the potential scan can be ignored. The value of the polarographic charging current thus depends on the time change of the electrode area:

$$i_c = \frac{dq}{dt} = (E - E_{\text{pzc}})C_{\text{dl}} \frac{dA}{dt} \tag{3-11}$$

By substituting the derivative of the area with time (from equation 3-2) one obtains

$$i_c = 0.00567(E - E_{\text{pzc}})C_{\text{dl}}m^{2/3}\ t^{-1/3} \tag{3-12}$$

Hence, the charging current decreases during the drop life, while the diffusion current increases (Figure 3-3):

$$i_{\text{total}}(t) = i_d(t) + i_c(t) = kt^{1/6} + k't^{-1/3} \tag{3-13}$$

The analytical significance of the charging current depends upon how large it is relative to the diffusion current of interest. When the analyte concentration is in the range 10^{-4} to 10^{-2} M, the current is mostly faradaic, and a well-defined polarographic wave is obtained. However, at low concentrations of the analyte, the charging current contribution becomes comparable to the analytical signal, and the measurement becomes impossible. The charging current thus limits the detection

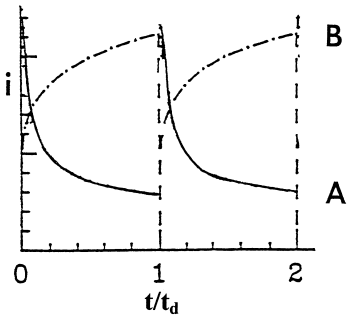

FIGURE 3-3 Variation of the charging (curve A) and diffusion currents (curves B) during the lifetime of a drop.

limit of classical polarography to the 5×10^{-6} to 1×10^{-5} M region. Lower detection limits are obtained for analytes with redox potentials closer to E_{pzc}, i.e., when i_c approaches its smaller value, (equation 3-11). Advanced (pulse) polarographic techniques, discussed in Section 3-3, offer lower detection limits by taking advantage of the different time dependences of the analytical and charging currents (equation 3-13). Such developments have led to a decrease in the utility of DC polarography.

3-3 PULSE VOLTAMMETRY

Pulse voltammetric techniques, introduced by Barker and Jenkin (3), are aimed at lowering the detection limits of voltammetric measurements. By substantially increasing the ratio between the faradaic and nonfaradaic currents, such techniques permit convenient quantitation down to the 10^{-8} M concentration level. Because of their greatly improved performance, modern pulse techniques have largely supplanted classical polarography in the analytical laboratory. The various pulse techniques are all based on a sampled current potential-step (chronoamperometric) experiment. A sequence of such potential steps, each with a duration of about 50 ms, is applied to the working electrode. After the potential is stepped, the charging current decays rapidly (exponentially) to a negligible value (equation 1-49), while the faradaic current decays more slowly. Thus, by sampling the current late in the pulse life, an effective discrimination against the charging current is achieved.

The difference between the various pulse voltammetric techniques is the excitation waveform and the current sampling regime. With both normal-pulse and differential-pulse voltammetry, one potential pulse is applied for each drop of mercury when the DME is used. (Both techniques can also be used at solid electrodes.) By controlling the drop time (with a mechanical knocker), the pulse is synchronized with the maximum growth of the mercury drop. At this point, near the end of the drop lifetime, the faradaic current reaches its maximum value, while the contribution of the charging current is minimal (based on the time dependence of the components).

3-3.1 Normal-Pulse Voltammetry

Normal-pulse voltammetry consists of a series of pulses of increasing amplitude applied to successive drops at a preselected time near the end of each drop lifetime (4). Such a normal-pulse train is shown in Figure 3-4. Between the pulses, the electrode is kept at a constant (base) potential at which no reaction of the analyte occurs. The amplitude of the pulse increases linearly with each drop. The current is measured about 40 ms after the pulse is applied, at which time the contribution of the charging current is nearly zero. In addition, because of the short pulse duration, the diffusion layer is thinner than that in DC polarography (i.e., there is larger flux of

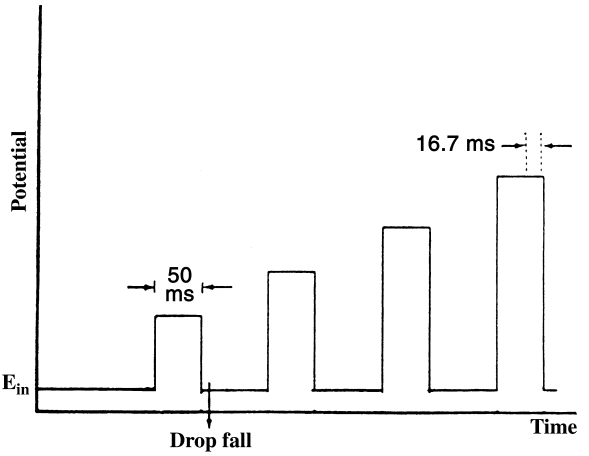

FIGURE 3-4 Excitation signal for normal pulse voltammetry.

analyte) and hence the faradaic current is increased. The resulting voltammogram has a sigmoidal shape, with a limiting current given by a modified Cottrell equation:

$$i_l = \frac{nFAD^{1/2}C}{\sqrt{\pi t_m}} \tag{3-14}$$

where t_m is the time after application of the pulse at which the current is sampled. This current can be compared to that measured in DC polarography:

$$\frac{i_{l,\mathrm{NF}}}{i_{l,\mathrm{DC}}} = \left(\frac{3t_d}{7t_m}\right)^{1/2} \tag{3-15}$$

This ratio predicts that normal-pulse polarography will be 5 to 10 times more sensitive than DC polarography (for typical values of t_d and t_m). Normal-pulse polarography may also be advantageous when using solid electrodes. In particular, by maintaining a low initial potential during most of the operation, it is possible to alleviate surface fouling problems (due to adsorbed reaction products).

A related technique, reverse-pulse voltammetry, has a pulse sequence that is a mirror image of that of normal-pulse voltammetry (5). In this case, the initial potential is on the plateau of the wave (i.e., where reduction occurs), and a series of positive-going pulses of decreasing amplitude is applied.

3-3.2 Differential-Pulse Voltammetry

Differential-pulse voltammetry is an extremely useful technique for measuring trace levels of organic and inorganic species. In differential-pulse voltammetry, fixed-magnitude pulses—superimposed on a linear potential ramp—are applied to the working electrode at a time just before the end of the drop (Figure 3-5). The current

is sampled twice, just before the pulse application (at 1) and again late in the pulse life (after ~40 ms, at 2, when the charging current has decayed). The first current is instrumentally subtracted from the second, and this current difference [$\Delta i = i(t_2) - i(t_1)$] is plotted versus the applied potential. The resulting differential pulse voltammogram consists of current peaks, the height of which is directly proportional to the concentration of the corresponding analytes:

$$i_p = \frac{nFAD^{1/2}C}{\sqrt{\pi t_m}} \left(\frac{1-\sigma}{1+\sigma}\right) \tag{3-16}$$

where $\sigma = \exp[(nF/RT)(\Delta E/2)]$. ($\Delta E$ is the pulse amplitude.) The maximum value of the quotient $(1-\sigma)/(1+\sigma)$, obtained for large pulse amplitudes, is unity (6).

The peak potential (E_p) can be used to identify the species, as it occurs near the polarographic half-wave potential:

$$E_p = E_{1/2} - \Delta E/2 \tag{3-17}$$

The differential-pulse operation results in a very effective correction of the charging background current. The charging-current contribution to the differential current is negligible, as described by

$$\Delta i_c \simeq -0.00567 C_i \, \Delta E \, m^{2/3} t^{-1/3} \tag{3-18}$$

where C_i is the integral capacitance. Such a background contribution is smaller by more than an order of magnitude than the charging current of normal-pulse voltammetry. Accordingly, differential pulse voltammetry allows measurements at concentrations as low as 10^{-8} M (about 1 μg L^{-1}). The improved detectability over DC polarography is demonstrated in Figure 3-6, which compares the response of the two techniques for the antibiotic chloramphenicol present at the 1.3×10^{-5} M level. Similarly, the improvements over normal-pulse polarography are illustrated in Figure 3-7.

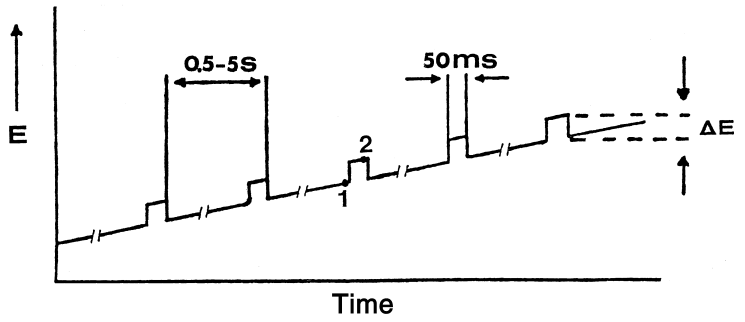

FIGURE 3-5 Excitation signal for differential-pulse voltammetry.

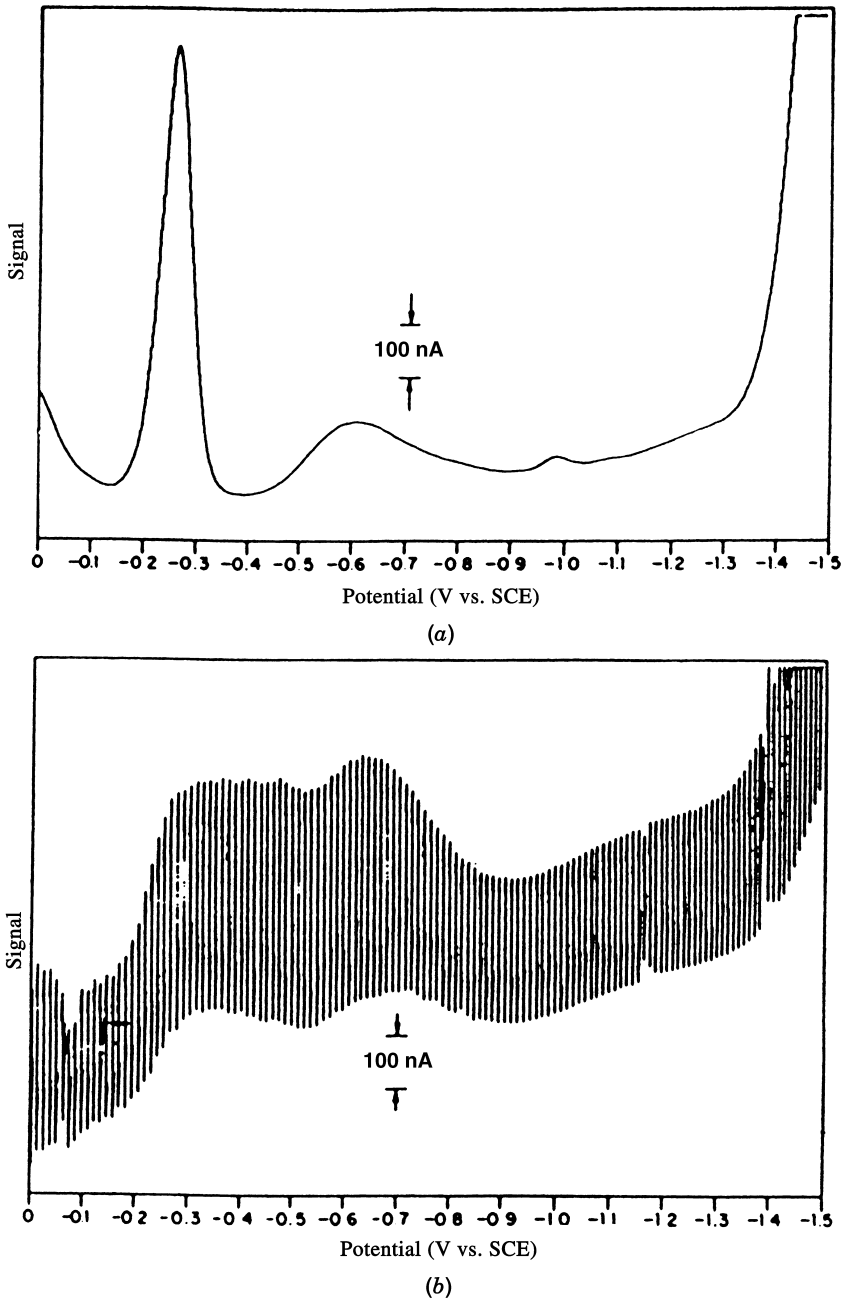

FIGURE 3-6 Differential pulse (*a*) and DC (*b*) polarograms for a 1.3×10^{-5} M chloramphenicol solution. (Reproduced with permission from reference 7.)

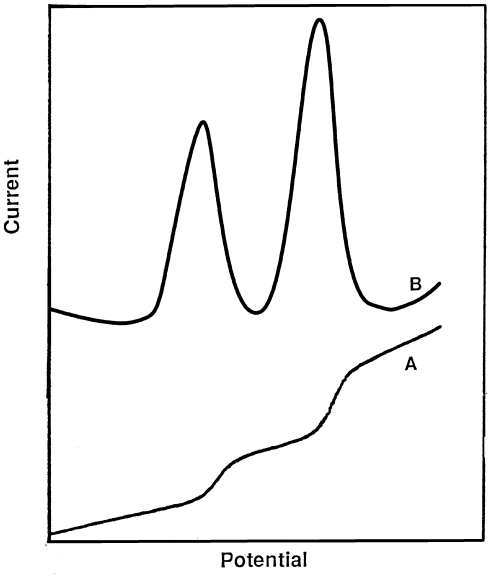

FIGURE 3-7 Normal-pulse (curve A) and differential-pulse (curve B) polarograms for a mixture of 1 mg L^{-1} cadmium and lead ions. The electrolyte is 0.1 M HNO_3.

The peak-shaped response of differential-pulse measurements results in improved resolution between two species with similar redox potentials. In various situations, peaks separated by 50 mV may be measured. Such quantitation depends not only upon the corresponding peak potentials but also on the widths of the peak. The width of the peak (at half-height) is related to the electron stoichiometry:

$$W_{1/2} = \frac{3.52RT}{nF} \tag{3-19}$$

and thus corresponds to 30.1 mV for $n = 1$ (at 25°C). The peak-shaped response, coupled with the flat background current, makes the technique particularly useful for analysis of mixtures.

The selection of the pulse amplitude and potential scan rate usually requires a trade-off among sensitivity, resolution, and speed. For example, larger pulse amplitudes result in larger and broader peaks. Pulse amplitudes of 25–50 mV, coupled with a 5 mV s^{-1} scan rate, are commonly employed. Irreversible redox systems result in lower and broader current peaks (i.e., inferior sensitivity and resolution) compared with those predicted for reversible systems (6). In addition to improvements in sensitivity and resolution, the technique can provide information about the chemical form in which the analyte appears (oxidation states, complexation, etc.).

3-3.3 Square-Wave Voltammetry

Square-wave voltammetry is a large-amplitude differential technique in which a waveform composed of a symmetrical square wave, superimposed on a base staircase potential, is applied to the working electrode (8) (Figure 3-8). The current is sampled twice during each square-wave cycle, once at the end of the forward pulse (at t_1) and once at the end of the reverse pulse (at t_2). Since the square-wave modulation amplitude is very large, the reverse pulses cause the reverse reaction of the product (of the forward pulse). The difference between the two measurements is plotted versus the base staircase potential. A dimensionless plot of the theoretical forward, reverse, and difference currents is given in Figure 3-9 for a rapid reversible redox system. The resulting peak-shaped voltammogram is symmetrical about the half-wave potential, and the peak current is proportional to the concentration. Excellent sensitivity accrues from the fact that the net current is larger than either the forward or reverse components (since it is the difference between them); the sensitivity is higher than that of differential pulse polarography (in which the reverse current is not used). Coupled with the effective discrimination against the charging background current, very low detection limits near 1×10^{-8} M can be attained. Comparison of square-wave and differential pulse voltammetry for reversible and irreversible cases indicated that the square-wave currents are 4 and 3.3 times higher, respectively, than the analogous differential-pulse response (10).

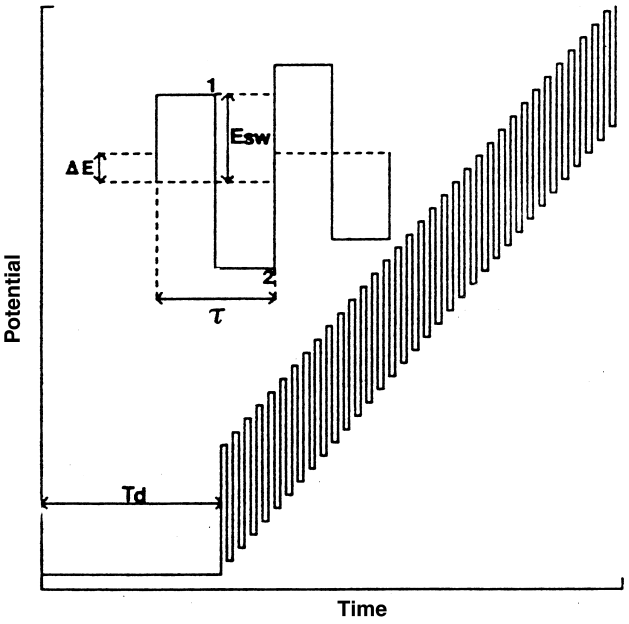

FIGURE 3-8 Square-wave waveform showing the amplitude, E_{sw}; step height, ΔE; square-wave period, τ; delay time, T_d; and current measurement times, 1 and 2. (Reproduced with permission from reference 9.)

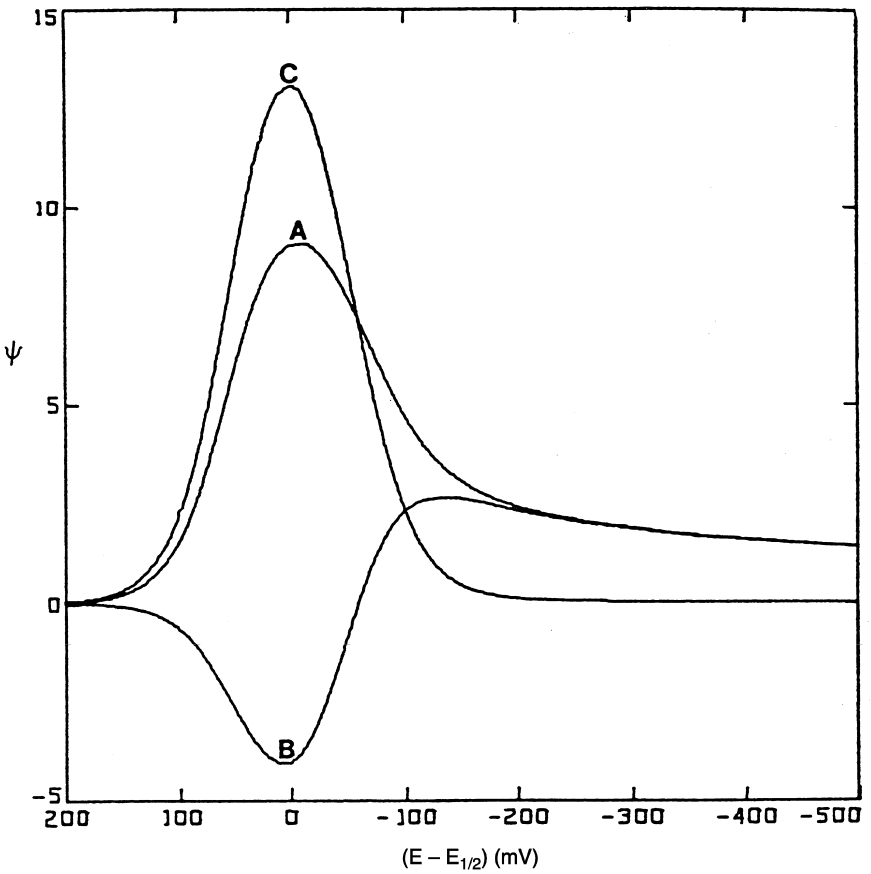

FIGURE 3-9 Square-wave voltammograms for reversible electron transfer. Curve A: forward current. Curve B: reverse current. Curve C: net current. (Reproduced with permission from reference 9.)

The major advantage of square-wave voltammetry is its speed. The effective scan rate is given by $f\ \Delta E_s$. The term f is square-wave frequency (in Hz) and ΔE_s is the step height. Frequencies of 1 to 100 cycles per second permit the use of extremely fast potential scan rates. For example, if $\Delta E_s = 10\,\text{mV}$ and $f = 50\,\text{Hz}$, then the effective scan rate is $0.5\ \text{V s}^{-1}$. As a result, the analysis time is drastically reduced; a complete voltammogram can be recorded within a few seconds, as compared with about 2–3 minutes in differential-pulse voltammetry. Because of the fast scan rates, the entire voltammogram is recorded on a single mercury drop. Hence, such an operation consumes few drops (compared to other pulse techniques). The inherent speed of square-wave voltammetry can greatly increase sample throughputs in batch (11) and flow (12) analytical operations. In addition, square-wave voltammetric detection for liquid chromatography and capillary electrophoresis can be used to

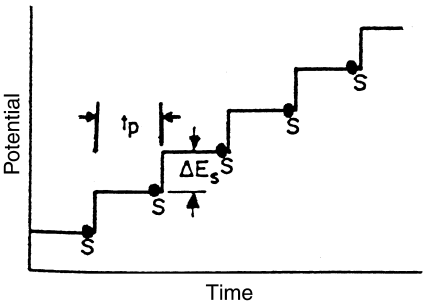

FIGURE 3-10 Potential–time waveform used in staircase voltammetry.

resolve coeluting or comigrating species and assist in the peak identification (13, 14). Kinetic studies can also benefit from the rapid scanning capability and the reversal nature of square-wave voltammetry.

3-3.4 Staircase Voltammetry

Staircase voltammetry has been proposed as a useful tool for rejecting the background charging current. The potential–time waveform involves successive potential steps of ~10 mV height and about 50 ms duration (Figure 3-10). The current is sampled at the end of each step, where the charging current has decayed to a negligible value. Hence, this waveform couples the discrimination against the charging current with the experimental speed of linear-scan voltammetry. Such an operation results in a peak-shaped current response, similar to that of linear-scan experiments. Indeed, as the steps become smaller, the equations for the staircase voltammetric response converge with those of linear-scan voltammetry (15). As such, staircase voltammetry can be considered as the digital version of linear-scan voltammetry. Similarly, cyclic staircase voltammetric experiments, in which the direction of the potential steps is reversed at a switching potential, result in a voltammetric response resembling that of cyclic voltammetry (but with a much-reduced charging-current contribution).

3-4 AC VOLTAMMETRY

Alternating current (AC) voltammetry is a frequency-domain technique that involves the superimposition of a small-amplitude AC voltage on a linear ramp (Figure 3-11). Usually the alternating potential has a frequency of 50–100 Hz and an amplitude of 10–20 mV. The AC signal thus causes a perturbation in the surface concentration, around the concentration maintained by the DC potential ramp. The resulting AC current is displayed versus the potential. Such a voltammogram shows a peak, the potential of which is the same as the polarographic half-wave potential. (In this region the sinusoid has maximum impact on the surface concentration, i.e., on the

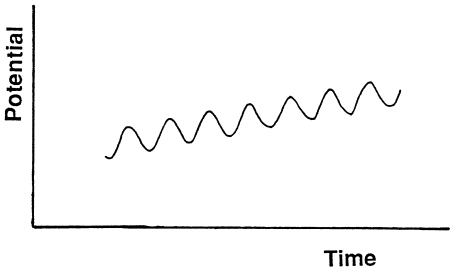

FIGURE 3-11 Potential–time waveform used in alternating current (AC) voltammetry.

current.) For a reversible system, such a response is actually the derivative of the DC polarographic response. The height of the AC voltammetric peak is proportional to the concentration of the analyte and, for a reversible reaction, to the square root of the frequency (ω):

$$i_p = \frac{n^2F^2A\omega^{1/2}D^{1/2}C\ \Delta E}{4RT} \tag{3-20}$$

The term ΔE is the amplitude. The peak width is independent of the AC frequency, and is $90.4/n$ mV (at 25°C).

The detection of the AC component allows one to separate the contributions of the faradaic and charging currents. The former is phase shifted 45° relative to the applied sinusoidal potential, while the background component is 90° out of phase. The charging current is thus rejected using a phase-sensitive lock-in amplifier (able to separate the in-phase and out-of-phase current components). As a result, reversible electrode reactions yield a detection limit around 5×10^{-7} M.

Substantial loss in sensitivity is expected for analytes with slow electron-transfer kinetics. This may be advantageous for measurements of species with fast electron-transfer kinetics in the presence of a species (e.g., dissolved oxygen) that is irreversible. (For the same reason, the technique is very useful for the study of electron processes.) Theoretical discussions on AC voltammetry are available in the literature (16–18).

3-5 STRIPPING ANALYSIS

Stripping analysis is an extremely sensitive electrochemical technique for measuring trace metals (19,20). Its remarkable sensitivity is attributed to the combination of an effective preconcentration step with advanced measurement procedures that generate an extremely favorable signal-to-background ratio. Since the metals are preconcentrated into the electrode by factors of 100 to 1000, detection limits are lowered by 2 to 3 orders of magnitude compared to solution-phase voltammetric measurements. Hence, four to six metals can be measured simultaneously in various matrices at concentration levels down to 10^{-10} M, utilizing relatively inexpensive

instrumentation. The ability to obtain such low detection limits depends strongly on the degree to which contamination can be minimized. Expertise in ultratrace chemistry is required.

Essentially, stripping analysis is a two-step technique. The first, or deposition, step involves the electrolytic deposition of a small portion of the metal ions in solution into the mercury electrode to preconcentrate the metals. This is followed by the stripping step (the measurement step), which involves the dissolution (stripping) of the deposit. Different versions of stripping analysis can be employed, depending upon the nature of the deposition and measurement steps.

3-5.1 Anodic Stripping Voltammetry

Anodic stripping voltammetry (ASV) is the most widely used form of stripping analysis. In this case, the metals are preconcentrated by electrodeposition into a small-volume mercury electrode (a thin mercury film or a hanging mercury drop). The preconcentration is done by cathodic deposition at a controlled time and potential. The deposition potential is usually 0.3–0.5 V more negative than E° for the least easily reduced metal ion to be determined. The metal ions reach the mercury electrode by diffusion and convection, where they are reduced and concentrated as amalgams:

$$M^{n+} + ne^- + Hg \rightarrow M(Hg) \tag{3-21}$$

The convective transport is achieved by electrode rotation or stirring of the solution (in conjunction with the mercury film electrode) or by stirring of the solution (when using the hanging mercury drop electrode). Quiescent solutions can be used when using mercury ultramicroelectrodes. The duration of the deposition step is selected according to the concentration level of the metal ions in question, from less than 0.5 min at the 10^{-7} M level to about 20 min at the 10^{-10} M level. The concentration of the metal in the amalgam, C_{Hg}, is given by Faraday's law:

$$C_{Hg} = \frac{i_l t_d}{nFV_{Hg}} \tag{3-22}$$

where i_l is the limiting current for the deposition of the metal, t_d is the length of the deposition period, and V_{Hg} is the volume of the mercury electrode. The deposition current is related to the flux of the metal ion at the surface. The total amount of metal plated represents a small (but reproducible) fraction of the metal present in the bulk solution.

Following the preselected time of the deposition, the forced convection is stopped, and the potential is scanned anodically, either linearly or in a more sensitive potential–time (pulse) waveform that discriminates against the charging background current (usually square-wave or differential-pulse ramps). Such pulse excitations also offer reduced oxygen interferences and analyte replating, respectively. During this

anodic scan, the amalgamated metals are reoxidized, stripped out of the electrode (in an order that is a function of each metal standard potential), and a current flows:

$$\mathrm{M(Hg)} \rightarrow \mathrm{M}^{n+} + ne^- + \mathrm{Hg} \tag{3-23}$$

The potential–time sequence used in ASV, along with the resulting stripping voltammogram, is shown in Figure 3-12. The voltammetric peak reflects the time-dependent concentration gradient of the metal in the mercury electrode during the potential scan. Peak potentials serve to identify the metals in the sample. The peak current depends upon various parameters of the deposition and stripping steps, as well as on the characteristics of the metal ion and the electrode geometry. For example, for a mercury film electrode, the peak current is given by

$$i_p = \frac{n^2F^2v^{1/2}AlC_{\mathrm{Hg}}}{2.7RT} \tag{3-24}$$

where A and l are the area and thickness, respectively, of the film and v is the potential scan rate (during the stripping). The corresponding concentration profile in the film and nearby solution is displayed in Figure 3-13. (For very thin mercury films, diffusion in the film can be ignored and the peak current is directly proportional to the scan rate.) For the hanging mercury drop, the following expression describes the stripping peak current:

$$i_p = 2.72 \times 10^5\ n^{3/2}AD^{1/2}v^{1/2}C_{\mathrm{Hg}} \tag{3-25}$$

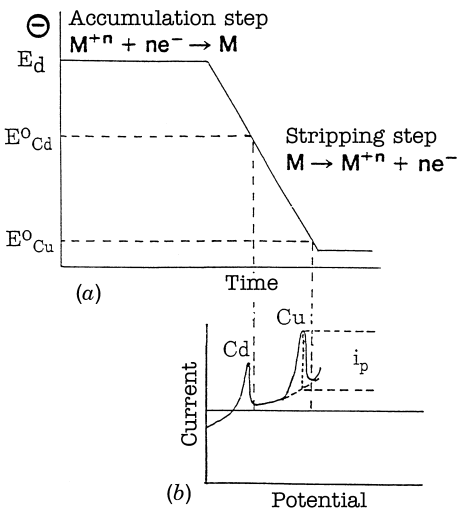

FIGURE 3-12 Anodic stripping voltammetry: the potential-time waveform (*a*), along with the resulting voltammogram (*b*).

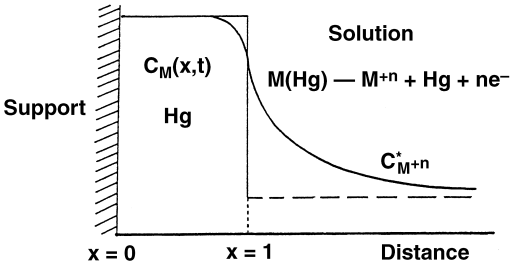

FIGURE 3-13 Concentration gradient of the metal in the mercury film electrode and nearby solution during the stripping step.

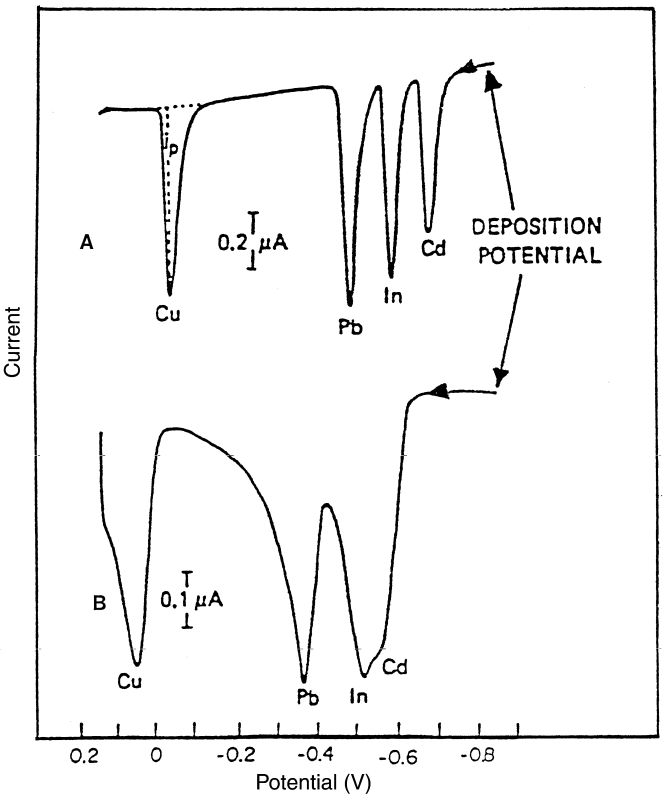

FIGURE 3-14 Stripping voltammograms for 2×10^{-7} M Cu^{2+}, Pb^{2+}, In^{3+} and Cd^{2+} at the mercury film (A) and hanging mercury drop (B) electrodes. (Reproduced with permission from reference 21.)

The mercury film electrode has a higher surface-to-volume ratio than the hanging mercury drop electrode and consequently offers a more efficient preconcentration and higher sensitivity (equations 3-22 through 3-25). In addition, the total exhaustion of thin mercury films results in sharper peaks and hence improved peak resolution in multicomponent analysis (Figure 3-14).

The major types of interferences in ASV procedures are overlapping stripping peaks caused by a similarity in the oxidation potentials (e.g., of the Pb, Tl, Cd, Sn or Bi, Cu, Sb groups), the presence of surface-active organic compounds that adsorb on the mercury electrode and inhibit the metal deposition, and the formation of intermetallic compounds (e.g., Cu-Zn) which affects the peak size and position. Knowledge of these interferences can allow prevention through adequate attention to key operations.

Improved signal-to-background characteristics can be achieved using dual-working-electrode techniques, such as ASV with collection or subtractive ASV (but at the expense of more complex instrumentation).

Other versions of stripping analysis, including potentiometric stripping, adsorptive stripping, and cathodic stripping schemes, have been developed to further expand its scope and power.

3-5.2 Potentiometric Stripping Analysis

Potentiometric stripping analysis (PSA), known also as stripping potentiometry, differs from ASV in the method used for stripping the amalgamated metals (22). In this case, the potentiostatic control is disconnected following the preconcentration, and the concentrated metals are reoxidized by an oxidizing agent [such as O_2 or Hg(II)] that is present in the solution:

$$\mathrm{M(Hg)} + \text{oxidant} \rightarrow \mathrm{M}^{n+} \tag{3-26}$$

A stirred solution is also used during the stripping step to facilitate the transport of the oxidant. Alternately, the oxidation can be carried out by passing a constant anodic current through the electrode. During the oxidation step, the variation of the working electrode potential is recorded, and a stripping curve, like the one shown in Figure 3-15a, is obtained. When the oxidation potential of a given metal is reached, the potential scan is slowed down as the oxidant (or current) is used for its stripping. A sharp potential step thus accompanies the depletion of each metal from the electrode. The resulting potentiogram thus consists of stripping plateaus, as in a redox titration curve. The transition time needed for the oxidation of a given metal, t_{M}, is a quantitative measure of the sample concentration of the metal:

$$t_M \propto C_{\mathrm{M}^{n+}} t_d / C_{\mathrm{ox}} \tag{3-27}$$

where C_{ox} is the concentration of the oxidant. Hence, the signal may be increased by decreasing the oxidant concentration. The qualitative identification relies on

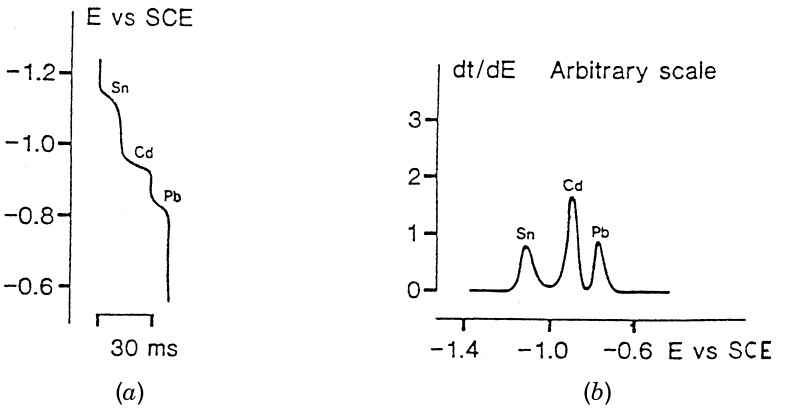

FIGURE 3-15 Stripping potentiograms for a solution containing 100 μg L^{-1} tin, cadmium, and lead; 80 s accumulation at −1.40 V. Original (*a*) and differential (*b*) displays. (Reproduced with permission from reference 22.).

potential measurements (in accordance with the Nernst equation for the amalgamated metal):

$$E = E^{\circ} + \frac{RT}{nF} \ln \frac{[M^{n+}]}{[M(Hg)]} \tag{3-28}$$

where E° denotes the standard potential for the redox couple $M^{n+}/M(Hg)$.

Modern PSA instruments use microcomputers to register fast stripping events and to convert the wave-shaped response to a more convenient peak over a flat baseline. Such a differential display of dt/dE vs. E is shown in Figure 3-15*b*. The use of nondeaerated samples represents an important advantage of PSA (over analogous ASV schemes), particularly in connection with field applications. In addition, such potential–time measurements eliminate the need for amplification when microelectrodes are concerned. By obviating the need for stirring or deoxygenating the solution, the coupling of PSA with microelectrodes permits convenient trace analysis of very small (5 μL) samples. PSA is also less susceptible to interfering surfactant effects, and hence can simplify the pretreatment of biological samples. A more detailed treatment of the theoretical foundation of PSA is given in reference 22.

About 20 amalgam-forming metals, including Pb, Sn, Cu, Zn, Cd, Bi, Sb, Tl, Ga, In and Mn, are easily measurable by stripping strategies (ASV and PSA) based on cathodic deposition onto mercury electrodes. Additional metals, such as Se, Hg, Ag, Te and As are measurable at bare solid electrodes such as carbon or gold.

3-5.3 Adsorptive Stripping Voltammetry and Potentiometry

Adsorptive stripping analysis greatly enhances the scope of stripping measurements toward numerous trace elements (23,24). This relatively new strategy involves the

formation, adsorptive accumulation, and reduction of a surface-active complex of the metal (Figure 3-16). Both voltammetric and potentiometric stripping schemes, with a negative-going potential scan or constant cathodic current, respectively, can be employed for measuring the adsorbed complex. Most procedures involve the reduction of the metal in the adsorbed complex (although it is possible also to exploit the reduction of the ligand). The response of the surface-confined species is directly related to its surface concentration, with the adsorption isotherm (commonly that of Langmuir, discussed in Section 2-1), providing the relationship between the surface and bulk concentrations of the adsorbate. As a result, calibration curves display nonlinearity at high concentrations. The maximum adsorption density is related to the size of the adsorbed complex, and to its surface concentration.

Short adsorption times (1–5 min) result in a very effective interfacial accumulation. The reduction step is also very efficient as the entire collected complex is reduced. Such a combination thus results in extremely low detection limits (10^{-10}–10^{-11} M) for important metals, including chromium, uranium, vanadium, iron, aluminum or molybdenum. Even lower levels, for example 10^{-12} M of platinum or titanium, can be measured by coupling the adsorption accumulation with catalytic reactions. In this case, the response of the accumulated complex is greatly amplified through a catalytic cycle, for example, in the presence of an oxidant. The adsorptive approach may also offer improvements in selectivity or sensitivity for metals (e.g., tin, nickel) that are also measurable by conventional stripping analysis. Examples of adsorptive stripping schemes for measuring trace metals are listed in Table 3-2. All procedures rely on a judicious choice of the chelating agent. The resulting complex should be surface active and electroactive; in addition, selective complexation can be used to enhance the overall selectivity.

Besides trace metals, adsorptive stripping voltammetry has been shown to be highly suitable for measuring organic compounds (including cardiac or anticancer drugs, nucleic acids, vitamins, and pesticides) that exhibit surface-active properties.

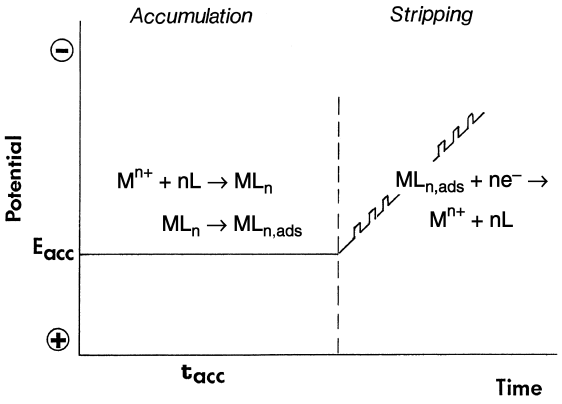

FIGURE 3-16 Accumulation and stripping steps in adsorptive stripping measurements of a metal ion (M^{n+}) in the presence of an appropriate chelating agent (L).

TABLE 3-2 Common Adsorptive Stripping Schemes for Measurement of Trace Metals

Metal	Complexing Agent	Supporting Electrolyte	Detection Limit, (M)	Reference
Al	Dihydroxyanthraquinone-sulfonic acid	BES buffer	1×10^{-9}	25
Be	Thorin	Ammonia buffer	3×10^{-9}	26
Co	Nioxime	Hepes buffer	6×10^{-12}	27
Cr	Diethylenetriamine-Pentaacetic acid	Acetate buffer	4×10^{-10}	28
Fe	Solochrome violet RS	Acetate buffer	7×10^{-10}	29
Mn	Eriochrome Black T	Pipes buffer	6×10^{-10}	30
Mo	Oxine	Hydrochloric acid	1×10^{-10}	31
Ni	Dimethylglyoxime	Ammonia buffer	1×10^{-10}	32
Pt	Formazone	Sulfuric acid	1×10^{-12}	33
Sn	Tropolone	Acetate buffer	2×10^{-10}	34
Ti	Mandelic acid	Potassium chlorate	7×10^{-12}	35
U	Oxine	Pipes buffer	2×10^{-10}	36
V	Catechol	Pipes buffer	1×10^{-10}	37

Depending on their redox activity, the quantitation of the adsorbed organic compounds may proceed through oxidation or reduction. For example, modern adsorptive stripping voltammetric and potentiometric methods represent highly sensitive tools for detecting ultratrace levels of nucleic acids. Figure 3-17 displays the adsorptive stripping potentiometric response of the carbon paste electrode for 0.5 ppm calf-thymus DNA following different adsorption times. Note the rapid increase of the oxidation peak (of the guanine nucleobase) upon extending the accumulation period. Nonelectroactive macromolecules may also be determined following their interfacial accumulation from tensammetric peaks (resulting from their adsorption–desorption mechanism).

3-5.4 Cathodic Stripping Voltammetry

Cathodic stripping voltammetry (CSV) is the "mirror image" of ASV. It involves anodic deposition of the analyte, followed by stripping in a negative-going potential scan:

$$A^{n-} + Hg \underset{\text{stripping}}{\overset{\text{deposition}}{\rightleftharpoons}} HgA + ne^- \tag{3-29}$$

The resulting reduction peak current provides the desired quantitative information. Cathodic stripping voltammetry is used to measure a wide range of organic and inorganic compounds capable of forming insoluble salts with mercury. Among these are various thiols or penicillins, as well as halide ions, cyanide, and sulfide. Highly

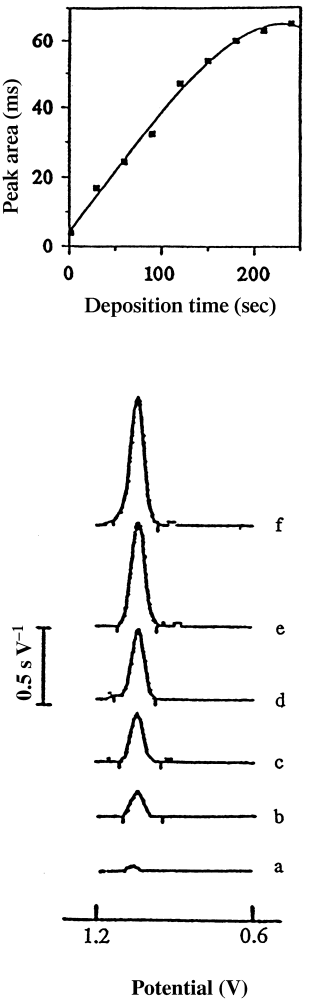

FIGURE 3-17 Adsorptive stripping potentiograms for 0.5 ppm calf-thymus DNA following different adsorption times of 1–150 s (curves a–f) (Reproduced with permission from reference 38.)

sensitive measurements can thus be performed, as illustrated in Figure 3-18 for the direct determination of subnanomolar concentrations of iodide in seawater.

Anions (e.g., halides) that form insoluble silver salts can be measured at a rotating silver disk electrode. In this, the deposition and stripping steps involve the reaction

$$Ag + X^- \rightleftharpoons AgX + e^- \qquad X^- = Cl^-, Br^- \tag{3-30}$$

Copper-based electrodes can also be employed for the same task.

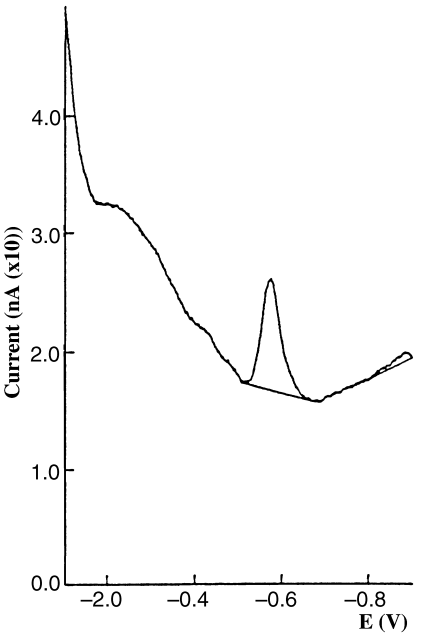

FIGURE 3-18 Stripping voltammograms for trace iodide in seawater. (Reproduced with permission from reference 39.)

3-5.5 Applications

The remarkable sensitivity, broad scope, and low cost of stripping analysis have led to its application in a large number of analytical problems. As illustrated in Figure 3-19, over 30 trace elements can conveniently be measured in various matrices by the various versions of stripping analysis. The technique has thus proved useful for the determination of numerous trace metals in environmental, industrial, and clinical samples, as well as for assays of foodstuffs, beverages, gunshot residues, and pharmaceutical formulations. Selected applications are listed in Table 3-3. Figure 3-20 displays adsorptive stripping voltammograms for chromium in various environmental (soil and ground water) samples from contaminated nuclear energy sites. Stripping analysis has also been an important technique for screening for blood lead in children (46). Many other unique applications of stripping analysis have been reported, including studies of metal speciation (oxidation state, metal–ligand interactions) in natural waters, on-line monitoring of industrial processes, in-situ oceanographic surveys, or remote environmental sensing (40,55,56).

3-6 FLOW ANALYSIS

An electrochemical detector uses the electrochemical properties of target analytes for their determination in a flowing stream. While parameters such as current, potential,

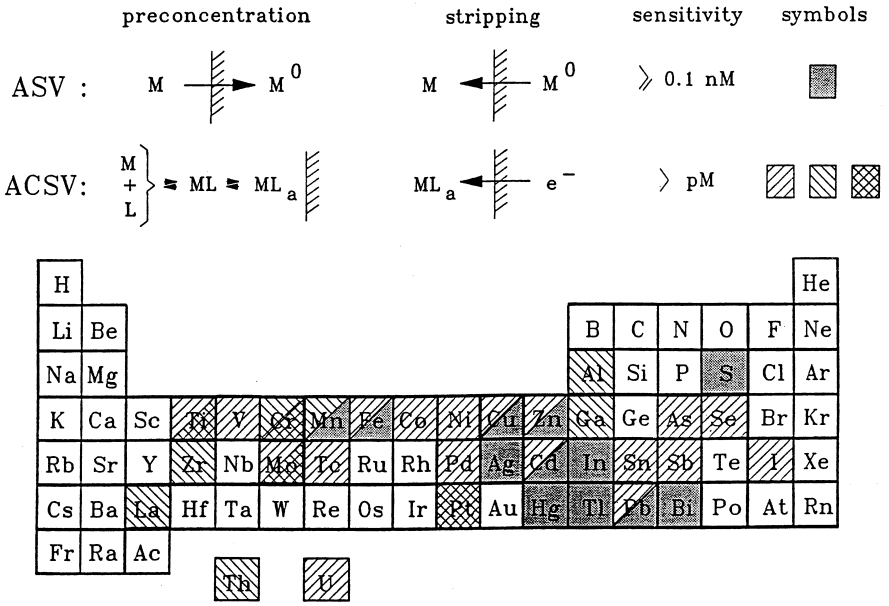

FIGURE 3-19 Elements measured by conventional ASV ■, and adsorptive stripping schemes with reduction of the element in the complex ▨, reduction of the ligand ▧, or catalytic process ▩. (Reproduced with permission from reference 40.)

TABLE 3-3 Representative Applications of Stripping Analysis

Metal	Sample Matrix	Stripping Mode	Working Electrode	Reference
Antimony	Gunshot residue	ASV	MFE	41
Cadmium	Lake water	ASV	MFE	42
Chromium	Soil	AdSV	HMDE	43
Cobalt	Sea water	AdSV	HMDE	27
Copper	Steel	ASV	HMDE	44
Iodide	Sea water	CSV	HMDE	39
Iron	Wine	AdSV	HMDE	45
Lead	Blood	PSA	MFE	46
Lead	Paint	ASV		47
Mercury	Fish	ASV	Au	48
Nickel	Plant leaves	AdSV	HMDE	49
Platinum	Gasoline	AdSV	HMDE	50
Selenium	Soil	CSV	HMDE	51
Thallium	Urine	ASV	HMDE	52
Titanium	Sea water	AdSV	HMDE	35
Uranium	Ground water	AdSV	HMDE	53
Zinc	Eye tissue	ASV	HMDE	54

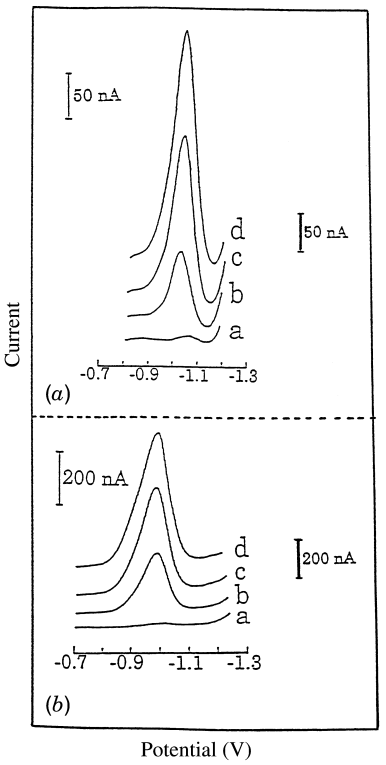

FIGURE 3-20 Adsorptive stripping voltammograms of chromium in ground water (*a*) and soil (*b*) samples, using cupferron as a chelating agent. (*a*) Curve a, response for electrolyte; Curve b, same as a but after spiking 20 μL of the sample (500-fold dilution); curves c and d, same as b, but after additions of 0.1 μg L^{-1} chromium; 20 s adsorption. (*b*) Curve a, response for the electrolyte; curve b, same as a but after spiking 5 μL^{-1} of the soil extract (2000-fold dilution); curves c and d, same as b but after additions of 0.5 μL^{-1} chromium; 15 s adsorption. (Reproduced with permission from reference 43.)

conductivity, and capacitance can be monitored by various electrochemical detectors, our discussion will focus primarily on the most popular constant-potential measurements. Controlled-potential detectors are ideally suited for monitoring analytes that are electroactive at modest potentials. Such devices are characterized by a remarkable sensitivity (down to the picogram level), high selectivity (toward electroactive species), wide linear range, low dead volumes, fast response, and relatively simple and inexpensive instrumentation. Such detectors are commonly used in many clinical, environmental, and industrial laboratories in connection with automated flow systems (e.g., flow injection analyzers) or separation techniques (particularly liquid chromatography and more recently capillary zone electrophoresis and on-line microdialysis). Such coupling with advanced separation steps allows electroanalysis to address highly complex samples.

3-6.1 Principles

Electrochemical detection is usually performed by controlling the potential of the working electrode at a fixed value (corresponding to the limiting current plateau region of the compounds of interest) and monitoring the current as a function of time. The current response thus generated reflects the concentration profiles of these compounds as they pass through the detector. Detection for liquid chromatography or flow injection systems results in sharp current peaks (reflecting the passage of the eluted analyte or sample zone, respectively). Accordingly, the magnitude of the peak current serves as a measure of the concentration. Typical response peaks recorded during an automated flow injection operation are displayed in Figure 3-21. The current peaks are superimposed on a constant background current (caused by redox reactions of the mobile phase or carrier solutions). Larger background currents, expected at high potentials, result in increased (flow rate-dependent) noise level. In particular, the cathodic detection of reducible species is hampered by the presence of traces of oxygen in the flowing solution. Such background noise is strongly influenced by the pulsation of the pump.

The applied potential affects not only the sensitivity and signal-to-noise characteristics but also the selectivity of amperometric measurements. In general, a lower potential is more selective, and a higher one more universal. Thus, compounds undergoing redox potentials at lower potentials can be detected with greater selectivity. The selection of the applied potential relies on the construction of

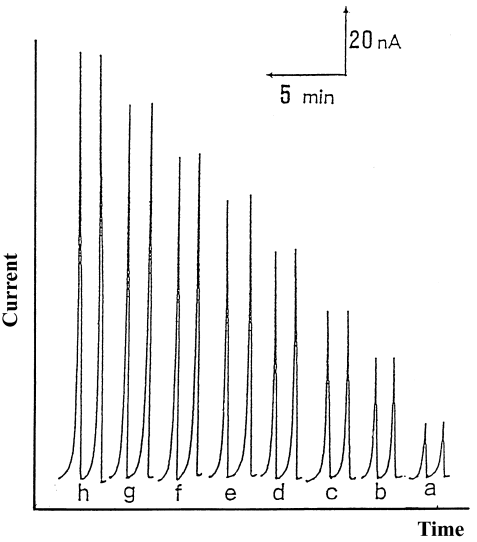

FIGURE 3-21 Typical amperometric readout during automated flow injection assays of ethanol at an enzyme carbon-paste electrode. Peaks a through h: 2×10^{-5} M to 1.6×10^{-4} M ethanol.

hydrodynamic voltammograms. These can be obtained by making repeated flow injections of the analyte solution while recording the current at different potentials. The resulting voltammogram has a characteristic wave (sigmoidal) shape. Although it is common to operate the detector on the limiting-current plateau region, a lowering of the operating potential (to the rising portion of the wave) can be used to improve the selectivity and lower the detection limit. Comparison of hydrodynamic voltammograms for the sample and standard solutions can provide important qualitative information.

Depending on their conversion efficiency, electrochemical detectors can be divided into two categories: those that electrolyze only a negligible fraction (0.1–5%) of the electroactive species passing through the detector (amperometric detectors), and those for which the conversion efficiency approaches 100% (coulometric detectors). Unfortunately, the increased conversion efficiency of the analyte is accompanied by a similar increase for the electrolyte (background) reactions, and no lowering of detection limits is realized.

3-6.2 Cell Design

A wide range of cell designs have been used for electrochemical monitoring of flowing streams. The cell design must fulfill the requirements of high signal-to-noise ratio, low dead volume, well-defined hydrodynamics, small ohmic drop, and ease of construction and maintenance (polishing). In addition, the reference and counter electrodes should be located on the downstream side of the working electrode, so that reaction products at the counter electrode or leakage from the reference electrode do not interfere with the working electrode.

The most widely used amperometric detectors are based on the thin-layer and wall-jet configurations (Figure 3-22). The thin-layer cell relies on a thin layer of solution that flows parallel to the planar electrode surface, which is imbedded in a

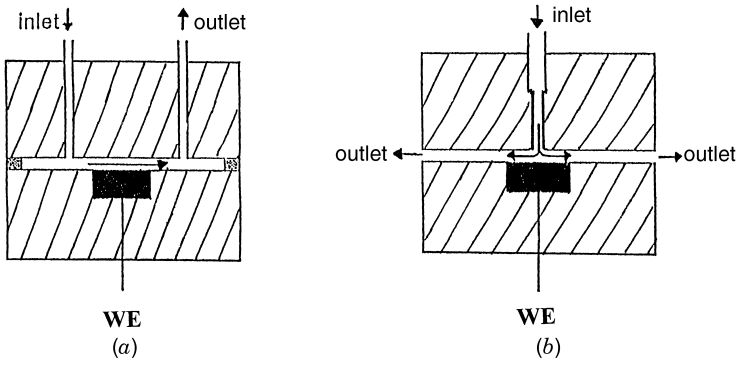

FIGURE 3-22 Common detector configurations: (*a*) thin-layer (channel) and (*b*) wall-jet flow cells. WE = working electrode.

rectangular channel. The flow channel is formed by two plastic blocks pressing a thin Teflon gasket, which defines the very small dead volume (~1 μL). In the wall-jet design, the stream flows from a nozzle perpendicularly onto a flat electrode surface (the wall), and then spreads radially over the surface. The electrode diameter is significantly larger than that of the nozzle inlet. Since the jet remains intact up to quite large inlet–electrode separations, it is possible to employ large-volume wall-jet detectors that offer decreased sensitivity to the properties of the mobile phase and simplified fabrication.

It is possible to employ detectors with solutions flowing over a static mercury drop electrode or a carbon-fiber microelectrode, or to use flow-through electrodes, with the electrode simply an open tube or porous matrix. The latter can offer complete electrolysis, that is coulometric detection. The extremely small dimensions of ultramicroelectrodes (discussed in Section 4-5.4) offer the advantages of flow rate independence (and hence a low noise level) and operation in nonconductive mobile phases (such as those of normal-phase chromatography or supercritical fluid chromatography). Ultramicroelectrodes can also greatly benefit modern microseparation techniques such as open-tubular liquid chromatography or capillary zone electrophoresis (CZE) (57). For example, cylindrical-shaped carbon or copper fibers can be inserted into the end of the capillary electrophoresis separation capillary (e.g., Figure 3-23). Such alignment of the working electrode with the end of the capillary represents a challenge in combining electrochemistry with CZE.

CZE has recently established itself as an important separation tool due to its impressive separation power. Since CZE separations rely on the application of strong electric fields for separating the analytes, it is essential to isolate the low detection potential from the high voltage (10–30 kV) used to affect the separation (59, 59a). This can be accomplished by using a decoupling device (e.g., Nafion joint, porous glass) or via end-column detection (i.e., placement of the detector opposite to the capillary outlet in a wall-jet configuration). The latter relies on the dramatic drop of the potential across small capillaries (of 25 μm or less). The distance between the detector and the capillary outlet should be as short as possible, as needed for

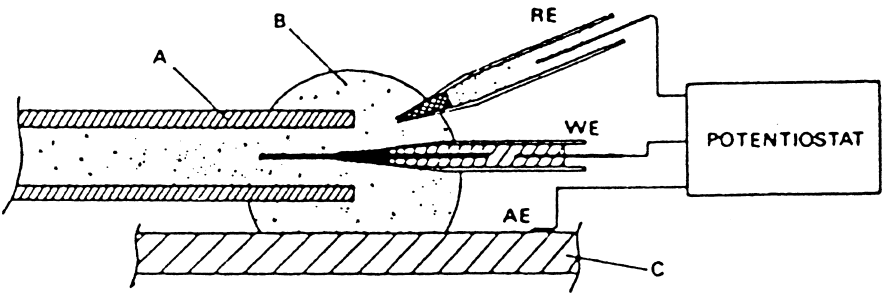

FIGURE 3-23 Schematic of a carbon-fiber amperometric detector for capillary electrophoresis: A, fused silica capillary; B, eluent drop; C, stainless steel plate; RE, reference electrode; WE, working electrode, AE, auxiliary electrode. (Reproduced with permission from reference 58.)

minimizing postcapillary zone broadening. Figure 3-24 depicts a typical end-column electropherogram for femtomole quantities of dopamine, isoproterenol, and catechol. Microfabricated electrochemical detectors are also being developed for on-chip integration with microscale separation systems, such as capillary electrophoresis (61, 61a), and for other chip-based analytical microsystems (e.g., "Lab-on-a-Chip") discussed in Section 6-3. Since the sensitivity of electrochemical detection is not compromised by the low volumes used in CZE systems, extremely low mass detection limits (in the attomole range) can be obtained. Such high sensitivity toward easily oxidizable or reducible analytes rivals that of laser-induced fluorescence (which is currently the method of choice for most CZE applications), and makes CZE/electrochemistry an ideal tool for assay of many small-volume samples.

3-6.3 Mass Transport and Current Response

Well-defined hydrodynamic conditions, with high rate of mass transport, are essential for successful use of electrochemical detectors. Based on the Nernst approximate approach, the thickness of the diffusion layer (δ) is empirically related to the solution flow rate (U) via

$$\delta = \frac{B}{U^{\alpha}} \tag{3-31}$$

where B and α are constants for a given set of conditions, with α ranging between 0.33 and 1.0. By substituting equation (3-31) in the general current response for

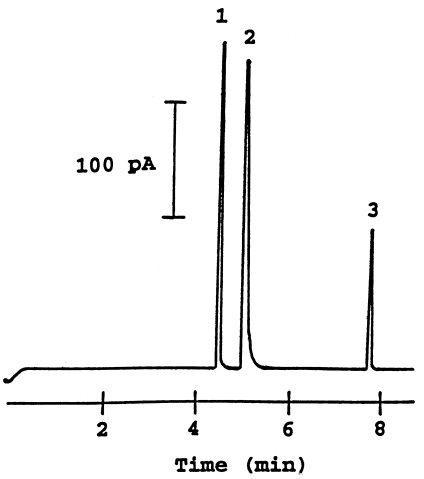

FIGURE 3-24 Electrophoretic separation of catechols with end-column detection. Detection potential, +0.8 V; separation capillary, 20 kV. The peaks correspond to 4.6 fmol dopamine (1), 4.1 fmol isoproterenol (2), and 2.7 fmol catechol (3). (Reproduced with permission from reference 60.)

mass transport controlled reactions ($i_l = nFADC/\delta$), one obtains the limiting steady-state response of flow-through electrodes:

$$i_l = nFAK_mCU^{\alpha} \tag{3-32}$$

where K_m is the mass-transport coefficient (D/B).

A more rigorous treatment takes into account the hydrodynamic characteristics of the flowing solution. Expressions for the limiting currents (under steady-state conditions) have been derived for various electrodes geometries by solving the three-dimensional convective diffusion equation:

$$\frac{\partial C}{\partial t} = D\left(\frac{\partial^2 C}{\partial x^2} + \frac{\partial^2 C}{\partial y^2} + \frac{\partial^2 C}{\partial z^2}\right) - \left(U_x\frac{\partial C}{\partial x} + U_y\frac{\partial C}{\partial y} + U_z\frac{\partial C}{\partial_z}\right) \tag{3-33}$$

The resulting equations, arrived at by setting appropriate initial and boundary conditions (depending on the particular electrode), are given in Table 3-4.

A generalized equation for the limiting-current response of different detectors, based on the dimensionless Reynolds (Re) and Schmidt (Sc) numbers has been derived by Hanekamp and co-workers (62):

$$i_l = nkFCD(Sc)^{\beta}b(Re)^{\alpha} \tag{3-34}$$

where k is a dimensionless constant and b is the characteristic electrode width.

In the case of coulometric detectors (with complete electrolysis), the limiting current is given by Faraday's law:

$$i_l = nFCU \tag{3-35}$$

TABLE 3-4 The Limiting-Current Response of Various Flow-Through Electrodes

Electrode Geometry	Limiting Current Equation
Tubular	$i = 1.61\ nFC(DA/r)^{2/3}U^{1/3}$
Planar (parallel flow)	$i = 0.68\ nFCD^{2/3}v^{-1/6}(A/b)^{1/2}U^{1/2}$
Thin-layer cell	$i = 1.47\ nFC(DA/b)^{2/3}U^{1/3}$
Planar (perpendicular)	$i = 0.903nFCD^{2/3}v^{-1/6}A^{3/4}u^{1/2}$
Wall-jet detector	$i = 0.898nFCD^{2/3}v^{-5/12}a^{-1/2}A^{3/8}U^{3/4}$

a = diameter of inlet; A = electrode area; b = channel height; C = concentration (mM); F = Faraday constant; D = diffusion coefficient; v = kinematic viscosity; r = radius of tubular electrode; U = average volume flow rate; u = velocity (cm s^{-1}); n = number of electrons.

Adapted from reference 62.

3-6.4 Detection Modes

The simplest, and by far the most common, detection scheme is the measurement of the current at a constant potential. Such fixed-potential amperometric measurements have the advantage of being free of double-layer charging and surface-transient effects. As a result, extremely low detection limits—on the order of 1–100 pg (about 10^{-14} moles of analyte)—can be achieved. In various situations, however, it may be desirable to change the potential during the detection (scan, pulse, etc.).

Potential-scanning detectors can increase the information content over that of fixed-potential operation. By rapidly recording numerous voltammograms during the elution, one obtains a three-dimensional detector response of the current against potential and time. Such addition of the redox potential selectivity can offer immediate identification of eluting peaks, and helps in resolving chromatographically coeluting components. Different approaches to swept-potential detectors based on square-wave voltammetry (13,14) or phase-sensitive AC voltammetry (63) have been reported. The greater selectivity of potential-scanning detection is accompanied by higher detection limits (versus fixed-potential amperometry), because of the additional background current associated with the potential scan.

Pulsed amperometric detection (PAD), introduced by Johnson and LaCourse (64, 65) has greatly enhanced the scope of liquid chromatography/electrochemistry (66). This detection mode overcomes the problem of loss of activity of noble metal electrodes associated with the fixed-potential detection of compounds such as carbohydrates, alcohols, amino acids, or aldehydes. Pulsed amperometric detection couples the process of anodic detection with anodic cleaning and cathodic reactivation of a noble metal electrode, thus assuring a continuously cleaned and active

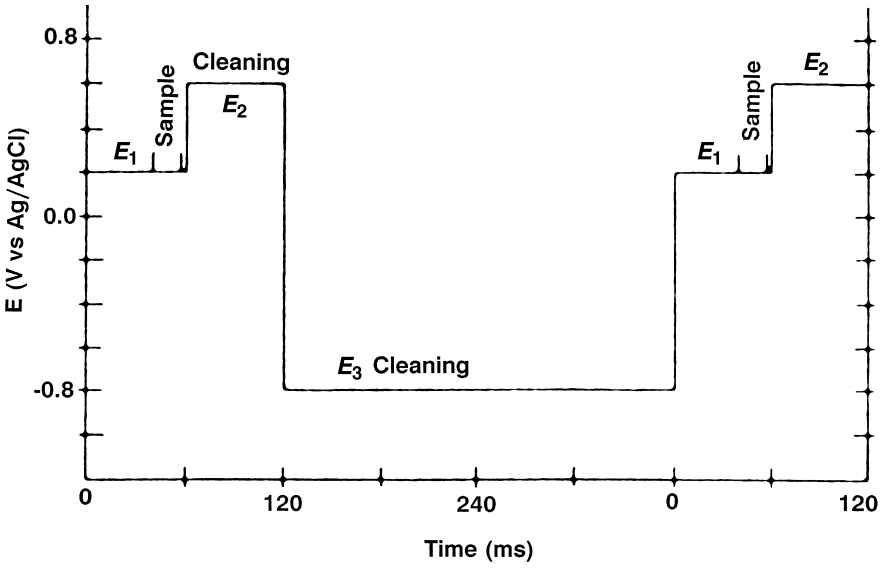

FIGURE 3-25 Triple-pulse amperometric waveform.

surface. This is usually accomplished with a three-step potential waveform, combining anodic and cathodic polarizations (e.g., Figure 3-25). The analytical response results primarily from adsorbed analyte, with detection limits approaching 50 ng (for 50 μL samples). Other automated multistep potential waveforms are possible. Such waveforms are commonly executed at a frequency of 1–2 Hz, in connection with gold or platinum working electrodes.

The power of electrochemical detection can be improved by using more than one working electrode (67). Different strategies, based primarily on dual-electrode detection, can thus be employed. For example, in the series mode (Figure 3-26*a*) the first upstream electrode can be used to generate an electroactive species that is more easily detected at the downstream electrode. Discrimination against compounds with irreversible redox chemistry can also be achieved. Significantly improved qualitative information can be achieved using a parallel (side-by-side) dual-electrode configuration (Figure 3-26*b*). Two simultaneous chromatograms can be generated by holding these electrodes at different potentials. The current ratios at these two potential settings provide real-time "fingerprints" of the eluting peaks. Such ratio values are compared with those of standards to confirm the peak identity. Further improvements in the information content can be achieved using multichannel amperometric detection (analogous to diode array optical detection) (68). For example, Figure 3-27 displays a three-dimensional chromatogram for a mixture of several biologically significant compounds at a 16-electrode detector array. By rapidly applying a five-potential sequence to the individual electrodes, an 80-channel chromatographic detection can be obtained. Such an electrochemical profile across

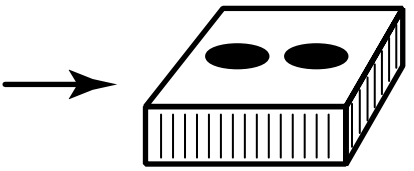

Series

(*a*)

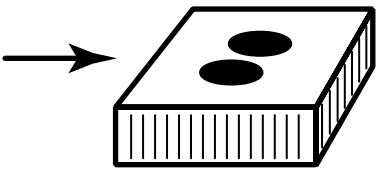

Parallel adjacent

(*b*)

FIGURE 3-26 Dual-electrode thin-layer detector configurations for operation in the series (*a*) and parallel (*b*) amperometric modes.

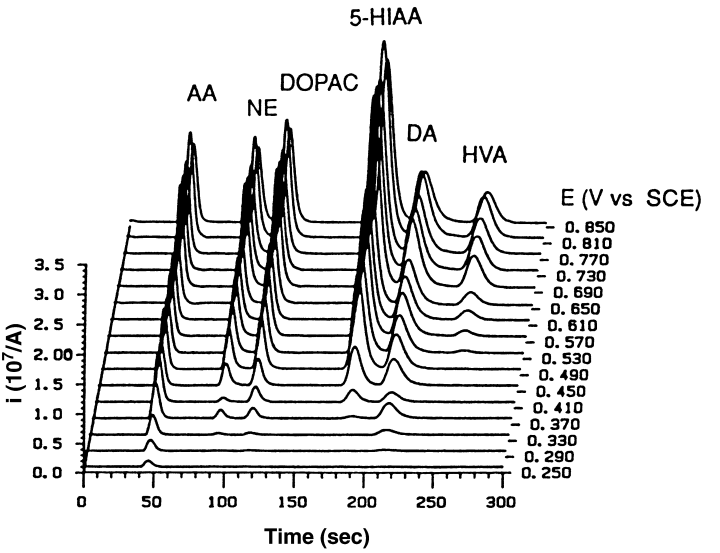

FIGURE 3-27 Three-dimensional chromatogram for oxidizable biological compounds at a multichannel amperometric detection system, consisting of an array of 16 carbon-paste electrodes held at different potentials. AA = ascorbic acid; NE = norepinephrine; DOPAC = 3,4-dihydroxyphenylacetic acid; 5-HIAA = 5-hydroxyindole-3-acetic acid; DA = dopamine; HVA = homovanillic acid. (Reproduced with permission from reference 68.)

the array provides confirmation of peak purity and improved identification of target analytes. Additional information can be achieved by using arrays comprising different electrode materials (see Section 6-4). For a more detailed description of on-line electrochemical detectors, the reader is referred to a monograph by Stulik and Pacáková (69). Comparison of various commercial detectors is also available (70).

REFERENCES

1. D. Ilkovic, *Coll. Czech. Chem. Commun*, 64, 498 (1934).
2. J. Lingane, *Chem. Rev.* 29, 1 (1941).
3. G.C. Barker and I.L. Jenkin, *Analyst*, 77, 685 (1952).
4. G.C. Barker and A.W. Gardner, *Z. Anal. Chem.*, 173, 79 (1960).
5. J. Osteryoung and E Kirowa-Eisner, *Anal. Chem.*, 52, 62 (1980).
6. E.P. Parry and R.A. Osteryoung, *Anal. Chem.*, 37, 1634 (1964).
7. J.B. Flato, *Anal. Chem.*, 44, 75A (1972).
8. J. Osteryoung and R.A. Osteryoung, *Anal. Chem.*, 57, 101A (1985).
9. J.J. O'Dea, J. Osteryoung and R.A. Osteryoung, *Anal. Chem.*, 53, 695 (1981).
10. S. Borman, *Anal. Chem.*, 54, 698A (1982).

11. C. Yarnitzky, *Anal. Chem.*, 57, 2011 (1985).
12. J. Wang, E. Ouziel, C. Yarnitzky and M Ariel, *Anal. Chim. Acta*, 102, 99 (1978).
13. R. Samuelsson, J.J. O'Dea and J. Osteryoung, *Anal. Chem.*, 52, 2215 (1980).
14. G.C. Gerhardt, R.M. Cassidy and A.S. Baranski, *Anal. Chem.*, 70, 2167 (1998).
15. S. Stefani and R Seeber, *Anal. Chem.*, 54, 2524 (1982).
16. B. Breyer and H Bauer, *Rev. Polarogr.*, 8, 157 (1960).
17. D.E. Smith, *CRC Crit. Rev. Anal. Chem.*, 2, 247 (1971).
18. B. Breyer and H Bauer, *Alternating Current Polarography and Tensammetry*, Wiley-Interscience, New York, 1963.
19. J. Wang, *Stripping Analysis: Principles, Instrumentation and Applications*, VCH Publishers, Deerfield Beach, FL, 1985.
20. T.R. Copeland and R.K. Skogerboe, *Anal. Chem.*, 46, 1257A (1974).
21. T.M. Florence, *J. Electroanal. Chem.*, 27, 273 (1970).
22. D. Jagner, *Trends Anal. Chem.* 2(3), 53 (1983).
23. J. Wang, "Voltammetry after Nonelectrolytic Proconcentration," in A.J. Bard Ed., *Electroanalytical Chemistry*, Vol. 16, p. 1, Marcel Dekker, New York, 1989.
24. C.M.G. van den Berg, *Anal. Chim. Acta*, 250, 265 (1991).
25. C.M.G. van den Berg, K. Murphy and J.P. Riley, *Anal. Chim. Acta*, 188, 177 (1986).
26. J. Wang and T. Baomin, *Anal. Chim. Acta*, 270, 137 (1992).
27. J.R. Donat and K.W. Bruland, *Anal. Chem.*, 60, 240 (1988).
28. J. Golimowski, P. Valenta and H.W. Nürnberg, *Fres. Z. Anal. Chem.*, 322, 315 (1985).
29. J. Wang and J.S. Mahmoud, *Fres. Z. Anal. Chem.*, 327, 789 (1987).
30. J. Wang and J.S. Mahmoud, *J. Electroanal. Chem.*, 208, 383 (1986).
31. C.M.C. van den Berg, *Anal. Chem.*, 57, 1532 (1985).
32. B. Pihlar, P. Valenta and H.W. Nürnberg, *Fres. Z. Anal. Chem.*, 307, 337 (1981).
33. J. Wang, J. Zadeii and M.S. Lin, *J. Electroanal. Chem.*, 237, 281 (1987).
34. J. Wang and J. Zadeii, *Talanta*, 34, 909 (1987).
35. K. Yokoi and C.M.C. van den Berg, *Anal. Chim. Acta*, 245, 167 (1991).
36. C.M.G. van den Berg and N. Nimmo, *Anal. Chem.*, 59, 269 (1987).
37. C.M.G. van den Berg, *Anal. Chem.*, 56, 2383 (1984).
38. J. Wang, X. Cai, C. Jonsson and M Balakrishan, *Electroanalysis*, 8, 20 (1996).
39. G.W. Luther, C. Swartz and W Ullman, *Anal. Chem.*, 60, 1721 (1988).
40. M. Tercier and J Buffle, *Electroanalysis*, 5, 187 (1993).
41. N.K. Komanur and G.W. van Loon, *Talanta*, 24, 184 (1977).
42. J. Poldoski and G Glass, *Anal. Chim. Acta*, 101, 79 (1978).
43. J. Wang, J. Lu and K Olsen, *Analyst*, 117, 1913 (1992).
44. S. Gottesfeld and M Ariel, *J. Electroanal. Chem.*, 9, 112 (1965).
45. J. Wang and S Mannino, *Analyst*, 114, 643 (1989).
46. P. Ostapczuk, *Clin. Chem.*, 38, 1995 (1992).
47. P. Lai and K Fung, *Analyst*, 103, 1244 (1978).
48. J. Golimoski and I Gustavsson, *Fres. Z. Anal. Chem.*, 317, 484 (1984).
49. S.B. Adeloju, A.M. Bond and M.H. Briggs, *Anal. Chim. Acta*, 164, 181 (1984).

50. K. Hoppstock and M Michulitz, *Anal. Chim. Acta*, 350, 135 (1997).
51. S. Porbes, G. Bound and T West, *Talanta*, 26, 473 (1979).
52. D.I. Levit, *Anal. Chem.*, 45, 1291 (1973).
53. J. Wang, R. Setiadji, L. Chen, J. Lu and S Morton, *Electroanalysis*, 4, 161 (1992).
54. T. Williams, O. Foy and C Benson, *Anal. Chim. Acta*, 75, 250 (1975).
55. T.M. Florence, *Analyst*, 111, 489 (1986).
56. J. Wang, *Analyst*, 119, 763 (1994).
57. A.G. Ewing, J.M. Mesaros and P.F. Gavin, *Anal. Chem.*, 66, 527A (1994).
58. P. Curry, C. Engstrom and A Ewing, *Electroanalysis*, 3, 587 (1991).
59. L.A. Holland and S.M. Lunte, *Anal. Commun.*, 35, 1H (1998).
59a. T. Kappes and P. Hanser, *Electroanalysis*, 3, 165 (2000).
60. S. Sloss, A.G. Ewing, *Anal. Chem.*, 63, 577 (1993).
61. A. Woolley, K. Lao, A. Glazer and R Mathies, *Anal. Chem.*, 70, 684 (1998).
61a. J. Wang, B. Tian and E. Sahlin, *Anal. Chem.*, 71, 5436(1999).
62. H.B. Hanekamp, P. Box and R.W. Frei, *Trends Anal. Chem.*, 1, 135 (1982).
63. A. Trojanek and H.G. De Jong, *Anal. Chim. Acta*, 141, 115 (1982).
64. D.C. Johnson and W.R. LaCourse, *Anal. Chem.*, 62, 589A (1990).
65. D.C. Johnson and W.R. LaCourse, *Electroanalysis*, 4, 367 (1992).
66. W.R. LaCourse, *Pulsed Electrochemical Detection in HPLC*, Wiley, New York, 1997.
67. D.A. Roston, R.E. Shoup and P.T. Kissinger, *Anal. Chem.*, 54, 1417A (1982).
68. J. Hoogvliet, J. Reijn and W van Bennekom, *Anal. Chem.*, 63, 2418 (1991).
69. K. Stulik and V Pacáková, *Electroanalytical Measurements in Flowing Liquids*, Ellis Horwood, Chichester, 1987.
70. M. Warner, *Anal. Chem.*, 66, 601A (1994).

EXAMPLES

Example 3-1 Voltammogram (*a*) was obtained for adsorptive stripping measurements of Fe(III) in sea water. Voltammograms (*b*) and (*c*) show successive standard additions of 4 ppb Fe(III). Find the concentration of Fe(III) in the sample.

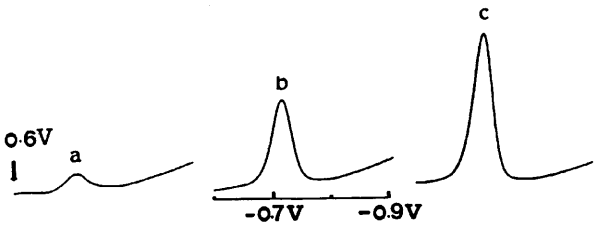

Solution The resulting current peaks lead to the following standards additions plot:

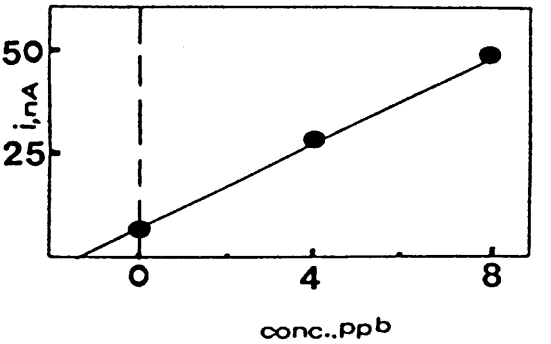

From which an Fe(III) concentration of 1.47 ppb can be obtained for the sample.

Example 3-2 Calculate the limiting current that would be expected from the reduction of 2×10^{-4} M Pb^{2+}, using the DME characteristics $m = 2.0\,\text{mg s}^{-1}$ and $t = 4\,\text{s}$. The diffusion coefficient of Pb^{2+} is $1.01 \times 10^{-5}\,\text{cm}^2\,\text{s}^{-1}$.

Solution The lead reduction is a two-reduction process:

$$Pb^{2+} + 2e^- \rightleftharpoons Pb$$

Hence, from the Ilkovic equation, (equation 3.3), we obtain

$$i_d = 708 \times 2 \times (1.01 \times 10^{-5})^{1/2}(2.0)^{2/3} \times 4^{1/6} \times 0.2. = 1.81\ \mu\text{A}$$

Example 3-3 Draw clearly the DC polarographic response for a mixture containing 3 mM Cu^{2+}, 2 mM Zn^{2+} and 1 mM Cd^{2+}. The half-wave potentials for the Cu, Zn and Cd ions are -0.12 V, -0.95 V and -0.62 V, respectively.

Solution

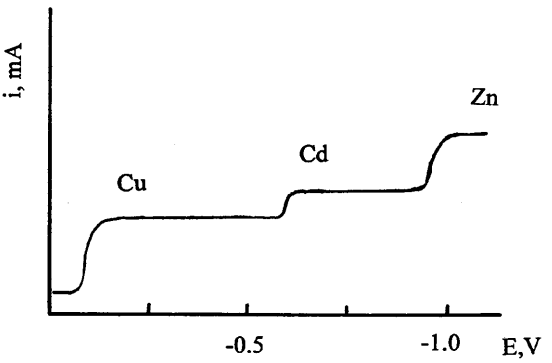

Example 3-4 A sample containing cadmium gives a polarographic reduction current of 6.0 μA. The current increases to 9 and 12 μA upon increasing the cadmium concentration in two steps of 2 mM each. Calculate the cadmium concentration in the original sample.

Solution

$$6 = KC \qquad 9 = K(C + 2) \qquad 12 = K(C + 4)$$

to yield a C value of 4 mM.

Example 3-5 Polarogram A was obtained for a 10 mL lead-containing sample. The limiting current increased (to B) after adding 100 μL of a 0.10 M lead standard to the 10 ml sample. Calculate the original lead concentration in the sample.

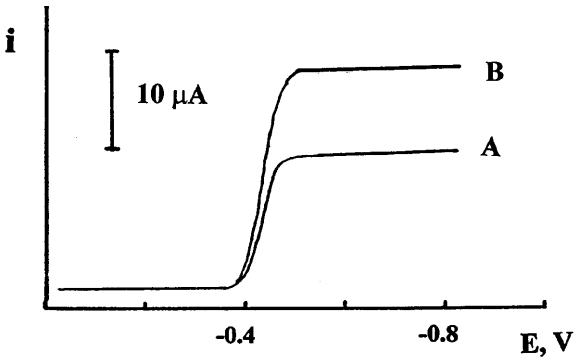

Solution The sample lead ion yielded a limiting current of 13 μA (A). The current increases by 8.5 μA upon spiking the sample with 1 mM lead standard (considering the 1 : 100 dilution; B − A).

$$i_l = KC \qquad 8.5 = \text{K}(1\text{ mM}) \qquad K{=}8.5$$

$$13.5. = 8.5.C_{\text{sample}}$$

$$C_{\text{sample}} = 1.53\text{ mM}$$

Example 3-6 Flow analysis of a urine sample at a thin-layer amperometric detector, with a flow rate of 1.25 mL min^{-1}, yielded a limiting current value of 1.6 μA for its unknown uric acid content. A larger current of 2.4 μA was observed for a sample containing 1×10^{-4} M uric acid and flowing at a rate of 0.9 mL min^{-1}. Calculate the original concentration of uric acid in the sample.

Solution From Table 3-4:

$$i_l = KCU^{1/3}$$

$$2.4. = K(1 \times 10^{-4})0.9^{1/3} \qquad K = 2.49 \times 10^4$$

$$1.6 = 2.49 \times 10^4(C)1.25^{1/3}$$

$$C = 6 \times 10^{-5} \text{ M}$$

QUESTIONS

1. Describe clearly the principle and operation of potentiometric stripping analysis (PSA). How it is differed from anodic stripping voltammetry (ASV)? What is the quantitative signal? What is its advantage over ASV?
2. Draw clearly schematic diagrams of a thin-layer flow detector utilizing (1) single working electrode, and (2) dual electrode. Explain how the latter improves the power and information content.
3. Describe and draw clearly the waveform employed in square-wave voltammetry. Explain how the current is measured.
4. Describe clearly the use of polarographic analysis for obtaining the values of the formation constant and stoichiometric number of metal complexes.
5. Describe clearly the challenges of interfacing electrochemical detectors to capillary electrophoresis separation systems. How can these challenges be overcome?
6. Explain clearly how and why the coupling of stripping voltammetry to a differential pulse waveform can enhance the power of stripping measurements of trace metals.
7. Select an electroanalytical technique most suitable for detecting trace levels of nickel in ground water. Justify this choice.
8. A liquid chromatographic experiment resulted in the same retention time for the electroactive compounds A and B. Which electrochemical detection scheme would offer a selective detection of the two coeluting analytes? Explain your selection. ($E^\circ_A = +0.43$ V; $E^\circ_B = +0.77$ V.)
9. Use the adsorption theory (of Section 2-1-3) to explain why adsorptive stripping voltammetry results in nonlinear calibration plots.
10. Derive the Cottrell equation by combining Fick's first law of diffusion with the time-dependent change of the concentration gradient during a potential-step experiment.

Analytical Electrochemistry, Second Edition. Joseph Wang

ISBNs: 0-471-28272-3 (Hardback); 0-471-22823-0 (Electronic)

CHAPTER 4

PRACTICAL CONSIDERATIONS

The basic instrumentation required for controlled-potential experiments is relatively inexpensive and readily available commercially. The basic necessities include a cell (with a three-electrode system), a voltammetric analyzer (consisting of a potentiostatic circuitry and a voltage ramp generator), and an *X–Y–t* recorder (or plotter). Modern voltammetric analyzers are versatile enough to perform many modes of operation. Depending upon the specific experiment, other components may be required. For example, a faradaic cage is desired for work with ultramicroelectrodes. The system should be located in a room free from major electrical interferences, vibrations, and drastic fluctuations in temperature.

4-1 ELECTROCHEMICAL CELLS

Three-electrode cells (e.g., Figure 4-1) are commonly used in controlled-potential experiments. The cell is usually a covered beaker of 5–50 mL volume, and contains the three electrodes (working, reference, and auxiliary), which are immersed in the sample solution. While the working electrode is the electrode at which the reaction of interest occurs, the reference electrode provides a stable and reproducible potential (independent of the sample composition), against which the potential of the working electrode is compared. Such "buffering" against potential changes is achieved by a constant composition of both forms of its redox couple, for example, Ag/AgCl or Hg/Hg_2Cl_2, as with the commonly used silver–silver chloride and the saturated calomel reference electrodes, respectively. To minimize contamination of the sample solution, the reference electrode may be insulated from the sample

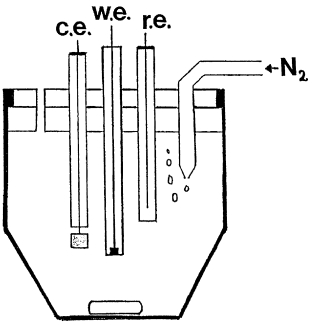

FIGURE 4-1 Schematic diagram of a cell for voltammetric measurements: w.e., working electrode; r.e., reference electrode; c.e., counter electrode. The electrodes are inserted through holes in the cell cover.

FIGURE 4-2 A complete cell stand. (Courtesy of BAS Inc.)

through an intermediate bridge. An inert conducting material, such as platinum wire or graphite rod, is usually used as the current-carrying auxiliary electrode. Attention should be given to the relative position of these electrodes, and to their proper connection to the electrochemical analyzer (see Section 4-4). The three electrodes, as well as the tube used for bubbling the deoxygenating gas (see Section 4-3), are supported in five holes in the cell cover. Complete systems, integrating the three-electrode cell, built-in gas control, and magnetic stirrer, along with proper cover, are available commercially (e.g., Figure 4-2).

The exact cell design and the material used for its construction are selected according to the experiment at hand and the nature of the sample. The various designs differ with respect to size, temperature-control capability, stirring requirement, shape, or number of cell compartments. Various micro cells with 20–500 μL volumes can be used when the sample volume is limited. Particularly attractive are thin-layer cells in which the entire sample is confined within a thin layer (less than 10 μm thick) at the electrode surface (1). Smaller sample volumes can be accommodated in connection with ultramicroelectrodes (discussed in Section 4-4) and advanced microfabrication processes (discussed in Section 6-3). In particular, lithographically fabricated picoliter microvials (2) hold great promise for assays of ultrasmall environments (e.g., single-cell systems). Specially designed flow cells (discussed in Section 3-6) are used for on-line applications. Glass is commonly used as the cell material because of its low cost, transparency, chemical inertness, and impermeability. Teflon and quartz represent other possible cell materials. The cell cover can be constructed of any suitable material that is inert to the sample. Accurate temperature control is readily achieved by immersing or jacketing the cell in a constant-temperature bath.

4-2 SOLVENTS AND SUPPORTING ELECTROLYTES

Electrochemical measurements are commonly carried out in a medium that consists of solvent containing a supporting electrolyte. The choice of the solvent is dictated primarily by the solubility of the analyte and its redox activity, and by solvent properties such as the electrical conductivity, electrochemical activity, and chemical reactivity. The solvent should not react with the analyte (or products) and should not undergo electrochemical reactions over a wide potential range.

While water has been used as a solvent more than any other media, nonaqueous solvents [e.g., acetonitrile, propylene carbonate, dimethylformamide (DMF), dimethyl sulfoxide (DMSO), or methanol] have also frequently been used. Mixed solvents may also be considered for certain applications. Double-distilled water is adequate for most work in aqueous media. Triple-distilled water is often required when trace (stripping) analysis is concerned. Organic solvents often require drying or purification procedures. These and other solvent-related considerations have been reviewed by Mann (3).

Supporting electrolytes are required in controlled-potential experiments to decrease the resistance of the solution, to eliminate electromigration effects, and to maintain a constant ionic strength (i.e., “swamping out” the effect of variable

amounts of naturally occurring electrolyte). The inert supporting electrolyte may be an inorganic salt, a mineral acid, or a buffer. While potassium chloride or nitrate, ammonium chloride, sodium hydroxide, or hydrochloric acid are widely used when using water as a solvent, tetraalkylammonium salts are often employed in organic media. Buffer systems (such as acetate, phosphate, or citrate) are used when a pH control is essential. The composition of the electrolyte may affect the selectivity of voltammetric measurements. For example, the tendency of most electrolytes to complex metal ions can benefit the analysis of mixtures of metals. In addition, masking agents [such as ethylenediaminetetraacetic acid (EDTA)] may be added to "remove" undesired interferences. The supporting electrolyte should be prepared from highly purified reagents, and should not be easily oxidized or reduced. The usual electrolyte concentration range is 0.1–1.0 M, in other words, in large excess of the concentration of all electroactive species. Significantly lower levels can be employed in connection with ultramicro working electrodes (see Section 4-5.4).

4-3 OXYGEN REMOVAL

The electrochemical reduction of oxygen usually proceeds via two well-separated two-electron steps. The first step corresponds to the formation of hydrogen peroxide:

$$O_2 + 2H^+ + 2e^- \rightarrow H_2O_2 \tag{4-1}$$

and the second step corresponds to the reduction of the peroxide:

$$H_2O_2 + 2H^+ + 2e^- \rightarrow 2H_2O \tag{4-2}$$

The half-wave potentials of these steps are approximately -0.1 and -0.9 V (versus the saturated calomel electrode). The exact stoichiometry of these steps is dependent on the medium. The large background current accruing from this stepwise oxygen reduction interferes with the measurement of many reducible analytes. In addition, the products of the oxygen reduction may affect the electrochemical process under investigation.

A variety of methods have been used for the removal of dissolved oxygen (4). The most common method has been purging with an inert gas (usually purified nitrogen) for 4–8 min prior to recording of the voltammogram. Longer purge times may be required for large sample volumes or for trace measurements. To prevent oxygen from reentering, the cell should be blanketed with the gas while the voltammogram is being recorded. Passage of the gas through a water-containing presaturator is desirable to avoid evaporation. The deaeration step, while time consuming, is quite effective and suitable for batch analysis. (The only exception is work with microsamples, where deoxygenation may lead to errors caused by the evaporation of solvent or loss of volatile compounds.)

Other methods have been developed for the removal of oxygen (particularly from flowing streams). These include the use of electrochemical or chemical (zinc) scrubbers, nitrogen-activated nebulizers, and chemical reduction (by addition of sodium sulfite or ascorbic acid). Alternately, it may be useful to employ voltam-

metric methods that are less prone to oxygen interference. The background connection capability of modem (computerized) instruments is also effective for work in the presence of dissolved oxygen.

4-4 INSTRUMENTATION

Rapid advances in microelectronics, and in particular the introduction of operational amplifiers, have led to major changes in electroanalytical instrumentation. Tiny and inexpensive integrated circuits can now perform many functions that previously required very large instruments. Such trends have been reviewed recently (5). Various voltammetric analyzers are now available commercially from different sources (Table 4-1) at relatively modest prices (ranging from $5,000 to $25,000 in 1999). Such instruments consist of two circuits: a polarizing circuit that applies the potential to the cell, and a measuring circuit that monitors the cell current. The characteristic of modern voltammetric analyzers is the potentiostatic control of the working electrode, which minimizes errors from cell resistance (i.e., poorly defined voltammograms with lower current response and shifted and broadened peaks). Equation 4-3 explains the cause for this ohmic distortion:

$$E_{\text{app}} = E_{\text{w.e.}} - E_{\text{r.e.}} - iR \tag{4-3}$$

where iR is the ohmic potential drop.

TABLE 4-1 Suppliers of Voltammetric Analyzers

Supplier	Address
Analytical Instrument Systems	P.O. Box 458, Flemington, NJ 08822, U.S.A. www.aishome.com
Bioanalytical Systems	2701 Kent Ave., W. Lafayette, IN 47906, U.S.A. www.bioanalytical.com
Cypress	P.O. Box 3931, Lawrence, KS 66044, U.S.A. www.cypresshome.com
CH Instruments	3700 Tennison Hill Dr., Austin, TX 78733, U.S.A. chinstr@worldnet.att.net
ECO Chemie	P.O. Box 85163, 3508 AD Utrecht, The Netherlands autolab@ecochemie.nl www.brinkmann.com
EG&G PAR	801 S. Illinois Ave, Oak Ridge, TN, 37830, U.S.A. www.egg.inc.com/par
ESA	45 Wiggins Ave., Bedford, MA 01730, U.S.A.
Metrohm	CH-9109 Herisau, Switzerland www.brinkmann.com
Radiometer/Tacussel	27 rue d'Alscace, F-69627 Villeurbanne, France Analytical@clevelandOH.com
Solartron	964 Marcon Blvd., Allentown, PA 18103, USA www.solartron.com

The potentiostatic control, aimed at compensating a major fraction of the cell resistance, is accomplished with a three-electrode system and a combination of operational amplifiers and feedback loops (Figure 4-3). Here, the reference electrode is placed as close as possible to the working electrode and is connected to the instrument through a high-resistance circuit that draws no current from it. Because the flow cannot occur through the reference electrode, a current-carrying auxiliary (counter) electrode is placed in the solution to complete the current path. Hence, the current flows through the solution between the working and the auxiliary electrodes. Symmetry in the placement of these electrodes is important for the assumption that the current paths from all points on the working electrode are equivalent. Because no current passes through the reference electrode and because of its position close to the working electrode, the potential drop caused by the cell resistance (iR) is minimized. If the potential sensed by the reference electrode is less than the desired value, the operational amplifier control loop provides a corrective potential. By adding an operational amplifier current-to-voltage converter (called a "current follower") to the working electrode, it is possible to measure the current without disturbing the controlled parameters. The instrument also includes a ramp generator to produce various regularly changing potential waveforms.

As was pointed out earlier, effective potential control requires very close proximity between the working and reference electrodes. This can be accomplished using a specially designed bridge of the reference electrode, known as a *Luggin probe*. The tip of this bridge should be placed as close as twice its diameter to the working electrode. A smaller distance will result in blockage (shielding) of the current path and hence a nonhomogeneous current density. The Luggin bridge should also not interfere with the convective transport toward the surface of the working electrode.

It should be pointed out that not all of the iR drop is removed by the potentiostatic control. Some fraction, called iR_u (where R_u is the uncompensated solution resistance between the reference and working electrodes) will still be included in the measured potential. This component may be significantly large when resistive nonaqueous media are used, and thus may lead to severe distortion of the

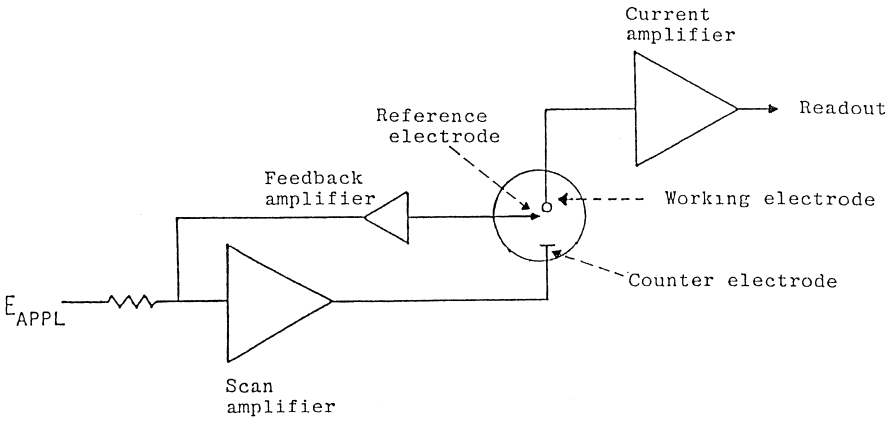

FIGURE 4-3 Schematic diagram of a three-electrode potentiostat.

voltammetric reponse. Many modern instruments, however, automatically subtract (compensate) the iR_u drop from the potential signal given to the potentiostat via an appropriate positive feedback.

Bipotentiostats, offering simultaneous control of two working electrodes (e.g., ring-disk) are also available. Such instruments consist of a conventional potentiostat with a second voltage-control circuit. Multipotentiostats, controlling more than two working electrodes, have also been described (6). The development of ultramicroelectrodes, with their very small currents (and thus negligible iR losses even when R is large), allows the use of simplified, two-electrode, potential control (see Section 4-5.4). In contrast, ultramicroelectrode work requires efficient current-measurement circuitry to differentiate between the faradaic response and the extraneous electronic noise and for handling low currents down to the picoamp range. Other considerations for the noise reduction involve the grounding and shielding of the instrument and cell.

The advent of inexpensive computing power has changed dramatically the way voltammetric measurements are controlled and data are acquired and manipulated. Computer-controlled instruments, available from most manufacturers (5), provide flexibility and sophistication in the execution of a great variety of modes. In principle, any potential waveform that can be defined mathematically can be applied with commands given through a keyboard. Such instruments offer various data-processing options, including autoranging, blank subtraction, noise reduction, curve smoothing, differentiation, integration, and peak search. The entire voltammogram can be presented as a plot or printout (of the current-potential values). In addition, computer control has allowed automation of voltammetric experiments and hence has greatly improved the speed and precision of the measurement. Since the electrochemical cell is an analog element, and computers work only in the digital domain, analog-to-digital (A/D) and digital-to-analog (D/A) converters are used to interface between the two. Unattended operation has been accomplished through the coupling of autosamplers and microprocessor-controlled instruments (e.g., Figure

FIGURE 4-4 Microprocessor-controlled voltammetric analyzer, in connection with an autosampler. (Courtesy of Metrohm Inc.)

4-4). The autosampler can accommodate over 100 samples, as well as relevant standard solutions. Such coupling can also address the preliminary stages of sample preparation (as dictated by the nature of the sample). The role of computers in electroanalytical measurements and in the development of "smarter" analyzers has been reviewed by Bond (7) and He et al. (8).

The nature of electrochemical instruments makes them very attractive for decentralized testing. For example, compact, battery-operated voltammetric analyzers, developed for on-site measurements of metals (9,10), readily address the growing needs for field-based environmental studies. Similarly, portable (hand-held) instruments are being designed for decentralized clinical testing (11).

4-5 WORKING ELECTRODES

The performance of the voltammetric procedure is strongly influenced by the material of the working electrode. The working electrode should provide high signal-to-noise characteristics, as well as a reproducible response. Thus, its selection depends primarily on two factors: the redox behavior of the target analyte and the background current over the potential region required for the measurement. Other considerations include the potential window, electrical conductivity, surface reproducibility, mechanical properties, cost, availability, and toxicity. A range of materials have found application as working electrodes for electroanalysis. The most popular are those involving mercury, carbon, or noble metals (particularly platinum and gold). Figure 4-5 displays the accessible potential window of these electrodes in various solutions. The geometry of these electrodes must also be considered.

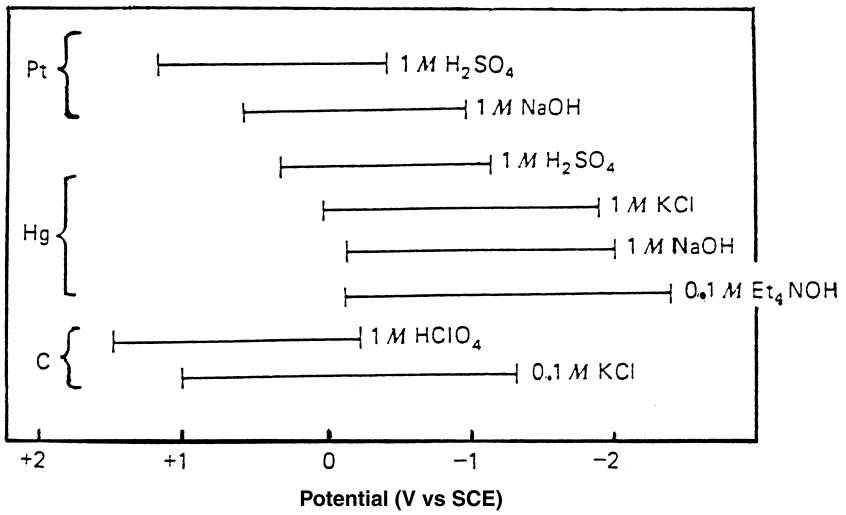

FIGURE 4-5 Accessible potential window of platinum, mercury, and carbon electrodes in various supporting electrolytes.

4-5.1 Mercury Electrodes

Mercury is a very attractive choice of electrode material because it has a high hydrogen overvoltage that greatly extends the cathodic potential window (compared to solid electrode materials) and possesses a highly reproducible, readily renewable, and smooth surface. In electrochemical terms, its roughness factor equals unity (i.e., identical geometrical and actual surface areas). Disadvantages of the use of mercury are its limited anodic range (due to the oxidation of mercury) and its toxicity.

There are several types of mercury electrodes. Of these, the dropping mercury electrode (DME), the hanging mercury drop electrode (HMDE), and mercury film electrode (MFE) are the most frequently used.

The DME, used in polarography (Section 3-2) and for electrocapillary studies (Section 1-4), consists of glass capillary tubing, 12–20 cm in length with an internal diameter of 30–50 μm, connected by a flexible tube to an elevated reservoir of mercury (Figure 4-6). Electrical contact is made through a wire inserted into the mercury reservoir. Mercury flows by gravity through the capillary at a steady rate, emerging from its tip as continuously growing drops. By adjusting the height of the mercury column, one may vary the drop time; the lifetime of the drop is typically 2–6 s. Such continuous exposure of fresh spherical drops eliminates passivation problems that may occur at stable solid electrodes. The key to successful operation of the DME is proper maintenance of its capillary (which prevents air bubbles,

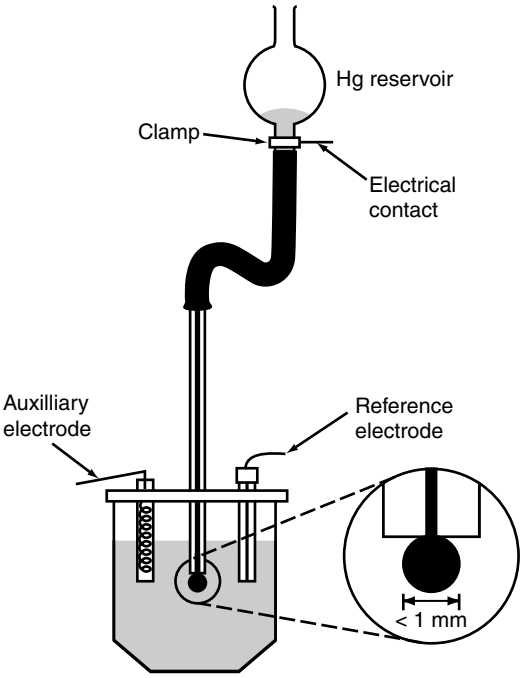

FIGURE 4-6 The dropping mercury electrode.

solution creeping, and accumulation of dirt). More elaborate DMEs, based on a mechanical drop detachment after reproducible time intervals, are used for pulse polarography.

The hanging mercury drop electrode is a popular working electrode for stripping analysis and cyclic voltammetry. In this configuration, stationary mercury drops are displaced from a reservoir through a vertical capillary. Early (Kemula-type) HMDE designs relied on mechanical extrusion (by a micrometer-driven syringe) from a reservoir through a capillary (12). The mercury reservoir should be completely filled with mercury; air must be fully eliminated. Modern HMDEs (particularly with the Model 303 of EG&G PAR, shown in Figure 4-7) employ electronic control of the drop formation, which offers improved reproducibility and stability (13). For this purpose, a solenoid-activated valve dispenses the mercury rapidly, with the drop size being controlled by the time during which the valve is opened. A wide-bore capillary allows a mercury drop to be grown very rapidly when the valve is opened. Three valve opening times produce drops that are described as small, medium, or large. Since the potential scan is accomplished after the valve has been closed (i.e., with a stationary electrode), charging-current contributions due to drop growth are eliminated. All the components of this electrode, including the mercury reservoir, are contained in a compact unit. Such a commercial probe allows the conversion from

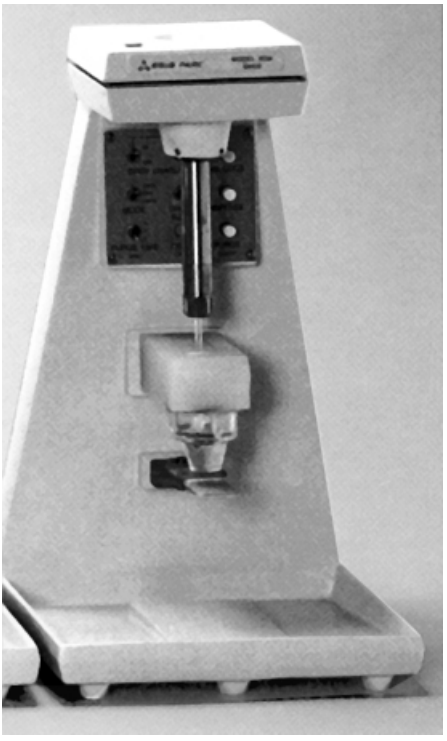

FIGURE 4-7 The static mercury drop electrode and its cell stand.

the HMDE to DME by operation of a single switch. When used in the DME mode, it exhibits a very rapid growth to a given area, which then remains constant (as desired for minimizing charging-current contributions). The performance of HMDEs can be improved by siliconizing the interior bore of the capillary.

Several mercury electrodes combine the features of the DME and HMDE. In particular, one employs a narrow-bore capillary that produces DMEs with drop lives of 50–70 s (14). Another involves a controlled-growth mercury drop (15). For this purpose, a fast-response valve offers a wide range of drop sizes and a slowly (step-by-step) growing drop.

The mercury film electrode, used for stripping analysis or flow amperometry, consists of a very thin (10–100 μm) layer of mercury covering a conducting support. Because of the adherent oxide films on metal surfaces, and the interaction of metals with mercury, glassy carbon is most often used as a substrate for the MFE. The mercury film formed on a glassy carbon support is actually composed of many droplets. As a result of not being a pure mercury surface, such film electrodes exhibit a lower hydrogen overvoltage and higher background currents. Another useful substrate for the MFE is iridium (because of its very low solubility in mercury and the excellent adherence of the resulting film). Mercury film electrodes are commonly preplated by cathodic deposition from a mercuric nitrate solution. An in-situ-plated MFE is often employed during stripping analysis (16). This electrode is prepared by simultaneous deposition of the mercury and the measured metals. Most commonly, a disk-shaped carbon electrode is used to support the mercury film. Mercury film ultramicroelectrodes, based on coverage of carbon fiber or carbon microdisk surfaces, have also received increasing attention in recent years.

4-5.2 Solid Electrodes

The limited anodic potential range of mercury electrodes has precluded their utility for monitoring oxidizable compounds. Accordingly, solid electrodes with extended anodic potential windows have attracted considerable analytical interest. Of the many different solid materials that can be used as working electrodes, the most often used are carbon, platinum, and gold. Silver, nickel, and copper can also be used for specific applications. A monograph by Adams (17) is highly recommended for a detailed description of solid-electrode electrochemistry.

An important factor in using solid electrodes is the dependence of the response on the surface state of the electrode. Accordingly, the use of such electrodes requires precise electrode pretreatment and polishing to obtain reproducible results. The nature of these pretreatment steps depends on the materials involved. Mechanical polishing (to a smooth finish) and potential cycling are commonly used for metal electrodes, while various chemical, electrochemical, or thermal surface procedures are added for activating carbon-based electrodes. Unlike mercury electrodes, solid electrodes present a heterogeneous surface with respect to the electrochemical activity (18). Such surface heterogeneity leads to deviations from the behavior expected for homogeneous surfaces.

Solid electrodes can be stationary or rotating, usually in a planar disk configuration. Such electrodes consist of a short cylindrical rod of the electrode material embedded in a tightly fitting tube of an insulating material (Teflon, Kel-F, etc.). The construction of a typical disk electrode is illustrated in Figure 4-8. It is essential to avoid crevices between the sleeve and the electrode materials, and thus to prevent solution creeping (and an increased background response). Electrical contact is made at the rear face. Disk solid electrodes are also widely employed in flow analysis in connection with thin-layer or wall-jet detectors (see Section 3-6). Growing attention is being given to other configurations of solid electrodes, including various ultramicroelectrodes (Section 4-5.4) and microfabricated screen-printed strips or silicon-based thin-film chips (Section 6-5).

4-5.2.1 Rotating Disk and Ring-Disk Electrodes The rotating disk electrode (RDE) is vertically mounted in the shaft of a synchronous controllable-speed motor and rotated with constant angular velocity (ω) about an axis perpendicular to the plain disk surface (Figure 4-9*a*). ($\omega = 2\pi f$, where f is the rotation speed in rps.) As a result of this motion, the fluid in an adjacent layer develops a radial velocity that moves it away from the disk center. This fluid is replenished by a flow normal to the surface. Hence, the RDE can be viewed as a pump that draws a fresh solution up from the bulk solution. Under laminar flow conditions (usually up to about 4000 rpm), the thickness of the diffusion layer decreases with increasing electrode angular velocity according to

$$\delta = 1.61 D^{1/3} \omega^{-1/2} v^{1/6} \tag{4-4}$$

where v is the kinematic viscosity (defined as the viscosity divided by the density in $cm^2\ s^{-1}$). Rotation speeds of 100–4000 rpm thus correspond to δ values in the 5–50 μm range. Equation (4-4) suggests that the thickness of the diffusion layer is

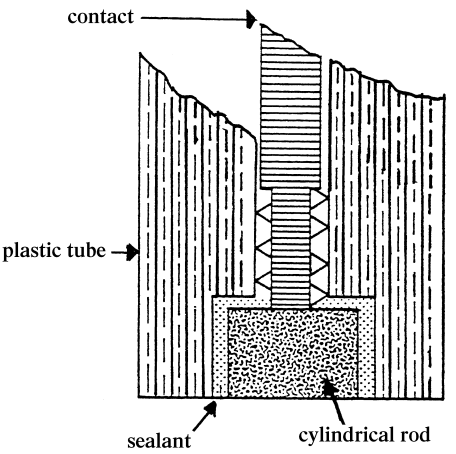

FIGURE 4-8 Construction of a typical disk electrode.

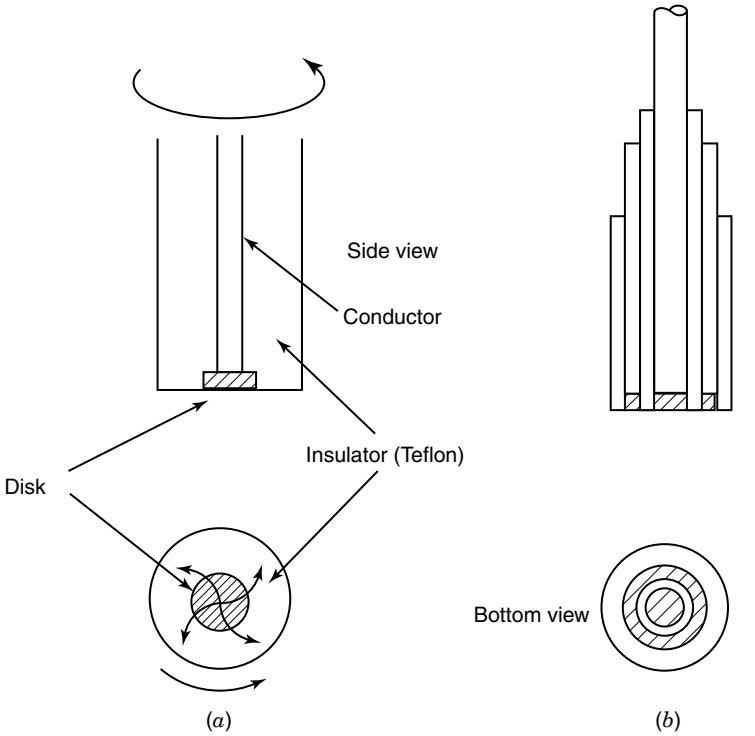

FIGURE 4-9 (*a*) Rotating disk and (*b*) ring-disk electrodes.

independent of the disk diameter, that is, a uniform layer across the surface. The limiting current (for a reversible system) is thus proportional to the square root of the angular velocity, as described by the *Levich equation*:

$$i_l = 0.62nFAD^{2/3}\omega^{1/2}v^{-1/6}C \tag{4-5}$$

An increase in ω from 400 to 1600 rpm thus results in a twofold increase of the signal. A deviation from linearity of a plot of i_l vs. $\omega^{1/2}$ suggests some kinetic limitations. In addition, at very low rotation speeds (0–100 rpm), a slight upward bend is observed due to contribution by natural convection. The voltammetric wave has a sigmoidal shape; for reversible systems it is identical to that common in DC polarography (described in Section 3-2), and independent of ω.

For quasi-reversible systems the limiting current is controlled by both mass transport and charge transfer:

$$i_l = nFADC\left(\frac{1}{1.61}D^{1/3}\omega^{-1/2}v^{1/6} + \frac{k}{D}\right) \tag{4-6}$$

where k is the specific heterogeneous rate constant. In the limit of purely kinetically controlled process ($k < 10^{-6}$ m s^{-1}) the current becomes independent of the rotation speed:

$$i_l = nFAkC \tag{4-7}$$

Overall, the RDE provides an efficient and reproducible mass transport and hence the analytical measurement can be made with high sensitivity and precision. Such well-defined behavior greatly simplifies the interpretation of the measurement. The convective nature of the electrode results also in very short response times. The detection limits can be lowered via periodic changes in the rotation speed and isolation of small mass transport-dependent currents from simultaneously flowing surface-controlled background currents. Sinusoidal or square-wave modulations of the rotation speed are particularly attractive for this task. The rotation-speed dependence of the limiting current (equation 4-5) can also be used for calculating the diffusion coefficient or the surface area. Further details on the RDE can be found in Adam's book (17).

An extension of the RDE involves an addition of a concentric-ring electrode surrounding the disk (and separated from it by a small insulating gap) (19). The resulting rotating ring-disk electrode (RRDE), shown in Figure 4-9b, has been extremely useful for elucidating various electrode mechanisms (through generation and detection reactions at the disk and ring, respectively). Because of the electrode rotation, the product of the disk reaction is hydrodynamically transported across the insulating gap toward the ring where it can be detected. Such "collection" experiments rely on measurements of the collection efficiency (N), which is the ratio of the ring and disk currents:

$$N = -i_R/i_D \tag{4-8}$$

and corresponds to the fraction of the species generated at the disk that is detected at the ring. (The negative sign arises from the fact that the currents pass in opposite directions.) Hence, the "collection" current is proportional to the "generation" current. The value of N reflects the dimensions of the electrodes and the gap. Such experiments are particularly useful for detecting short-lived intermediate species, generated at the disk and consumed before reaching the ring (i.e., EC mechanism). Such consumption during the disk-to-ring transition time results in current ratios smaller than the "geometric" N. The RRDE has also been useful for studying ion transport (doping/undoping) in conducting polymer films.

4-5.2.2 Carbon Electrodes Solid electrodes based on carbon are currently in widespread use in electroanalysis, primarily because of their broad potential window, low background current, rich surface chemistry, low cost, chemical inertness, and suitability for various sensing and detection applications. In contrast, electron-transfer rates observed at carbon surfaces are often slower than those observed at metal electrodes. The electron-transfer reactivity is strongly affected by the origin

and history of the carbon surface (20,21). While all common carbon electrode materials share the basic structure of a six-membered aromatic ring and sp^2 bonding, they differ in the relative density of the edge and basal planes at their surfaces. The edge orientation is more reactive than the graphite basal plane toward electron transfer and adsorption. Materials with different edge-to-basal plane ratios thus display different electron-transfer kinetics for a given redox analyte. The edge orientation also displays undesirably high background contributions. A variety of electrode pretreatment procedures have been proposed to increase the electron-transfer rates. The type of carbon, as well as the pretreatment method, thus has a profound effect upon the analytical performance. The most popular carbon electrode materials are those involving glassy carbon, carbon paste, carbon fiber, screen-printed carbon strips, carbon films, or other carbon composites (e.g., graphite epoxy, wax-impregnated graphite, Kelgraf). The properties of different types of carbon electrodes are discussed below.

4-5.2.2.1 Glassy-Carbon Electrodes Glassy (or "vitreous") carbon has been very popular because of its excellent mechanical and electrical properties, wide potential window, chemical inertness (solvent resistance), and relatively reproducible performance. The material is prepared by means of a carefully controlled heating program of a premodeled polymeric (phenol–formaldehyde) resin body in an inert atmosphere (22). The carbonization process is carried out very slowly over the 300–1200°C temperature range to insure the elimination of oxygen, nitrogen, and hydrogen. The structure of glassy carbon involves thin, tangled ribbons of cross-linked graphite-like sheets. Because of its high density and small pore size, no impregnating procedure is required. However, a surface pretreatment is usually employed to create active and reproducible glassy-carbon electrodes and to enhance their analytical performance (18,23). Such pretreatment is usually achieved by polishing (to a shiny "mirror-like" appearance) with successively smaller alumina particles (down to 0.05 μm) on a polishing cloth. The electrode should then be rinsed with deionized water before use. Additional activation steps, such as electrochemical, chemical, heat, or laser treatments, have also been used to enhance the performance. The improved electron-transfer reactivity has been attributed to the removal of surface contaminants, exposure of fresh carbon edges, and an increase in the density of surface oxygen groups (which act as interfacial surface mediators). Several reviews provide more information on the physical and electrochemical properties of glassy-carbon electrodes (20,24).

A similar, but highly porous, vitreous carbon material—reticulated vitreous carbon (RVC)—has found widespread application for flow analysis and spectroelectrochemistry (25). As shown in Figure 4-10, RVC is an open-pore ("sponge-like") material; such a network combines the electrochemical properties of glassy carbon with many structural and hydrodynamic advantages. These include a very high surface area ($\sim 66\ cm^2\ cm^{-3}$ for the 100-ppi grade), 90–97% void volume, and a low resistance to fluid flow.

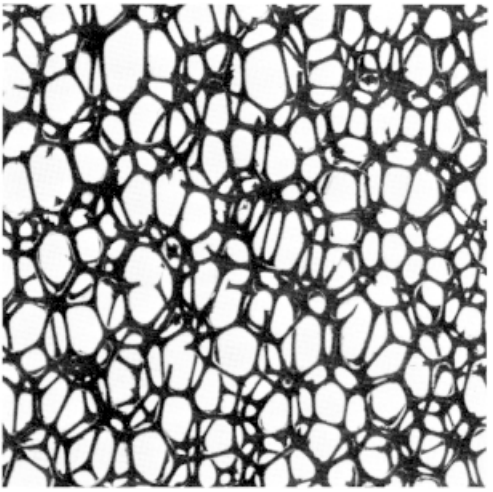

FIGURE 4-10 The open-pore structure of reticulated vitreous carbon.

4-5.2.2.2 Carbon-Paste Electrodes Carbon-paste electrodes, which use graphite powder mixed with various water-immiscible organic binders (pasting liquids), offer an easily renewable and modified surface, low cost, and very low background current contributions (26–28). A wide choice of pasting liquids is possible, but practical considerations of low volatility, purity, and economy narrow the choice to a few. These include Nujol (mineral oil), paraffin oil, silicone grease, and bromonaphthalene. The first appears to perform the best. The paste composition strongly affects the electrode reactivity, with increase in the pasting-liquid content decreasing electron-transfer rates, as well as the background-current contributions (28). In the absence of pasting liquid, the dry graphite electrode yields very rapid electron-transfer rates (approaching those of metallic surfaces). Despite their growing popularity, the exact behavior of carbon-paste electrodes is not fully understood. It is possible that some of the electrochemistry observed at these electrodes involves permeation of the pasting liquid layer by the electroactive species (i.e., solvent extraction). Carbon paste represents a convenient matrix for the incorporation of appropriate modifying moieties (29). The modifier is simply mixed together with the graphite/binder paste (with no need to devise individualized attachment schemes for each modifier). Enzyme-containing carbon pastes have been used as fast-responding reagentless biosensors (see Chapter 6). A disadvantage of carbon pastes is the tendency of the organic binder to dissolve in solutions containing an appreciable fraction of organic solvent.

4-5.2.2.3 Carbon-Fiber Electrodes The growing interest in ultramicroelectrodes (Section 4-5.4) has led to widespread use of carbon fibers in electroanalysis. Such materials are produced, mainly in connection with the preparation of high-strength composites, by high-temperature pyrolysis of polymer textiles or via

catalytic chemical vapor deposition. Different carbon fiber microstructures are available, depending upon the manufacturing process. They can be classified into three broad categories, namely, low-, medium-, and high-modulus types. The last type is most suitable for electrochemical studies because of its well-ordered graphite-like structure and low porosity (30). Improved electron transfer performance can be achieved by various electrode pretreatments, particularly "mild" and "strong" electrochemical activations, or heat treatment (31). Most electroanalytical applications rely on fibers of 5–20 μm diameter that provide the desired radial diffusion. Such fibers are typically mounted at the tip of a pulled glass capillary with epoxy adhesive, and are used in cylindrical or disk configurations. Precautions should be taken not to contaminate the carbon surface with the epoxy. The main advantage of carbon-fiber microelectrodes is their small size (5–30 μm diameter for commercially available fibers), which makes, them very attractive for anodic measurements in various microenvironments—for example, the detection of neurotransmitter release in the extracellular space of the brain. Nanometer-sized carbon fibers can be prepared by etching the fiber in flame or under ion beam (e.g., Figure 4-11). The various electroanalytical applications of carbon fibers have been reviewed by Edmonds (32).

FIGURE 4-11 Scanning electron image of a carbon-fiber electrode.

4-5.2.3 Metal Electrodes While a wide choice of noble metals is available, platinum and gold are the most widely used metallic electrodes. Such electrodes offer a very favorable electron-transfer kinetics and a large anodic potential range. In contrast, the low hydrogen overvoltage at these electrode limits the cathodic potential window (to the -0.2 to -0.5 V region, depending upon the pH). More problematic are the high background currents associated with the formation of surface-oxide or adsorbed hydrogen layers (e.g., Figure 4-12). Such films can also strongly alter the kinetics of the electrode reaction, leading to irreproducible data. These difficulties can be addressed with a pulse potential (cleaning/reactivation) cycle, as common in flow amperometry (34). The surface layers problem is less severe in nonaqueous media where noble metals are often an ideal choice. Compared to platinum electrodes, gold ones are more inert, and hence are less prone to the formation of stable oxide films or surface contamination. Gold electrodes are also widely used as substrates for self-assembled organosulfur monolayers or for stripping measurements of trace metals (Sections 4-5.3 and 3.5). Other metals, such as copper, nickel, or silver have been used as electrode materials in connection with specific applications, such as the detection of amino acids or carbohydrates in

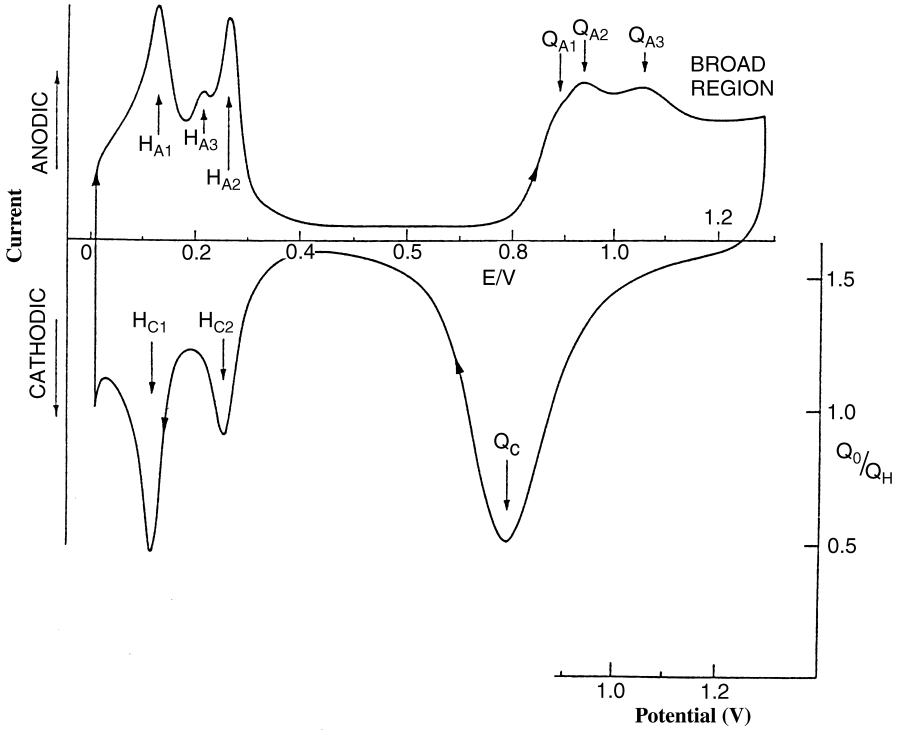

Figure 4-12 Current–potential curve for a platinum electrode in 0.5 M H_2SO_4. Regions of oxide formation (Q_A) and reduction (Q_C) as well as formation, of hydrogen (H_C) and its oxidation (H_A) are indicated. (Reproduced with permission from reference 33.)

alkaline medium (copper and nickel) and of cyanide or sulfur compounds (silver). Unlike platinum or gold electrodes, the copper electrode offers a stable response for carbohydrates at constant potential.

4-5.3 Chemically Modified Electrodes

Chemically modified electrodes (CMEs) represent a modem approach to electrode systems. These rely on the placement of a reagent onto the surface, to impart the behavior of that reagent to the modified surface. Such deliberate alteration of electrode surfaces can thus meet the needs of many electroanalytical problems, and may form the basis for new analytical applications and different sensing devices.

There are various ways in which CMEs can benefit analytical applications. These include acceleration of electron-transfer reactions, preferential accumulation, or selective membrane permeation. Such steps can impart higher selectivity, sensitivity, or stability to electrochemical devices. These analytical applications and improvements have been extensively reviewed (35–37). Many other important applications, including electrochromic display devices, controlled release of drugs, electrosynthesis, and corrosion protection, should also benefit from the rational design of electrode surfaces.

One of the most common approaches for incorporating a modifier onto the surface has been coverage with an appropriate polymer film. Polymer modified electrodes are often prepared by casting a solution containing the dissolved polymer onto the surface and allowing the solvent to evaporate, or via electropolymerization in the presence of the dissolved monomer. The latter offers precise control of the film thickness (and often the morphology) and is particularly attractive in connection with miniaturized sensor surfaces. The structures of some common polymeric coatings are shown in Figure 4-13. For example, the Dupont Nafion perfluorinated sulfonated cation exchanger (*a*) has been widely used as an electrode modifier due to its attractive permselective, ion-exchange, and antifouling properties (see examples below). Additional advantages can be obtained by coupling two (or more) polymers in a mixed or multilayer configuration. Other useful modification schemes include bulk modification of composite carbon materials, covalent (chemical) attachment, sol-gel encapsulation, physical adsorption, and spontaneous chemisorption.

4-5.3.1 Self-Assembled Monolayers Spontaneously adsorbed monolayers of *n*-alkanethiols ($X(CH_2)_nSH$ with $n > 10$) on gold surfaces, based on the strong interaction between gold and sulfur, are particularly well-suited for controlling and manipulating the reactivity at the interface. Such monolayers are commonly formed by immersing the gold electrode overnight in ethanolic solutions containing millimolar concentrations of the alkanethiol. The formation of self-assembled organosulfur monolayers (SAMs) has attracted considerable attention due to its many potential scientific and technological applications (38–40). In addition to fundamental studies on the structure of such monolayers and long-range electron transfer, such applications include chemical sensors and biosensors, information storage devices, or lithography.

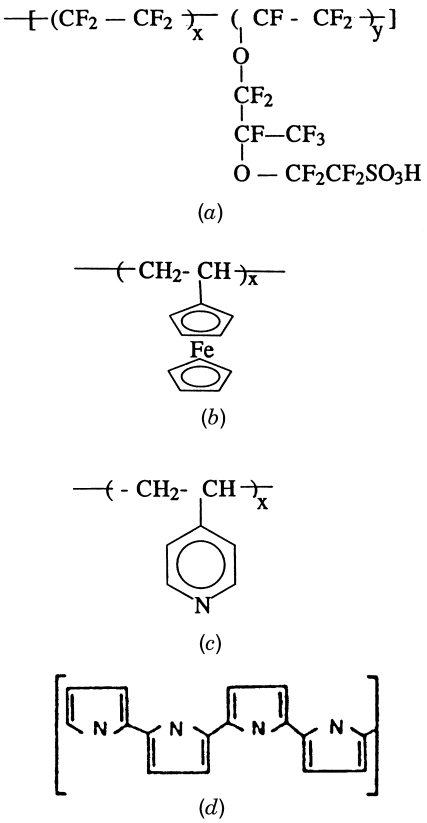

FIGURE 4-13 Structures of common polymeric coatings: (*a*) Nafion, (*b*) polyvinyllferrocene; (*c*) polyvinylpyridine; (*d*) polypyrrole.

Cleavage of the S–H bond is central to this monolayer formation:

$$\mathrm{RSH} + \mathrm{Au} \rightleftharpoons \mathrm{RS{-}Au} + e^- + \mathrm{H}^+ \tag{4-9}$$

Van-der Waals forces between the methylene groups orient the monolayer. Such a self-assembly process thus results in well-organized and stable monolayers, with the hydrocarbon tails packed parallel to each other, tilted at $\sim 30^\circ$ relative to the surface normal (Figure 4-14). The closely-packed pinhole-free films (surface coverage of $\sim 9 \times 10^{-10}$ mol cm^{-2}) block transport of species to the underlying gold surface. The packing and order are influenced by factors such as the chain length, nature of the end group, nature of the solvent, immersion time, and substrate morphology. Increasingly disordered structures with lower packing density and coverage are observed upon decreasing the chain length ($n < 10$). These and other structural disorders and defects (e.g., pinholes) often lead to degraded performance. Coassembled monolayers, formed from mixtures of alkanethiols, can offer compositional

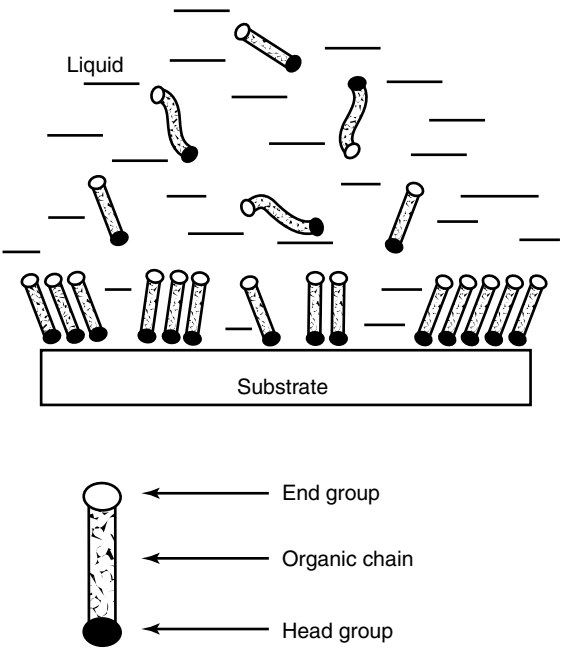

FIGURE 4-14 Formation of a self-assembled monolayer at a gold sustrate. (Reproduced with permission from reference 38.)

and topographical variations in the film architecture. The novelty of using SAMs stems from their ability to be further modified into chemically or biologically reactive surface layers (via covalent coupling of different materials to the functional end group, X). This use of SAMs for anchoring various functionalities can impart specific interactions essential for various sensing applications (see Chapter 6). These applications can benefit from the use of mixed SAMs that minimize steric hindrance effects. The high degree of order has also allowed detailed structure–function relationships to be developed for various electron-transfer processes. Other highly ordered films, such as of alkyl siloxane, can be formed on metal oxide surfaces (particularly SiO_2).

4-5.3.2 Sol-Gel Encapsulation of Reactive Species Another new and attractive route for tailoring electrode surfaces involves the low-temperature encapsulation of recognition species within sol-gel films (41,42). Such ceramic films are prepared by the hydrolysis of an alkoxide precursor such as, $Si(OCH_3)_4$ under acidic or basic condensation, followed by polycondensation of the hydroxylated monomer to form a three-dimensional interconnected porous network. The resulting porous glass-like material can physically retain the desired modifier but permits its interaction with the analyte that diffuses into the matrix. Besides their ability to entrap the modifier, sol-gel processes offer tunability of the physical characteristics

(e.g., porosity), thermal stability, and mechanical rigidity. Sol-gel-derived composite electrodes have also been prepared by dispersing carbon or gold powders in the initial sol-gel mixture (43,44).

4-5.3.3 Electrocatalytic Modified Electrodes Often the desired redox reaction at the bare electrode involves slow electron-transfer kinetics and therefore occurs at an appreciable rate only at potentials substantially higher than its thermodynamic redox potential. Such reactions can be catalyzed by attaching to the surface a suitable electron transfer mediator (45,46). Knowledge of homogeneous solution kinetics is often used to select the surface-bound catalyst. The function of the mediator is to facilitate the charge transfer between the analyte and the electrode. In most cases the mediated reaction sequence (e.g., for a reduction process) can be described by

$$M_{ox} + ne^- \rightarrow M_{red} \tag{4-10}$$

$$M_{red} + A_{ox} \rightarrow M_{ox} + A_{red} \tag{4-11}$$

where M represents the mediator and A the analyte. Hence, the electron transfer takes place between the electrode and mediator and not directly between the electrode and analyte. The active form of the catalyst is electrochemically regenerated. The net results of this electron shuttling are a lowering of the overvoltage to the formal potential of the mediator and an increase in current density. The efficiency of the electrocatalytic process also depends upon the actual distance between the bound redox site and the surface (since the electron-transfer rate decreases exponentially when the electron-tunneling distance is increased).

The improvements in sensitivity and selectivity that accrue from electrocatalytic CMEs have been illustrated for numerous analytical problems, including the biosensing of dihydronicotinamide–adenine dinucleotide (NADH) at a Meldola-Blue coated electrode (47), the liquid-chromatographic amperometric detection of thiols at cobalt-phthalcocyanine-coated electrodes (48), detection of nitric oxide release from a single cell by a porphyrin-based microsensor (49), and flow-injection measurements of carbohydrates at ruthenium dioxide containing carbon-paste detectors (50). Cyclic voltammograms for various carbohydrates at the ruthenium dioxide carbon-paste electrodes are shown in Figure 4-15. As expected for redox mediation, the peaks of the surface-bound ruthenium species (dotted lines) increase upon addition of the carbohydrate analytes (solid lines). Figure 4-16 illustrates the electrocatalytic scheme involved in the detection of NADH. The implications of this scheme for various biosensors are discussed in Section 6-1.

4-5.3.4 Preconcentrating Electrodes Preconcentrating CMEs, with surfaces designed for reacting and binding of target analytes, hold great promise for chemical sensing (51–54). The concept is analogous to stripping voltammetric schemes, with the target analyte being preferentially partitioned from the dilute sample into the preconcentrating surface layer, and subsequently being reduced or

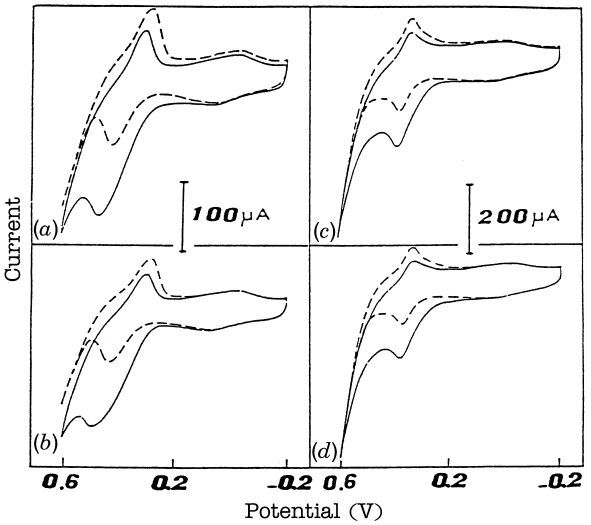

FIGURE 4-15 Cyclic voltammograms for 1.5×10^{-3} M ribose (*a*), glucose (*b*), galactose (*c*), and fructose (*d*) recorded at a RuO_2-modified carbon-paste electrode. Dotted lines were obtained in carbohydrate-free solutions. (Reproduced with permission from reference 50.)

oxidized during a potential scan. Unlike conventional stripping procedures, the preconcentration step is nonelectrolytic. Most preconcentrating CMEs employ electrostatic binding or coordination reactions for collecting the analyte. Schemes based on hydrophobic partition into a lipid coating or covalent reactions have also been reported. The preconcentrating agent may be incorporated within the interior of a carbon-paste matrix or via functionalized polymeric and alkanethiol films. For example, as shown in Figure 4-17, ligand centers can covalently bind to a polymer backbone on the electrode to effectively accumulate and measure target metals. The major requirements for a successful analytical use of preconcentrating electrodes are strong and selective binding, prevention of saturation, and convenient surface regeneration. Following the accumulation, the electrode can be transferred to more suitable solutions that facilitate the measurement and "cleaning" steps.

Practical examples of using preconcentrating CMEs include the use of a mixed 2,9-dimethyl-1,10-phenanthroline/carbon-paste electrode for trace measurements of copper (55), the use of clay-containing carbon pastes for voltammetric measurements of iron (56), the use of polyelectrolyte coatings for the uptake and

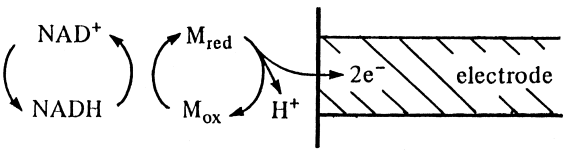

FIGURE 4-16 Electrocatalytic detection of NADH.

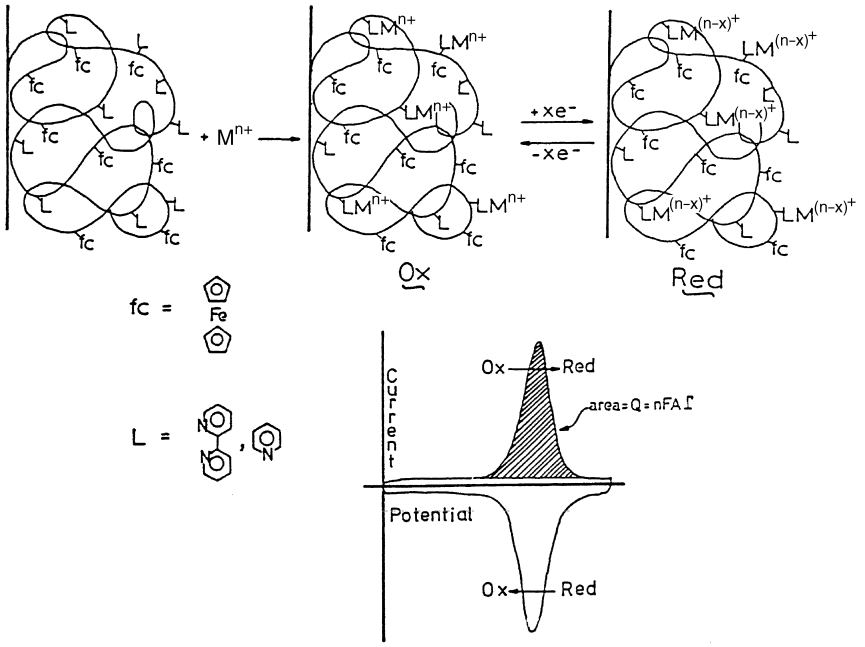

FIGURE 4-17 Preconcentrating surfaces based on covalent binding of the ligand to a polymer backbone. Q = charge; A = electrode area; Γ = surface coverage. (Reproduced with permission from reference 52.)

voltammetry of multiply charged metal complexes (57,58), the use of surface-bound crown ethers and cryptands for trace measurements of lead (59), ion-exchange voltammetric measurements of lanthanide ions at a Nafion-coated electrode (60), the collection of ultratrace cadmium onto mercaptocarboxylic-acid monolayers (61), and the quantitation of nickel at porphyrin-coated electrodes (62).

4-5.3.5 Permselective Coatings Permselective coatings offer to bring higher selectivity and stability to electrochemical devices. This is accomplished by exclusion from the surface of unwanted matrix constituents, while allowing transport of the target analyte. Different avenues for controlling the access to the surface have been proposed, based on different transport mechanisms. These include the use of size-exclusion poly(1,2-diaminobenzene) films (63), charge-exclusion ionomeric Nafion coatings (64), hydrophobic lipid (65) or alkylthiols (66) layers, or bifunctional (mixed) coatings (67). Such anti-interference membrane barriers offer an effective separation step (in situ on the surface), and hence protect the surface against adsorption of large macromolecules or minimize overlapping signals from undesired electroactive interferences. For example, the poly(1,2-diaminobenzene)-coated flow detector rapidly responds to the small hydrogen peroxide molecule, but not to the larger ascorbic acid, uric acid, or cysteine species (Figure 4-18). Note also

the protection from foulants present in the serum sample. Such size-exclusion (sieving) properties are attributed to the morphology of electropolymerized films (Figure 4-19). Similarly, Nafion-coated microelectrodes are often used for in-vivo monitoring of cationic neurotransmitters (e.g., dopamine) in the presence of otherwise interfering ascorbic acid (64). Such anionic interference is excluded from the surface through electrostatic repulsion with the negatively charged sulfonated groups (Figure 4-20). Examples of these and other discriminative films are given in Table 4-2.

4-5.3.6 Conducting Polymers Electronically conducting polymers (such as polypyrrole, polythiophene, and polyaniline) have attracted considerable attention due to their ability to switch reversibly between the positively charged conductive state and a neutral, essentially insulating, form and to incorporate and expel anionic species (from and to the surrounding solution), upon oxidation or reduction:

$$P^0 + A^- \rightarrow P^+A^- + e^- \tag{4-12}$$

where P and A^- represent the polymer and the "dopant" anion, respectively. The latter serves to maintain the electrical neutrality, that is, to counterbalance the positive charge of the polymer backbone. The electrical conductivity of these films, which originates from the electronic structure of their polymeric backbone (i.e., electron hopping involving the delocalized π electrons), thus varies with the applied potential. The structure of common conducting polymers, and their conductivity ranges (from the undoped to doped states) are displayed in Figure 4-21. The redox

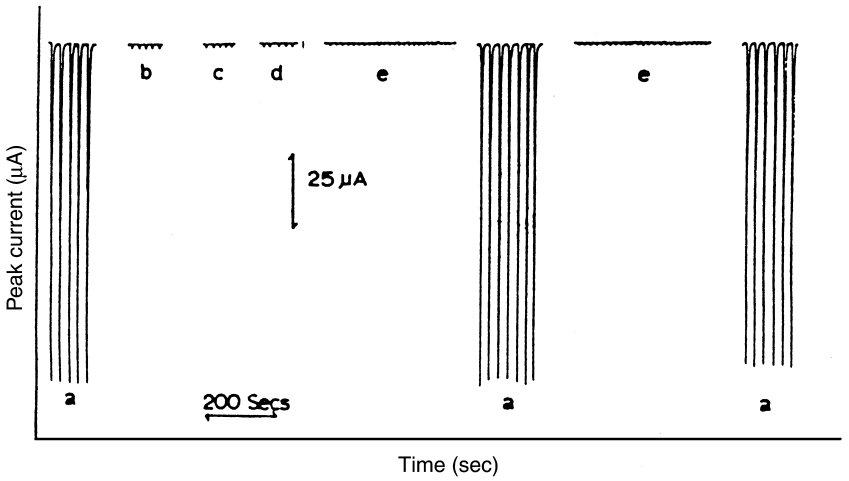

FIGURE 4-18 Permselective coatings: flow injection response of a poly(1,2-diaminobenzene)-coated electrode to the following: a, hydrogen peroxide (1 mM); b, ascorbic acid (1 mM); c, uric acid (1 mM); d, L-cysteine (1 mM); and e, control human serum. (Reproduced with permission from reference 63.)

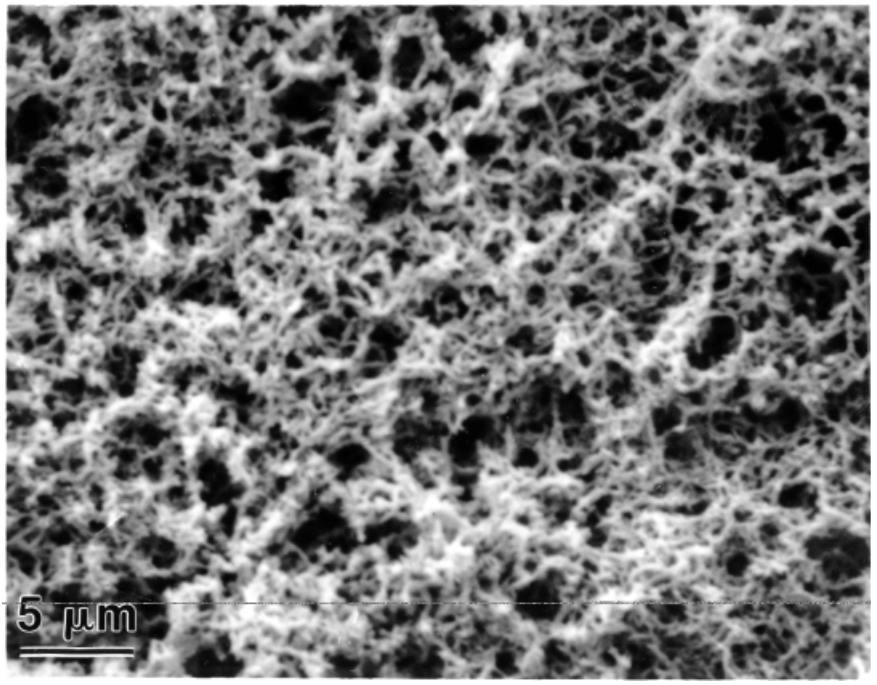

FIGURE 4-19 Scanning electron micrograph of a polyaniline-coated electrode.

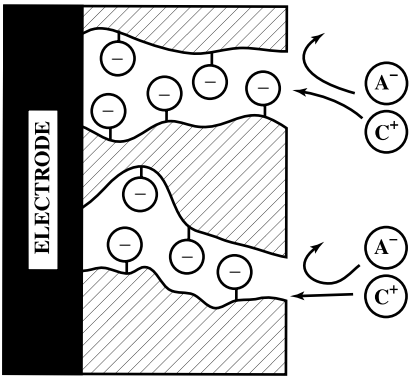

FIGURE 4-20 Use of negatively charged polymeric films for excluding anionic interferences.

TABLE 4-2 Commonly Used Membrane Barriers

Transport Mechanism	Membrane Barrier	Reference
Size exclusion	Cellulose acetate	68
	Poly(1,2-diaminobenzene)	63
	Polyphenol	69
Hydrophobic barriers	Phospholipid	65
	Self-assembled thiols	66
Charge exclusion	Nafion	64
	Poly(ester-sulfonic acid)	70
	Self-assembled thioctic acid	71
Mixed control	Cellulose acetate/Nafion	67

changes (equation 4-12) are not localized at a specific center, but rather delocalized over a number of conducting polymer groups.

These polymers are readily prepared by in-situ electropolymerization (from the monomer solution). The oxidation of the monomer proceeds according to

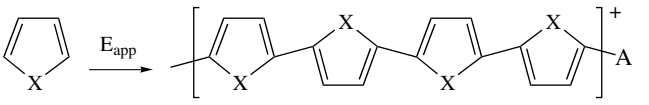

(4-13)

X=NH (polypyrrole)
S (polythiophene)
O (polyfuran)

Often the first step in the electropolymerization process is the electrooxidative formation of a radical cation from the starting monomer. This step is commonly followed by a dimerization process, followed by further oxidation and coupling reactions. Well-adhered films can thus be formed on the surface in galvanostatic, potentiostatic, or multi scan experiments. The behavior of electropolymerized films can be controlled by the polymerization conditions, including the electrolyte (particularly the nature and level of the anion serving as the dopant), solvent, monomer concentration, applied potential or current, and duration. The dynamics of the redox switching reaction (equation 4-12) strongly depend upon the ionic fluxes that accompany the process. The tight entrapment of large anionic dopants (e.g., polyelectrolytes) precludes their removal from the film, and hence the charge compensation is dominated by the movement of a "pseudo-dopant" cation.

Changes in the polymer properties can be induced by attaching various chemical or biological functionalities to the monomer prior to polymerization. It is possible also to impart molecular recognition or electrocatalytic action via the incorporation of functional dopants (e.g., complexing agents or an electron-transfer mediator). Hence, conducting polymers can act as efficient molecular interfaces between recognition elements and electrode transducers. The unique physical and chemical

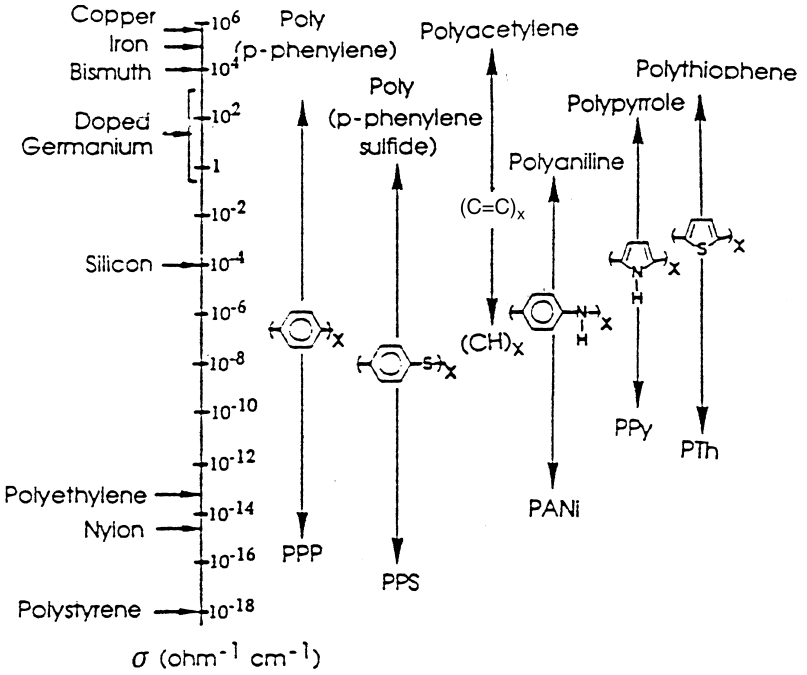

FIGURE 4-21 Conductivity range of common conducting polymers, along with their chemical structure. (Reproduced with permission from reference 72.)

properties of conducting polymers, and particularly the controllable and dramatic change in electrical conductivity and rapid exchange of the doping ion, offer diverse electrochemical applications, including batteries, fuel cells, corrosion protection, or chemical sensing (73). The latter include amperometric flow detection of nonelectroactive ions, solid-state gas sensing, entrapment/attachment and stabilization of biological entities, direct monitoring of biological interactions (e.g., DNA hybridization), electrochemical control of membrane permeability, sensor arrays based on multiple films, new potentiometric recognition of ions, preconcentration/stripping of trace metals, and controlled release of chemicals. For example, Figure 4-22 shows typical flow injection peaks for submillimolar concentrations of carbonate ions (utilizing the doping–updoping of the polypyrrole-based detector). Such anodic

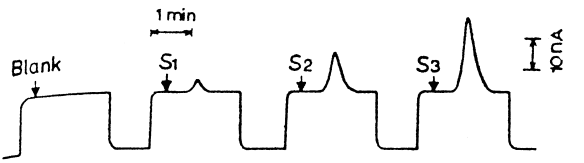

FIGURE 4-22 Typical response of polypyrrole detector to carbonate (S_1, 1×10^{-4} M; S_2, 2.5×10^{-4} M; S_3, 5×10^{-4} M) based on the doping–undoping process. (Reproduced with permission from reference 74.)

peaks reflect the passage of the carbonate anions [which are capable of penetrating into the film, equation (4-12)] over the surface. These and other analytical opportunities have been reviewed by Ivaska (75), Wallace (76), and Bidan (72). The widespread use of polypyrrole is attributed to its electropolymerization from aqueous media at neutral pH (which allows the entrapment of a wide range of dopants). Other films are more limited in this regard. For example, thiophene is soluble only in organic solvents, and aniline in acidic media. The electropolymerization growth can also lead to nonconducting, self-limiting films, which are often used as permselective/protective layers (Section 4-5.3.5) or for the physical entrapment of biomolecules (Chapter 6).

4-5.4 Microelectrodes

Miniaturization is a growing trend in the field of analytical chemistry. The miniaturization of working electrodes not only has obvious practical advantages, but also opens some fundamentally new possibilities (77–79). The term "microelectrode" is reserved here for electrodes with at least one dimension not greater than 25 μm.

Such dimensions offer obvious analytical advantages, including the exploration of microscopic domains, measurements of local concentration profiles, detection in microflow systems or within very narrow electrophoresis capillaries, and analysis of very small (microliter) sample volumes. Particularly fascinating are recent studies aimed at time-resolved probing of dynamic processes (e.g., secretion of chemical messengers) in single cells (80), the in-vivo monitoring of neurochemical events (e.g., stimulated dopamine release), and the use of nanoscopic electrode tips for single molecule detection (81) or high-resolution spatial characterization of surfaces (see Section 2-3). Figure 4-23 illustrates the use of a carbon-fiber microelectrode for measuring the vesicular release of dopamine following cellular stimulation.

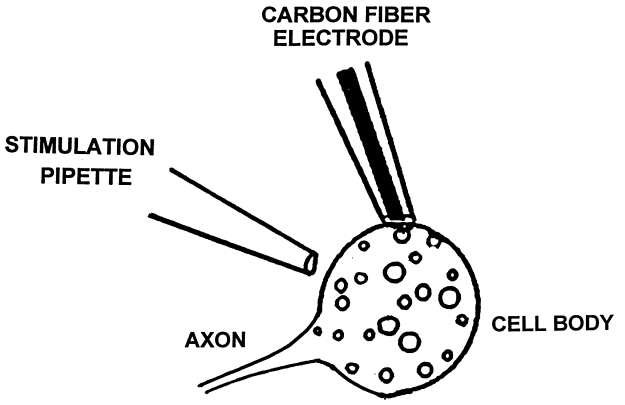

FIGURE 4-23 Experimental setup for monitoring dopamine release by exocytosis, from a cell body. The microelectrode and glass capillary (containing the chemical stimulant) are micromanipulated up to the cell body. (Reproduced with permission from reference 82.)

Microelectrodes exhibit several other attractive and important properties that have expanded the possibilities of electrochemistry:

- Because of the very small total currents at microelectrodes, it is possible to work in highly resistive solutions that would develop large ohmic (iR) drops with conventional electrodes. The decreased ohmic distortions allow electrochemical measurements to be made in new and unique chemical environments that are not amenable to macroscopic electrodes. Microelectrode experiments have thus been reported in low-dielectric solvents (e.g., benzene, toluene), frozen acetonitrile, low-temperature glasses, gaseous and solid phases, supercritical carbon dioxide, ionically conductive polymers, oil-based lubricants, and milk. In addition, more traditional systems can be studied with little or no deliberately added supporting electrolyte, and with two-electrode systems. The use of electrolyte-free organic media can greatly extend the electrochemical potential window, thus allowing studies of species with very high oxidation potentials. Acetonitrile, for example, can be used to about 4 V (versus a silver reference electrode), making possible studies of short-chain alkanes.
- The greatly reduced double-layer capacitance of microelectrodes, associated with their small area, results in electrochemical cells with small RC time constants. For example, for a microdisk the RC time constant is proportional to the radius of the electrode. The small RC constants allow high-speed voltammetric experiments to be performed on the microsecond time scale (scan rates higher than 10^6 V s^{-1}) and hence to probe the kinetics of very fast electron-transfer and coupling-chemical reactions (83), or the dynamic of processes such as exocytosis (e.g., Figure 4-23). More discussion of such high-speed experiments is given in Section 2-1.
- Enhanced rates of mass transport of electroactive species accrue from the radial (nonplanar) diffusion to the edges of microelectrodes. Such "edge effects" contribute significantly to the overall diffusion current. The rate of mass transport to and from the electrode (and hence the current density) increases as the electrode size decreases. As a consequence of the increase in mass-transport rates and the reduced charging currents, microelectrodes exhibit excellent signal-to-background characteristics in comparison to their larger counterparts. In addition, steady-state or quasi-steady-state currents are rapidly attained, and the contribution of convective transport is negligible. The fact that redox reactions that are limited by mass transport at macroscopic electrodes become limited by the rate of electron transfer can also benefit many kinetic studies.

4-5.4.1 Diffusion at Microelectrodes The total diffusion-limited current is composed of the planar flux and radial flux diffusion components:

$$i_{\text{total}} = i_{\text{planar}} + i_{\text{radial}} \tag{4-14}$$

For disk, spherical, and hemispherical geometries, the general expression for the radial component in equation (4-14) is given by

$$i_{\text{radial}} = arnFDC \tag{4-15}$$

where r is the electrode radius and a is a function of the electrode geometry. For disks, spheres, and hemispheres the a values are equal to 4, 4π, and 2π, respectively. Such radial diffusion leads to a larger flux at the perimeter of the electrode than at the center, and hence to a nonuniform current density.

The extent to which the planar or radial component dominates depends on the relative dimensions of the electrode and the diffusion layer, as expressed by the dimensionless parameter Dt/r_0^2 where t is the electrolysis time and r_0 is the smallest dimension of the electrode (84). For large (>1) values of Dt/r_0^2 (i.e., diffusion layer thickness that exceeds the size of the electrode), the current approaches steady state, and sigmoidal voltammograms are observed. In contrast, planar diffusion dominates at small values of Dt/r_0^2, and a peak-shaped behavior is observed. Hence, depending on the time scale of the experiment (i.e., the scan rate), the same electrode may exhibit peak-shaped or sigmoidal voltammograms (e.g., Figure 4-24). Similarly, in chronoamperometric experiments, a modified Cottrell equation predicts that a steady-state current is reached rapidly after the potential step (e.g., within ~ 10 ms and 1.3 s for 1 μm and 10 μm diameter disks, respectively). The change from semi-infinite planar diffusion to semi-infinite hemispherical diffusion, associated with the decrease in the electrode dimension, is illustrated in Figure 4-25, which displays computed concentration profiles for a given time after the start of a chronoamperometric experiment at a disk with different radii.

4-5.4.2 Configurations of Microelectrodes Electrodes of different materials have been miniaturized in many geometrical shapes (Figure 4-26), with the common characteristic that the electrode dimension is significantly smaller than the diffusion layer at the surface (for ordinary voltammetric time scales, e.g., 1–10 s). The most commonly used is a circular conductor (of around 10 μm diameter), embedded in an insulating plane (the so-called microdisk electrode) (a). Other common geometries include the microring (b), microcylinder (c), microhemisphere (d), or microband (e) electrodes. Cylinder and band (line) microelectrodes, which can be several millimeters long, yield larger (and hence more easily measured) currents, while maintaining an enhanced diffusional flux. Band electrodes of nanoscopic dimensions can be fabricated by sealing ("sandwiching") ultrathin carbon and metal films between insulating supports and polishing one end of the sandwich, or via photolithographic deposition of a thin metal film on an insulating substrate. The fabrication of most microelectrode geometries (with the exception of microcylinders) is technically demanding. Special attention should be given to proper sealing (between the active surface and insulating sheath) to assure good performance and to minimize stray capacitances. Fine metal (Pt, Au, Ir) wires, carbon fibers, or thin metal films are commonly used for these preparations. Molecular (nanometer)-sized electrodes being developed in several laboratories

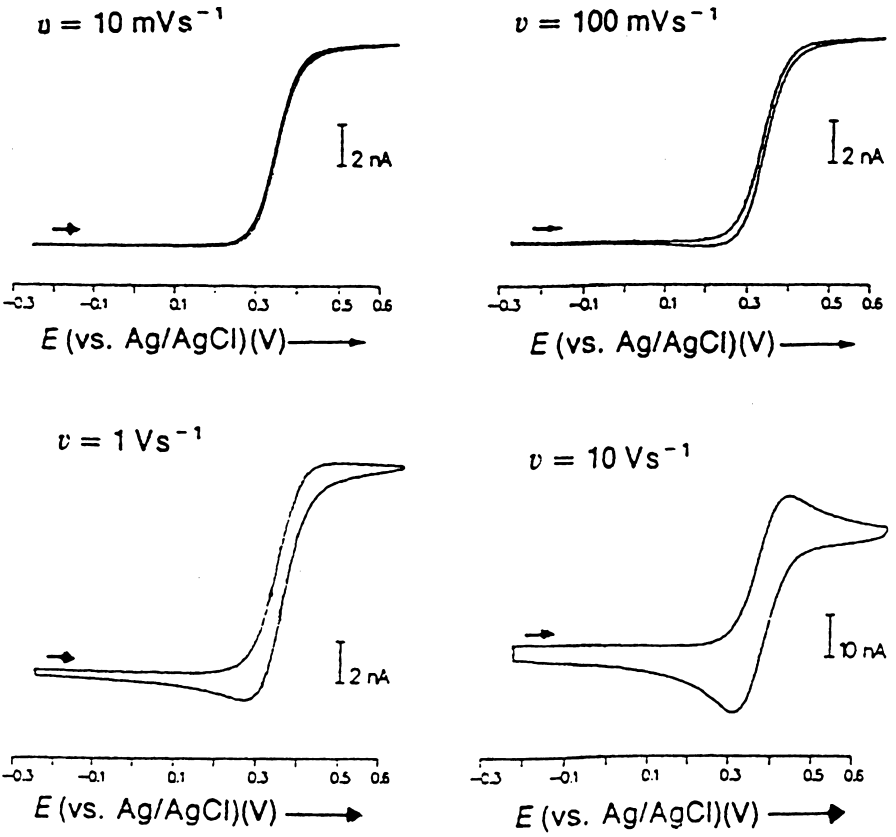

FIGURE 4-24 Cyclic voltammograms for the oxidation of ferrocene at a 6 μm platinum microdisk at different scan rates. (Reproduced with permission from reference 84.)

(85) should offer additional spatial and temporal advantages, including a closer look at interfacial chemistry processes. The construction of such nanoscopic electrodes is even more challenging than that of their microscopic counterparts (86).

4-5.4.3 Composite Electrodes Composite electrodes couple the advantages of single microelectrode systems with significantly higher currents due to larger surface areas (86). Such electrodes thus address instrumental difficulties of monitoring the extremely small (subnanoampere) currents at single microelectrodes. The surfaces of composite electrodes consist of uniform (array) or random (ensemble) dispersions of a conductor region within a continuous insulating matrix (Figure 4-27). Examples of arrays include closely spaced microdisks or interdigitated microband electrodes (e.g. Figure 4-28). Lithographic techniques are often used for fabricating such arrays (with various patterning), allowing precise control of the spacing (88). Ensembles can be fabricated by mixing or pressing a powdered

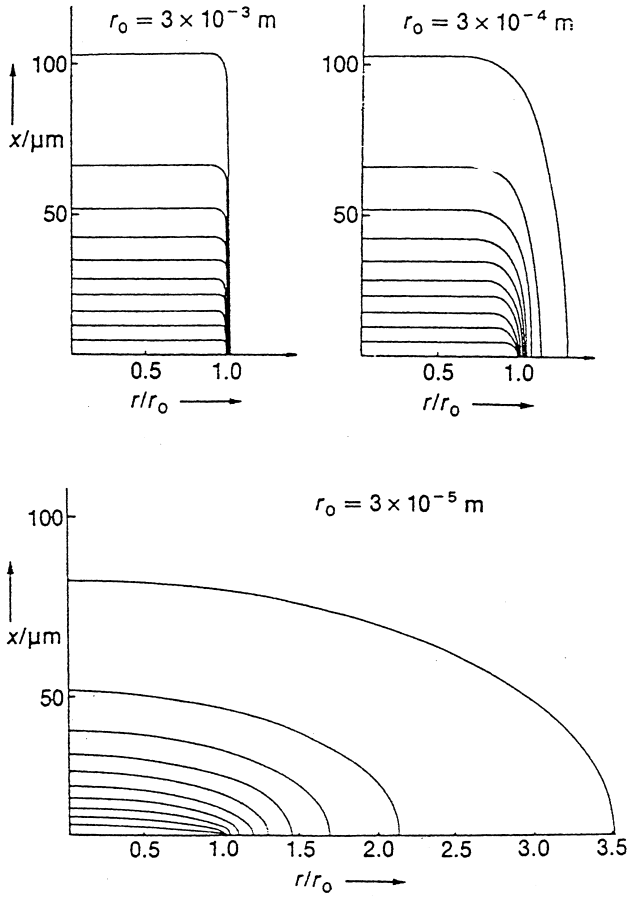

FIGURE 4-25 Normalized calculated concentration profiles for disk electrodes with different radii (r_0), one second after start of a chronoamperometric experiment. (Reproduced with permission from reference 84.)

conductor with an insulator [e.g. Kel-F/graphite (89)], by impregnation of a porous conductor with an insulator [e.g., microcellular carbon/epoxy (90)], embedding carbon fibers in an insulating epoxy (91), or via deposition of a metal conductor into the pores of a microporous host membrane (92).

As long as there is a negligible overlap of the diffusion layers from adjacent sites (i.e., so long as each member maintains its own radial diffusional field), the current of a composite electrode is the sum of currents of the individual sites. At sufficiently long times, the diffusion layers overlap, and the electrode behaves as though its entire geometric surface were active. For example, a slow scanning cyclic voltammetric experiment displays a current peak proportional to the total geometric area. The exact time scale for the change from isolated to merged diffusion layers depends on the spacing between the individual electrodes and their size. Larger distances and

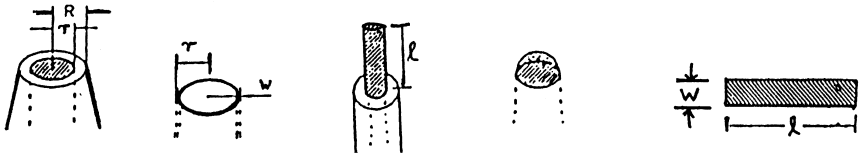

(*a*) (*b*) (*c*) (*d*) (*e*)

FIGURE 4-26 Common configurations of microelectrodes. *a*, disk; *b*, ring; *c*, cylinder; *d*, hemisphere; *e*, line (bond); l = length, w = width, r = radius.

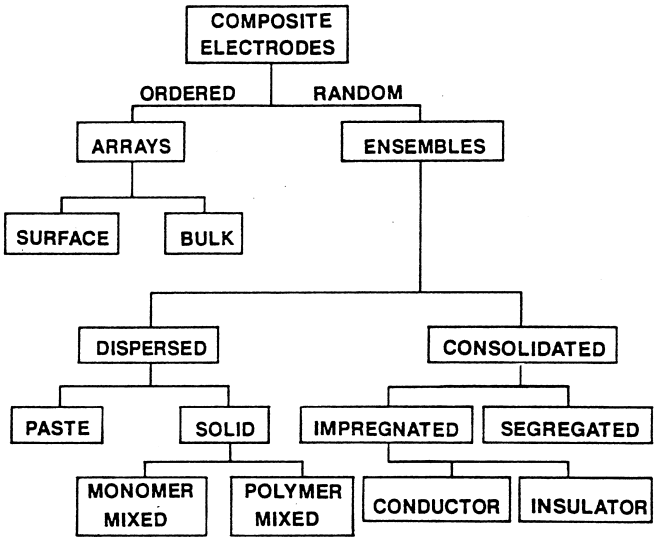

FIGURE 4-27 Classification of composite electrodes used in controlled-potential electrochemical techniques. (Reproduced with permission from reference 87.)

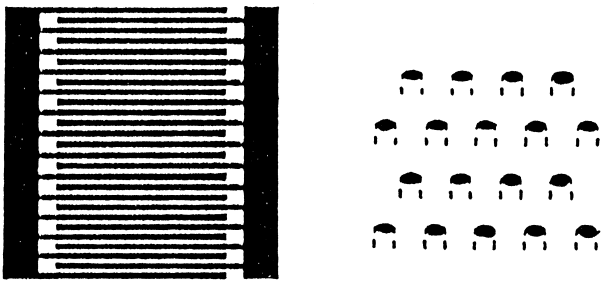

(*a*) (*b*)

FIGURE 4-28 Schematic representation of an interdigitated microarray electrode (*a*) and closely-spaced microdisk electrodes (*b*).

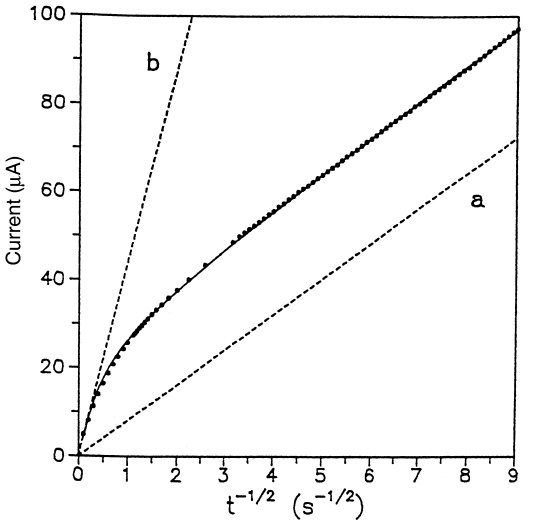

FIGURE 4-29 Cottrell plot of the chronoamperometric response for 1×10^{-3} M $Ru(NH_3)_6^{3+}$ at a Kel-F/gold composite electrode. Points are experimental data, the solid line is the least-squares fit to theory. Dashed lines are theoretical Cottrell plots for a macroelectrode with active area equal to the active area of the composite (curve a) and to the geometric area of the composite (curve b). (Reproduced with permission from reference 87.)

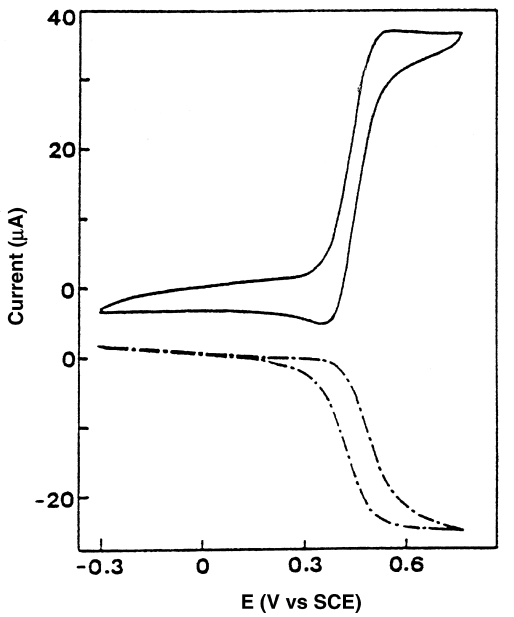

FIGURE 4-30 Cyclic voltammogram for ferrocene at a 3 μm width, 2 μm gap interdigitated microband (solid line). The dotted line represents the current of the collector electrode held at a potential of -0.1 V. (Reproduced with permission from reference 95.)

smaller dimensions are preferred. Chronoamperometric experiments, such as the one shown in Figure 4-29, can be used to estimate the transition between these time regimes, and the fraction of the conductive surface in accordance with the theoretical model (93). In addition to their large collective current, enhanced signal-to-noise ratios, and flow-rate independence (in the flow detection), composite electrodes hold great promise for incorporating appropriate modifiers within the bulk of the composite matrix.

Closely spaced band electrodes (pairs or triples), with each electrode within the diffusion layer of the other, can be used for studying reactions in a manner analogous to ring-disk generation–collection and redox recycling experiments (94,95). Unlike with rotating ring-disk electrodes, the product of the reaction at the collector electrode can diffuse back across the narrow gap to the generator electrode to give higher collection efficiencies (and hence sensitivity). A typical generation–collection experiment at such an array is illustrated in Figure 4-30. The covering of such closely spaced microelectrodes with conducting polymers can form the basis for novel microelectronic (transistor-like) sensing devices (see Chapter 6). The properties and applications of interdigitated arrays of microband electrodes have been reviewed (96).

REFERENCES

1. T.P. DeAngelis, R.E. Bond, E.E. Brooks, and W.R. Heineman. *Anal. Chem.*, 49, 1792 (1977).
2. R. Clark and A.G. Ewing. *Anal. Chem.*, 70, 1119 (1998).
3. C.K. Mann, in A.J. Bard, Ed., *Electroanalytical Chemistry*, Vol. 3, p. 57, Marcel Dekker, New York, 1969.
4. G.G. Wallace, *Trends Anal. Chem.*, 4, 145 (1985).
5. A. Newman, *Anal. Chem.*, 69, 369A (1997).
6. T. Matsue, A. Aoki, E. Ando, and I. Uchida. *Anal. Chem.*, 62, 409 (1990).
7. A.M. Bond, *Modern Polarographic Methods in Analytical Chemistry*, Marcel Dekker, New York, 1980.
8. P. He, J. Avery, and L.R. Faulkner, *Anal. Chem.*, 54, 1314 (1982).
9. A.M. Bond, D. Luscombe, S.N. Tan, and F.L Walter, *Electroanalysis*, 2, 195 (1990).
10. J. Wang, *Analyst*, 119, 763 (1994).
11. K.A. Erickson and P. Wilding, *Clin. Chem.*, 39, 283 (1993).
12. W. Kemula, and K. Kublik, *Anal. Chim. Acta*, 18, 104 (1958).
13. W. Peterson, *Am. Lab.*, 12, 69 (1979).
14. G. Macchi, *J. Electroanal. Chem.*, 9, 290 (1965).
15. Z. Kowalski, K. Wang, R. Osteryoung, and J. Osteryoung. *Anal. Chem.*, 59, 2216 (1987).
16. T.M. Florence, *J. Electroanal. Chem.*, 27, 273 (1970).
17. R.N. Adams, *Electrochemistry at Solid Electrodes*, Marcel Dekker, New York, 1969.
18. R.C. Engstrom, *Anal. Chem.*, 54, 2310 (1982).
19. W.J Albery and M. Hitchman, *Ring-Disk Electrodes*, Clarendon Press, Oxford, 1971.

20. R.L. McCreery, "Carbon Electrodes: Structural Effects on Electron Transfer Kinetics," in A.J. Bard, Ed., *Electroanalytical Chemistry*, Vol 18, Marcel Dekker, New York, 1991.
21. P. Chen and R.L. McCreery, *Anal. Chem.*, 68, 3958 (1996).
22. J.C. Bokros, *Carbon*, 15, 355 (1977).
23. D. Fagan, I. Hu, and T. Kuwana, *Anal. Chem.*, 57, 2759 (1985).
24. W.E. van der Linden and J.W. Dieker, *Anal. Chim. Acta*, 119, 1 (1980).
25. J. Wang, *Electrochim. Acta*, 26, 1721 (1981).
26. C. Olson and R.N. Adams, *Anal. Chim. Acta*, 22, 582 (1960).
27. C. Urbaniczky and K. Lundstrom, *J. Electroanal. Chem.*, 176, 169 (1984).
28. M. Rice, Z. Galus, and R.N. Adams, *J. Electroanal. Chem.*, 143, 89 (1983).
29. K. Kalcher, *Electroanalysis*, 2, 419 (1990).
30. E. Csöregi, L. Gorton, and G. Marko-Varga, *Anal. Chim. Acta*, 273, 59 (1993).
31. J. Feng, M. Brazell, K. Renner, R. Kasser, and R.N. Adams, *Anal. Chem.*, 59, 1863 (1987).
32. T. Edmonds, *Anal. Chim. Acta*, 175, 1 (1985).
33. H. Kozlowska, B. Conway, and W. Sharp, *J. Electroanal. Chem.*, 43, 9 (1973).
34. D.C. Johnson and W. LaCourse, *Anal. Chem.*, 62, 589A (1990).
35. R.W. Murray, A.G. Ewing, and R.A. Durst, *Anal. Chem.*, 59, 379A (1987).
36. J. Wang, *Electroanalysis*, 3, 255 (1991).
37. R.P. Baldwin and K.N. Thomsen, *Talanta*, 38, 1 (1991).
38. C. Zhong and M.D. Porter, *Anal. Chem.*, 67, 709A (1995).
39. C. Bain and G. Whitsides, *Angew. Chem. Int. Ed. Eng.*, 28(4), 506 (1989).
40. D. Mandler, and I. Turyan, *Electroanalysis*, 8, 207 (1996).
41. O. Lev, M. Tsionsky, I. Rabinovich, V. Glezer, S. Sampath, I. Pankratov, and J. Gun. *Anal. Chem.*, 67, 22A (1995).
42. M. Petit-Dominquez, H. Shen, W.R. Heineman, and C.J. Seliskar, *Anal. Chem.*, 69, 703 (1997).
43. M. Tsionsky, G. Gun, V Glezer, and O Lev, *Anal. Chem.*, 66, 1747 (1994).
44. J. Wang and P. Pamidi, *Anal. Chem.*, 69, 4490 (1997).
45. J. Zak and T. Kuwana, *J. Electroanal. Chem.*, 150, 645 (1983).
46. J. Cox, R. Jaworski, and P. Kulesza, *Electroanalysis*, 3, 869 (1991).
47. L.J. Gorton, *Chem. Soc. Faradays Trans.*, 82, 1245 (1986).
48. M. Halbert and R. Baldwin, *Anal. Chem.*, 57, 591 (1985).
49. T. Malinski and Z. Taha, *Nature*, 358, 676 (1992).
50. J. Wang and Z. Taha, *Anal. Chem.*, 62, 1413 (1990).
51. J. Wang, "Voltammetry after Nonelectrolytic Preconcentration," in A.J. Bard, Ed., *Electroanalytical Chemistry*, Vol. 16, p. 1, Marcel Dekker, New York, 1989.
52. A. Guadalupe and H. Abruna, *Anal. Chem.*, 57, 142 (1985).
53. D.W. Arrigan, *Analyst*, 119, 1953 (1994).
54. P. Ugo and L.M. Moreto, *Electroanalysis*, 7, 1105 (1995).
55. S. Prabhu, R. Baldwin, and L. Kryger, *Anal. Chem.*, 59, 1074 (1987).
56. J. Wang and T. Martinez, *Electroanalysis*, 1, 167 (1989).
57. N. Oyama and F.C. Anson, *Anal. Chem.*, 52, 1192 (1980).

58. J. Wang and Z. Lu, *J. Electroanal. Chem.*, 266, 287 (1989).
59. S. Prabhu, R. Baldwin, and L. Kryger, *Electroanalysis*, 1, 13 (1989).
60. P. Ugo, B. Ballarin, S. Daniele, and G. Mazzocchin, *Anal. Chim. Acta*, 244, 29 (1991).
61. I. Turyan and D. Mandler, *Anal. Chem.*, 66, 58 (1994).
62. T. Malinski, A. Ciszewski, J. Fish, and L. Czuchajowski, *Anal. Chem.*, 62, 909 (1990).
63. S.V. Sasso, R. Pierce, R. Walla and A. Yacynych, *Anal. Chem.*, 62, 1111 (1990).
64. G. Nagy, G. Gerhardt, A. Oke, M. Rice, and R.N. Adams, *J. Electroanal. Chem.*, 188, 85 (1985).
65. J. Wang and Z. Lu, *Anal. Chem.*, 62, 826 (1990).
66. J. Wang, H. Wu, and L. Angnes, *Anal. Chem.*, 65, 1893 (1993).
67. J. Wang and P. Tuzhi, *Anal. Chem.*, 58, 3257 (1986).
68. G. Sittampalam and G. Wilson, *Anal. Chem.*, 55, 1608 (1983).
69. T. Ohsaka, T. Hirokawa, H. Miyamoto, and N. Oyama, *Anal. Chem.*, 59, 1758 (1987).
70. J. Wang and T. Golden, *Anal. Chem.*, 61, 1397 (1989).
71. Q. Cheng and A. Brajter-Toth, *Anal. Chem.*, 64, 1998 (1992).
72. G. Bidan, *Sensors and Actuators B*, 6, 45 (1992).
73. M. Kanatzidis, *Chem. Eng. News*, Dec. 3, 36 (1990).
74. T. Ikariyama and W.R. Heineman, *Anal. Chem.*, 58, 1803 (1986).
75. A. Ivaska, *Electroanalysis*, 3, 247 (1991).
76. P. Teasdale and G. Wallace, *Analyst*, 118, 329 (1993).
77. R.M. Wightman, *Science*, 240, 415 (1988).
78. R.M. Wightman, *Anal. Chem.*, 53, 1125A (1981).
79. A.M. Bond, *Analyst*, 119, RI (1994).
80. R. Kennedy, L. Huang, M. Atkinson, and P. Dush, *Anal. Chem.*, 65, 1882 (1993).
81. F. Fan, J. Kwak, and A.J. Bard, *J. Am. Chem. Soc.*, 118, 9669 (1996).
82. B.B. Anderson and A.G. Ewing, *J. Pharm. Biomed. Anal.*, 19, 15 (1999).
83. C.P. Andrieux, P. Hapiot, and J.M. Saveant, *Electroanalysis*, 2, 183 (1990).
84. J. Heinze, *Angew. Chem. (Eng. Ed.)*, 32, 1268 (1993).
85. R. Penner, N. Lewis, *Chem. Industry*, Nov. 4, 788 (1991).
86. Y. Shao, M.V. Mirkin, G. Fish, S. Kokotov, D. Palankar, and A. Lewis, *Anal. Chem.*, 69, 1627 (1997).
87. D.E. Tallman and S.L. Petersen, *Electroanalysis*, 2, 499 (1990).
88. W. Thormann, P. van den Bosch, and A.M. Bond, *Anal. Chem.*, 57, 2764 (1985).
89. D.E. Weisshaar and D.E. Tallman, *Anal. Chem.*, 55, 1146 (1983).
90. J. Wang, A. Brennsteiner, and A.P. Sylwester, *Anal. Chem.*, 62, 1102 (1990).
91. R. Deutscher and S. Fletcher, *J. Electroanal. Chem.*, 239, 17 (1988).
92. R.M. Penner and C.R. Martin *Anal. Chem.*, 59, 2625 (1987).
93. T. Gueshi, K. Tokuda, and H. Matsuda, *J. Electroanal. Chem.*, 89, 247 (1978).
94. A.J. Bard, J. Crayton, G. Kittlesen, T. Shea, and M.S. Wrighton, *Anal. Chem.*, 58, 2321 (1986).
95. O. Niwa, M. Morita, and H. Tabei, *Anal. Chem.*, 62, 447 (1990).
96. O Niwa, *Electroanalysis*, 7, 606 (1995).

Examples

Example 4-1 A rotating ring-disk electrode (1600 rpm) yields a disk current of 12.3 μA for the oxidation of a 2×10^{-3} M potassium ferrocyanide solution. Calculate the reduction current observed at the surrounding ring using a 6×10^{-3} M potassium ferrocyanide solution and a rotation speed of 2500 rpm ($N = 0.33$).

Solution From the Levich equation, (4-5), one can calculate first the disk current under the new conditions:

$$\frac{i_D}{12.3} = \frac{K \times (6 \times 10^{-3}) \times (2500)^{1/2}}{K \times (2 \times 10^{-3}) \times (1600)^{1/2}}$$

$$i_D = 46.125\ \mu\text{A}$$

Then, from equation (4-8), we can solve for the ring current:

$$i_R = -Ni_D = -0.33 \times 12.125 = -15.221 \mu\text{A}$$

Example 4-2 A rotating mercury film electrode (2 mm diameter) yielded a stripping peak current of 2.2 μA for a 1×10^{-8} M lead(II) solution following a 3 min deposition at −1.0 V with a 1600 rpm rotation. Calculate the peak current for a 2.5×10^{-8} M lead(II) solution following a 2 min deposition with a 2500 rpm rotation.

Solution

$$2.2 = K \times (1 \times 10^{-8}) \times 3 \times (1600)^{1/2}$$

$$K = 1.83 \times 10^6$$

$$i_p = 1.83 \times 10^6\ (2.5 \times 10^{-8}) \times 2 \times (2500)^{1/2} \quad i_p = 4.6\ \mu\text{A}$$

QUESTIONS

1. What are the advantages of using ultramicroelectrodes for electrochemical measurements?
2. Explain clearly how chemically modified electrodes can benefit electrochemical measurements?

3. Explain clearly why a carbon composite disk electrode offers improved signal-to-background characteristics compared to a carbon disk electrode of the same geometric area.

4. Describe clearly why the oxidation of polypyrrole film results in the uptake of an anion from the surrounding solution.

5. Derive the Levich equation for the limiting current at the rotating disk electrode [based on combining equations (4-4) and (1-12)].

6. How can you use the rotating ring disk electrode for detecting short-lived intermediate species?

7. Explain clearly why effective compensation of the ohmic drop is essential for diagnostic applications of cyclic voltammetry (e.g., estimating n from ΔE_p).

8. Describe the rationale of using electrodes coated with Nafion films for selective detection of the cationic neurotransmitter dopamine in the presence of the common interference from anionic ascorbic acid.

9. Explain the reason for including the time-consuming oxygen removal step in pulse-polarographic measurements of tin ion in juice samples.

10. Explain clearly why and how a change of the scan rate affects the shape of the cyclic voltammetric response of an ultramicroelectrode.

11. Propose a modified electrode surface suitable for detecting in-situ micromolar concentrations of ferric ion in an industrial stream. What are the challenges of such in-situ monitoring?

Analytical Electrochemistry, Second Edition. Joseph Wang

ISBNs: 0-471-28272-3 (Hardback); 0-471-22823-0 (Electronic)

CHAPTER 5

POTENTIOMETRY

5-1 PRINCIPLES OF POTENTIOMETRIC MEASUREMENTS

In potentiometry, information on the composition of a sample is obtained through the potential appearing between two electrodes. Potentiometry is a classical analytical technique with roots before the turn of the twentieth century. However, the rapid development of new selective electrodes and more sensitive and stable electronic components over the last 25 years of the twentieth century has expanded tremendously the range of analytical applications of potentiometric measurements. Selective potentiometric electrodes are currently widely used in many fields, including clinical diagnostics, industrial process control, environmental monitoring, and physiology. The speed with which this field has developed is a measure of the degree to which potentiometric measurements meet the need of the analytical chemist for rapid, low-cost, and accurate analysis. In this chapter, the principles of direct potentiometric measurements, based on ion-selective electrodes, will be described. (The second major aspect of potentiometry, the so-called potentiometric titrations, will not be covered.) General books devoted exclusively to direct potentiometry may be found in references 1 to 5.

The equipment required for direct potentiometric measurements includes an ion-selective electrode (ISE), a reference electrode, and a potential-measuring device (a pH/millivolt meter that can read 0.2 mV or better) (Figure 5-1). Conventional voltmeters cannot be used because only very small currents are allowed to be drawn. The ion-selective electrode is an indicator electrode capable of selectively measuring the activity of a particular ionic species. Such electrodes exhibit a fast response and a wide linear range, are not affected by color or turbidity, are not

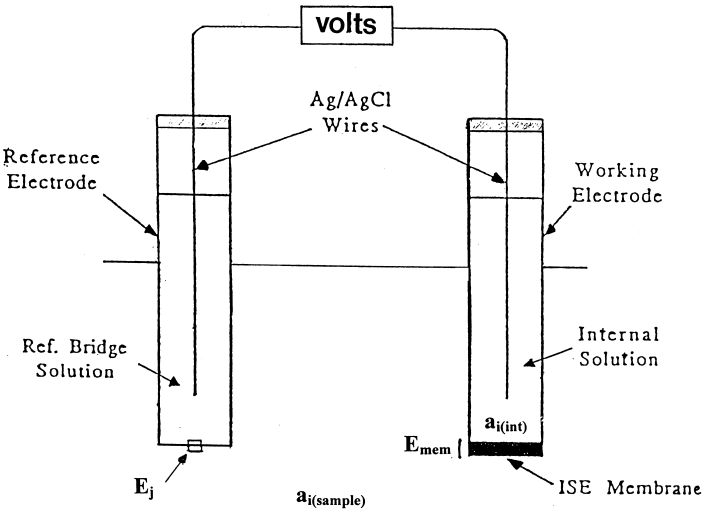

FIGURE 5-1 Schematic diagram of an electrochemical cell for potentiometric measurements.

destructive, and are very inexpensive. Ion-selective electrodes can be assembled conveniently in a variety of shapes and sizes. Specially designed cells allow flow or microliter analyses (see, for example, Section 5-3).

Ion-selective electrodes are mainly membrane-based devices, consisting of permselective ion-conducting materials, which separate the sample from the inside of the electrode. On the inside is a filling solution containing the ion of interest at a constant activity. The membrane is usually nonporous, water insoluble, and mechanically stable. The composition of the membrane is designed to yield a potential that is primarily due to the ion of interest (via selective binding processes, e.g., ion exchange, which occur at the membrane–solution interface). The trick is to find a membrane that will selectively bind the analyte ions, leaving co-ions behind. Membrane materials, possessing different ion-recognition properties, have thus been developed to impart high selectivity (see Section 5-2). The detailed theory of the processes at the interface of these membranes, which generate the potential, is available elsewhere (6–8). Thermodynamic arguments, which will not be elaborated here, tell us that the gradient of activity across the membrane (of the analyte ions in the outer and inner solutions) produces a gradient of free energy:

$$\Delta G = -RT \ln\left(\frac{a_{i,\text{sample}}}{a_{i,\text{int.soln}}}\right) \tag{5-1}$$

where R is the universal gas constant ($8.134\ \text{J K}^{-1}\ \text{mol}^{-1}$) and T is the absolute temperature. The potential produced across the membrane corresponds to this free energy difference:

$$E = -\frac{\Delta G}{n\text{F}} = \frac{RT}{nF} \ln\left(\frac{a_{i,\text{sample}}}{a_{i,\text{int.soln}}}\right) \tag{5-2}$$

Such a potential arises whenever the membrane separates two solutions of different ion activity (Figure 5-2). The ion-recognition (binding) event generates a phase boundary potential at the membrane–sample interface. Another phase boundary potential is developed at the inner surface of the membrane (at the membrane–filling solution interface). The membrane potential corresponds to the potential difference across the membrane. The resulting potential of the ion-selective electrode, which reflects the unequal distribution of the analyte ions across the boundary, is generally monitored relative to the potential of a reference electrode. Since the potential of the reference electrode is fixed, and the activity of the ion in the inner solution is constant, the measured cell potential reflects the potential of the ISE, and can thus be related to the activity of the target ion in the sample solution. Ideally, the response of the ISE should obey equation (5-3):

$$E = K + (2.303RT/z_iF) \log a_i \tag{5-3}$$

where E is the potential, and z_i and a_i are the ionic charge and activity, respectively, of the ion. The constant K includes all sample-independent potential contributions, which depend upon various factors (influenced by the specific design of the ISE). Equation (5-3) predicts that the electrode potential is proportional to the logarithm of the activity of the ion monitored. For example, at room temperature a 59.1 mV change in the electrode potential should result from a 10-fold change in the activity of a monovalent ion ($z = 1$). Similar changes in the activity of a divalent ion should result in a 29.6 mV change of the potential. A 1 mV change in the potential

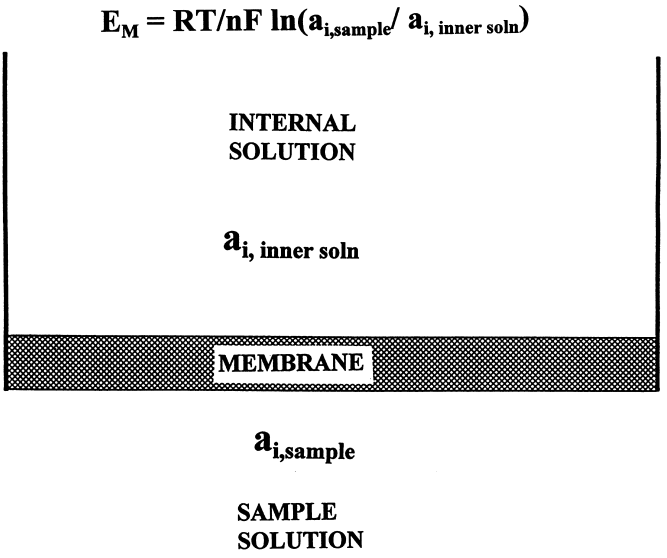

FIGURE 5-2 Membrane potential reflects the gradient of activity of the analyte ion in the inner and outer (sample) solutions.

corresponds to 4% and 8% changes in the activity of monovalent and divalent ions, respectively. The term "Nernstian" behavior is used to characterize such behavior. In contrast, when the slope of the electrode response is significantly smaller than $59.1/z_i$, the electrode is characterized by a sub-Nernstian behavior.

It should be noted again that ISEs sense the activity, rather than the concentration of ions in solution. The term "activity" is used to denote the effective (active) concentration of the ion. The difference between concentration and activity arises because of ionic interactions (with oppositely charged ions) that reduce the effective concentration of the ion. The activity of an ion i in solution is related to its concentration, c_i, by

$$a_i = f_i c_i \tag{5-4}$$

where f_i is the activity coefficient. The activity coefficient depends on the types of ions present and on the total ionic strength of the solution. The activity coefficient is given by the *Debye–Hückel equation*:

$$\log f_i = \frac{-0.51 z_i^2 \sqrt{\mu}}{1 + \sqrt{\mu}} \qquad (\text{at } 25^\circ\text{C}) \tag{5-5}$$

where μ is the ionic strength. The activity coefficient thus approaches unity (i.e., $a_i \cong c_i$) in very dilute solutions. The departure from unity increases as the charge of the ion increases.

Equation (5-3) has been written on the assumption that the electrode responds only to the ion of interest, i. In practice, no electrode responds exclusively to the ion specified. The actual response of the electrode in a binary mixture of the primary and interfering ions (i and j, respectively) is given by the *Nikolskii–Eisenman equation* (9):

$$E = K + (2.303RT/z_iF) \log(a_i + k_{ij} a_j^{z_i/z_j}) \tag{5-6}$$

where k_{ij} is the selectivity coefficient, a quantitative measure of the electrode ability to discriminate against the interfering ion (i.e., a measure of the relative affinity of ions i and j toward the ion-selective membrane). For example, if an electrode is 50 times more responsive to i than to j, k_{ij} has a value of 0.02. A k_{ij} of 1.0 corresponds to a similar response for both ions. When $k_{ij} \gg 1$, then the ISE responds better to the interfering ion j than to the target ion i. Usually, k_{ij} is smaller than 1, which means that the ISE responds more selectively to the target ion. The lower the value of k_{ij}, the more selective is the electrode. Selectivity coefficients lower than 10^{-5} have been achieved for several electrodes. For an ideally selective electrode, k_{ij} would equal zero (i.e., no interference). Obviously, the error in the activity a_i due to the interference of j would also depend upon their relative levels. The term z_i/z_j corrects for a possible charge difference between the target and interfering ions. Normally, the most serious interferences have the same charge as the primary ion, so that

$z_i/z_j = 1$. In practice, the contribution of all interfering ions present in the sample matrix ($\sum k_{ij} a_j^{z_i}/z_j$) should be included in the Nikolskii–Eisenman equation. For example, for a sodium electrode immersed in a mixture of sodium, potassium, and lithium, the response is given by

$$E = K + \frac{2.303RT}{F} \log(a_{\mathrm{Na}} + k_{\mathrm{Na,K}} a_{\mathrm{K}} + k_{\mathrm{Na,Li}} a_{\mathrm{Li}}) \tag{5-7}$$

Accordingly, an ISE displays a selective response when the activity of the primary ion is much larger than the summation term of the interferents; that is, when $a_i \gg \sum k_{ij} a_j^{z_i/z_j}$. Under this condition, the effect of interfering ions is negligible, and changes in the measured potential can be related with confidence to variations in the activity of the target ion. The selectivity coefficients thus serve as guidelines of how far a given ISE should be applicable for a particular analytical problem. Nonselective ISEs are rarely useful for real-life applications (with the exception of their combination with the operation of ISE arrays; see Section 6-4). In reality, equations with more than two components are rarely used. Deviations from the Nikolski–Eisenman equation have been reported for various situations (particularly for mixtures of ions of different charge, in the case of non-Nernstian behavior of interfering ions, and due to the concentration dependence of k_{ij}).

It is important for the analytical chemist to realize the selectivity coefficient of a particular electrode. Various methods have been suggested for determining the selectivity coefficient, including the fixed-interference method, separate-solution method, and the fixed primary-ion method (10,11). The most popular fixed-interference method involves two solutions, one containing a constant concentration of the interfering ion and the second containing a zero concentration. Also popular is the separate-solution method, which involves the preparation of calibration curves for each ion. As selectivity is a complex function of the membrane composition and the experimental design, the values of selectivity coefficients should be regarded as operationally defined (i.e., valid for the particular set of conditions used for their determination).

Usually the analytical chemist needs to determine the concentration of the ion of interest rather than its activity. The obvious approach for converting potentiometric measurements from activity to concentration is to make use of an empirical calibration curve, such as the one shown in Figure 5-3. Electrode potentials of standard solutions are thus measured and plotted (on semilog paper) versus the concentration. Since the ionic strength of the sample is usually unknown, it is often useful to add a high concentration of an electrolyte to the standards and the sample to maintain about the same ionic strength (i.e., the same activity coefficient). The ionic-strength adjuster is usually a buffer (since pH control is also desired for most ISEs). The empirical calibration plot thus yields results in terms of concentration. Theoretically, such a plot should yield a straight line with a slope of approximately $59/z_i$ mV (Nernstian slope). Detection by means of ion-selective electrodes may be performed over an exceedingly broad concentration range, which, for certain electrodes, may embrace five orders of magnitude. In practice, the usable range

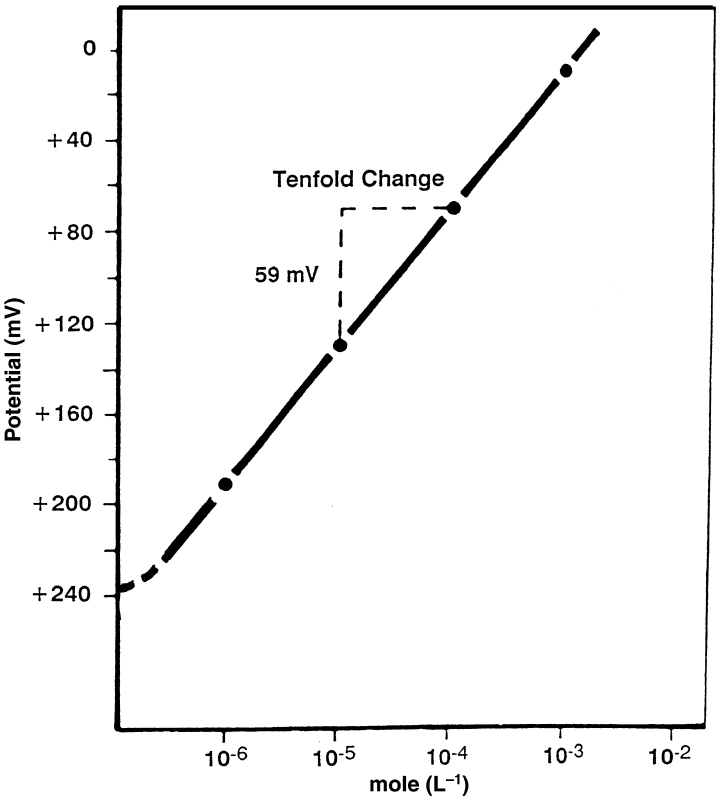

FIGURE 5-3 Typical calibration plot for a monovalent ion.

depends on other ions in the solution. Departure from linearity is commonly observed at low concentrations (about 10^{-5}–10^{-6} M) due to the presence of coexisting ions (equation 5-6). The extent of the departure depends on the selectivity coefficient as well as upon the level of the interfering ion (Figure 5-4). The detection limit for the analyte ion is defined by

$$a_{i,\min} = k_{ij} a_j^{z_i/z_j} \tag{5-8}$$

and corresponds to the activity of i at the intersection of the asymptotes in the E vs. $\log a_i$ calibration plot, that is, where the extrapolated linear and zero-slope segments meet (12) (see Figure 5-5). It is only when the plot becomes almost horizontal that the activity measurement becomes impossible. At high concentrations of the ions of interest, interference by species of opposite charge [not described by equation (5-6)] may lead to deviation from the linear electrode response.

The logarithmic response of ISEs can cause major accuracy problems. Very small uncertainties in the measured cell potential can cause large errors. (Recall that an

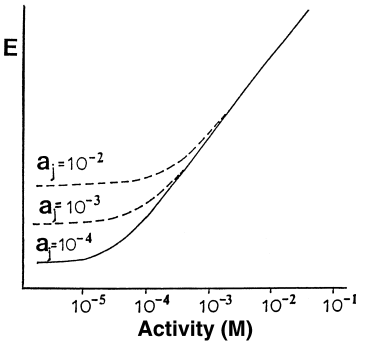

FIGURE 5-4 The potential response of an ion-selective electrode versus activity of ion *i* in the presence of different levels of an interfering ion *j*.

uncertainty of ± 1 mV corresponds to a relative error of about 4% in the concentration of a monovalent ion.) Since potential measurements seldom have better than 0.1 mV uncertainty, the best measurements of monovalent ions are limited to about 0.4% relative concentration error. In many practical situations, the error is significantly larger. The main source of error in potentiometric measurements is

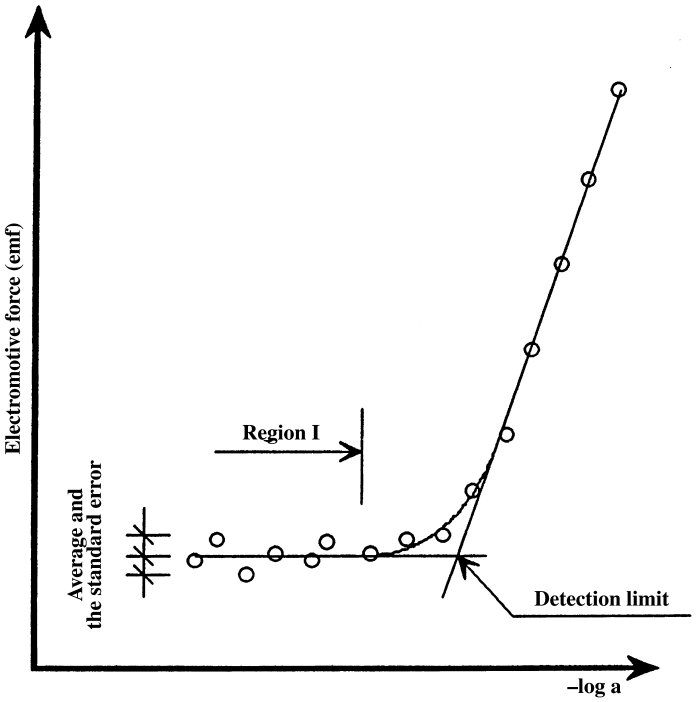

FIGURE 5-5 Determination of the detection limit of an ion-selective electrode. (Reproduced with permission from reference 12.)

actually not the ISE but rather changes in the reference electrode junction potential, that is, the potential difference generated between the reference electrolyte and sample solution. The junction potential is caused by an unequal distribution of anions and cations across the boundary between two dissimilar electrolyte solutions (which results in ion movement at different rates). When the two solutions differ only in the electrolyte concentration, the liquid junction potential is proportional to the difference in transference numbers of the positive and negative ions and to the logarithm of the ratio of the ions on both sides of the junction:

$$E = \frac{RT}{F}(t_1 - t_2) \ln \frac{a_i(1)}{a_i(2)} \tag{5-9}$$

Changes in the reference electrode junction potential result from differences in the composition of the sample and standard solutions (e.g., upon switching from whole blood samples to aqueous calibrants). One approach to alleviate this problem is to use an intermediate salt bridge, with a solution (in the bridge) of ions of nearly equal mobility (e.g., concentrated KCl). Standard solutions with an electrolyte composition similar to that of the sample are also desirable. These precautions, however, will not eliminate the problem completely. Other approaches to address this and other changes in the cell constant have been reviewed (13).

5-2 ION-SELECTIVE ELECTRODES

The discussion of Section 5-1 clearly illustrates that the most important response characteristic of an ISE is selectivity. Depending on the nature of the membrane material used to impart the desired selectivity, ISEs can be divided into three groups: glass, liquid, or solid electrodes. More than two dozen ISEs are commercially available and are widely used (although many more have been reported in the literature). Such electrodes are produced by firms such as Orion Research, Radiometer, Corning Glass, Beckman, Hitachi, or Sensorex.

5-2.1 Glass Electrodes

Glass electrodes are responsive to univalent cations. The selectivity for these cations is achieved by varying the composition of a thin ion-sensitive glass membrane.

5-2.1.1 pH Electrodes The most common potentiometric device is the pH electrode. This electrode has been widely used for pH measurements for several decades. Besides use for direct pH measurements, the pH glass electrode is commonly employed as the transducer in various gas and biocatalytic sensors, involving proton-generating or proton-consuming reactions (see Chapter 6). Its remarkable success is attributed to its outstanding analytical performance, and in particular its extremely high selectivity for hydrogen ions, its remarkably broad response range, and to its fast and stable response. The phenomenon of glass

selectivity was reported by Cremer in 1906 (14). Glass pH electrodes of different configurations and dimensions have been in routine use for over six decades since their commercial introduction by A. Beckman. A schematic of a commonly used configuration is shown in Figure 5-6. This consists of a thin pH-sensitive glass membrane sealed to the bottom of an ordinary glass tube. The composition of the glass membrane is carefully controlled. Usually, it consists of a three-dimensional silicate network, with negatively charged oxygen atoms available for coordinating cations of suitable size. Some of the more popular glasses have three-component compositions of 72% SiO_2–22% Na_2O–6% CaO or 80% SiO_2–10% Li_2O–10% CaO. Inside the glass bulb are a dilute hydrochloric acid solution and a silver wire coated with a layer of silver chloride. The electrode is immersed in the solution whose pH is to be measured, and connected to an external reference electrode. (In the so-called combination electrode, the external reference electrode is combined with the ion-selective electrode into one body.) The rapid equilibrium established

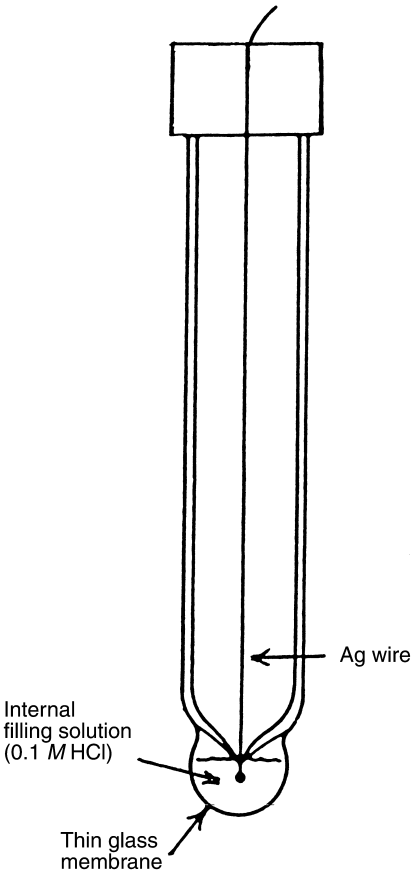

FIGURE 5-6 A glass pH electrode.

across the glass membrane, with respect to the hydrogen ions in the inner and outer solutions, produces a potential:

$$E = K + \frac{RT}{F} \ln \frac{[H^+]_{inner}}{[H^+]_{outer}} \tag{5-10}$$

The potential of the electrode is registered with respect to the external reference electrode. Hence, the cell potential (at 25°C and after introducing the definition of pH) follows the relation

$$E_{cell} = K' + 0.059\text{pH} \tag{5-11}$$

The measured potential is thus a linear function of pH; an extremely wide (10–14 decades) linear range is obtained, with calibration plots yielding a slope of 59 mV per pH unit. The overall mechanism of the response is complex. The selective response is attributed to the ion-exchange properties of the glass surface, and in particular the replacement of sodium ions associated with the silicate groups in the glass by protons:

$$Na^+_{glass} + H_3O^+_{soln} \rightleftharpoons Na^+_{soln} + H_3O^+_{glass} \tag{5-12}$$

The theory of the response mechanism has been thoroughly discussed (15).

The user must be alert to some shortcomings of the glass pH electrode. For example, in solutions of pH 11 or more, the electrode shows a so-called alkaline error in which it responds also to changes in the level of alkali metal ions (particularly sodium):

$$E_{cell} = K + 0.059 \log([H_3O^+] + k_{H,Na}[Na^+]) \tag{5-13}$$

As a result, the pH reading is lower than the true value (Figure 5-7). This error is greatly reduced if the sodium oxide in the glass is replaced by lithium oxide. Still, even with new glass formulations (with $k_{H,Na} < 10^{-10}$), errors can be appreciable when measurements are carried out in highly basic solutions (e.g., NaOH). Many glass electrodes also exhibit erroneous results in highly acidic solutions (pH < 0.5); the so-called acid error yields higher pH readings than the true value (Figure 5-7).

Before the pH electrode is used, it should be calibrated using two (or more) buffers of known pH. Many standard buffers are commercially available, with an accuracy of ±0.01 pH unit. Calibration must be performed at the same temperature at which the measurement will be made; care must be taken to match the temperature of samples and standards. The exact procedure depends on the model of pH meter used. Modern pH meters, such as the one shown in Figure 5-8, are microcomputer controlled, and allow double-point calibration, slope calculation, temperature adjustment, and accuracy to ±0.001 pH unit, all with few basic steps. The electrode must

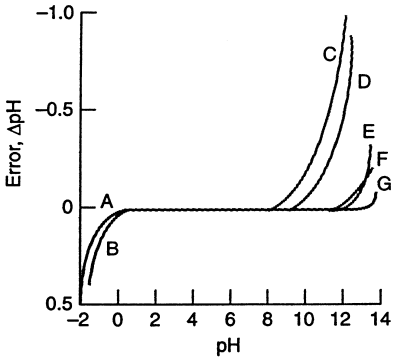

FIGURE 5-7 The alkaline and acid errors of several glass pH electrodes. A, Corning 015/H_2SO_4; B, Corning 015/HCl; C, Corning 015/1 M Na^+; D, Beckman-GP/1 M Na^+; E, L&N BlackDot/1 M Na^+; F, Beckman E/1M Na^+; G, Ross electrode. (Reproduced with permission from reference 16.)

FIGURE 5-8 A modern microprocessor-controlled pH meter.

be stored in an aqueous solution when not in use, so that the hydrated gel layer of the glass does not dry out. A highly stable response can thus be obtained over long time periods. As with other ion-selective electrodes, the operator should consult the manufacturer's instructions for proper use. Commercial glass electrodes are remarkably robust and, with proper care, will last for more than a year. Proper maintenance of the reference electrode is also essential to minimize errors.

Measurements of pH can also be performed using other types of potentiometric sensors. Non-glass electrodes offer various advantages for certain pH measurements (particularly intravascular and intraluminal clinical applications, food assays, and operation in fluoride media), including ease of preparation, low electrical resistance, and safety in handling. The most common examples are the quinhydrone electrode (in which the response is due to a proton-transfer redox reaction of the quinone–hydroquinone couple), and the antimony electrode (based on the redox reaction between antimony and antimony oxide involving protons). Other metal–metal oxide couples, such as palladium–palladium oxide, have been applied for pH measurements. Membrane electrodes based on various neutral hydrogen ion carriers (e.g. tridodecylamine) can also be employed (17). The resulting electrodes exhibit excellent selectivity, reproducibility, and accuracy, but their dynamic range is inferior to that of glass electrodes. (The dynamic range appears to depend on the acidity constant of the incorporated ionophore.) New pH sensors based on new glass compositions or non-glass formulations are currently being developed in various laboratories. While such electrodes may be useful for specific applications, glass electrodes are likely to remain the choice for routine analytical applications.

5-2.1.2 Glass Electrodes for Other Cations From the early days of glass pH electrodes, it was noticed that alkaline solutions display some interference on the pH response. Deliberate changes in the chemical composition of the glass membrane (along with replacements of the internal filling solution) have thus led to electrodes responsive to monovalent cations other than hydrogen, including sodium, ammonium, and potassium (15). This usually involves the addition of B_2O_3 or Al_2O_3 to sodium silicate glasses, to produce anionic sites of appropriate charge and geometry on the outer layer of the glass surface. For example, the sodium- and ammonium-selective glasses have the compositions 11% Na_2O–18% Al_2O_3–71% SiO_2 and 27% Na_2O–4% Al_2O_3–69% SiO_2, respectively. Unlike sodium silicate glasses (used for pH measurements), these sodium aluminosilicate glasses possess what may be termed $AlOSiO^-$ sites with a weaker electrostatic field strength and a marked preference for cations other than protons. The overall mechanism of the electrode response is complex but involves a combination of surface ion-exchange and ion-diffusion steps. To further minimize interference from hydrogen ions, it is desirable to use solutions with pH values higher than 5. Improved mechanical and electrical properties can he achieved using more complex glasses containing various additives.

5-2.2 Liquid-Membrane Electrodes

Liquid-membrane type ISEs, based on water-immiscible liquid substances impregnated in a polymeric membrane, are widely used for direct potentiometric measurements (17,18). Such ISEs are particularly important because they permit direct measurements of several polyvalent cations as well as certain anions. The polymeric membrane [commonly made of plasticized poly(vinyl chloride) (PVC)] separates the test solution from the inner compartment, containing a standard solution of the target ion (into which a silver/silver chloride wire is dipped). The filling solution usually contains a chloride salt of the primary ion, as desired for establishing the potential of the internal silver/silver chloride wire electrode. The membrane-active (recognition) component can be a liquid ion exchanger or a neutral macrocyclic compound. The selective extraction of the target ion at the sample/membrane interface creates the electrochemical phase boundary potential. The membranes are commonly prepared by dissolving the recognition element, a plasticizer (e.g., *o*-nitrophenyl ether) that provides the properties of liquid phase, and the PVC in a solvent such as tetrahydrofuran. (The recognition element is usually present in 1–3% amount.) Slow evaporation of the solvent over 1–2 days leaves a flexible membrane of 10–100 μm thickness, which can be cut (with a cork borer) and mounted on the end of plastic tube. The ion-discriminating ability (and hence the selectivity coefficient) depend not only upon the nature of the recognition element but also upon the exact membrane composition, including the membrane solvent and the nature and content of the plasticizer. The extraction properties of the membrane can be further improved by adding ion-pairing agents to the plasticizer. The PVC matrix provides mechanical strength and permits diffusion of analytes to the recognition sites. The hydrophobic nature of the membrane prevents leaching of the sensing element and the plasticizer into the aqueous sample solution, and thus extends the operational lifetime. In contrast, release of the primary ion (from the inner solution) leads to its higher activity at the layer adjacent to the membrane (relative to the bulk sample), and hence to increased detection limits of carrier-based liquid-membrane electrodes (19). Such a localized accumulation of ions makes it impossible to measure dilute samples. By choosing an internal electrolyte with low activity of the primary ion and preventing its leakage, it is possible to greatly lower the detection limits by up to six orders of magnitude down to the picomolar range (20). Active research in various laboratories is elucidating these interfacial ion fluxes in connection with the development of potentiometric sensors for trace analysis. Lowering of the detection limits would require careful attention to the selectivity of the resulting ISE. The selectivity of most ISEs is currently not sufficient to reach the picomolar level.

5-2.2.1 Ion-Exchanger Electrodes One of the most successful liquid-membrane electrodes is selective toward calcium. Such an electrode relies on the ability of phosphate ions to form stable complexes with the calcium ion. It uses a liquid cation exchanger, consisting of an aliphatic diester of phosphoric acid [$(RO)_2PO_2^-$ with R groups in the C_8–C_{16} range] that possesses high affinity for calcium ions. The ion exchanger is held in a porous, plastic filter membrane that

separates the test solution from the inner compartment, containing a standard calcium chloride solution (Figure 5-9). The preferential uptake of calcium ions into the membrane can thus be represented as

$$Ca^{2+} + 2(RO)_2PO_2^- \rightleftharpoons [(RO)_2PO_2]_2Ca \tag{5-14}$$

The resulting cell potential is given by

$$E_{cell} = K + \frac{0.059}{2} \log a_{Ca} \tag{5-15}$$

Calcium activities as low as 5×10^{-7} M can be measured, with selectivity coefficients $K_{Ca,Mg}$ and $K_{Ca,K}$ of 0.02 and 0.001, respectively. Such potential response is independent of the pH over the pH range from 5.5 to 11.0. Above pH 11, $Ca(OH)^+$ is formed, while below pH 5.5, protons interfere. Because of its attractive response characteristics, the calcium ISE has proved to be a valuable tool for the determination of calcium ion activity in various biological fluids.

Liquid anion exchangers, such as lipophilic quaternary ammonium salts (e.g., Figure 5-10) or phosphonium salts, have been employed for the preparation of anion-selective sensors. The resulting ISEs usually lack an anion-recognition function, and hence display anion selectivity corresponding to the anion partition into the supporting hydrophobic membrane. This gives rise to the following order of selectivities, which is known as the *Hofmeister series*: large liphophilic anions $> ClO_4^- > IO_4^- > SCN^- > I^- > NO_3^- > Br^- > CI^- > HCO_3^- > H_2PO_4^-$; that is, maximum response to lipophilic anions (21). Accordingly, several commercial sensors (e.g., NO_3^- "selective" electrodes) based on ion-exchange type membranes, suffer interference from liphohilic anions (e.g., ClO_4^-). Useful electrodes for nitrate (22), thiocyanate (23), and chloride (24) ions have been developed. Sensors responsive to anionic macromolecules have also been developed despite the greater

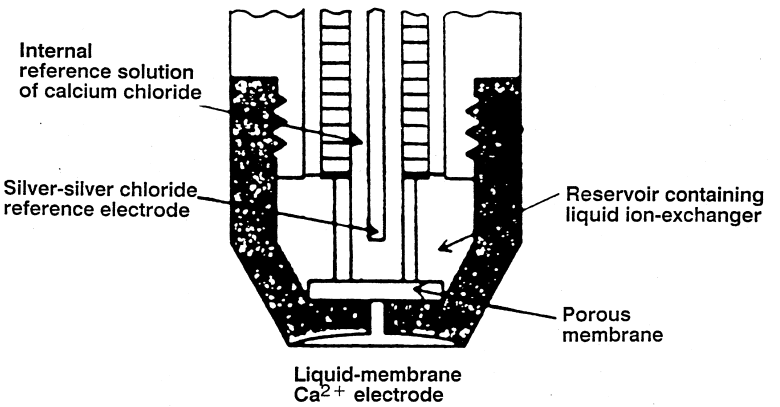

FIGURE 5-9 Schematic diagram of a calcium ion-selective electrode.

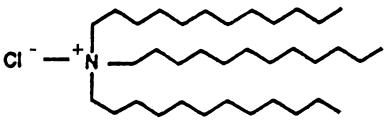

FIGURE 5-10 A quaternary alkyl ammonium chloride.

difficulty in identifying appropriate membrane chemistry that yields a significant and selective response (25,26). A very successful example is the use of the quaternary ammonium salt tridodecylmethylammonium chloride (TDMAC) for detecting the clinically-important drug heparin (25). Apparently, the polyionic heparin is favorably extracted into the membrane through ion-pairing interaction with the positively charged nitrogen atoms (Figure 5-11). The extraction process results in a steady-state change in the phase boundary potential at the membrane–sample interface. Analogous potentiometric measurements of other macromolecular polyanionic species have also been reported (26). Ion-exchange electrodes sensitive to large organic cations have also been described. For example, PVC membranes containing dinonylnaphthalenesulfonic acid (DNNS) have been used for the detection of drugs of abuse (e.g., opiate alkaloids) (27). Such organic-responsive electrodes, however, lack sufficient selectivity and are limited to simple samples such as pharmaceutical formulations.

5-2.2.2 Neutral Carrier Electrodes In addition to charged liquid ion exchangers, liquid-membrane electrodes often rely on the use of complex-forming neutral carriers. Much effort has been devoted to the isolation or synthesis of compounds containing cavities of molecular dimensions. Such use of chemical recognition principles has made an enormous impact upon widespread acceptance of ISEs. The resulting neutral carriers can be natural macrocyclic molecules or synthetic crown

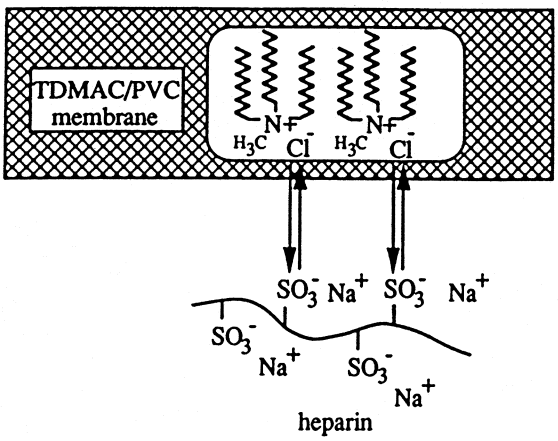

FIGURE 5-11 The recognition process occurring at the TDMAC/PVC membrane/sample interface used for measurements of heparin. (Reproduced with permission from reference 26.)

compounds (e.g., tailor-made cyclic polyethers) capable to envelop various target ions in their pocket. Electron-donor atoms, present in the polar host cavity, further facilitate and influence the interaction with the target ion. For example, while oxygen-containing crown ethers form stable complexes with alkali or alkaline earth metals, sulfur-containing ones are best suited for binding heavy metals. The extent of this interaction is determined by the "best-fit" mechanism, with larger ions not able to fit the molecular cavity while smaller ones are weakly coordinated. Often, a subunit group is added to the crown compound to impart higher selectivity (through steric or blockage effects) and improved lipophilicity. The ion recognition process is thus influenced by the cavity (ring) size, the number and positioning of the electron-donor atoms, and the nature of the subunit. For example, 14-crown-4-ether compounds (i.e., 4 oxygens in a 14-atom ring) offer selective recognition of lithium. Overall, these ionophores serve as reversible and reusable binding reagents that selectively extract the target analyte into the membrane. Such a binding event creates the phase boundary potential at the membrane–sample interface. To assure reversible binding, it is essential to keep the free energy of activation of the analyte–ionophore reaction sufficiently small (28). Molecular modeling techniques are being used to guide the design of ionophores toward target analytes. The specific design takes into consideration the selectivity demands imposed by clinical or environmental samples.

A host of carriers, with a wide variety of ion selectivities, have been proposed for this task. Most of them have been used for the recognition of alkali and alkaline earth metal cations (e.g., clinically relevant electrolytes). A classical example is the cyclic depsipeptide valinomycin (Figure 5-12), used as the basis for the widely used ISE for potassium ion (29). This doughnut-shaped molecule has an electron-rich pocket in the center into which potassium ions are selectively extracted. For example, the electrode exhibits a selectivity for K^+ over Na^+ of approximately 5000. The basis for the selectivity seems to be the fit between the size of the potassium ion (radius 1.33 Å) and the volume of the internal cavity of the macrocyclic molecule. The hydrophobic side chains of valinomycin stretch into the lipophilic part of the membrane. In addition to its excellent selectivity, the electrode is well behaved and has a wide working pH range. Strongly acidic media can be employed because the electrode is 18,000 times more responsive to K^+ than to H^+. A Nernstian response to potassium ion activities, with a slope of 59 mV per pK^+, is commonly observed from 10^{-6} to 10^{-1} M. Such attractive performance characteristics have made the valinomycin ISE extremely popular for clinical analysis (with 200 million assays of blood potassium being carried out annually in the United States using this device).

Many other cyclic and noncyclic organic carriers with remarkable ion selectivities have been used successfully as active hosts of various liquid membrane electrodes. These include the 14-crown-4-ether for lithium (30); 16-crown-5 derivatives for sodium; bis-benzo-18-crown-6 ether for cesium; the ionophore ETH 1001 [(*R*,*R*)-*N*,*N*^{1}-bis(11-ethoxycarbonyl)undecyl-*N*,*N*^{1}-4,5-tetramethyl-3,6-dioxaoctanediamide] for calcium; the natural macrocyclics nonactin and monensin for ammonia and sodium (31), respectively; the ionophore ETH 1117 for magnesium; calixarene derivatives for sodium (32); and macrocyclic thioethers for mercury and silver (33).

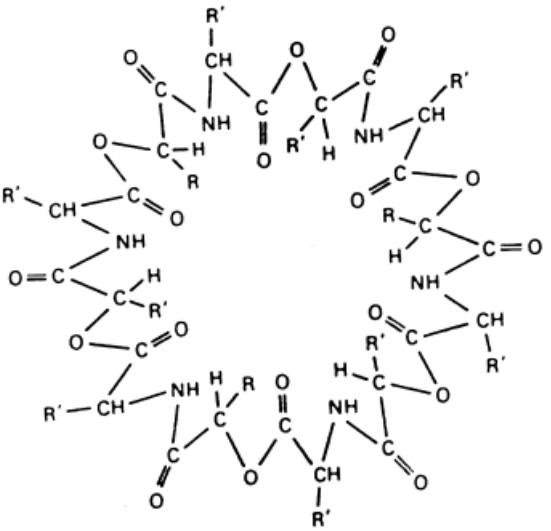

FIGURE 5-12 Valinomycin.

Some common ionophores used for sensing different cations are displayed in Figure 5-13. The development of highly selective lithium electrodes for clinical monitoring of psychiatric patients (receiving lithium-based drugs) has been particularly challenging considering the large sodium interference. Similarly, highly selective ionophores for sodium are needed for addressing the large excess of potassium in the intracellular fluid.

Anion-selective liquid-membrane electrodes have also been developed based on the coordination of the anionic guest to host materials, such as metallophorphyrin or hydrophobic vitamin B_{12} derivatives, alkyltin compounds or macrocyclic polyamines (34–38) (Figure 5-14). Such biomimetically designed ionophores offer effective sensing of inorganic and organic anions, such as thiocyanate, carbonate, salicylate, phosphate, or adenosine nucleotides. Unlike anion-exchanger electrodes, these anion sensors display selectivity patterns greatly different from the Hofmeister sequence (due to the direct interaction of the host with the specific anion). Often, this interaction involves an exchange of the coordinated anion at the metal center of the organometallic ionophore with the target anion in the sample solution. Useful reviews describe in detail individual carrier-based ISEs, (according to the analyte for which they were developed) and their practical limits. (39,39a). Many exciting developments based on novel host–guest chemistry (e.g., recognition by steric shapes) are anticipated.

5-2.3 Solid-State Electrodes

Considerable work has been devoted to the development of solid membranes that are selective primarily to anions. The solid-state membrane can be made of single

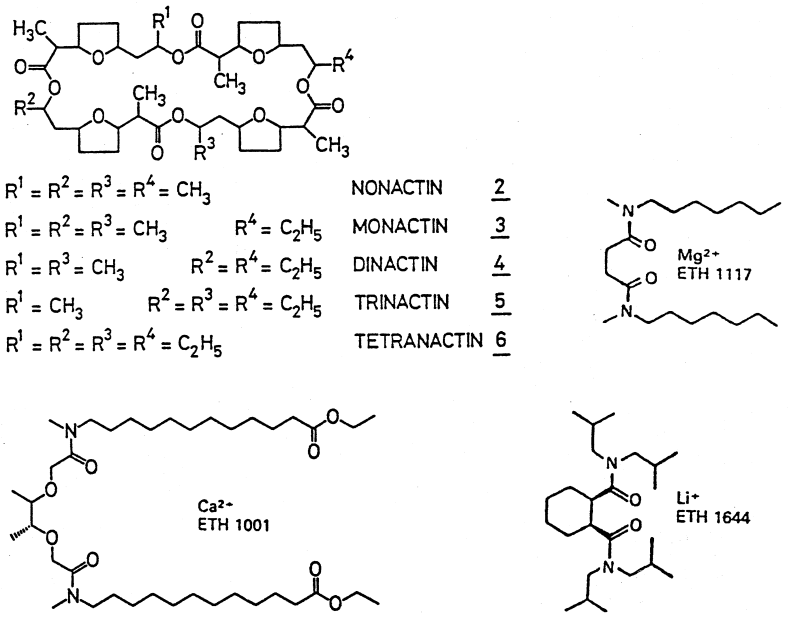

FIGURE 5-13 Structures of neutral carriers used in liquid-membrane ion-selective electrodes.

crystals, polycrystalline pellets, or mixed crystals. The resulting solid-state membrane electrodes have found use in a great number of analytical applications.

An example of a very successful solid-state sensor is the fluoride ion-selective electrode. This single-crystal device is by far the most successful anion-selective electrode. It consists of a LaF_3 crystal and an internal electrolyte solution (consisting of 0.1 M NaF and 0.1 M KCl, and containing the Ag/AgCl wire). The LaF_3 crystal is doped with EuF_2 to provide vacancies ("holes") at anionic sites (Figure 5-15). Since each EuF_2 introduces only two F^- instead of three, there is a vacant fluoride site for each EuF_2 added. Such a solid-state membrane derives its selectivity from restriction of the movement of all ions, except the fluoride of interest. The latter moves by migration through the crystal lattice (by jumping from one vacancy defect to another), thus establishing the desired potential difference. A Nernstian response

$$E = K - 0.059 \log a_{F^-} \tag{5-16}$$

is obtained down to about 10^{-6} M. The only interfering ion (due to similarity in size and charge) is OH^-, for which the selectivity coefficient (K_{F^-/OH^-}) is 0.1. Hence, the electrode is limited to use over the pH range 0–8.5. Other halide ions are considerably larger than F^- and so do not interfere. The electrode exhibits at least a 1000 : 1 preference for fluoride over chloride or bromide ions. In acidic solutions (pH $< \sim 4$) the fluoride activity is less than the formal concentration (due to the formation of HF).

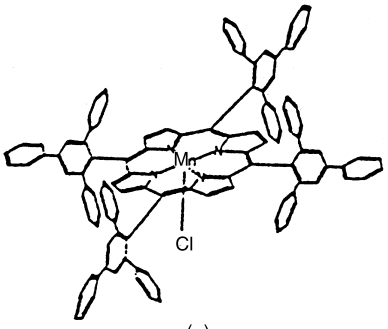

(*a*)

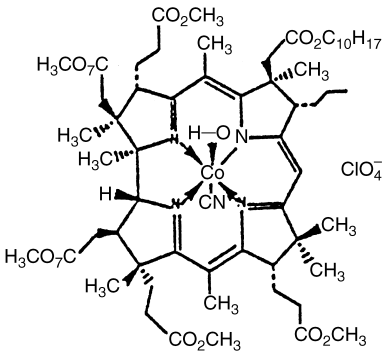

(*b*)

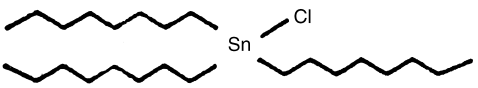

(*c*)

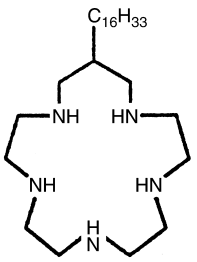

(*d*)

FIGURE 5-14 Structures of some chemical species useful for designing anion-selective electrodes: (*a*) Mn(III) porphyrin; (*b*) vitamin B_{12} derivative; (*c*) tri-*n*-octyltin chloride; (*d*) lipophilic polyamine macrocyclic compound.

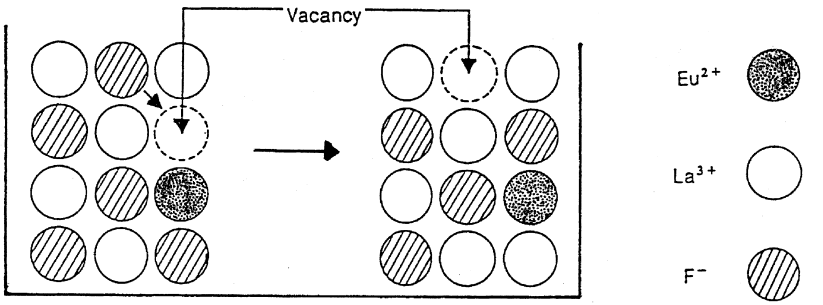

FIGURE 5-15 Migration of the fluoride ion through the LaF_3 lattice (doped with EuF_2). The vacancies created within the crystal cause jumping of neighboring F^- into the vacancy.

Other useful solid-state electrodes are based on silver compounds (particularly silver sulfide). Silver sulfide is an ionic conductor, in which silver ions are the mobile ions. Mixed pellets containing Ag_2S–AgX (where X = Cl, Br, I, SCN) have been successfully used for the determination of one of these particular anions. The behavior of these electrodes is determined primarily by the solubility products involved. The relative solubility products of various ions with Ag^+ thus dictate the selectivity (i.e., $k_{ij} = K_{SP(Agi)}/K_{SP(Agj)}$). Consequently, the iodide electrode (membrane of Ag_2S/AgI) displays high selectivity over Br^- and Cl^-. In contrast, the chloride electrode suffers from severe interference from Br^- and I^-. Similarly, mixtures of silver sulfide with CdS, CuS, or PbS provide membranes that are responsive to Cd^{2+}, Cu^{2+}, or Pb^{2+}, respectively. A limitation of these mixed-salt electrodes is that the solubility of the second salt must be much larger than that of silver sulfide. A silver sulfide membrane by itself responds to either S^{2-} or Ag^+ ions, down to the 10^{-8} M level.

Sensors for various halide ions can also be prepared by suspending the corresponding silver halide in an inert support material, such as silicone rubber (40). Such support material provides a flexible, heterogeneous membrane with resistance to cracking and swelling. The resulting membrane is called a heterogeneous or precipitate-impregnated membrane. For example, a chloride-selective electrode is based on a heterogeneous membrane prepared by polymerizing monomeric silicone rubber in the presence of an equal weight of silver chloride particles. A 0.5 mm thick disk of this heterogeneous membrane is sealed to the bottom of a glass tube; potassium chloride and a silver wire are placed in the tube. The sensitivity of the electrode is limited by the solubility of silver chloride. Chloride concentrations from 5×10^{-5} to 1.0 M can be measured. Such an electrode operates over the pH range 2–12, and at temperatures between 5 and 5000°C. Ion-selective electrodes for thiocyanate (SCN^-) or cyanide (CN^-) can be prepared in a similar fashion. Such electrodes rely on a "corrosion" reaction between the silver halide (AgX) and the target ion, for example:

$$AgX + 2CN^- \rightarrow Ag(CN)_2^- + X^- \qquad (5\text{-}17)$$

(Safety considerations dictate that cyanide measurements should be carried out in strongly basic media.) The interference mechanism with silver-based solid-state ISEs differs from that of ISEs described earlier. Depending on the K_{SP} value, an excess of the interfering ion may result in its deposition as silver salt on the membrane surface. Removal of the interfering film (by scrubbing) is thus required to restore the electrode activity. Table 5-1 lists some solid-state electrodes from a commercial source, along with their dynamic range and major interferences.

5-2.4 Coated-Wire Electrodes

Coated-wire electrodes (CWEs), introduced by Freiser in the mid-1970s, are prepared by coating an appropriate polymeric film directly onto a conductor (Figure 5-16). The ion-responsive membrane is commonly based on poly(vinyl chloride), while the conductor can be metallic (Pt, Ag, Cu) or graphite-based of any conventional shape such as wire or disk. The conductor is usually dipped in a solution of PVC and the active substance, and the resulting film is allowed to air dry. Other polymers and modified polymers, including poly(acrylic acid) and modified poly(vinylbenzyl chloride) can also be useful for various applications. In addition to the miniaturization capability, CWEs are extremely simple, inexpensive, and easy to prepare and function well over the 10^{-5}–10^{-1} M concentration range. The exact mechanism of the behavior of the CWE continues to be a mystery, in view of the lack of internal reference components. Coated-wire electrodes may suffer from reproducibility and long-term stability (drifting potential) problems. Nevertheless, such devices have been found useful for various important applications, provided the electrodes are calibrated periodically. Determinations of basic drugs (e.g., cocaine, methodone) (42), amino acids (43), potassium, and sodium (44) represent some of the useful applications of CWE. New concepts for preparing CWEs appear to improve their analytical performance, particularly with respect to stability and

TABLE 5-1 Characteristics of Solid-State Crystalline Electrodes[a]

Analyte Ion	Concentration Range (M)	Major Interferences
Br^-	10^0 to 5×10^{-6}	CN^-, I^-, S^{2-}
Cd^{2+}	10^{-1} to 1×10^{-7}	Fe^{2+}, Pb^{2+}, Hg^{2+}, Ag^+, Cu^{2+}
Cl^-	10^0 to 5×10^{-5}	CN^-, I^-, Br^-, S^{2-}
Cu^{2+}	10^{-1} to 1×10^{-8}	Hg^{2+}, Ag^+, Cd^{2+}
CN^-	10^{-2} to 1×10^{-6}	S^{2-}
F^-	Saturated to 1×10^{-6}	OH^-
I^-	10^0 to 5×10^{-8}	
Pb^{2+}	10^{-1} to 1×10^{-6}	Hg^{2+}, Ag^+, Cu^{2+}
Ag^+/S^{2-}	Ag^+: 10^0 to 1×10^{-7} S^{2-}: -10^0 to 1×10^{-7}	Hg^{2+}
SCN^-	10^0 to 1×10^{-6}	I^-, Br^-, CN^-, S^{2-}

[a]From *Orion Guide to Ion Analysis*, Orion Research, Cambridge, MA, 1983. With permission.

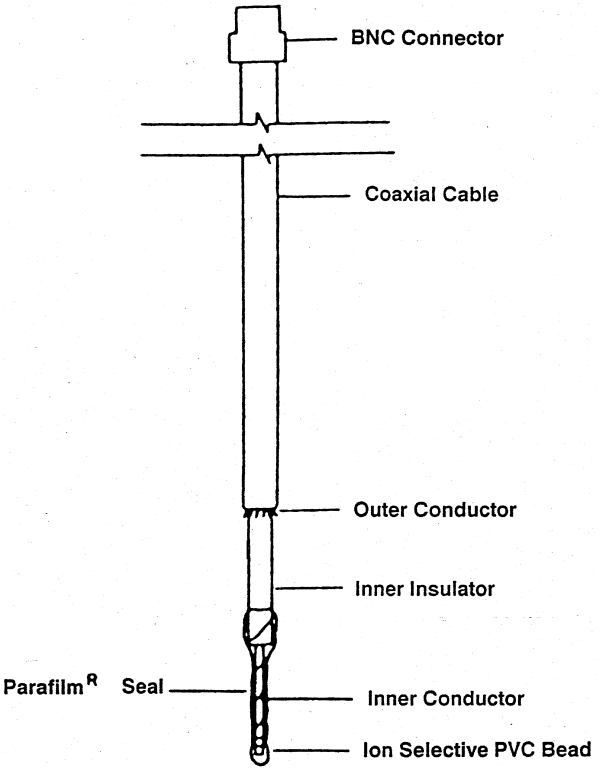

FIGURE 5-16 Coated-wire ion-selective electrode. (Reproduced with permission from reference 41.)

reproducibility. The principles and applications of CWEs have been reviewed (4). The possibility of eliminating the internal filling solution is receiving considerable interest in connection with mass production of potentiometric sensors and sensor arrays (see Section 6-3.2).

5-3 ON-LINE AND IN-VIVO POTENTIOMETRIC MEASUREMENTS

Various on-line monitoring systems can benefit from the inherent specificity, wide scope, dynamic behavior, and simplicity of ISEs. In particular, ISEs have become widely used as detectors in high-speed automated flow analyzers, such as air-segmented or flow injection systems (45,46). For example, Figure 5-17 shows the flow injection determination of physiologically important potassium in serum, using a tubular potassium selective electrode, at a rate of 100 samples per hour. Even higher throughputs, reaching 360 samples per hour, have been employed in connection with air-segmented flow systems (48). Such analyzers are now being

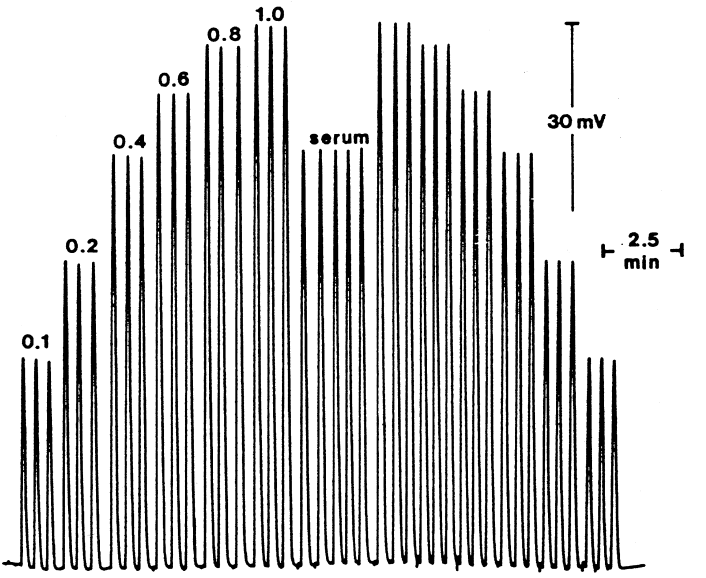

FIGURE 5-17 Flow injection potentiometric determination of potassium in serum. (Reproduced with permission from reference 47.)

routinely employed in most hospitals for the high-speed determination of physiologically important cationic electrolytes (e.g., K^+, Na^+, Ca^{2+}, Mg^{2+}, and H^+) or anions (e.g. Cl^-) in body fluids. The corresponding ISEs are usually placed in series, along the flow channel. Additional advantages accrue from the coupling of arrays of potentiometric detectors with chemometric (statistical) procedures (see Section 6-4). The transient nature of flow-injection potentiometric measurements (e.g., Figure 5-17) nicely addresses the potential-drift problem common to analogous batch measurements. It can also be exploited for enhancing the selectivity by operating under kinetic (rather than equilibrium) control. Improved selectivity can also be achieved by deliberately adding the interfering ion to the flow-injection carrier solution. Several designs of low-volume potentiometric flow detectors have been reported (47,48). The simplest design consists of an ISE fitted tightly with a plastic cap, with an inlet and outlet for the flowing stream (Figure 5-18). The reference electrode is usually placed downstream from the ISE. It can also be immersed in a parallel (potassium chloride) flowing stream. Other common detector designs include the flow-through tubular ISE (used in Figure 5-17), and tangential or wall-jet ISEs. Multi-ion detectors, based on ion-sensitive field-effect transistors (discussed in Section 6-3) have been combined with miniaturized micromachined flow-injection systems (50). Such coupling offers improved response times and reduced consumption of samples and reagents.

In addition to automated analysis, ISEs can be used to detect ionic species in chromatographic effluents. Particularly powerful is the coupling of modern ion

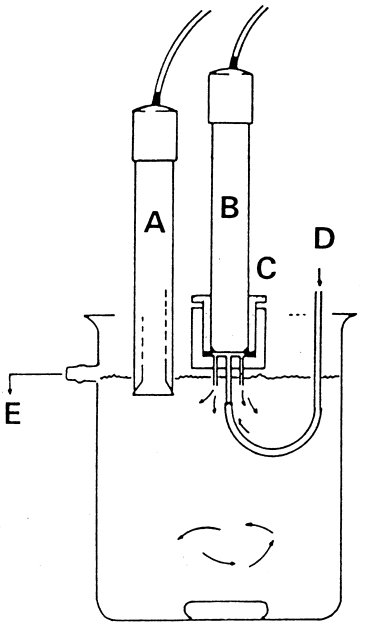

FIGURE 5-18 Flow-through potentiometric cell-cap design. A, reference electrode; B, iodide electrode; C, flow-through cap; D, inlet; E, outlet. (Reproduced with permission from reference 49.)

chromatography with potentiometric detection (51). Similarly, liquid-membrane microelectrodes have been used as small-dead-volume detectors in open tubular column liquid chromatography (52). Miniaturization has also permitted the recent adaptation of ISEs as on-column detectors for capillary zone electrophoresis in connection with femtoliter detection volumes (53,54). The small dimensions in capillary electrophoresis require proper attention to the positioning of the ISE detector. Both micropipette and coated-wire ISEs have been useful for this task, with the latter offering a simplified electrode alignment (54). Micropipette ISEs have also been used as tips in scanning electrochemical microscopy (55; see Section 2-3). The suitability to miniaturization is attributed to the fact that the potentiometric signal does not depend on the sensing area; but further miniaturization of ISEs to the nanometer domain is limited by the electrical resistance of the bulk liquid membrane.

Potentiometric microelectrodes are very suitable for in-vivo real-time clinical monitoring of blood electrolytes, intracellular studies, in-situ environmental surveillance or industrial process control. For example, Simon's group described the utility of a system for on-line measurements of blood potassium ion concentration during an open-heart surgery (56); Buck and co-workers (57) reported on the use of flexible planar electrode arrays for the simultaneous in-vivo monitoring of the pH and potassium ion in the porcine beating heart during acute ischemia (Figure 5-19).

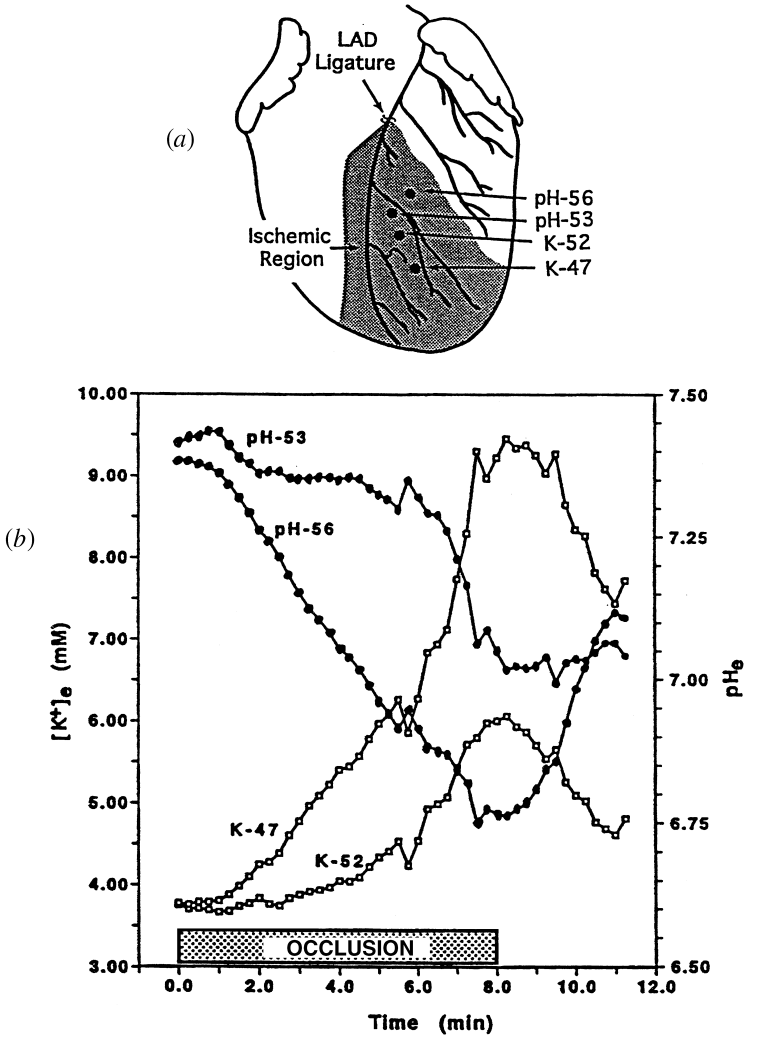

FIGURE 5-19 (*a*) Placement of the two pH and two potassium sensors (0.5 mm diameter) in the porcine heart. (*b*) Recorded fall in the pH and increased potassium activity LAD = left anterior descending coronory artery. (Reproduced with permission from reference 57.)

Miniaturized catheter-type ISE sensors, such as the implantable probe shown in Figure 5-20 represent the preferred approach for routine clinical in-vivo monitoring of blood electrolytes. For these intravascular measurements the reference electrode is placed outside the artery (in the external arm of the catheter), thus obviating biocompatability and drift problems associated with its direct contact with the blood.

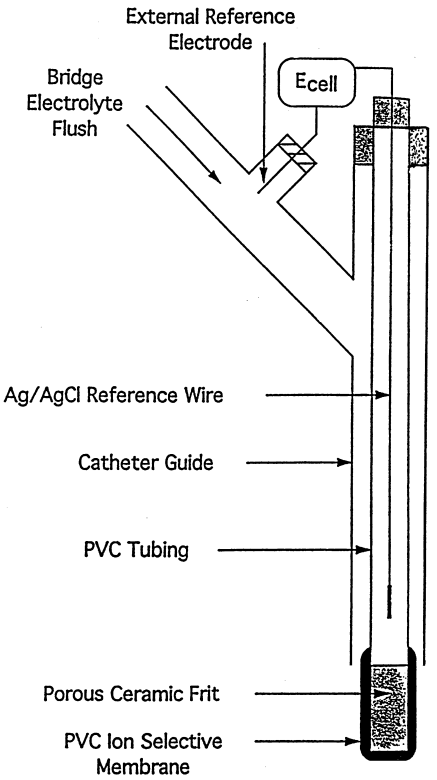

FIGURE 5-20 Miniaturized ISE catheter sensor for continuous monitoring of blood electrolytes. (Reproduced with permission from reference 58.)

REFERENCES

1. J. Koryta, *Ions, Electrodes and Membranes*, Wiley, New York, 1982.
2. W.E. Morf, *The Principles of Ion-Selective Electrodes and of Membrane Transport*, Elsevier, Amsterdam, 1981.
3. A.K. Covington, Ed., *Ion-Selective Electrode Methodology*, CRC Press, Boca Raton, FL, 1979.
4. H. Freiser, Ed., *Ion Selective Electrodes in Analytical Chemistry*, Vol. 1 and 2, Plenum Press, New York, 1978 and 1980.
5. N. Lakshminarayanaiah, *Membrane Electrodes*, Academic Press, New York, 1976.
6. P.P. Buck, *CRC Crit. Rev. Anal. Chem.*, 5, 323 (1976).
7. D. Ammann, W. Morf, P. Anker, P. Meier, E. Pret, and W. Simon, *Ion Sel. Electrode Rev.*, 5, 3 (1983).
8. A.K. Covington, *CRC Crit. Rev. Anal. Chem.*, 3, 355 (1974).
9. B.P. Nikolskii, *Acta Physiochim. U.S.S.R.*, 7, 597 (1937).

10. Y. Umezawa, Ed., *Handbook of Ion-Selective Electrodes: Selectivity Coefficients*, CRC Press, Boca Raton, FL, 1990.
11. E. Bakker, *Electroanalysis*, 9, 7 (1997).
12. R.P. Buck and E. Lindner, *Pure Appl. Chem.*, 66, 2527 (1995).
13. A. Lewenstam, M. Maj-Zurawska, and A. Hulanicki, *Electroanalysis*, 3, 727 (1991).
14. M. Cremer, *Z. Biol. (Munich)*, 47, 562 (1906).
15. G. Eisenman, Ed., *Glass Electrodes for Hydrogen and Other Cations*, Marcel Dekker, New York, 1976.
16. R.G. Bates, *Determination of pH: Theory and Practice*, Wiley, New York, 1973.
17. P. Anker, D. Ammann, and W. Simon, *Mikrochim, Acta*, I, 237 (1983).
18. U. Oesch, D. Ammann, and W. Simon, *Clin. Chem.*, 38, 1448 (1986).
19. S. Mathison, and E. Bakker, *Anal. Chem.*, 70, 303 (1998).
20. T. Sokalski, A. Ceresa, T. Zwicki, and E. Pretsch, *J. Am. Chem. Soc.*, 119, 11347 (1997).
21. F. Hofmeister, *Arch. Exp. Pathol. Pharmakol.*, 24, 247 (1888).
22. A. Hulanicki, M. Maj-Zurawska, and R. Lewandowski, *Anal. Chim. Acta*, 98, 151 (1978).
23. C.J. Coetzee and H. Freiser, *Anal. Chem.*, 40, 207 (1968).
24. J.L. Walker, *Anal. Chem.*, 43, 89A (1971).
25. S. Ma, V. Yang, and M. Meyerhoff, *Anal. Chem.*, 64, 694 (1992).
26. B. Fu, E. Bakker, J. Yum, E. Wang, V. Yang, and M.E. Meyerhoff, *Electroanalysis*, 7, 823 (1995).
27. C.R. Martin, and H. Freiser, *Anal. Chem.*, 52, 562 (1980).
28. E. Pretsch, M. Badertscher, M. Welti, T. Maruizumi, W. Morf, and W. Simon, *Pure Appl. Chem.*, 60, 567 (1988).
29. W.E. Morf, D. Ammann, and W. Simon, *Chimica*, 28, 65 (1974).
30. V. Gadzekpo, J. Hungerford, A. Kadry, Y. Ibrahim, and G. Christian, *Anal. Chem.*, 57, 493 (1985).
31. O. Kedem, E. Loebel, and M. Furmansky, *Gen. Offenbar*, No. 2027128 (1970).
32. A. Cadogan, D. Diamond, M. Smyth, M. Deasy, A. McKervey, and S. Harris, *Analyst*, 114, 1551 (1989).
33. Z. Brzozka, P. Cobben, D. Reinhaudt, J. Edema, J. Buter, and R. Kellogg, *Anal. Chim. Acta*, 273, 1139 (1993).
34. U. Wuthier, H. Viet Pham, R. Zund, D. Welti, R.J. Funck, A. Bezegh, D. Ammann, E. Pretsch, and W. Simon, *Anal. Chem.*, 56, 535 (1984).
35. K. Tohda, M. Tange, K. Odashima, Y. Umezawa, H. Furuta, and J. Sessler, *Anal. Chem.*, 64, 960 (1992).
36. S. Park, W. Matuszewski, M. Meyerhoff, Y. Liu, and K. Kadish, *Electroanalysis*, 3, 909 (1991).
37. S. Glazier and M. Arnold, *Anal. Chem.*, 63, 754 (1991).
38. Q. Chang, S.B. Park, D. Kliza, G.S. Cha, H. Yim, and M.E. Meyerhoff, *Amer. Lab*, Nov., 10 (1990).
39. P. Buhlmann, E. Pretsch, and E. Bakker, *Chem. Rev.*, 98, 1593 (1998).
39a. E. Bakker, P. Buhlmann, and E. Pretsch, *Electroanalysis* 11, 915 (1999).
40. E. Pungor and K. Toth, *Pure Appl. Chem.*, 31, 521 (1972).

41. C.R. Martin and H. Freiser, *J. Chem. Educ.*, 57, 152 (1980).
42. L. Cunningham and H. Freiser, *Anal. Chim. Acta*, 139, 97 (1982).
43. H. James, G. Carmack, and H. Freiser, *Anal. Chem.*, 44, 856 (1972).
44. H. Tamura, K. Kimura, and T. Shono, *Anal. Chem.*, 54, 1224 (1982).
45. K. Toth, J. Fucsko, E. Lindner, Z. Feher, and E. Pungor, *Anal. Chim. Acta*, 179, 359 (1986).
46. M. Trojanowich, and W. Matuszewski, *Anal. Chim. Acta*, 138, 71 (1982).
47. M.E. Meyerhoff and P.M. Kovach, *J. Chem. Educ.*, 60, 766 (1983).
48. P.S. Alexander and P. Seegopaul, *Anal. Chem.*, 52, 2403 (1980).
49. R. Llenado and G.A. Rechnitz, *Anal. Chem.*, 45, 2165 (1973).
50. B. van der Schoot, S. Jeanneret, A. van den Berg, and N. de Rooji, *Anal. Methods Instrum.*, 1, 38 (1993).
51. I. Isildak and A. Covington, *Electroanalysis*, 5, 815 (1993).
52. A. Manz and W. Simon, *J. Chromatogr. Sci.*, 21, 326 (1983).
53. A. Nann, I. Silverstri, and W. Simon, *Anal. Chem.*, 65, 1662 (1993).
54. T. Kappes and P.C. Hauser, *Anal. Chem.*, 70, 2487 (1998).
55. K. Toth, G. Nagy, C. Wei, and A.J. Bard, *Electroanalysis*, 7, 801 (1995).
56. H.F. Osswald, R. Asper, W. Dimai, and W. Simon, *Clin. Chem.*, 25, 39 (1979).
57. R.P. Buck, V. Cosorfet, E. Lindner, S. Ufer, M. Madaras, T. Johnson, R. Ash, and M. Neuman, *Electroanalysis*, 7, 846 (1995).
58. C. Espadas-Torre, M. Telting-Diaz, and M.E. Meyerhoff, *Interface*, Spring Issue, 41 (1995).

EXAMPLES

Example 5-1 Calculate the relative error (in proton concentration) that would occur if the pH of a 1×10^{-2} M NaOH solution were measured with a pH glass electrode ($k_{H,Na} = 10^{-10}$; assuming activity coefficient of 1.0).

Solution The concentration of the interfering sodium ion is 1×10^{-2} M, while that of the target proton is

$$[H^+] = K_w/[OH^-] = 10^{-14}/10^{-2} = 1 \times 10^{-12}\text{M}$$

From equation (5.6), we thus obtain

$$E_{cell} = K + 0.059 \log[1 \times 10^{-12} + 10^{-10} \times (1 \times 10^{-2})]$$

The relative error in concentration is thus

$$[10^{-10} \times (1 \times 10^{-2})/10^{-12}] \times 100 = 100\%$$

Example 5-2 The following potentials were observed for a calcium electrode immersed in standard calcium solutions:

$[Ca^{2+}]$ M	E (mV)
1×10^{-5}	100
1×10^{-4}	129
1×10^{-3}	158

What potential is expected for a calcium concentration of 5×10^{-4} M? (Assume activity coefficient of 1.0.)

Solution Plotting E vs. $\log[Ca^{2+}]$ gives a straight line with a slope of 29 mV/decade and an intercept of 245 mV. A calcium concentration of 5×10^{-4} M thus yields:

$$E = K + 29 \log [5 \times 10^{-4}] = 245 - 95.7 = 149.3 \text{ mV}$$

EXAMPLE 5-3 Calculate the error in millivolts that would occur if a solution containing 5×10^{-5} M F^- (pH 10) were measured with a fluoride ISE. ($k_{F,OH} = 0.1$)

Solution The concentration of the interfering hydroxyl ion at pH = 10 can be obtained:

$$[OH^-] = K_w/[H^+] = 10^{-14}/10^{-10} = 10^{-4} \text{ M}$$

From equation (5.4) we obtain:

$$E_{cell} = K - 0.059 \log(5 \times 10^{-5} + 0.1 \times 10^{-4}) = K + 0.249$$

In the absence of hydroxyl ion:

$$E_{cell} = K - 0.059 \log(5 \times 10^{-5}) = K + 0.254$$

Therefore the error in mV is

$$\text{Error} = K + 249 - (K + 254) = -5 \text{ mV}$$

Example 5-4 A student calibrated a Mg^{2+} ion-selective electrode using two standard solutions at 25°C and constant ionic strength. He obtained the following results:

$[Mg^{+2}]$ (M)	E(mV)
1×10^{-3}	142
1×10^{-4}	113

What is the concentration of the test solution that gave a potential reading of 125 mV under the same conditions?

Solution Plotting E vs. $\log[Mg^{2+}]$ gives a straight line; the magnesium concentration (2.6×10^{-4} M) corresponding to the 125 mV reading can be read directly from the axis.

EXAMPLE 5-5 Calculate the error caused by sodium ion, $a_{Na} = 0.01$, in the measurement of lithium, $a_{Li} = 0.01$, using a lithium ion-selective electrode $k_{Li,Na} = 0.06$

Solution From equation (5.6), we obtain

$$E = K + 0.059 \log[0.001 + 0.06(0.01)] = K - 0.165 \text{ V}$$

Without sodium the potential is

$$E = K + 0.059 \log(0.001) = K - 0.177 \text{ V}$$

Thus

$$\text{Error} = (0.012/0.177) \times 100 = 6.8\%$$

QUESTIONS

1. Discuss clearly the structural requirements for designing selective ionophores for ISE work. Give examples of such structures.
2. Explain clearly (using equations) why a highly selective ISE is not always sufficient for accurate potentiometric measurements.
3. Explain how the ion-recognition event is translated to the response of the corresponding ISE.
4. Explain clearly (using equations) why the sodium ISE is more sensitive than the calcium one.
5. Describe the source of errors in pH measurements using the glass pH electrode.

6. Describe the response mechanism of the fluoride ion-selective electrode. Explain clearly why the OH^- is the major interfering ion in F^- ISE measurements.

7. Discuss the significance of the selectivity coefficient of an ISE. How would you determine its value?

8. Give example of a successful ISE for measuring a macromolecular polyanionic compound.

9. Use the Nikolskii–Eisenman equation to explain why lowering of the detection limits requires careful attention to the selectivity of the resulting ISE.

10. Explain clearly how the presence of magnesium ion can influence the response of the calcium ISE.

11. By how many millivolts will the potential of a calcium ISE change if the electrode is removed from a 1×10^{-3} M $CaCl_2$ solution and placed in 1×10^{-3} M $CaCl_2$?

12. Explain clearly why small uncertainties in the measured cell potential can cause large errors in the response of ISEs.

13. Discuss the major sources of errors in potentiometric measurements.

Analytical Electrochemistry, Second Edition. Joseph Wang

ISBNs: 0-471-28272-3 (Hardback); 0-471-22823-0 (Electronic)

CHAPTER 6

ELECTROCHEMICAL SENSORS

A chemical sensor is a small device that can be used for direct measurement of the analyte in the sample matrix. Ideally, such a device is capable of responding continuously and reversibly and does not perturb the sample. By combining the sample handling and measurement steps, sensors eliminate the need for sample collection and preparation. Chemical sensors consist of a transduction element covered with a chemical or biological recognition layer. This layer interacts with the target analyte and the chemical changes resulting from this interaction are translated by the transduction element into electrical signals.

The development of chemical sensors is currently one of the most active areas of analytical research. Electrochemical sensors represent an important subclass of chemical sensors in which an electrode is used as the transduction element. Such devices hold a leading position among sensors presently available, have reached the commercial stage, and have found a vast range of important applications in the fields of clinical, industrial, environmental, and agricultural analyses. The field of sensors is interdisciplinary and future advances are likely to derive from progress in several disciplines. Research into electrochemical sensors is proceeding in a number of directions, as described in the following sections. The first group of electrochemical sensors, the potentiometric ion-selective electrodes (based on "ionic receptors"), has been described in Chapter 5.

6-1 ELECTROCHEMICAL BIOSENSORS

Electrochemical biosensors combine the analytical power of electrochemical techniques with the specificity of biological recognition processes. The aim is to

biologically produce an electrical signal that relates to the concentration of an analyte. For this purpose, a biospecific reagent is either immobilized or retained at a suitable electrode, which converts the biological recognition event into a quantitative amperometric or potentiometric response. Such biocomponent–electrode combinations offer new and powerful analytical tools that are applicable to many challenging problems. A level of sophistication and state-of-the art technology are commonly employed to produce easy-to-use, compact, and inexpensive devices. Advances in electrochemical biosensors are progressing in different directions. Two general categories of electrochemical biosensors may be distinguished, depending on the nature of the biological recognition process: biocatalytic devices (utilizing enzymes, cells, or tissues as immobilized biocomponents) and affinity sensors (based on antibodies, membrane receptors, or nucleic acids).

6-1.1 Enzyme-Based Electrodes

Enzymes are proteins that catalyze chemical reactions in living systems. Such catalysts are not only efficient but are also extremely selective. Hence, enzymes combine the recognition and amplification steps, as needed for many sensing applications.

Enzyme electrodes are based on the coupling of a layer of an enzyme with an appropriate electrode. Such electrodes combine the specificity of the enzyme for its substrate with the analytical power of electrochemical devices. As a result of this coupling, enzyme electrodes have been shown to be extremely useful for monitoring a wide variety of substrates of analytical importance in clinical, environmental, and food samples.

6-1.1.1 Impractical and Theoretical Considerations The operation of an enzyme electrode is illustrated in Figure 6-1. The immobilized enzyme layer is chosen to catalyze a reaction, which generates or consumes a detectable species:

$$S + C \xrightarrow{\text{Enzyme}} P + C' \tag{6-1}$$

where S and C are the substrate and coreactant (cofactor), and P and C' are the corresponding products. The choice of the sensing electrode depends primarily upon the enzymatic system employed. For example, amperometric probes are highly suitable when oxidase or dehydrogenase enzymes (generating electrooxidizable peroxide or NADH species) are employed, pH-glass electrodes are used for enzymatic pathways that result in a change in pH, while gas (carbon dioxide) potentiometric devices will be the choice when decarboxylase enzymes are used.

The success of the enzyme electrode depends, in part, on the immobilization of the enzyme layer. The objective is to provide intimate contact between the enzyme and the sensing surface while maintaining (and even improving) the enzyme stability. Several physical and chemical schemes can thus be used to immobilize the enzyme onto the electrode. The simplest approach is to entrap a solution of the

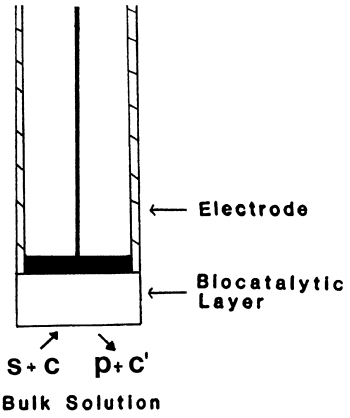

FIGURE 6-1 Enzyme electrode based on a biocatalytic layer immobilized on an electrode transducer.

enzyme between the electrode and a dialysis membrane. Alternately, polymeric films (e.g., polypyrrole, Nafion) may be used to entrap the enzyme (via casting or electropolymerization). Additional improvements can be achieved by combining several membranes and/or coatings. Figure 6-2 displays a useful yet simple immobilization based on trapping the enzyme between an inner cellulose acetate film and a collagen or polycarbonate membrane, cast at the tip of an amperometric transducer. Such coverage with a membrane or coating serves also to extend the linear range (via reduction of the local substrate concentration) and to reject potential interferences (e.g., coexisting electroactive species or proteins). In chemical immobilization methods, the enzyme is attached to the surface by means of a covalent coupling through a cross-linking agent (e.g., glutaraldehyde, amide). Covalent coupling may be combined with the use of functionalized thiolated monolayers for assembling multilayer enzyme networks on electrode surfaces (2). Other useful enzyme immobilization schemes include entrapment within a thick gel layer, low-temperature encapsulation onto sol-gel films, adsorption onto a graphite surface, incorporation (by mixing) within the bulk of three-dimensional carbon-paste or graphite-epoxy matrices (3,4), or electrochemical codeposition of the enzyme and catalytic metal particles (e.g., Pt, Rh). Such codeposition, as well as electropolymerization processes, are particularly suited for localizing the enzyme onto miniaturized sensor surfaces (5,6). The electropolymerization route can be accomplished by entrapping the enzyme within the growing film or anchoring it covalently to the monomer prior to the film deposition. These avenues can also reduce interferences and fouling of the resulting biosensors. The mixed-enzyme/carbon-paste immobilization strategy is attractive for many routine applications as it couples the advantages of versatility (controlled doping of several modifiers, e.g., enzyme, cofactor mediator), speed (due to close proximity of biocatalytic and sensing sites, and absence of membrane barriers), ease of fabrication, and renewability.

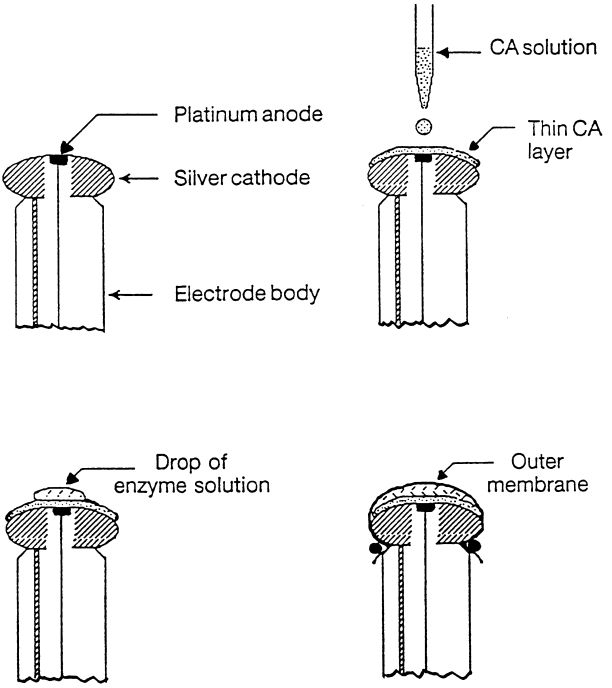

FIGURE 6-2 Steps in the preparation of an amperometric enzyme electrode with simple enzyme immobilization by trapping between an inner cellulose acetate and outer collagen membrane, cast on the electrode body. (Reproduced with permission from reference 1.)

The immobilization procedure may alter the behavior of the enzyme (compared to its behavior in homogeneous solution). For example, the apparent parameters of an enzyme-catalyzed reaction (optimum temperature or pH, maximum velocity, etc.) may all be changed when an enzyme is immobilized. Improved stability may also accrue from the minimization of enzyme unfolding associated with the immobilization step. Overall, careful engineering of the enzyme microenvironment (on the surface) can be used to greatly enhance the sensor performance. More information on enzyme immobilization schemes can be found in several reviews (7,8).

The response characteristics of enzyme electrodes depend on many variables, and an understanding of the theoretical basis of their function would help to improve their performance. Enzymatic reactions involving a single substrate can be formulated in a general way as

$$\mathrm{E} + \mathrm{S} \underset{k_{-1}}{\overset{k_1}{\rightleftharpoons}} \mathrm{ES} \xrightarrow{k_2} \mathrm{E} + \mathrm{P} \tag{6-2}$$

In this mechanism, the substrate S combines with the enzyme E to form an intermediate complex ES, which subsequently breaks down into products P and

liberates the enzyme. At a fixed enzyme concentration, the rate v of the enzyme-catalyzed reaction is given by the Michaelis–Menten equation:

$$v = \frac{V_m[S]}{(K_m + [S])} \tag{6-3}$$

where K_m is the *Michaelis–Menten constant* and V_m is the maximum rate of the reaction. The term K_m corresponds to the substrate concentration for which the rate is equal to half of V_m. In the construction of enzyme electrodes, it is desirable to obtain the highest V_m and the lowest K_m. Figure 6-3 shows the dependence of the reaction rate upon substrate concentration, together with the parameters K_m and V_m. The initial rate increases with substrate, until a nonlimiting excess of substrate is reached, after which additional substrate causes no further increase in the rate. Hence, a leveling-off of calibration curves is expected at substrate concentrations above the K_m of the enzyme. Accordingly, low K_m values—while offering higher sensitivity—result in a narrower linear range (which reflects the saturation of the enzyme). The above discussion assumes that the reaction obeys the Michaelis–Menten kinetics theory. Experimentally, the linear range may exceed the concentration corresponding to K_m, because the local substrate concentration in the electrode containment region is often less than the bulk concentration (as common with amperometric probes coated with diffusion-limiting membranes). The level of the cosubstrate (coreactant) may also influence the linear range [through stoichiometric limitation of equation (6-1)].

Improved sensitivity and scope can be achieved by coupling two (or more) enzymatic reactions in a chain, cycling, or catalytic mechanism (9). For example, a considerable enhancement of the sensitivity of enzyme electrodes can be achieved by enzymatic recycling of the analyte in two-enzyme systems. Such an amplification

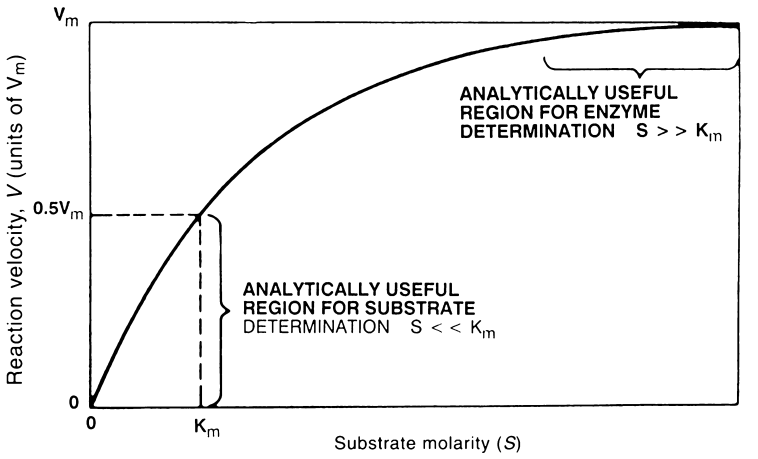

FIGURE 6-3 Dependence of the velocity of an enzyme-catalyzed reaction upon the substrate concentration (at a constant level of enzyme activity).

scheme generates more than a stoichiometric amount of product and hence large analytical signals for low levels of the analyte. In addition, a second enzyme can be used to generate a detectable (electroactive) species, from a nonelectroactive product of the first reaction.

6-1.1.2 Enzyme Electrodes of Analytical Significance

6-1.1.2.1 Glucose Sensors The determination of glucose in blood plays a crucial role in the diagnosis and therapy of diabetes. Electrochemical biosensors for glucose play a key role in this direction. The glucose amperometric sensor, developed by Updike and Hicks (10), represents the first reported use of an enzyme electrode. The electrode is commonly based on the entrapment of glucose oxidase (GOx) between polyurethene and permselective membranes on a platinum working electrode (Figure 6-4). The liberation of hydrogen peroxide in the enzymatic reaction

$$\text{Glucose} + O_2 \xrightarrow{\text{glucose oxidase}} \text{gluconic acid} + H_2O_2 \qquad (6\text{-}4)$$

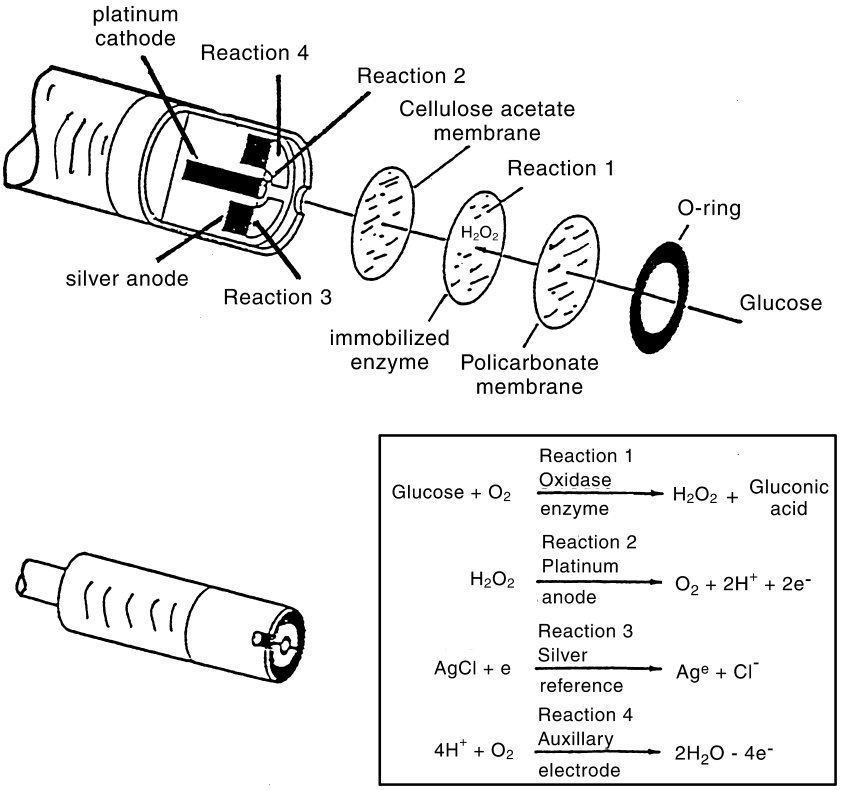

FIGURE 6-4 Schematic of a "first-generation" glucose biosensor (based on a probe manufactured by YSI Inc.).

can be monitored amperometrically at the platinum surface:

$$H_2O_2 \xrightarrow{\text{electrode}} O_2 + 2H^+ + 2e^- \tag{6-5}$$

The multilayer membrane coverage (Figure 6-4) improves the relative surface availability of oxygen (by decreasing the ratio of glucose/oxygen flux) and excludes potential interferences (common at the potentials used for detecting the peroxide product). The enzymatic reaction can also he followed by monitoring the consumption of the oxygen cofactor.

Further improvements can be achieved by replacing the oxygen with a non-physiological (synthetic) electron acceptor, which is able to shuttle electrons from the flavin redox center of the enzyme to the surface of the working electrode. Glucose oxidase (and other oxidoreductase enzymes) do not directly transfer electrons to conventional electrodes because their redox center is surrounded by a thick protein layer. This insulating shell introduces a spatial separation of the electron donor–acceptor pair, and hence an intrinsic barrier to direct electron transfer, in accordance with the distance dependence of the electron transfer rate (11):

$$K_{et} = 10^{13} e^{-0.91(d-3)} e^{[-(\Delta G+\lambda)/4RT\lambda]} \tag{6-6}$$

where ΔG and λ correspond to the free and reorganization energies accompanying the electron transfer, respectively, and d is the actual electron transfer distance.

As a result of using artificial (diffusional) electron-carrying mediators, measurements become insensitive to oxygen fluctuations and can be carried out at lower potentials that do not provoke interfering reactions from coexisting electroactive species (Figure 6-5). Many organic and organometallic redox compounds have been considered for this role of enzyme mediator. Some common examples are displayed in Figure 6-6. In particular, ferrocene derivatives (e.g., Figure 6-6*a*) have been very successful for shuttling electrons from glucose oxidase to the electrode by the following scheme:

$$\text{Glucose} + GOx_{(ox)} \rightarrow \text{gluconic acid} + GOx_{(red)} \tag{6-7}$$

$$GOx_{(red)} + 2M_{(ox)} \rightarrow GOx_{(ox)} + 2M_{(red)} + 2H^+ \tag{6-8}$$

$$2M_{(red)} \rightarrow 2M_{(ox)} + 2e^- \tag{6-9}$$

where $M_{(ox)}$ and $M_{(red)}$ are the oxidized and reduced forms of the mediator. This chemistry has led to the development of a pen-sized meter for personal glucose monitoring in a single drop of blood. Such rapid (~ 30 s) self-testing assays commonly rely on a chronoapmerometric operation (e.g., Example 6-1). The single-use disposable strips used with this device are made of poly(vinyl chloride) and a screen-printed carbon electrode containing a mixture of glucose oxidase and

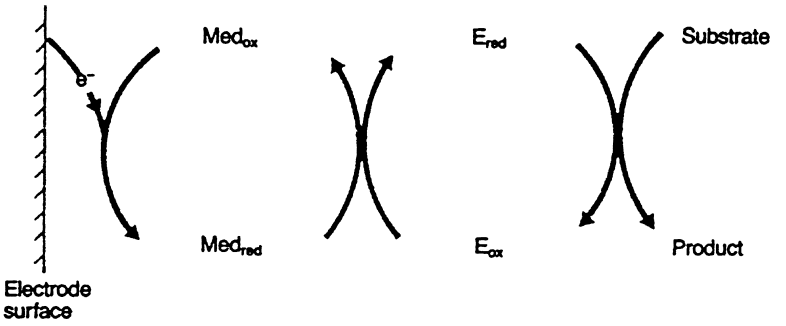

FIGURE 6-5 "Second-generation" enzyme electrode: sequence of events that occur in a mediated system. (Reproduced with permission from reference 12.)

the mediator (Figure 6-7). The screen-printing technology used for mass-scale production of this and similar biosensors is discussed in Section 6-3. Other classes of promising mediators for glucose oxidase are quinone derivatives, ruthenium complexes, ferricyanide, phenothiazine compounds, and organic conducting salts (particularly tetrathiafulvalene-tetracyanoquinodimethane, TTF-TCNQ). An elegant nondiffusional route for establishing electrical communication between GOx and the electrode is to "wire" the enzyme to the surface with a long polymer having a dense array of electron relays [e.g., osmium(bipyridyl) bound to poly(vinylpyridine); Figure 6-8 (14)]. Such a polymeric chain is flexible enough to fold along the enzyme structure. The resulting three-dimensional redox-polymer/enzyme network offers high current outputs and stabilizes the mediator to the surface. An even more elegant possibility is chemical modification of the enzyme with the redox-active mediator (15). Glucose electrodes of extremely efficient electrical communication with the electrode can be generated by the enzyme reconstitution process (16). For this purpose, the flavin active center of GOx is removed to allow positioning of the electron-mediating ferrocene unit prior to the reconstitution of the enzyme (Figure 6-9). The challenges in establishing electrical communication between redox enzymes and electrode surfaces have been reviewed (2,17). Ultimately, these and similar developments would lead to invasive (needle-type) and noninvasive devices for continuous real-time monitoring of glucose (18). Such probes would offer a tight control of diabetes, in connection with an alarm detecting hypo- or hyperglycemia or a future closed-loop insulin-releasing system (i.e., artificial pancreas).

6-1.1.2.2 Ethanol Electrodes The reliable sensing of ethanol is of great significance in various disciplines. The enzymatic reaction of ethanol with the cofactor nicotinamide–adenine dinucleotide (NAD^+), in the presence of alcohol dehydrogenase (ADH)

$$C_2H_5OH + NAD^+ \xrightarrow{ADH} C_2H_5O + NADH \qquad (6\text{-}10)$$

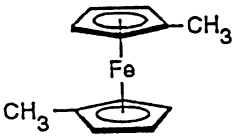

(*a*)

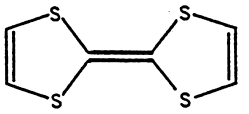

(*b*)

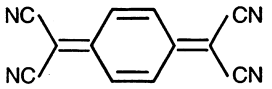

(*c*)

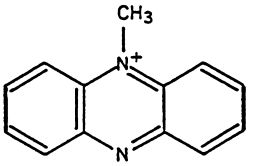

(*d*)

FIGURE 6-6 Chemical structure of some common redox mediators: (*a*) dimethyl ferrocene; (*b*) tetrathiafulvalene; (*c*) tetracyanoquinodimethane; (*d*) Meldola Blue.

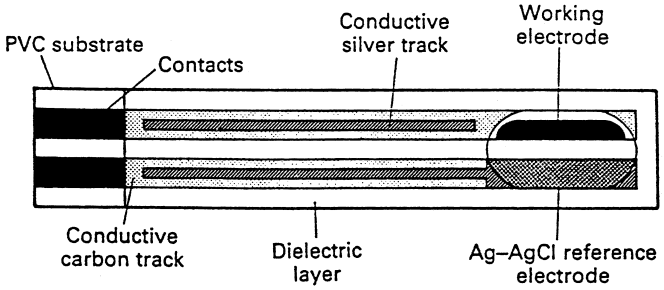

FIGURE 6-7 Schematic representation of a disposable glucose sensor strip. (Reproduced with permission from reference 13.)

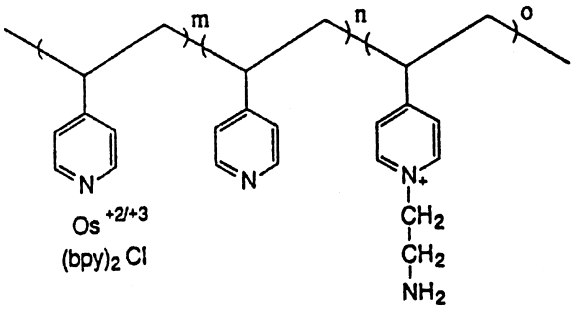

FIGURE 6-8 Composition of an electron-relaying redox polymer used for "wiring" enzymes to electrode transducer. (Reproduced with permission from reference 14.)

serves as a basis of amperometric sensors for ethanol (19). Reagentless devices based on the coimmobilization of ADH and NAD^+ to various carbon or platinum anodes are employed (e.g., Figure 6-10). NAD^+ is regenerated electrochemically by oxidation of the NADH, and the resulting anodic current is measured:

$$NADH \rightarrow NAD^+ + 2e^- + H^+ \tag{6-11}$$

To circumvent high overvoltage and fouling problems encountered with the direct oxidation of NADH at conventional electrode (equation 6-11), much work has been devoted to the development of modified electrodes with catalytic properties for

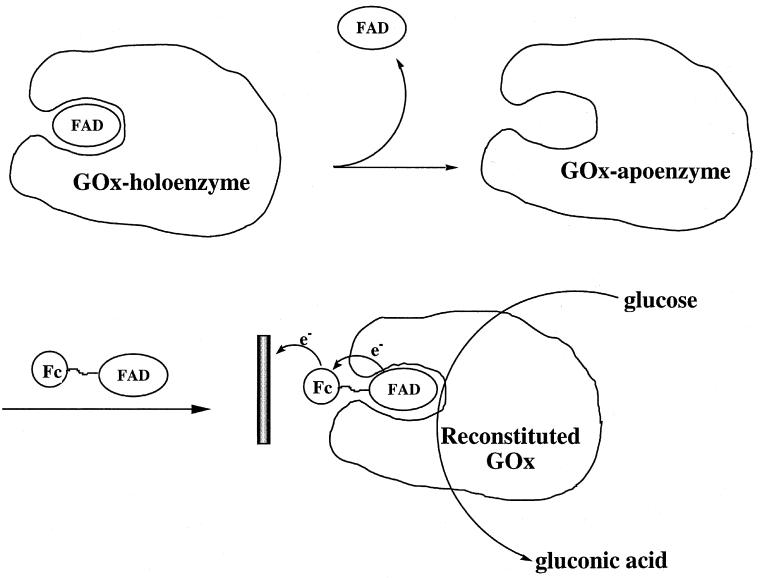

FIGURE 6-9 Electrical contact of a flavoenzyme by its reconstitution with a relay-FAD semisynthetic cofactor. Fc = ferrocene. (Reproduced with permission from reference 2.)

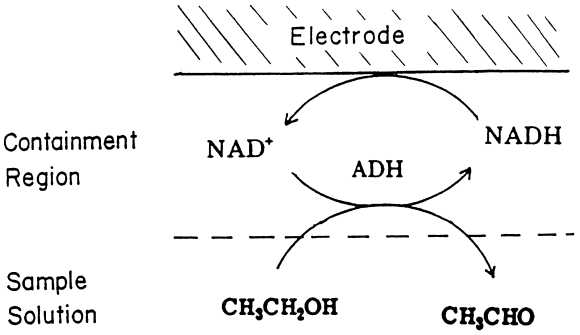

FIGURE 6-10 Reagentless ethanol bioelectrode.

NADH. Immobilized redox mediators, such as the phenoxazine Meldola Blue or phenothiazine compounds, have been particularly useful for this purpose (20) (see also Figure 4-12). Such mediation should be useful for many other dehydrogenase-based biosensors. High sensitivity and speed are indicated from the flow-injection response of Figure 3-21. The challenges of NADH detection and the development of dehydrogenase biosensors have been reviewed (21). Alcohol biosensing can also be accomplished in the presence of alcohol oxidase, based on measurements of the liberated peroxide product.

6-1.1.2.3 Urea Electrodes The physiologically important substrate urea can be sensed based on the following urease-catalyzed reaction:

$$NH_2CONH_2 + 2H_2O + H^+ \xrightarrow{\text{urease}} 2NH_4^+ + HCO_3^- \qquad (6\text{-}12)$$

The sensor is an ammonium ion-selective electrode surrounded by a gel impregnated with the enzyme urease (Figure 6-11) (22). The generated ammonium ions are detected after 30–60 s to reach a steady-state potential. Alternately, the changes in the proton concentration can be probed with glass pH or other pH-sensitive electrodes. As expected for potentiometric probes, the potential is a linear function of the logarithm of the urea concentration in the sample solution.

Enzyme electrodes for other substrates of analytical significance have been developed. Representative examples are listed in Table 6-1. Further advances in enzyme technology, and particularly the isolation of new and more stable enzymes, should enhance the development of new biocatalytic sensors. New opportunities (particularly assays of new environments or monitoring of hydrophobic analytes) derive from the finding that enzymes can maintain their biocatalytic activity in organic solvents (31,32).

6.1.1.2.4 Toxin (Enzyme Inhibition) Biosensors Enzyme affectors (inhibitors and activators) that influence the rate of biocatalytic reactions can also be measured. Sensing probes for organophosphate and carbamate pesticides, for the respiratory

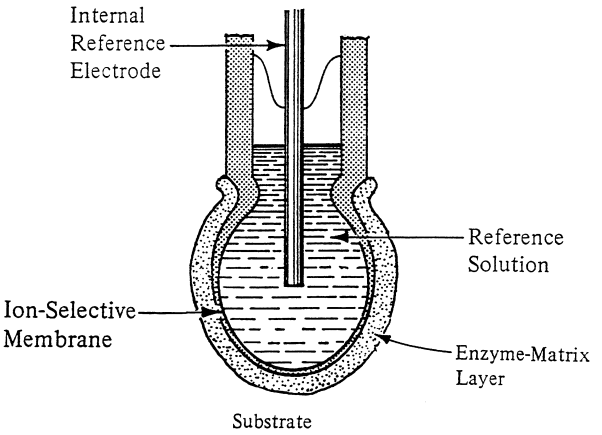

FIGURE 6-11 Urea electrode, based on the immobilization of urease onto an ammonium ion-selective electrode.

poisons cyanide or azide, or for toxic metals have been developed using enzymes such as acetylcholinesterase, horseradish peroxidase, or tyrosinase (33,34). The analytical information is commonly obtained from the decreased electrochemical response to the corresponding substrate (associated with the inhibitor–enzyme interaction). Pesticide measurements with cholinesterase systems often employ a bienzyme cholinesterase/choline oxidase system, in connection to amperometric monitoring of the liberated peroxide species. Changes in the substrate response can also be exploited for measuring the activity of enzymes.

6-1.1.3 Tissue and Bacteria Electrodes The limited stability of isolated enzymes, and the fact that some enzymes are expensive or even unavailable in the pure state, has prompted the use of cellular materials (plant tissues, bacterial cells, etc.) as a source for enzymatic activity (35). For example, banana tissue (which is rich with polyphenol oxidase) can be incorporated by mixing within the carbon paste

TABLE 6-1 Some Common Enzyme Electrodes

Measured Species	Enzyme	Detected Species	Type of sensing	Reference
Cholesterol	Cholesterol oxidase	O_2	Amperometric	23
Creatinine	Creatinase	NH_3	Potentiometric gas sensing	24
Lactate	Lactate dehydrogenase	NADH	Amperometric	25
	Lactate oxidase	H_2O_2	Amperometric	26
Penicillin	Penicillinase	H^+	Potentiometric	27
Phenol	Tyrosinase	Quinone	Amperometric	28
Salicylate	Salicylate hydroxylase	CO_2	Potentiometric gas sensing	29
Uric acid	Uricase	CO_2	Potentiometric gas sensing	30

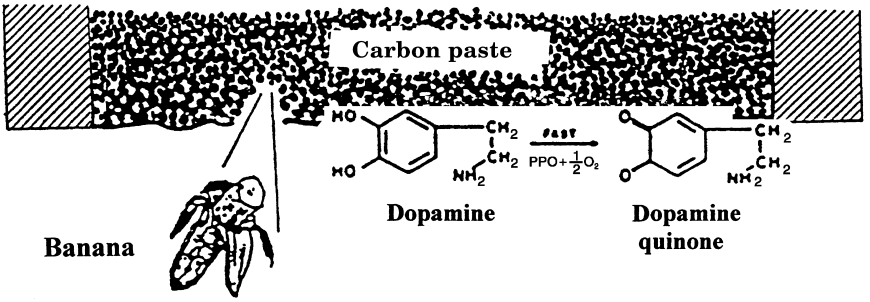

FIGURE 6-12 The mixed tissue (banana) carbon-paste sensor for dopamine. PPO = polyphenol oxidase. (Reproduced with permission from reference 36.)

matrix to yield a fast-responding and sensitive dopamine sensor (Figure 6-12). These biocatalytic electrodes function in a manner similar to that of conventional enzyme electrodes (i.e., enzymes present in the tissue or cell produce or consume a detectable species).

Other useful sensors rely on the coupling of microorganisms and electrochemical transducers. Changes in the respiration activity of the microorganism, induced by the target analyte, result in decreased surface concentration of electroactive metabolites (e.g., oxygen), which can be detected by the transducer.

6-1.2 Affinity Biosensors

Affinity sensors exploit selective binding of certain biomolecules (e.g., antibodies, receptors, or polynucleotides) toward specific target species. The biomolecular recognition process is governed primarily by the shape and size of the receptor pocket and the ligand of interest (the analyte). An associative process of this kind is governed by thermodynamic considerations (in contrast to the kinetic control exhibited by biocatalytic systems). The high specificity and affinity of these biochemical binding reactions lead to highly selective and sensitive sensing devices. As will be shown in the following sections, electrochemical transducers are very suitable for detecting these molecular recognition events. Such devices rely on measuring the electrochemical signals resulting from the binding process. Another type of interaction, the hybridization of two complementary DNA strands, can also be probed and used for sequence-selective biosensing of DNA. Such detection of specific DNA sequence, although still in its infancy, holds great promise for diagnosing infectious or genetic diseases.

6-1.2.1 Immunosensors Most reported affinity biosensors are based on immunological reactions involving the shape recognition of the antigen (Ag) by the antibody (Ab) binding site to form the antibody/antigen (AbAg) complex:

$$\mathrm{Ab} + \mathrm{Ag} \rightleftharpoons \mathrm{AbAg} \tag{6-13}$$

The antibody is a globular protein produced by an organism to bind to foreign molecules (i.e., antigens) and mark them for elimination from the organism. The remarkable selectivity of antibodies is based on the stereospecificity of the binding site for the antigen, and is reflected by large binding constants (ranging from 10^5 to 10^9 L mol^{-1}). Antibody preparations may be monoclonal or polyclonal. The former are produced by a single clone of antibody-producing cells, and thus have the same affinity. Polyclonal antibodies, in contrast, are cheaper but possess varying affinities.

Electrochemical immunosensors, combining specific immunoreactions with electrochemical transduction, have gained considerable attention in recent years (37–41). Such sensors are based on labeling of the antibody (or antigen) with an enzyme that acts on a substrate and generates an electroactive product that can be detected amperometrically. Enzyme immunosensors can employ competitive or sandwich modes of operation (Figure 6-13). In competitive-type sensors, the sample antigen (analyte) competes with an enzyme-labeled antigen for antibody-binding sites on a membrane held on an amperometric or potentiometric sensing probe. After the reaction is complete, the sensor is washed to remove unreacted components. The probe is then placed in a solution containing the substrate for the enzyme, and the product or reactant of the biocatalytic reaction is measured. Due to the competitive nature of the assay, the measurement signal is inversely proportional to the concentration of the analyte in the sample. Several enzymes, such as alkaline phosphatase, peroxidase, or catalase, have been particularly useful for this task.

Sandwich-type sensors are applicable for measuring large antigens that are capable of binding two different antibodies. Such sensors utilize an antibody that binds the analyte-antigen, which then binds an enzyme-labeled second antibody. After removal of the nonspecifically adsorbed label, the probe is placed into the substrate-containing solution, and the extent of the enzymatic reaction is monitored

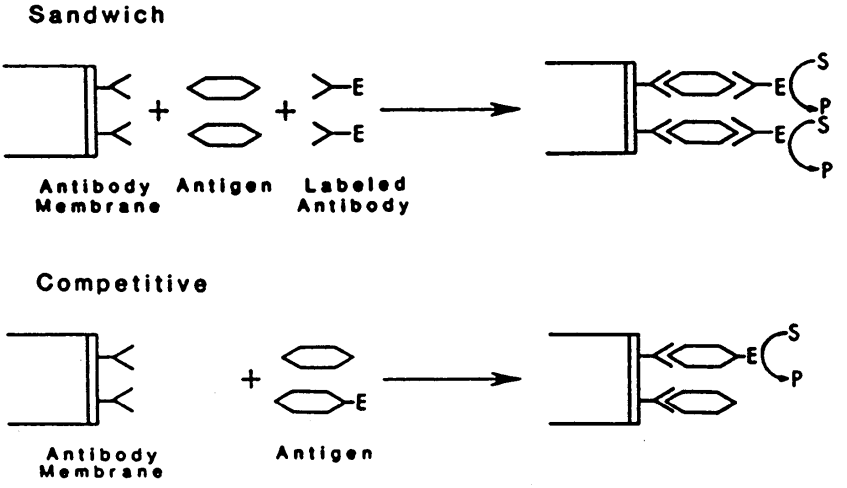

FIGURE 6-13 Enzyme immunosensors based on the competitive or sandwich modes of operation. (Reproduced with permission from reference 40.)

electrochemically. Other types of immunosensors based on labeling the antigen or antibody with an electroactive tag (e.g., a heavy metal), label-free capacitance measurements, immobilizing antigen–carrier conjugates at the tip of potentiometric electrodes, or amplifying the antigen–antibody complex equilibrium by liposome lysis are also being explored.

Instead of immobilizing the antibody onto the transducer, it is possible to use a bare (amperometric or potentiometric) electrode for probing enzyme immunoassay reactions (42). In this case, the content of the immunoassay reaction vessel is injected to an appropriate flow system containing an electrochemical detector, or the electrode can be inserted into the reaction vessel. Remarkably low (femtomolar) detection limits have been reported in connection with the use of the alkaline phosphatase label (43,44). This enzyme catalyzes the hydrolysis of phosphate esters to liberate easily oxidizable phenolic products.

6-1.2.2 DNA Hybridization Biosensors Nucleic acid recognition layers can be combined with electrochemical transducers to form new and important types of affinity biosensors. The use of nucleic acid recognition layers represents a relatively new and exciting area in biosensor technology. In particular, DNA hybridization biosensors offer considerable promise for obtaining sequence-specific information in a simpler, faster and cheaper manner, compared to traditional hybridization assays. Such new strategies hold enormous potential for clinical diagnosis of genetic or infectious diseases, for the detection of food-contaminating organisms, for environmental monitoring, or for criminal investigations.

The basis for these devices is the Watson–Crick DNA base pairing. Accordingly, these sensors rely on the immobilization of a relatively short (20–40 bases) single-stranded DNA sequence (the "probe") on the transducer surface, which upon hybridization to a specific complementary region of the target DNA gives rises to an electrical signal. Several studies have demonstrated the utility of electroactive indicators for monitoring the hybridization event (45). Such redox-active compounds have a much larger affinity for the resulting target:probe duplex (compared to their affinity for the probe alone). Their association with the surface duplex thus results in an increased electrochemical response. For example, Figure 6-14 displays the increased response of the $Co(phen)_3^{+3}$ indicator as recorded at a probe-coated strip electrode upon increasing the concentration of the *E. coli* DNA sequence. Control of the probe immobilization and of the hybridization conditions (e.g., ionic strength, temperature, time) is crucial for attaining high sensitivity and selectivity (including the detection of single point mutations). Sequence-specific electrochemical biosensors based on new innovative detection strategies are being developed for direct electrical detection of the hybridization event. These include the use of enzyme labels or indicator-free measurements (relying on the intrinsic electroactivity of DNA, on changes in interfacial properties, or on the conductivity of a DNA-functionalized electropolymerized film). Ultimately, these developments will lead to the introduction of miniaturized (on-chip) sensor arrays, containing numerous microelectrodes (each coated with a different oligonucleotide probe) for the simultaneous hybridization detection of multiple DNA sequences. The new gene

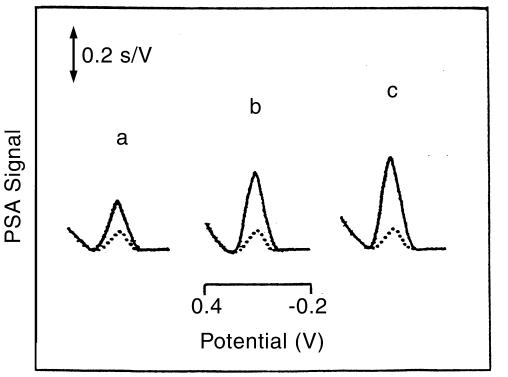

FIGURE 6-14 DNA hybridization biosensors: detection of DNA sequences from the *E. coli* pathogen. Chronopotentiometric response of the redox indicator upon increasing the target concentration in 1.0 μg/ml steps (a–c), in connection with a 2 min hybridization time. (Reproduced with permission from reference 46.)

chips would integrate a microfluidic network—essential for performing all the steps of the bioassay (see Section 6-3.2)—with the detection process, and would thus address the growing demands for shrinking DNA diagnostics in accordance with market needs in the twenty-first century.

Other modes of DNA interactions (besides base-pair recognition) can be used for the development of electrochemical DNA biosensors. In particular, dsDNA-modified electrodes can be designed for detecting small molecules (e.g., drugs or carcinogens) interacting with the immobilized nucleic acid layer (47,48). The intercalative accumulation of these molecules onto the surface-confined DNA layer can be used for their measurements at trace levels, in a manner analogous to the preconcentration/voltammetric schemes described in Section 4-5.3.4. In addition, the sensitivity of the intrinsic redox signals of DNA to its structure and conformation offers considerable opportunities for nucleic acid research, including the sensing of DNA damage.

6-1.2.3 Receptor-Based Sensors Another new and promising avenue of sensing is the use of chemoreceptors as biological recognition elements. Receptors are protein molecules embedded in the cellular membrane that specifically bind to target analytes. The receptor–analyte (host–guest) binding can trigger specific cellular events, such as modulation of the membrane permeability or activation of certain enzymes, that translate the chemical interaction to electrical signals. For example, ion-channel sensors utilizing receptors in a bilayer lipid membrane couple the specific binding process with intense signal amplification (49–51), attributed to the opening/closing switching of the ion flux through the membrane (Figure 6-15). A single selective binding event between the membrane receptor and the target analyte can thus result in an increase of the transmembrane conduction that involves thousands of ions. Unlike most antibody binding (aimed at specific substances),

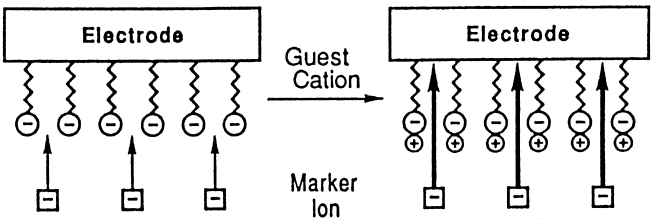

FIGURE 6-15 Schematic representation of the ion permeability modulation for cation-responsive voltammetric sensors based on negatively charged lipid membranes. Complexation of the guest cation to the phospholipid receptors causes an increase of the permeability for the anionic marker ion. (Reproduced with permission from reference 49.)

receptors tend to bind to classes of substances (possessing common chemical properties that dictate the binding affinity). Accordingly, receptor-based biosensors are usually class-specific devices.

Instead of isolating, stabilizing, and immobilizing chemoreceptors onto electrodes, it is possible to use intact biological sensing structures for determining relevant chemical stimulants (52,53). This novel concept was illustrated with antennule structures of the blue crab. Such structures are part of the crab's food-locating system, and thus can be exploited for the determination of amino acids. Similarly, various drugs can be monitored based on their stimulation of nerve fibers in the crayfish walking leg. A flow cell based on such a neuronal sensor is shown in Figure 6-16. Such a sensor responds to stimulant compounds at extremely low levels (down to 10^{-15} M!), with very short response times. The relationship between the response frequency (R) and the stimulant concentration (C) is given by

$$R = \frac{R_{\max}}{1 + (K/C)^n} \tag{6-14}$$

where $R_{\max}$ is the maximum response frequency, n is a cooperativity factor between receptors, and K is a constant.

In addition to the use of bioreceptors, it is possible to design artificial molecules that mimic bioreceptor functions (51). Such artificial receptors (hosts) can be tailored for a wide range of guest stimulants. For example, cyclodextrin derivatives have been used to provide a shape-discrimination effect in connection with ion-channel sensors (54). The receptors are incorporated within artificial lipid membranes, prepared by the Langmuir–Blodgett (LB) deposition method on the transducer surface. The LB method (which involves a transfer of a monomolecular film from an air–water interface onto the electrode surface) results in thin organic films that can be organized into multilayer molecular assemblies one monolayer at a time. Artificial sensor arrays (emulating biological sensory systems, e.g., the human nose) are also being explored in various laboratories (55) (see Section 6-4). High sensitivity and selectivity can be achieved also by using the receptor recognition process as an in-situ preconcentration step (56).

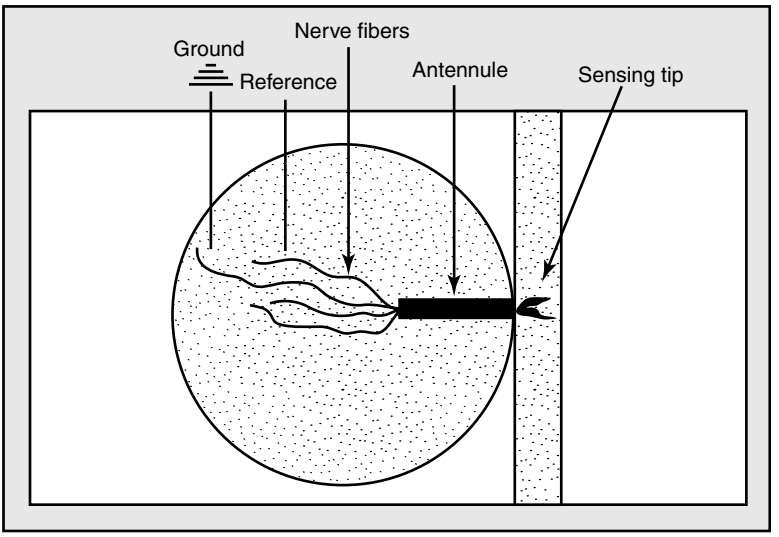

FIGURE 6-16 Neuronal sensing: top view of a flow cell with mounted antennule and the various electrode connections. (Reproduced with permission from reference 52.)

6-2 GAS SENSORS

Real-time monitoring of gases, such as carbon dioxide, oxygen, and ammonia, is of great importance in many practical environmental, clinical, and industrial situations. Gas-sensing electrodes are highly selective devices for measuring dissolved gases. They are reliable and simple and exhibit excellent selectivity, but tend to have relatively slow response times (particularly as the limit of detection is approached).

Gas sensors usually incorporate a conventional ion-selective electrode surrounded by a thin film of an intermediate electrolyte solution and enclosed by a gas-permeable membrane. An internal reference electrode is usually included, so that the sensor represents a complete electrochemical cell. The gas of interest in the sample solution diffuses through the membrane and comes to equilibrium with the internal electrolyte solution. In the internal compartment, between the membrane and the ion-selective electrode, the gas undergoes a chemical reaction, consuming or forming an ion to be detected by the ion-selective electrode. (Protonation equilibria in conjunction with a pH electrode are most common.) Since the local activity of this ion is proportional to the amount of gas dissolved in the sample, the electrode response is directly related to the concentration of the gas in the sample. The response is usually linear over a range of typically four orders of magnitude; the upper limit is determined by the concentration of the inner electrolyte solution. The permeable membrane is the key to the electrode's gas selectivity. Two types of polymeric material, microporous and homogeneous, are used to form the gas-permeable membrane. Typically, such hydrophobic membranes are 0.01–0.1 mm thick and are impermeable to water or ions. Hence, gas-sensing probes exhibit

excellent selectivity, compared with many ion-selective electrodes. Besides the membrane, the response characteristics are often affected by the composition of the internal solution and the geometric variables (57). Amperometric gas sensors based on different configurations have also been developed in recent years. Such developments have been reviewed (58).

6-2.1 Carbon Dioxide Sensors

Carbon dioxide devices were originally developed by Severinghaus and Bradley (59) to measure the partial pressure of carbon dioxide in blood. This electrode, still in use today (in various automated systems for blood gas analysis), consists of an ordinary glass pH electrode covered by a carbon dioxide membrane, usually silicone, with an electrolyte (sodium bicarbonate–sodium chloride) solution entrapped between them (Figure 6-17). When carbon dioxide from the outer sample diffuses through the semipermeable membrane, it lowers the pH of the inner solution:

$$CO_2 + H_2O \rightarrow HCO_3^- + H^+ \tag{6-15}$$

Such changes in the pH are sensed by the inner glass electrode. The overall cell potential is thus determined by the carbon dioxide concentration in the sample:

$$E = K + \frac{RT}{F} \ln[CO_2] \tag{6-16}$$

A Nernstian response of 59 mV per decade change in concentration is commonly observed (at 25°C). Relation to the partial pressure carbon dioxide is accomplished by the use of Henry's law. A catheter sensor configuration has been developed for in-vivo monitoring of blood carbon dioxide (61).

By using different membranes, it is possible to obtain potentiometric sensors for gases such as sulfur dioxide or nitrogen dioxide. Such sensors employ similar (acid–base) or other equilibrium processes. These devices, along with their equilibrium processes and internal electrodes, are summarized in Table 6-2. Membrane coverage

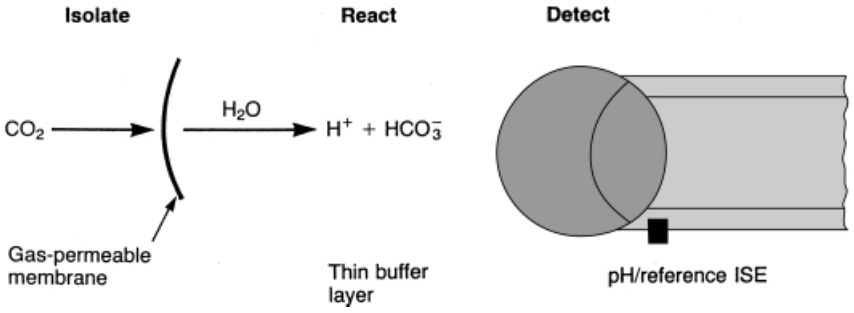

FIGURE 6-17 Schematic of the potentiometric sensor for carbon dioxide. (Reproduced with permission from reference 60.)

TABLE 6-2 Potentiometric Gas Sensors

Target Gas	Equilibrium Process	Sensing Electrode
CO_2	$CO_2 + H_2O \rightleftharpoons HCO_3^- + H^+$	H^+, CO_3^{2-}
NO_2	$2NO_2 + H_2O \rightleftharpoons NO_3^- + NO_2^- + 2H^+$	H^+
SO_2	$SO_2 + H_2O \rightleftharpoons HSO_3^- + H^+$	H^+
H_2S	$H_2S \rightleftharpoons 2H^+ + S^{2-}$	S^{2-}, H^+
HF	$HF \rightleftharpoons H^+ + F^-$	F^-, H^+

of other ion-selective electrodes (e.g., chloride) can be used for the sensing of other gases (e.g., chlorine).

6-2.2 Oxygen Electrodes

While most gas sensors rely on potentiometric detection, the important oxygen probe is based on amperometric measurements. In particular, membrane-covered oxygen probes based on the design of Clark et al. (62) have found acceptance for many applications. The sensor is based on a pair of electrodes immersed in an electrolyte solution and separated from the test solution by a gas-permeable hydrophobic membrane (Figure 6-18). The membrane is usually made of Teflon, silicon rubber, or polyethylene, while the electrolyte is a solution of potassium chloride and buffer. Oxygen diffuses through the membrane and is reduced at the surface of the sensing electrode. The resulting electrolytic current is proportional to the rate of diffusion of oxygen to the cathode, and hence to the partial pressure of oxygen in the sample. Such an electrode thus displays a linear response in contrast to the logarithmic dependence of most gas sensors (discussed in Section 6-2.1). The actual potential applied at the cathode (with respect to the anode/reference electrode) depends on the particular design. Cathodes made of platinum, gold, or silver are commonly incorporated in different commercial probes. The applied potential usually maintains the cathode on the diffusion-limited plateau region for the oxygen reduction process.

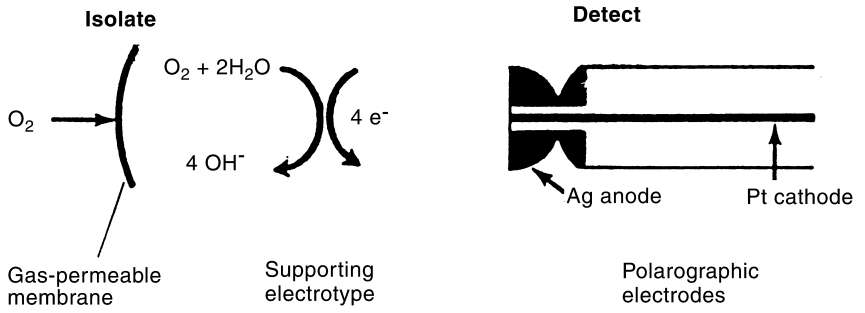

FIGURE 6-18 Membrane-covered oxygen probe based on the Clark electrode. (Reproduced with permission from reference 60.)

Periodic calibration is desired for addressing slow drifts. This is usually accomplished by exposure to samples with known oxygen content, for example, with air assumed 20.93% O_2. The response lime of the electrode is generally larger when changing from a high P_{O_2} to a low P_{O_2}, compared with a change in the opposite direction.

Membraneless oxygen sensors based on solid-state technology have also been reported. For example, coverage of a Y_2O_3-doped ZrO_2 disk with porous platinum electrodes results in a selective sensor, based on the coupling of the oxygen reduction process and the preferential transport of the oxide ion product through vacancies in the doped crystal (63). For this purpose, one of the platinum electrodes is exposed to the unknown gas while the second one is exposed to the reference gas. Such potentiometric sensors commonly operate at high temperatures, and are widely used in the automotive industry for controlling the ratio of air/fuel (with an annual worldwide market exceeding 150 million dollars).

Other useful gas sensors include the potentiometric ammonia (64) or hydrogen cyanide probes (65), and amperometric carbon monoxide (66) and nitrogen dioxide (67) devices. The hydrogen cyanide probe is an example of a modern device that relies on changes in the conductivity of electropolymerized film (polyaniline) in the presence of a given gas.

6-3 SOLID-STATE DEVICES

The integration of chemically sensitive membranes with solid-state electronics has led to the evolution of miniaturized, mass-produced potentiometric probes known as ion-selective field-effect transistors (ISFETs). The development of ISFETs is a logical extension of coated-wire electrodes (described in Section 5-2.4). The construction of ISFETs is based on the technology used to fabricate microelectronic chips. Ion-selective field-effect transistors incorporate the ion-sensing membrane directly on the gate area of a field-effect transistor (FET) (Figure 6-19). The FET is a solid-state device that exhibits high input impedance and low output impedance and is therefore capable of monitoring charge build-up on the ion-sensing membrane. As the charge density on this membrane changes because of interaction with the ions in solution, a drain current flows between the source and drain of the transistor. The increased voltage needed to bring the current back to its initial value represents the response. (This is commonly accomplished by placing the ISFET in a feedback loop.) From the standpoint of change in drain current as a result of change in activity of the ion of interest, the ISFET response is governed by the same Nernstian relationship (and the selectivity limitation) that characterizes conventional ion-selective electrodes.

Such sensors utilizing solid-state electronics have significant advantages. The actual sensing area is very small. Hence, a single miniaturized solid-state chip could contain multiple gates and be used to sense several ions simultaneously. Other advantages include the in-situ impedance transformation and the ability for temperature and noise compensation. While the concept of the ISFET is very

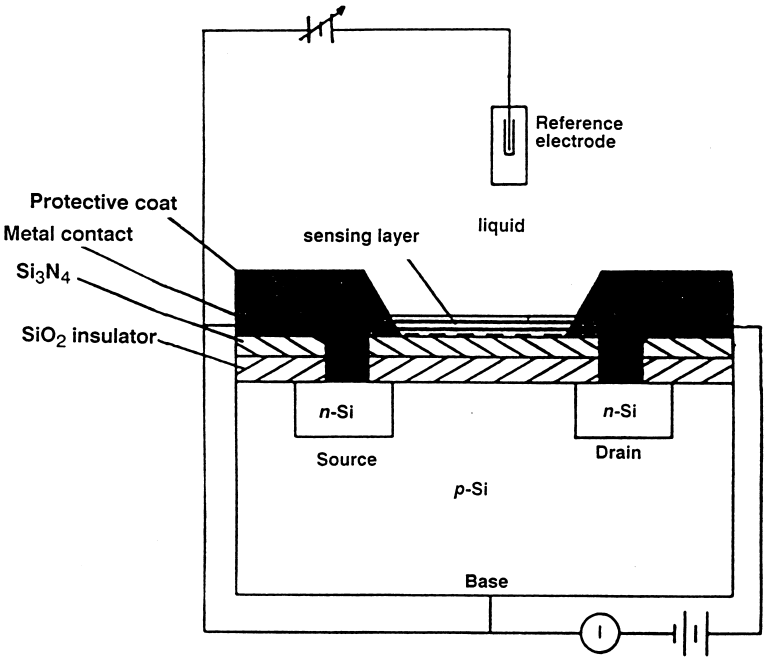

FIGURE 6-19 An ion-selective field-effect transistor.

exciting and intriguing, problems with stability and encapsulation still need to be solved before such devices reach the truly practical stage. One problem is the detachment of PVC-type ion-sensing membranes from the gates of FETs. This can be minimized by suspending a polyimide mesh over the gate (68); the polymer film thus becomes anchored in place by the mesh.

The coating on the gate is the key to the analytical chemistry that the ISFET can perform. Ion-selective field-effect transistors based on various ion-responsive layers have been developed. Among these are a sodium ISFET based on the synthetic sodium carrier ETH 227, an ammonium ISFET utilizing monactin–nonactin (69), and a chloride ISFET prepared by laying a membrane of methyltridodecylammonium chloride on a silicon nitride gate (70). Ion-selective field-effect transistors that are not covered with an ion-responsive membrane can be used directly as pH sensors. The silicon nitride coating on the transistor is itself sensitive to hydrogen ions (through its own surface properties) and develops phase boundary potentials proportional to the logarithm of the hydrogen ion activity in the contacting solution. The ability to sense several ions was illustrated using a quadruple-function ISFET probe that simultaneously monitored potassium, sodium, calcium, and pH in whole blood samples (71). Ion-selective field-effect transistors can be combined with various biological agents, such as enzymes or antigens, to form effective biosensors. The biological recognition process results in modulation of the gate voltage, and thus controls the drain current. For example, an enzyme field-effect transistor (ENFET)

was developed for continuous monitoring of glucose in body fluids (72). The theory and mode of operation of ISFETs have been reviewed (73).

6-3.1 Microfabrication of Solid-State Sensor Assemblies

Other miniaturized solid-state sensors can be fabricated by coupling microelectronics and chemically sensitive layers. In particular, Wrighton and co-workers (74) fabricated diode and transistor structures by combining a conducting polymer with lithographically defined interdigitated microarray electrodes. Such devices have been responsive to redox species such as oxygen or hydrogen. Interesting biosensing applications of this molecular electronic switching device involved the addition of an enzyme layer (75,76). Changes in the conductivity of the polymer resulting from pH changes (associated with the enzymatic reaction) have been exploited for monitoring the corresponding substrate (e.g., Figure 6-20). Miniaturized and disposable amperometric biosensors can be achieved by coupling microfabricated oxygen electrodes with various biocomponents (77).

6-3.2 Microfabrication Techniques

Microfabrication technology has made a considerable impact on the miniaturization of electrochemical sensors and systems. Such technology allows replacement of traditional bulky electrodes and "beaker-type" cells with mass-producible, easy-to-use sensor strips. These strips can be considered as disposable electrochemical cells onto which the sample droplet is placed. The development of microfabricated electrochemical systems has the potential to revolutionize the field of electroanalytical chemistry.

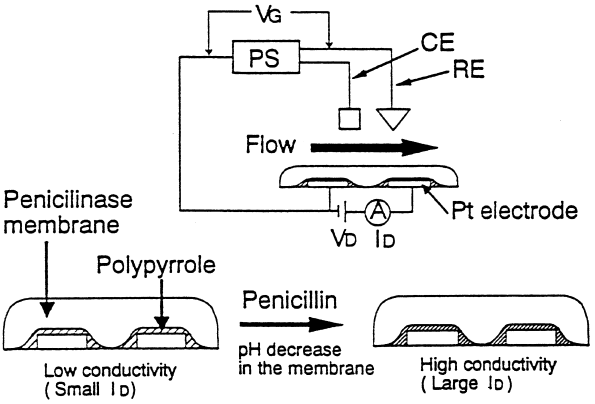

FIGURE 6-20 Configuration of a penicillin sensor based on an microarray electrode coated with a pH-responsive polypyrrole. V_G = gate voltage; V_D = drain voltage; I_D = drain current; PS = potentiostat; CE and RE = counter and reference electrodes, respectively. (Reproduced with permission from reference 76.)

The thin-film lithographic approach can be used for producing small (micrometer) dimension electrodes on silicon wafers (e.g. Figure 4-24) This technology couples various processes (based on electronic integrated circuit manufacturing), including vapor deposition of a thin metal film, its coverage with a UV-sensitive photoresist, photolithographic patterning (using an appropriate mask and UV radiation), removal of the exposed photopolymerized soluble zone of the photoresist with a developer, and chemical or plasma etching (78). Three-electrode microsystems can thus be readily prepared on a planar silicon wafer. This lithographic approach represents an attractive route for the production of sensor arrays. For example Figure 6-21 displays a multiple-analyte sensor array, commonly used for point-of-care clinical assays of small blood droplets (79).

Microfabricated electrodes can be integrated with other silicon microstructures (including micropumps, microchannels, mixing chambers, or valves) to produce complete miniaturized analytical systems (80). Due to their fluid manipulation capability such micromachined systems hold great promise for performing all the steps of a chemical or biological assay (including the sample preparatory steps, analytical reactions, separation and detection) on a single microchip platform. Such on-chip integration of the sample manipulations offers greatly improved efficiency with respect to sample size, reagent/solvent consumption, and response time, and should find use in numerous analytical applications. Eventually this would enable

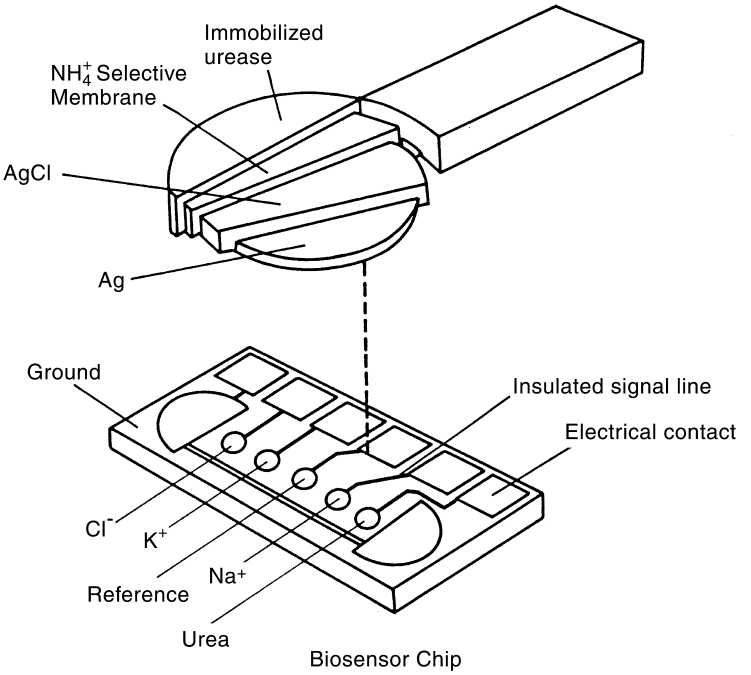

FIGURE 6-21 A silicon-based sensor array for monitoring various blood electrolytes, gases, and metabolites. (Courtesy of i-STAT Co.)

the laboratory to be transported to the sample. A range of assays have already been adapted to the microchip format. These possibilities have led to the concepts of μTAS (micro-total analytical systems) and "Lab-on-a-Chip", which are hot topics of analytical chemistry. The extremely small dimensions of electrochemical detectors, coupled with their remarkable sensitivity and compatibility with microfabrication technologies, make them very suitable for adaptation for "Lab-on-a-Chip" analytical microsystems. Microsystems relying on electrosmotic flow obviate the needs for pumps or valves but require proper attention to the decoupling of the detector potential from the high voltage used to control the microfluidics. Such precise fluid control is accomplished by regulating the applied potentials at the terminus of each channel of the microchip (81). The channel networks of these chips include mixing tees and cross intersections for mixing reagents and injecting samples with high reproducibility (e.g., Figure 6-22). Particularly powerful is the use of electrochemical detectors for monitoring on-chip electric-field-driven separations (see Section 3-6).

Large-scale sensor fabrication can be accomplished not only by lithographic techniques but also using modern screen-printing (thick-film) processes (82,83). The screen-printing technology relies on printing patterns of conductors and insulators onto the surface of planar (plastic or ceramic) substrates. Various conducting and insulating ink materials are available for this task. The screen-printing process involves several steps (as illustrated in Figure 6-23 for the fabrication of carbon electrodes), including placement of the ink onto a patterned screen or stencil, followed by forcing it through the screen with the aid of a squeegee, and drying/curing the printed patterns. Such a process yields mass-producible (uniform

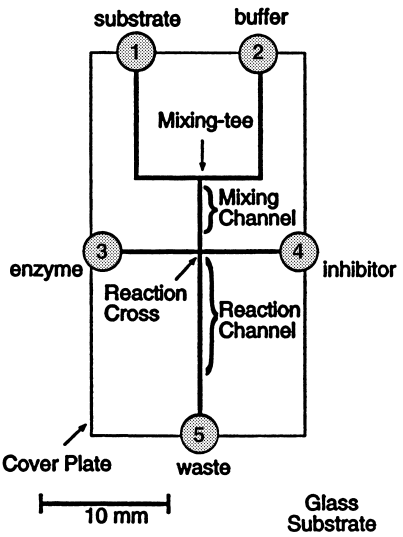

FIGURE 6-22 Schematic of a microchip system for enzymatic assays. The channels terminate at reservoirs containing the indicated solutions. (Reproduced with permission from reference 81.)

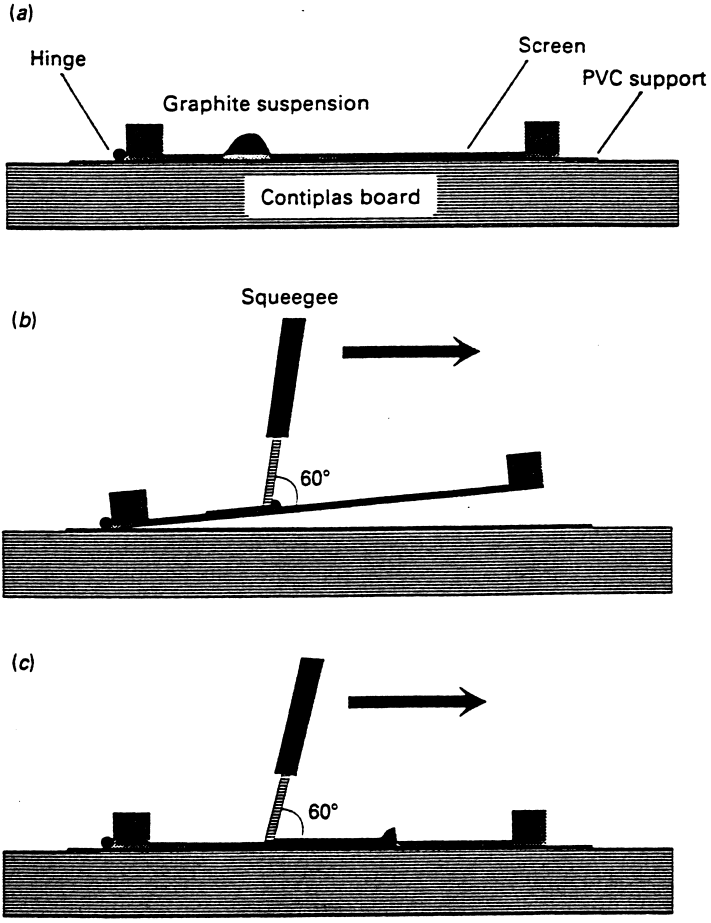

FIGURE 6-23 Steps involved in the screen-printing process: (*a*) deposit the graphite suspension onto the screen; (*b*) load the screen mesh with the graphite; (*c*) force the graphite onto the substrate. (Reproduced with permission from reference 83.)

and disposable) electrodes of different shapes or sizes, similar to the glucose strip shown in Figure 6-7. The electrochemical reactivity and overall performance of screen-printed electrodes are dependent upon the composition of the ink employed and on the printing and curing conditions (e.g., pressure, temperature). Disposable potentiometric sensors can be fabricated by combination of ion-selective polymeric membranes with dry reagent films. Such disposable ion-selective electrode slides require microliter (10–50 μL) sample volumes, and are ideally suited for various decentralized applications. Mass-produced potentiometric sensor arrays are also being developed in connection with future high-speed clinical analyzers. These are being combined with advanced materials (e.g., hydrogels) that obviate the need for internal filling solutions (common to ISE sensors; see Chapter 5). The screen-

printing technology requires lower capital and production costs than the thin-film lithographic approach, but is limited to electrode structures larger than 100 μm. It is also possible to fabricate electrochemical devices combining the thin- and thick-film processes.

6-4 SENSOR ARRAYS

So far we have discussed the one-sensor/one-analyte approach. However, arrays of independent electrodes can offer much more analytical information and thus hold a great potential for many practical applications. These include the development of "intelligent sensing systems" capable of responding to changes in the chemical environment of the array.

The use of multielectrode arrays takes advantage of the partial selectivity of an individual electrode by combining several electrodes and examining the relative responses of all the sensors together. The array's response for each analyte thus corresponds to a fingerprint pattern (e.g., Figure 6-24). In addition, the coupling of multielectrode arrays with a chemometric (multivariate calibration) approach allows analysis of a mixture of analytes. Two calibration techniques, partial least squares and multiple linear regression, are particularly useful for this task. High stability, rather than selectivity, is the primary concern in the operation of electrode arrays.

Various types of multielectrode arrays can be employed. For example, potentiometric electrode arrays exploit the fact that ion-selective electrodes respond to some degree to a range of ions (85–87). The first potentiometric array was described by Otto and Thomas (85). Diamond and co-workers have illustrated the utility of an array comprising of three highly selective electrodes and one sparingly selective electrode (87). Arrays of highly selective potentiometric electrodes can also be

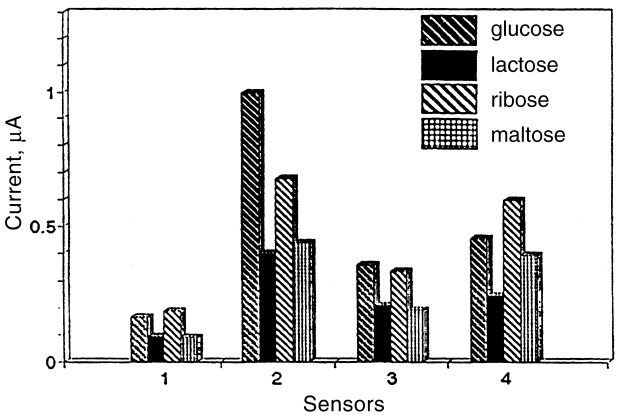

FIGURE 6-24 Response pattern of an amperometric sensor array for various carbohydrates. The array comprised carbon-paste electrodes doped with CoO (1), Cu_2O (2), NiO (3) and RuO_2 (4). (Reproduced with permission from reference 84.)

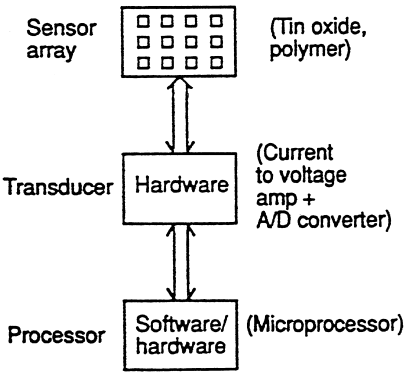

FIGURE 6-25 The flow of information in the array-based artificial nose. (Reproduced with permission from reference 94.)

useful when high-speed analysis is required (88). Arrays of voltammetric electrodes can be based on the use of different electrode materials (89) or catalytic surface modifiers (84) (with different voltammetric characteristics), on the use of partially selective coated electrodes (each covered with a different permselective film) (90), or on the use of different operating potentials or surface pretreatments (91,92). Microlithographic techniques are often used for the construction of such amperometric array electrodes, with multielectrode potentiostats controlling the potentials of the individual electrodes. A single (common) reference electrode is normally used with these arrays. Novel arrays of polymeric chemoresistors or metal oxide sensors have been used in connection with computer-assisted pattern-recognition algorithms for monitoring the flavor of beers (93) or for detecting various odorants (94). Changes in the resistivity of a series of conducting polymers upon the adsorption of different volatile compounds have been particularly useful for creating the response patterns. The distinct yet partially overlapping signals are achieved by preparing the individual polymers from modified monomer units or with different counter ions (dopants). Such arrays serve as electronic analogues for the human nose. The information flow in such arrays is displayed in Figure 6-25. Practical applications of electrode arrays have been facilitated by the availability of inexpensive multichannel data-acquisition cards for personal computers. The development of sensor arrays has been reviewed by Diamond (95). New advances are expected based on the development of user-friendly software, of new statistical tools, and of novel sensor fabrication technology.

REFERENCES

1. G. Sittamplam and G.S. Wilson, *J. Chem. Educ.*, 59, 70 (1982).
2. I. Willner, E. Katz, and B. Willner, *Electroanalysis*, 9, 965 (1997).
3. L. Gorton, *Electroanalysis*, 7, 23 (1995).

4. S. Algeret, *Analyst*, 121, 175 (1996).
5. J. Wang and L. Angnes, *Anal. Chem.*, 64, 456 (1992).
6. P.N. Bartlett and J.M. Cooper, *J. Electroanal. Chem.*, 362, 1 (1993).
7. D.N. Gray, M.H. Keyes, and B. Watson, *Anal. Chem.*, 49, 1067A (1977).
8. H.H. Weetall, *Anal. Chem.*, 46, 602A (1974).
9. X. Yang, G. Johansson, D. Pfeiffer, and F. Scheller, *Electroanalysis*, 3, 659 (1991).
10. S.J. Updike and G.P. Hicks, *Nature*, 214, 986 (1967).
11. R.A. Marcus and N. Sutin, *Biochim. Biophys. Acta*, 811, 265 (1985).
12. J.E. Frew and H.A.O. Hill, *Anal. Chem.*, 59, 933A (1987).
13. M.J. Green and P.I. Hilditch, *Anal. Proc.*, 28, 374 (1991).
14. M. Vreeke, R. Maidan, and A.J. Heller, *Anal. Chem.*, 64, 3085 (1992).
15. Y. Degani and A. Heller, *J. Phys. Chem.*, 91, 1285 (1987).
16. A. Riklin, E. Katz, I. Willner, A. Stocker, and A. Buckmann, *Nature*, 367, 672 (1995).
17. A. Guindilis, P. Atanasov, and E. Wilkins, *Electroanalysis*, 9, 661 (1997).
18. C. Henry, *Anal. Chem.*, 70, 594A (1998).
19. A. Malinauskas and J. Kulys, *Anal. Chim. Acta*, 98, 31 (1978).
20. L. Gorton, *J. Chem. Soc. Faraday Trans.*, 82, 1245 (1986).
21. M. Lobo, A. Miranda, and P. Tunon, *Electroanalysis*, 9, 191 (1997).
22. G.G. Guilbault and J.G. Montalvo, *J. Am. Chem. Soc.*, 92, 2533 (1970).
23. G.F. Hall and A.P.F. Turner, *Anal. Lett.*, 24, 1375 (1991).
24. H. Thompson and G.A. Rechnitz, *Anal. Chem.*, 46, 246 (1974).
25. W.J. Blaedel and R.A. Jenkins, *Anal. Chem.*, 48, 1240 (1976).
26. D. Pfeiffer, K. Setz, T. Schulmeister, F. Scheller, H. Lueck, and D. Pfeiffer, *Biosensors Bioelectron.*, 7, 661 (1992).
27. G.J. Papariello, A.K. Mukherji, and C.M. Shearer, *Anal. Chem.*, 45, 790 (1973).
28. G. Hall, D. Best, and A.F. Turner, *Anal. Chim. Acta*, 213, 113 (1988).
29. P. Seegopaul and G.A. Rechnitz, *Anal. Chem.*, 56, 852 (1984).
30. T. Kawashima and G.A. Rechnitz, *Anal. Chim. Acta*, 83, 9 (1976).
31. S. Saini, G. Hall, M. Downs, and A.F. Turner, *Anal. Chim. Acta*, 249, 1 (1991).
32. J. Wang, *Talanta*, 40, 1905 (1993).
33. J. Besombes, S. Cosiner, P. Labbe, and G. Reverdy, *Anal. Chim. Acta*, 311, 255 (1995).
34. J. Marty, D. Garcia, and R. Rouillon, *Trends Anal. Chem.*, 14, 329 (1995).
35. G.A. Rechnitz, *Science*, 214, 287 (1981).
36. J. Wang and M.S. Lin, *Anal. Chem.*, 60, 1545 (1988).
37. M. Aizawa, A. Moricka, and S. Suzuki, *Anal. Chim. Acta*, 115, 61 (1980).
38. P. Skladal, *Electroanalysis*, 9, 737 (1997).
39. I. Rosen, and J. Rishpon, *J. Electroanal. Chem.*, 258, 27 (1989).
40. R.K. Kobos, *Trends Anal. Chem.*, 6, 6 (1987).
41. S. Kaku, S. Nakanishi, and K. Horiguchi, *Anal. Chim. Acta*, 225, 283 (1989).
42. W.R. Heineman and H. Halsall, *Anal. Chem.*, 57, 1321A (1985).
43. C. Bauer, A. Eremenko, E. Forster, F. Bier, A. Makower, B. Halsall, W. Heineman, and F. Scheller, *Anal. Chem.*, 68, 2453 (1996).

44. O. Bagel, B. Limoges, B. Schollhorn, and C. Degrand, *Anal. Chem.*, 69, 4688 (1997).
45. S.R. Mikkelsen, *Electroanalysis*, 8, 15 (1996).
46. J. Wang, G. Rivas, and X. Cai, *Electroanalysis*, 9, 395 (1997).
47. M. Yang, M. McGovern, and M. Thompson, *Anal. Chim. Acta*, 346, 259 (1997).
48. J. Wang, G. Rivas, D. Luo, X. Cai, N. Dontha, P. Farias, and H. Shirashi, *Anal. Chem.*, 68, 4365 (1996).
49. S. Nagase, M. Kataoka, R. Naganawa, R. Komatsu, K. Odashimo, and Y. Umezawa, *Anal. Chem.*, 62, 1252 (1990).
50. I. Krull, D. Nikolelis, J. Brennan, R. Brown, M. Thompson, V. Ghaemmaghami, and K. Kallury, *Anal. Proc.*, 26, 370 (1991).
51. K. Odashima, M. Sugawara, and Y. Umezawa, *Trends Anal. Chem.*, 10, 207 (1991).
52. R.M. Buch and G.A. Rechnitz *Anal. Chem.*, 61, 533A (1989).
53. D. Leech and G.A. Rechnitz, *Electroanalysis*, 5, 103 (1993).
54. K. Odashima, M. Kotato, M. Sugawara, and Y. Umezawa, *Anal. Chem.*, 65, 927 (1993).
55. K.C. Persaud, *Anal. Proc.*, 28, 339 (1991).
56. J. Wang, Y. Lin, A. Eremenko, I. Kurochkin, and M. Mineyeva, *Anal. Chem.*, 65, 513 (1993).
57. J.W. Ross, J. Riseman, and J. Kruger, *Pure Appl. Chem.*, 36, 473 (1973).
58. Z. Gao, W. Buttner, and J. Stetter, *Electroanalysis*, 4, 253 (1990).
59. J.W. Severinghaus and A.F. Bradley, *J. Appl. Physiol.*, 13, 515 (1957).
60. J.D. Czaban, *Anal. Chem.*, 57, 345A (1985).
61. W. Opdycke and M.E. Meyerhoff, *Anal. Chem.*, 58, 950 (1986).
62. L.C. Clark, R. Wolf, D. Granger, and Z. Taylor, *J. Appl. Physiol.*, 9, 689 (1953).
63. *NASA Technical Briefs*, 9, 105 (1985).
64. M.E. Meyerhoff, *Anal. Chem.*, 52, 1532 (1980).
65. J. Langmaier and J. Janata, *Anal. Chem.*, 64, 523 (1992).
66. X. Xing and C.C. Liu, *Electroanalysis*, 3, 111 (1991).
67. S. Chang and J. Stetter, *Electroanalysis*, 2, 359 (1990).
68. G. Blackburn and J. Janata, *J. Electrochem. Soc.*, 129, 2580 (1982).
69. V. Oesch, S. Caras, and J. Janata, *Anal. Chem.*, 53, 1983 (1981).
70. T.V. Zhukova, *Zavod. Lab.*, 50, 18 (1984); *Chem. Abstr.*, 101, 221484S (1984).
71. A. Sibbard, A.K. Covington, and R.F. Carter, *Clin. Chem.*, 30, 135 (1984).
72. J. Kimura, *J Electrochem. Soc.*, 136, 1744 (1989).
73. J. Janata and R.J. Huber, *Ion-Sel. Electrode Rev.*, 1, 31 (1979).
74. G. Kittlesen, H. White, and M. Wrighton, *J. Am. Chem. Soc.*, 106, 7389 (1984).
75. P.N. Bartlett, and P. Birkin, *Anal. Chem.*, 65, 1118 (1993).
76. M. Nishizawa, T. Matsue, and I. Uchida, *Anal. Chem.*, 64, 2642 (1992).
77. H. Suzuki, E. Tamiya, and I. Karube, *Electroanalysis*, 3, 53 (1991).
78. G. Fiaccabrino and M. Koudelka-Hep, *Electroanalysis*, 10, 217 (1998).
79. K. Erickson and P. Wilding, *Clin. Chem.*, 39, 283 (1993).
80. G. Kovacs, K. Peterson, and M Albin, *Anal. Chem.*, 68, 407A (1996).
81. A. Hadd, D. Raymond, J. Halliwell, S. Jacobson, and J.M. Ramsey, *Anal. Chem.*, 69, 3407 (1997).

82. D. Craston, C. Jones, D. Williams, and N. El Murr, *Talanta*, 38, 17 (1991).
83. S. Wring and J. Hart, *Analyst*, 117, 1281 (1992).
84. Q. Chen, J. Wang, G.D. Rayson, B. Tian, and Y. Lin, *Anal. Chem.*, 65, 251 (1993).
85. M. Otto and J.D.R. Thomas, *Anal. Chem.*, 57, 2647 (1985).
86. K. Beebe, D. Verz, J. Sandifer, and B. Kowalski, *Anal. Chem.*, 60, 66 (1988).
87. R.J. Forster, F. Regan, and D. Diamond, *Anal. Chem.*, 63, 876 (1991).
88. D. Diamond, J. Lu, Q. Chen, and J. Wang, *Anal. Chim. Acta*, 281, 629 (1993).
89. R.S. Glass, S.P. Perone, and D.R. Ciarlo, *Anal. Chem.*, 62, 1914 (1990).
90. J. Wang, G.D. Rayson, Z. Lu, and H. Wu, *Anal. Chem.*, 62, 1924 (1990).
91. J. Stetter, P.C. Jurs, and S.L. Rose, *Anal. Chem.*, 58, 860 (1986).
92. P. Fielden and T. McCreedy, *Anal. Chim. Acta*, 273, 111 (1993).
93. T. Pearce, J. Gardner, S. Freil, P. Bartlett, and N. Blair, *Analyst*, 118, 371 (1993).
94. A. Newman, *Anal. Chem.*, 63, 586A (1991).
95. D. Diamond, *Electroanalysis*, 5, 795 (1993).

EXAMPLES

Example 6-1 Chronoamperogram a was obtained for the biosensing of glucose in whole blood. Subsequent standard additions of 1×10^{-3} M glucose yielded the chronoamperograms b to d. Find the concentration of glucose in the sample.

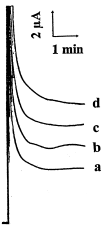

Solution The resulting current transients (sampled after 2 min) lead to the following standards additions plot:

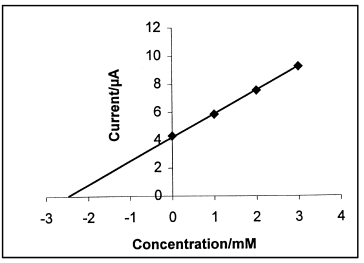

From which a glucose concentration of 2.4 mM can be obtained for the sample.

Example 6-2 The following standard addition plot was obtained for a competitive electrochemical enzyme immunoassay of the pesticide 2,4-D. A ground water sample (diluted 1 : 20 was subsequently assayed by the same protocol to yield a current signal of 65 nA. Calculate the concentration of 2,4-D in the original sample.

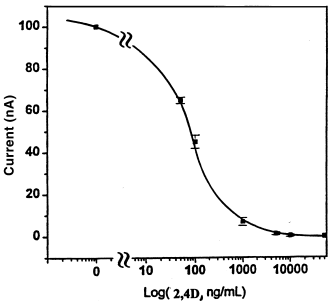

Solution The response of the diluted sample corresponds to 50 ng mL^{-1} 2,4-D. Considering the 20-fold dilution, the original sample concentration corresponds to 1.0 μg mL^{-1}.

QUESTIONS

1. Describe different schemes for immobilizing enzymes onto electrode transducers.
2. How would you extend the linear range of calibration plots based on the use of enzyme electrodes?
3. Describe a biosensing protocol for detecting mutations in DNA samples.
4. Suggest an enzyme electrode-based procedure for detecting organophosphate pesticides.
5. Describe various routes for facilitating the electrical communication between the redox center of glucose oxidase and an electrode surface.
6. Describe the major problems encountered in the detection of the NADH product of dehydrogenase-based amperometric biosensors. Discuss a common approach to circumvent these problems.
7. What are the improvements associated with performing analytical procedures on a microchip platform?
8. Give example of an enzyme electrode based on an ion-selective electrode transducer. What is the relationship between the substrate concentration and the potential response?

9. Explain clearly how the use of enzymes can enhance the power of electrochemical immunosensors.

10. Explain clearly why and how the response of glucose oxidase-based enzyme electrodes is influenced by fluctuations in the oxygen tension.

11. Use equations to explain why and how an increase in the sensitivity of an enzyme electrode is often coupled to a narrower linear range.

12. Explain clearly why highly selective individual electrodes are not desired for the operation of sensor arrays.

13. Discuss the major sources of errors in amperometric monitoring of blood glucose.

INDEX